Protected sulphonate nanoparticles, thiol-Michael functionalisation of nanogel decorated nanoparticles, and thiol-Michael microcapsules for agricultural mobility and adhesion applications

By

Andrew R. Edwards

A thesis submitted in fulfillment of the requirements for the degree of Doctor of Philosophy in Chemistry with Industrial Collaboration

University of Warwick, Department of Chemistry

Sept 2015

Table of contents

Figures and schemes

Tables

Acknowledgments

Firstly I would like to thank Associate Professor Stefan Bon for both funding of the project and for the support of himself and his group. He was the reason I got the funding that I did and for that I owe him my eternal gratitude. I would also like to thank the collaboration and support from the other University of Warwick staff, Professor Dave Haddleton, Professor Patrick Unwin, and Professor Julie Macpherson who also attended the group meetings with our industrial collaborator (Syngenta UK) and offered input and advice for the project that we worked on. I would also like to thank Stefan for the opportunity to visit three conferences, Glasgow for the Macro 2010 conference, Gothenburg for a conference in Sweden and the Macro 2012 conference at Warwick where I presented a poster at all three conferences and won a poser prize for second place at the Glasgow one.

As well as my supervisor I would also like to thank the sponsor for my project, Syngenta UK with big thanks to Ian M. Shirley for all the group meetings we regularly had with the Syngenta group. I also had the opportunity to visit the Jealotts Hill campus to see how the work is done at Syngenta and for project guidance and support. They provided the aims and criteria for the project as well as part of the funding. The rest of the funding was provided by the EPSRC.

I would also like to thank all the members of the Bon group over the past 4 years, including Dr Pat Colver, Dr Nadia Grossiord, Dr Catheline Colard, Dr Roberto Teixeira, Dr Attyah Alzhrani, Dr Nicholas Ballard, Dr Yunhua Chen, Dr Gabit Nurumbetov, Dr Rong Chen, Dr Holly McKenzie, Ashton Boyd, Dr Tom Skelhon, Dr Adam Morgan, Andy Ross, Dr Mike Brown and the various MChem students that had joined our group each year (specifically Qamreen Parker for her collaborative help with

the work in **Chapter 2**). The group has kept me happy in the lab and the office and I have made some lovely friends over my four years as a student.

Dr Nicole Jagielski, Dr Florence Gayet and Dr Paul Wilson also joined the Syngenta project in both Stefan Bon and Dave Haddletons' group and provided me with support and ideas about the chemistry involved.

I would also like to thank all the members of staff and faculty in the department of chemistry who have always been friendly, welcoming and provided chats each day. this combined with the lovely PhD students in various other groups made the department a lovely place to be and the coffee breaks and lunch times were as enjoyable as working in the lab. I would like to mention members of other groups in the department including Anisha, Mike, Dr Mike Snowden, Neil, Rob, James, Greg, Helena, Lara, Ian, Luke, Junliang, Dr Stefan Schumann, Nikola, Tom, Sang, Zhejia, Fran, Alex, Penny, Samiullah, Chris, Alan, Lihong, Deborah, Seng Soi Hoong, Jun, Julie Ann, Hazel, Helen, Deena, Pete, Ian, Vinh, Richard, Sarah, Robin, Mike, Liang, Yan, Gaidad, Dr Matt Gibson, Julian, George, James, Anthony, Rajan, Kayleigh, Muxiu, Qiang, Guanzhou, Yanzi, Stacy, Matt, Dr Remzi Becer and Claudia. They have all been friendly and helpful for keeping my mood happy.

I would also like to thank a few people for their expertise with equipment and training. I acknowledge Steve York and Ian Portman for providing training, use and help with electron microscopes (Department of Physics and School of Biology respectively), Birmingham Science city Innovative for some of the equipment used in this research (Uses for Advanced Materials in the Modern World, West Midlands Centre for Advanced Materials Project 2) with support from Advantage West Midlands (AWM) and partly funded by the European Regional Development Fund (ERDF).

Solid-state NMR measurements were provided and run by Jonathan Lamley in Dr Józef Lewandowski's group. ^{1}H and ^{13}C NMR were run thanks to Dr Ivan Prokes and Edward Tunnah. Dr Mike Brown provided expertise with the organic chemistry in Chapter II who joined our group for a short time. Raman microscopy was achieved thanks to the help from Andy Ross.

I would like to thank the support of all my friends from my previous university who kept me company when I visited them and to my oldest friend Tom for his lifelong friendship.

I would like to thank my Dad Will, my Mum Sally, my Brother Chris, my Sister-in-law Dolls (plus my new Niece Ruby), Auntie Jacky (Professor at Warwick) and her family, and my new step family Tina, Jack, and Jetson for all their support in life and for both raising and influencing my life into what it is today.

I also thank my newest family who have given me support while writing my corrections, so I thank my wife Elim for being my soulmate and my sunshine, and I thank my new family-in-law.

Declaration

I hereby declare that this thesis consists of my own work, and that none of the work has been submitted for any previous degree institutions. The work in **Chapter II** was done with collaboration with Qamreen Parker, MSc. The microfluidic section was aided by Dr Gabit Nurumbetov who fabricated the devices and provided me with inside about what was occurring.

Where other sources of information have been used, they have been acknowledged and referenced.

Signature: Andy Edwards **Date:** 18th Sept 2013

Abstract

Targeted delivery of an active ingredient to plant systems required extensive studies in areas of soil mobility, plant root adhesion and encapsulation. To accomplish the aims of mobility and adhesion to roots, specific surface charges and colloidal forces are required. These charges are required to provide sufficient repulsive forces preventing adhesion to soil and attractive forces allowing adhesion to roots. To accomplish the aims of synthesising colloids for mobility, adhesion and also encapsulation we formed a specific strategy. We aimed to increase the anionic surface charge on colloidal nanoparticles as a means to aid mobility studies of colloids through soil by providing increased repulsive forces to prevent adhesion to both air interfaces and soil. We also designed a way to decorate colloidal nanoparticles with microgel particles thus forming a soft adhesive surface layer with which further functionality could be incorporated i.e. surface charges. Finally we designed a simple methodology for the encapsulation of oil with post functionalisation in mind.

We synthesised colloidal nanoparticles, less than 200 nm, using soap-free emulsion polymerisation of styrene where up to 50 wt% of protected ethyl styrene sulphonate monomer was incorporated. The nanoparticles were hydrolysed to release the sulphonic charge using thermolysis in an autoclave. Soap-free emulsion polymerisation was used to synthesise raspberry-like and core-shell morphology decorated nanoparticles by the adhesion of crosslinked nanogel particles to a range of hydrophobic and hydrophilic seeds. Poly(acrylic) and poly(styrenic) seeds were synthesised with a range of hydrophobicities whereby more decoration of nanogel particles was achieved for hydrophilic seeds. The nanogel decoration was studied using di-, tri- and multi-functional acrylates and the morphologies changed from raspberry-like to core-shell as the functionality of the crosslinker increased. The presence of Vinyl

functional groups was proved using Raman microscopy. Post functionalisation with different thiols was carried out using nucleophilic thiol-Michael addition chemistry and a loss of vinyl groups was shown. Encapsulation of aromatic oil was carried out using an interfacial thiol-Michael addition reaction between a tetra- functional thiol and a penta-/hexa- functional ene using an amine nucleophilic catalyst. A microfluidic device was used to control the capsule sizes and dispersity and light microscopy was used to study capsule sizes and dry-down properties. No rupture was observed for the millimetre and microcapsules produced but unfortunately size scale-down could not be accomplished for the current system using high shear homogenisation.

In conclusion we increased the loading of sulphonate charge for colloidal poly(styrene) nanoparticles and we successfully increased the surface area of styrenic and acrylic seed nanoparticles using nanogel particle adhesion. We post functionalised decorated nanoparticles using thiol-Michael addition reactions and synthesised capsules using thiol-Michael addition reactions confined in a microfluidic device.

Abbreviations

AIBN	2,2'-azobis(2-methylpropionitrile)
DEGDA	Di-(ethylene glycol) di-acrylate
DDI	Double deionized water
DSC	Differential scanning calorimetry
DVB	Di-vinylbenzene
DLS	Dynamic light scattering
EMA	Ethyl methacrylate
ESS	Ethyl *4*-vinylbenzenesulphonate
FTIR	Fourier transform infra red
Tg	Glass transition temperature
Z_{Ave}	Average hydrodynamic diameter
NMR	Nuclear magnetic resonance
NSS	Neopentyl *4*-vinylbenzenesulphonate
MMA	Methyl methacrylate
X_m	Monomer conversion
PDI	Polydispersity index
PEGMEA	Poly (ethylene glycol) methyl ether acrylate
KPS	Potassium persulphate
SEM	Scanning electron microscopy
NaSS	Sodium *4*-vinylbenzenesulphonate
SSNMR	Solid-state nuclear magnetic resonance
TEM	Transmission electron microscopy
TGA	Thermal gravimetric analysis
X_m	Monomer conversion

Chapter 1 - Introduction

1.1. Abstract

In this chapter we discuss how plant systems function and the uptake of water. We also discuss soil and colloid mobility through soil media and the mechanisms for both colloid transport and retention. We discuss the synthesis of lyophobic colloidal particles *via* emulsion polymerisation and discuss the theory on particle formation, surface charge and colloidal stability. Finally we report the outlook and aims of the thesis.

1.2. Introduction to plants, soil, colloid mobility, water uptake and pesticides

Plant growth is controlled by environmental factors including the plants genetic make-up (this affects the growth and insect/pest resistance), moisture content or soil aeration (rainfall), sunlight intensity and duration, atmosphere conditions (humidity), soil composition (relative content of silica, silt and clay) and the mineral content (presence of metals, clays, nitrogen etc).[1-3] The use of artificial systems e.g. greenhouses and controlled water delivery systems can help reduce the variability in environmental factors.

A major problem for agriculture is the protection of crops against biotic creatures (insects, bugs, and weeds) that involves the use of insecticides, herbicides and pesticides. However, due to the toxicity of these additives being able to prevent waste contamination and leaching is an important aim. Strict rules control which products can be delivered to plant systems to prevent groundwater contamination.

Targeted delivery of protective additives to plants is a very crucial aim and most model systems used to predict uptake by plants are unreliable due to the great variability between actual and model systems. Soil chemistry is so complex that modelling colloid mobility through soil faces many issues. The ability to deliver insecticides, pesticides or herbicides (often called active ingredients, AIs) relies on three components: colloid mobilisation and transport through the soil phase, selective adhesion to roots systems for targeted release or protective root coatings and encapsulation of the AI to provide delivery to the target. Many factors need to be considered in order to approach solve

these three components and firstly a more detailed discussion on plants and soil subsystems is presented.

1.2.1. Plant structure

Plants are split into two zones, the shoot system and the root system (or rhizosphere when the soil surrounding the roots is factored). Plant structure is shown in **Figure 1.1-A.**).[1-4] Targeted delivery requires special attention to be made to the roots system which is where an active ingredient will be taken up.

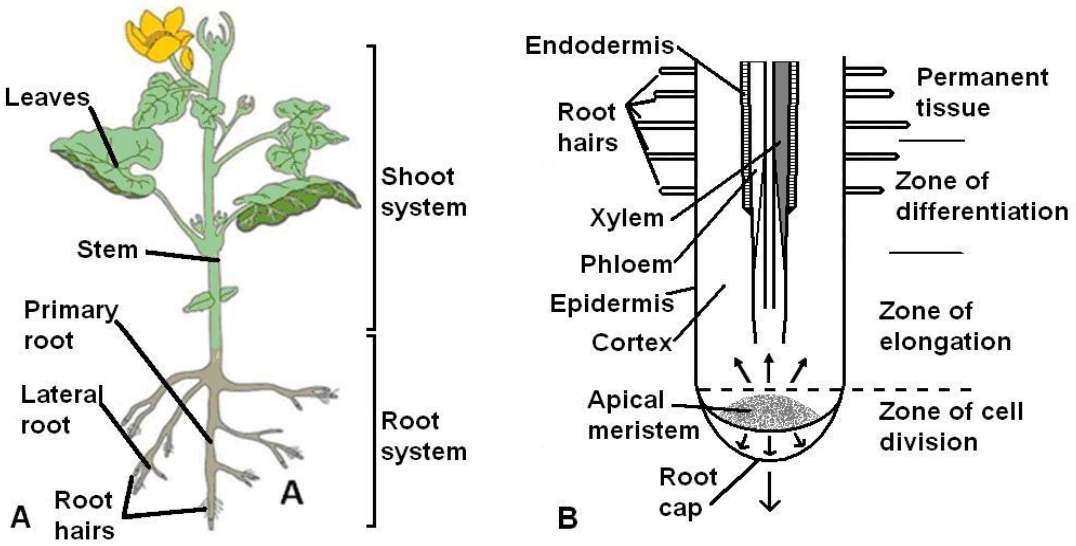

Figure 1.1. Image showing A) the highlighted structure of a plant and root system for a typical plant, B) the highlighted sections of a root [A) reproduced from reference 1 with some modifications, B) was reproduced from reference 2].

1.2.2. Root structure

The roots of plants typically serve three main functions. Anchorage of the plant, storage of photosynthesis products i.e. glucose, and uptake of water and nutrients from the soil.[4] The primary root is typically split into a number of different sections (see **Figure 1.1-B.**).[1-5] At the very tip is the root cap or meristem. This rigid cellular structure pushes the primary root through the soil allowing the roots to grow deeper.

The zone of elongation is where new cells are produced providing the root with an increasing length by pushing the root cap further into the soil. Lastly is the zone of differentiation or zone of maturation. This is the most interesting zone for targeted delivery as this region contains the root hairs of the plant. The root hairs are responsible for the uptake of water and nutrients to the plant and therefore influence the pathway that capsules or particles would take through the soil. The root hairs contain a very large surface area that increases the effectiveness for water uptake by absorption. The growth of maize plants (studied by our sponsor) was studied by both Kramer and Boyer[5] and Varner and Canny,[6] and they reported that root hairs have the highest density and greatest length at 30-60 cm from the root tip. Root surfaces are composed of complex carbohydrates such as cellulose, hemicelluloses and pectin and therefore contain many carbonyl and hydroxyl surface groups. Cellulose is a polysaccharide consisting of repeating units of β-(1-4)-*D*-glucose (structure of cellulose is shown in **Figure 1.2.**)[7].

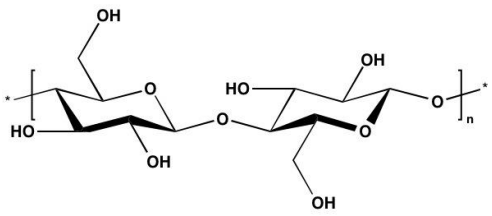

Figure 1.2. Structure of cellulose.

Hemicellulose is a mixture of xyloglucans, xilans, mannans and glucomannans and pectin consists of nearly 60% homogalacturonan (structures are reported in reference 7). The anionic nature of the surface of roots means that cationic particles will bind very strongly to cell walls due to electrostatic interactions. Schaffner *et al* reported the adhesion of cationic particles to cellulose and showed that anionic latex particles surrounded by cationic surfactants can adhere to cellulose due to charge reversal (charge reversal is shown in **Figure 1.3.**).[8] Charge reversals can also occur from adsorption of

cations in the soil. Cellulose has also been shown to bind or complex with alkali metals and heavy metal complexes as reported by Öztürk *et al*.[9]

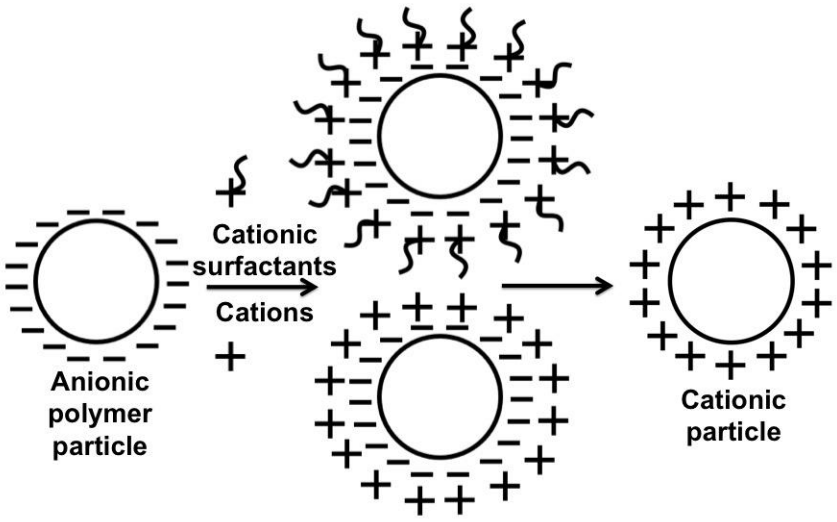

Figure 1.3. Charge reversal of anionic colloids by adsorption of cationic surfactants or cations.

1.2.3. Soil composition

Transport of colloids or capsules to the roots requires mobility through the porous soil medium Understanding what adheres or sticks to soil is vital in order to make colloids mobile. Soil composition is typically 25% air, 25% water, 5% organic matter and 45% minerals.[10] Composition will alter depending on the exact location and soil type e.g. loams or clay soil. The mineral compounds typically consist of silicates including sand, silt, and clay and the dimensions of these are 2-0.05 mm, 0.05-0.002 mm and <0.002 mm respectively.[10] Clays are also found as alumino-silicates e.g. kaolinite, mica, illite where the surface contains both oxygen and hydroxyl groups (similar to the root hair composition). Silica can exist with both anionic or cationic charges depending on soil acidity and surface heterogeneities as reported by Ryan and Elimelech.[11] The silica colloids in soil are often termed collector sites and are one of the main sources of adhesion for colloidal particles depending on the collector and particle

roughness as well as the surface charge of the particles and collector sites. The other source of adhesion is the air-water interface (AWI's) as discussed in **Section 1.2.4.2.** Many electrolytes are present in soil such as metal ions and organic matter e.g. humic substances including humic acids and fulvic acids (structure of a typical humic acid reported by Stevenson is shown in **Figure 1.4.**).[12] Pesticides have been reported to bind with humic acids[13-14] and these acids control the ionic strength and pH of the soil. The electrolytes can have a drastic influence on the double layer forces of the colloidal particles. Electrolytes can also adhere to the surface of particles as reported by McCarthy *et al* and Pelley *et al* which can provide additional steric and charge stabilisation.[14-15] The valence number of metals in the soil can severely influence the double layer forces around particles and a greater valency leads to greater double layer compression thereby influencing the stability of colloids towards aggregation (this is shown in **Figure 1.5.**).[16] This is related to the critical coagulation concentration (ccc) as expressed by the Schulze-Hardy rule which states that the ccc is related to the inverse sixth power law of counter ion charge e.g. the ccc ratio for metal valency 1:2:3 is 1000:16:1.3 (as predicted by the DLVO theory discussed in **Section 1.4.1.**).[17-18] So a thousand times more concentration of Na^{+} would be needed to compress a double layer the same amount as Ag^{3+}.

1.2.4. Colloid mobility through soil or porous media

Reporting mobility of colloids through porous media is extensively difficult due to the variability in natural conditions. Such conditions include pH of the water (affects colloid aggregation), surface roughness of particles and collector sites, soil porosity and pore size distribution (discussed in **Section 1.4.2.3.**) and the water content or influence of AWI's.

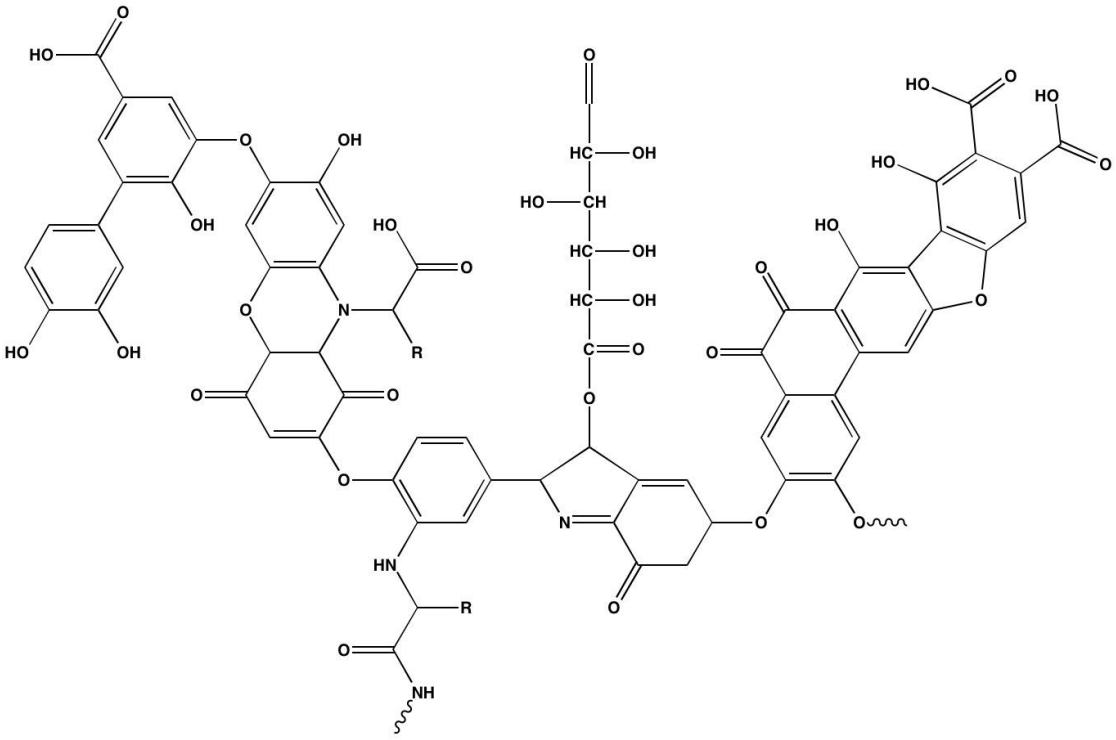

Figure 1.4. Structure of a typical humic acid [reported by Stevenson from reference 12].

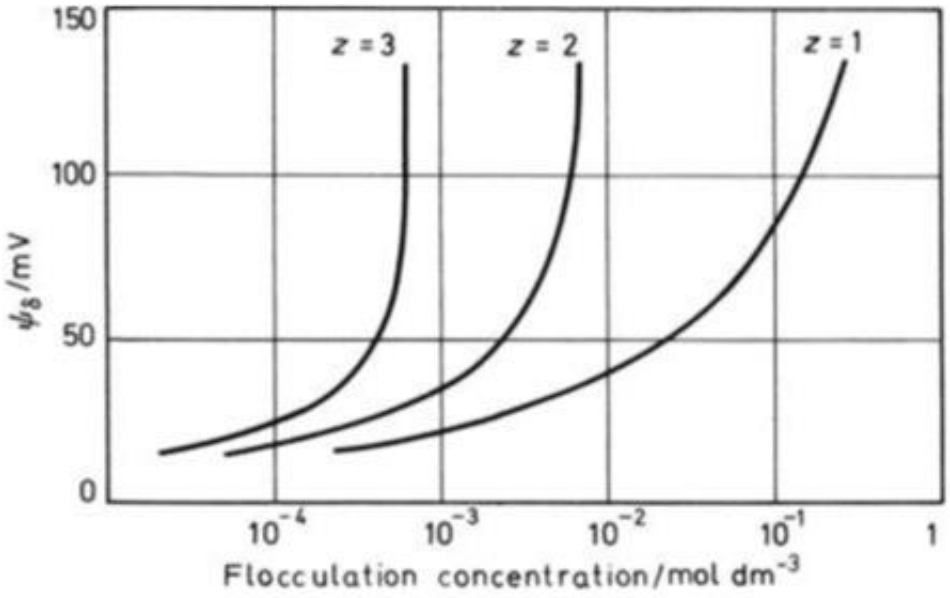

Figure 1.5. Graph showing the critical coagulation concentration for different Stern potentials using different valency counterions, z. Curves shown using values of A = 10^{-19} J, $\varepsilon/\varepsilon_o$ = 78.5 and T = 298 K [Reproduced from Shaw from reference 16].

Most model systems for studying particle mobility are carried out using idealised planar and curved surfaces as model collector sites and particles respectively. In nature surface heterogeneities exist on collector sites and therefore the adhesion or

repulsion of particles will be more complex. Reviews by both Ryan and Elimelech[11] and Sen and Khilar[19] have discussed the mobility of naturally occurring colloids through soil and discussed the methods to cause mobilisation. Mobilisation is affected by ionic strength and shear forces, adhesion and double layer forces (based on the DLVO theory), entrapment and straining of particles in pores by size exclusion, multi-particle bridging and surface deposition and the adhesion of organic mater to colloids (such as humic acid adhesion to particles). Ryan and Elimelech also discussed the different results between both experimental work and theoretical work.

1.2.4.1. Colloidal surface charge

Many authors have studied the mobility of synthetic latex particles through soil systems as well as model soil systems where typically the soil is represented by glass, silica or quartz beads of different diameters.

Studies by Grolimund *et al*, Bradford *et al* and Mishurov *et al* have shown that anionic carboxylate particles possess soil mobility.[11,20-24] Bradford *et al* discussed that colloid retention of hydrophobic carboxyl particles by straining is important when larger particle sizes (> 3 μm) and smaller soil grain sizes.[21] McDowell-Boyer *et al* and Pelley *et al* reported the mobility of anionic sulphate particles through soil.[25,15] Pelley *et al* reported that of 3 different particle sizes (50, 110 and 1500 nm) the attachment efficiency with quartz sand increased with particle size due to an increased secondary energy well.[15] However, cationic amine and amidine colloids have been reported to bind with the silicates or anionic collector sites present in the soil (when the silica is anionic) as reported by Grolimund *et al* and Elimelech *et al.*[20,26] The cause of the adhesion of cationic particles is coulombic attraction to anionic surfaces and the presence of attractive double layers.[20,26-27] Elimelech *et al* reported that at low ionic strength the

adhesion was far greater than at high ionic strength due to the thickness of the double layers.[26-27] Typically anionic particles show greater soil mobility in saturated water conditions where anionic colloids and soil both provide repulsive forces. The adhesion for anionic particles in soil is usually dependant on either size dependency (straining) or from the adhesion to an air-water interface.

1.2.4.2. The air-water Interface presence in soils

The presence of air in soil can have drastic influences on the mobility of particles through soil. Typically three scenarios exist which depend on the relative amount of air present: saturated, semi-saturated or unsaturated. These terms represent damp soil due to heavy rain, semi damp soil due to moderate rain with regions of drying and dry soil. The presence of air in soil systems leads to the formation of an AWI. DeNovio published an article reviewing the deposition and mobilisation of colloids under unsaturated soil conditions (deposition mechanisms are shown in **Figure 1.6.**).[28] Studies by Wan and Wilson,[29] Sharma *et al*,[30] Crist *et al*[31] and Sirivithayapakorn *et al*[32] have all shown that great attractive force drive particles to adhere to the AWI's reducing the release rates of colloids. Wan and Wilson reported that adhesion to an AWI can be considered irreversible due to strong capillary forces as well as non DLVO theory forces i.e. hydrophobic attraction and can be only be removed using high shearing forces.[29] This concept was further proved using modelling of particle adhesion to AWI's reported by Corapcioglu and Choi.[33] Adhesion of colloids to the AWI is dependent on the surface forces as discussed by Israelachvili.[34] These forces include van der Waals, electrostatic and solvation forces (discussed in **Section 1.4.**). The adhesion of colloids to an AWI is comparable to the theory of Pickering stabilisation only in this case the adhesion is between particles and air-water interface rather than a water-oil interface.

The colloidal particles will preferentially absorb onto the interface to reduce the total free energy of the system.

Sharma *et al* reported that moving AWI's can detach particles from collector sites (or surfaces), a moving liquid-gas interface was passed over a glass surface deposited with latex particles where the colloids preferentially adhered to the AWI.[30] Sharma *et al* also studied the effects of both surface charge and hydrophobicity on the adhesion to the AWI or removal from a collector surface. They reported that hydrophobic amidine and sulphate colloids adhered to the AWI 10 times more strongly than hydrophilic carboxylate and amino colloids. This adhesion effect was due to long-range hydrophobic interactions and this was in agreement with the results shown by Wan and Wilson.[29] However, the detachment of hydrophobic colloids showed little dependence on surface charge due to strong hydrophobic attractions whereas hydrophilic colloids (anionic carboxylate) were detached from the surface more efficiently than cationic (amino) particles. Their results were in agreement with the calculated DLVO theory calculations. Sharma *et al* and Dai *et al* also reported that slower AWI velocities allowed more particles to detach from solid surfaces and onto the AWI's.[30,35] Crist *et al*[31] and Wan and Tokunaga[36] reported that anionic colloids will not adhere to AWI's but cationic colloids do stick.

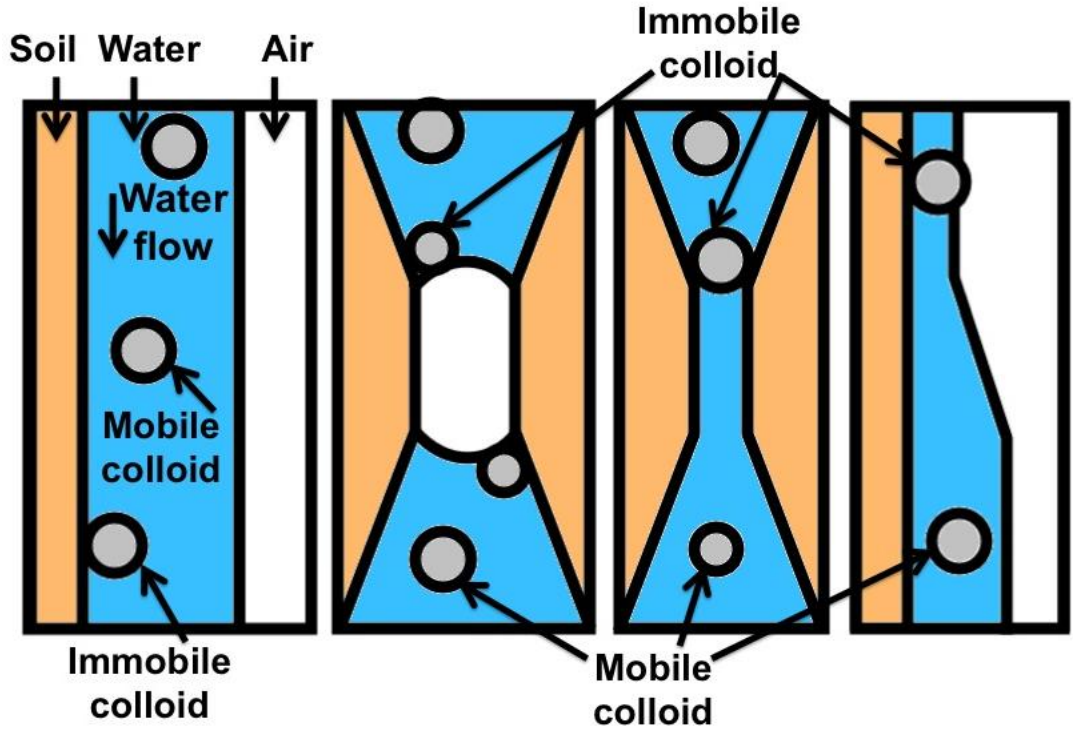

Figure 1.6. Four methods of colloid deposition. From left to right, attachment of particles to soil collector sites, attachment of particles to the air-water interface, straining of particles in narrow pores and attachment *via* film straining [Reproduced and adapted from DeNovio reference 28].

The adhesion of colloids to AWI's can allow the colloids to move with the infiltration front as reported by Sharma *et al* and Sirivithayapakorn *et al*.[30,32] Sirivithayapakorn *et al* reported that once the AWI dissolves that the colloidal latex particles cluster together and will move through the soil as aggregated clusters (shown in **Figure 1.7.**).[32] Crist *et al*[31] and Sirivithayapakorn *et al*[32] both reported that these colloidal clusters can block pores or adhere to collector sites and AWI's further down in the soil (**Figure 1.7.**). Hydrophobic colloids adhered to an AWI or collector site often cause further adhesion of subsequent hydrophobic colloids thus increasing the colloid retention. Mishurov *et al* reported that colloids of 0.02 μm adhere more strongly to an AWI than larger 0.2 μm and 1 μm colloids due to the increased surface area,[24] this effect was also reported by Zhuang *et al* for the adhesion of amphiphilic colloids.[37]

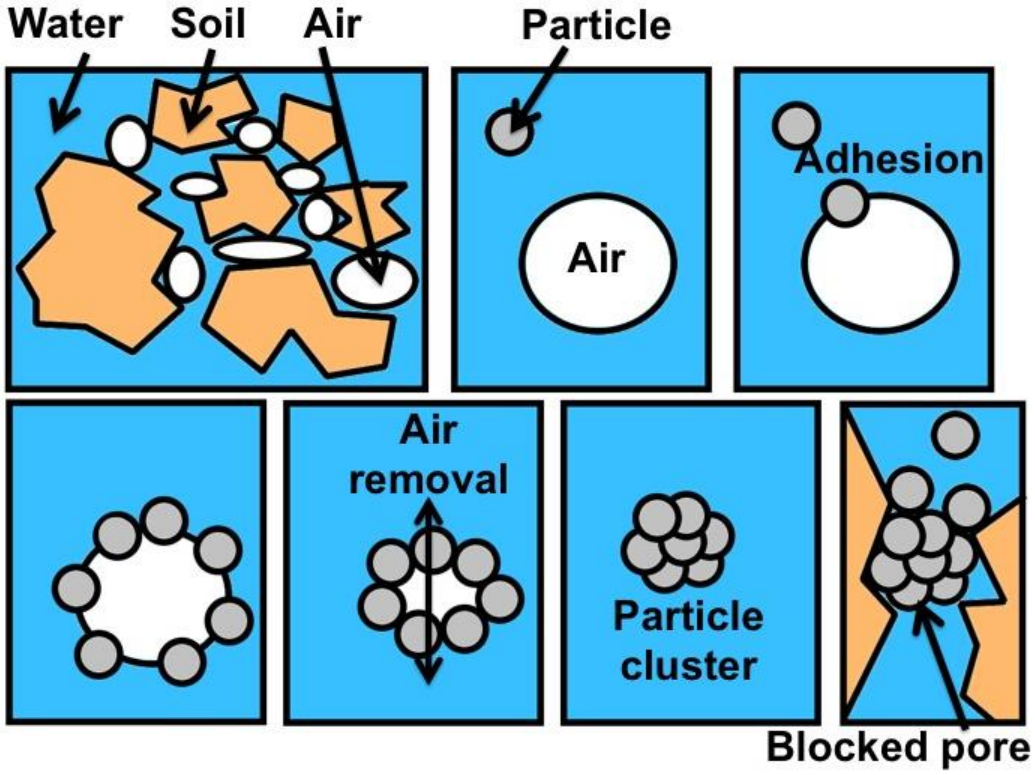

Figure 1.7. Representation of the adhesion of particles to an air-water interface followed by the dissolution of the air. The clusters formed can block pores throughout the soil.

1.2.4.3. Size of colloidal particles and soil porosity

Studies by Bradford *et al* reported that large 3 µm anionic carboxylate colloids passing through a glass bead and sand column are retained to a greater degree than smaller 0.45-1 µm colloids.[21-23] This retention difference is caused by smaller colloids passing through the pores thus causing colloid attachment to be the more important mechanism for retention.[21-23] Studies by Harvey *et al* have shown that colloids of approximately 1 µm were 1.25 times more mobile that particles smaller in size.[38] This is related to the pore size distribution of the soil where small colloids pass through to the groundwater and large colloids can become blocked in pores (straining). Large particles can also "cake" above the porous media restricting the ability of other colloids to be transported as reported by Ouyang *et al* and Torkzaban *et al*.[39-40] This mobility based on size heavily depends on many factors that cannot always be controlled. Large tunnels

caused by worms can lead to very fast throughput of colloids.[40] The porosity and pore sizes are controlled by the soil type and whether the soil is course or fine textured will have a large effect on which particle sizes can become entrapped.[40] However, in opposition to this theory Elimelech and O'Melia showed that particle size has less effect on their mobility.[41-42] Pelley *et al* reported that a larger retention was observed for 1.5 µm sulphate particles when compared to smaller 0.5 µm colloids.[15] DeNovio *et al* also reviewed the transport of colloid sized particles and the relationship with the soil structure.[28] Mishurov *et al*,[24] Zhuang *et al*[37] and Zvikelsky *et al*[43] all reported that ~200 nm anionic colloids colloids were the most mobile in an anionic column.

1.2.5. Water absorption by plant roots

As we discussed earlier the bulk of water in plant systems is taken up by the root hairs.[1-5] Water is absorbed by the osmotic pressure difference between the roots and the soil. A model by Roose *et al* studied the hydraulic pressure gradients between the inside of the roots and between the roots and soil to determine how the root length and diameters affect the water uptake.[44] They reported that greater numbers of roots absorb more water and thicker roots have a greater hydraulic pressure.[44] Roose *et al* also discussed that due to the uptake of water into the plant system, many areas of the soil remain dry which can severely affect the mobility of colloids by absorption to AWI's. This model was applied to primary and secondary root systems but the possibility of scaling up to provide water profiles more progressed root systems does exist. Due to this driving force for absorbing water being able to tailor particles or capsules to pass through the soil to the section of water absorption maxima would allow them to be pulled towards the roots system.

1.2.6. Delivery of pesticides to plants

As well as finding a solution for moving colloids through soil followed by adhesion to root hairs We are also interested in encapsulating a solid AI compound called abamectin (Agri-Mek, Avid and Zephyr are trade names) which is a mixture of 80% avermectin B_{1a} and 20% avermectin B_{1b} (avermectin is a 16 membered macrocyclic lactone as shown in **Figure 1.8.**).[45-46]

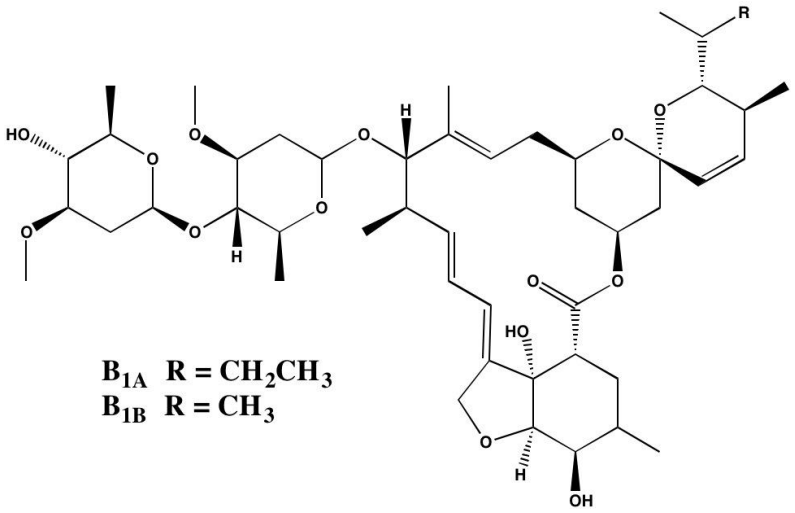

Figure 1.8. Stucture of avermectin B_{1a} and B_{1b}.

Abamectin is used to target mites and insects which can cause damage to crops. Abamectin is solid and immobile in soil and therefore is dissolved in a solvent called solvesso 200ND.[47] Solvesso 200ND is purchased from ExxonMobil and comprises of a mixture of heavy aromatic hydrocarbons (C_9-C_{13}, also called heavy aromatic naphtha solvent) and <1% naphthalene. Examples of the main chemicals found in solvesso 200ND are shown in **Figure 1.9.**.[48] Due to the toxicity toward aquatic organisms solvesso needs to be encapsulated into a capsule or carrier particle to reduce or prevent leeching into the groundwater. However, thermodynamics will typically cause release of the solvent from capsules due to the relative volatility of solvesso and permeability of capsule walls. Release of oil from capsules is typically prevented by a less porous wall

structure as well as greater wall thickness and this maintains the internal pressure of the liquid droplets (further discussed in **Chapter 4**). This internal Laplace pressure increases as the dimensions of capsule decrease (Laplace pressure measures the pressure difference between internal and external mediums). A capsule wall with low porosity reduces the amount of solvent that will be lost *via* diffusion. Typically the oil is encapsulated using interfacial polymerization techniques such as poly(urethane) and poly(urea) combined with the solvent evaporation technique (references and discussion located in **Chapter 4**).

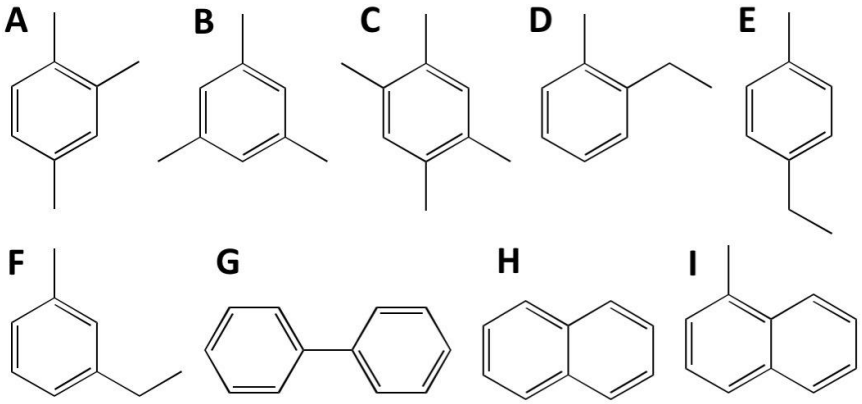

Figure 1.9. Structures of the major composition of solvesso 200ND, A) 1,2,4-tri-methyl benzene, B) 1,3,5- tri-methyl benzene, C) 1,2,4,5-tetra-methyl benzene, D) 1,2-ethyl toluene, E) 1,4-ethyl toluene, F) 1,3-ethyl toluene, G) biphenyl, H) naphthalene, I) 1-methyl naphthalene.[48]

1.3. Synthesis of colloidal particles

1.3.1. Lyophobic colloids

Fitch described a colloid as "a dispersion of fine particles suspended in a fluid medium".[49] Colloidal particles are typically in the order of 1-1000 nm in diameter. Colloidal particles can be either lyophilic or lyophobic depending on whether the interaction with the solvent is thermodynamically favourable or not. Lyophilic colloids form spontaneously and are thermodynamically stable whereas lyophobic colloids are

thermodynamically unstable and seek to aggregate to the lower surface area. Lyophobic colloids are "solvent hating" and aggregation (or flocculation) of the colloids will occur unless sufficient repulsive forces exist to maintain colloidal stability (Colloid stabilisation discussed in **Section 1.4.**). Typically lyophobic polymer colloids are synthesised using heterogeneous polymerisation techniques including emulsion, mini-emulsion, suspension, precipitation and dispersion polymerisation. Arshady analysed these techniques and their differences (excluding mini-emulsion) and discussed the particle sizes (shown in **Figure 1.10.**) from using either droplet nucleation techniques or nucleation and growth techniques.[50] Mini-emulsion polymerisation is reviewed in "*Colloids and Colloid Assemblies*" by Caruso.[51] Suspension, emulsion and precipitation polymerisation are discussed in "*Polymer Science and Technology*" by Ebewele.[52] Each book review provides an overview on the mechanism for particle formation and many examples of their industrial uses and applications. Due to the size range of our aims we are primarily interested in emulsion polymerisation and more specifically soap-free emulsion polymerisation.

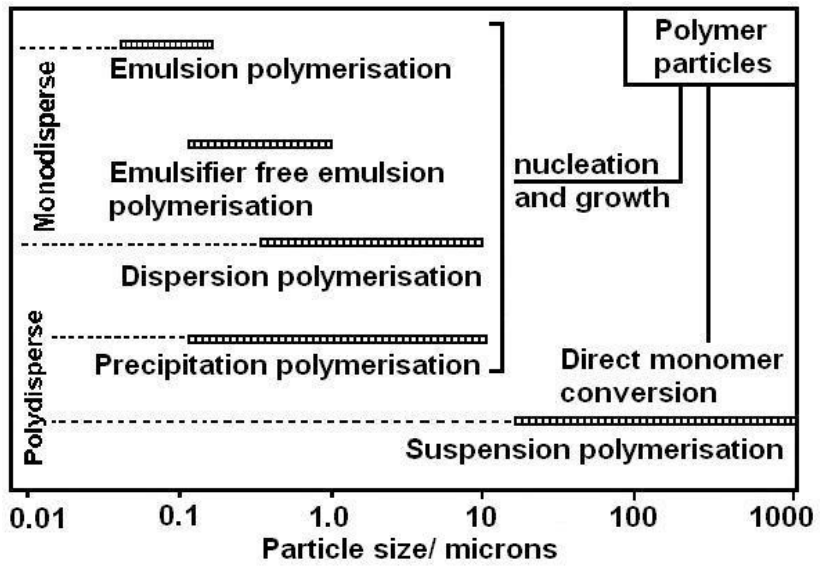

Figure 1.10. Colloidal particle sizes from both droplet nucleation and monomer conversion heterogeneous techniques [Reproduced from reference 50].

1.3.2. Emulsion polymerisation

Multiple authors have studied emulsion polymerisation since it was first used during World War 2 in the 1940s, but more recently Fitch provided an in-depth review on emulsion polymerisation in the book "*Polymer Colloids*".[49] Chern has also reviewed emulsion polymerisation in papers and a book called "*Principles and Applications of Emulsion Polymerisation*".[53-54] These books discuss emulsion polymerisation including theories and mechanisms for particle nucleation, particle growth, kinetics and potential applications of the technique. Emulsion polymerisation typically consists of three stages as reported in the 1940s by Harkins[55-56] and Smith and Ewart.[57] Stage 1. The number of particles increases and rate increases until all surfactant is adsorbed onto particles (2-15% conversion). Stage 2. Particle number and polymerisation rate remain constant, Stage 3. All monomer droplets in the continuous phase have been consumed and monomer is only present inside particles ([M] decreases and therefore the rate decreases). This theory is applicable for monomers with low water solubility and the presence of micelles where the presence of micelles causes particle formation to occur *via* micellar nucleation.[49,53-57] However, there is a greater interest for soap-free emulsion polymerisation to reduce the effects of surfactants in colloid synthesis. Surfactants are difficult to remove from the surface of particles and when the surfactant is removed often a decrease in colloidal stability occurs.

1.3.3. Soap-free emulsion polymerisation

1.3.3.1. Primary Particle formation

Homogeneous nucleation of polymer particles was proposed by Priest,[58] Roe,[59] Fitch and Tsai[49] and later adapted by Hansen and Ugelstad.[60-61] They discussed primary

particle formation occurring by the collapse and precipitation of surface active oligoradicals when a critical chain length is reached (j_{cr}). The primary particle contains an initiator fragment at the surface that is a polar hydrophilic group (dependant on the choice of initiator e.g. sulphate, peroxides, azo). Initiation and polymerisation is demonstrated for styrene using initiator potassium persulphate in **Figure 1.11-A** and **Figure 1.11-B** respectively where the primary particles grow by a combination of polymerisation and coagulative nucleation mechanisms (discussed in **Section 1.3.3.2.** and shown in **Figure 1.11-C** to **Figure 1.11-E.**).

1.3.3.2. Colloidal surface charge

Without the presence of micelles to provide colloidal stability (through electrostatic and steric stabilisation) primary particles produced using homogeneous nucleation require sufficient repulsive forces to be colloidally stable. Surface charge and therefore stability is gained by either adsorption of oligoradicals onto the particle surface (**Figure 1.11-D**) or by coagulative nucleation as reported by Lichti *et al*[62] and Feeney *et al* (**Figure 1.11-E.**).[63-64] Coagulative nucleation is where two primary particles coagulate into one particle with higher surface charge (the particle remains spherical due to the interfacial tension reducing the overall surface area) as shown in **Figure 1.11-E**. The shape of the particles produced *via* coagulative nucleation is affected by the addition of crosslinkers that can inhibit the ability to morph into spherical shaped particles. When coagulative nucleation occurs in soap-free emulsion polymerisation there are no micelles for nucleation to occur in so nucleation occurs in the aqueous phase. Micelles absorb different amounts of monomer and give broader dispersities whereas soap-free emulsion polymerisation generates low dispersities unless high amounts of water-soluble comonomers are added (discussed in more detail for the

polymerisation of styrene with sodium 4-vinylbenzenesulphonate in **Section 2.2.2.1.** in **Chapter 2**).

Generally particles produced *via* soap-free emulsion polymerisation can be tailored by a range of factors[49,53] These factors include the initiator type (cationic, anionic and neutral surface groups), initiator concentration (number of surface functional groups and number of particles), the monomer (hydrophobicity and glass transition temperature, T_g), reaction temperature (rate) and the addition of comonomers (additional surface charges or steric stabilisation and particle size).

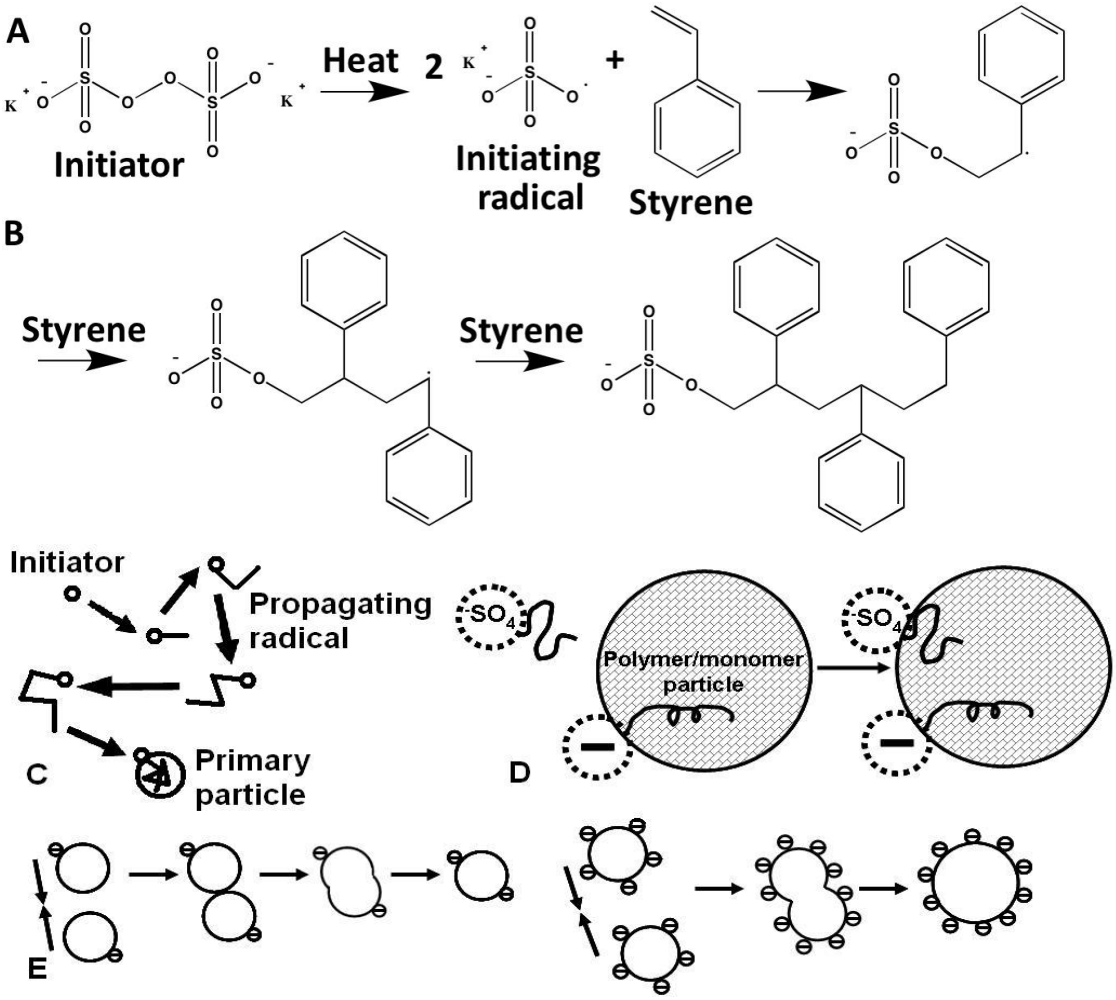

Figure 1.11. Scheme demonstrating the initiation and polymerisation of styrene using potassium persulphate initiator. A) Initiation of potassium persulphate and addition of one monomer unit, B) propagation of the initiating radical using more styrene, C) formation of a primary particle from propagating radial, D) adsorption of surface oligoradicals onto a polymer particle, E) coagulative stabilisation of surface charge [Figures C-E are reproduced and adapted from reference 49].

1.4. Colloid stabilisation

Typically the stabilisation of colloids is discussed by three main interactions: DLVO theory interactions (van der Waals and electrostatic double layer forces), the non DLVO theory interactions (hydration and hydrophobic forces) and steric interactions. Numerous book reviews provide in-depth theoretical background for these stabilisation mechanisms with specific references detailing their uses.[17,52,53,65-66]

1.4.1. DLVO theory interactions

The total interfacial interaction energy between particle-particle and particle-collector is generally calculated using the "DLVO" theory. DLVO theory studies the balance between the van der Walls interactions and electrostatic double layer repulsion.

1.4.1.1. Van der Waals interactions

Van der Waals interactions are the interactions of all atoms in a body and can be present between atoms, molecules and various surfaces with different geometries.[67] Van der Waals interactions can be attractive or repulsive depending on the specific medium which is related to the dielectric constant (as discussed by both Hamaker[68] and Derjaguin[69-70]). Van der Waals interactions are the sum of the Keesom (orientation), Debye (induction) and the London (dispersion) forces as caused by the interaction between two permanent dipoles, permanent and induced dipoles and two instantaneously induced dipoles respectively. The interaction energies between atoms and molecules vary to the power r^{-6}. Hamaker developed further extension of the theory of Van der Waals-London dispersion interactions for macroscopic objects[68] including sphere-sphere and sphere-wall interactions. Hamaker showed that additive collection of

each dispersion forces leads to longer range interactions than shown previously by London where the interaction energies scale to the power –A/6D (-Ar/12x) for sphere-sphere interactions. The model proposed by Hamaker has also been applied to other geometries of interacting objects. Israelachvilis' book "*Intermolecular and Surface Forces*" provides an overview of the equations for calculating the van der Waals interaction force for a multitude of different surfaces such as sphere-sphere, sphere-flat, flat-flat etc.[34] The pair potential for a typical van der Waals interaction is shown later in **Figure 1.13.,** in **Section 1.4.1.3.**.

1.4.1.2. Electric double layer interactions

For soap-free emulsion polymerisation we discussed that particle formation *via* homogeneous nucleation, adsorption of polyelectrolytes and coagulative nucleation leads to charged surface groups. Due to the requirement for electroneutrality a bound layer of adsorbed ions of opposite charge will absorb to the particle surface. The bound layer of ions was first studied first by Helmholtz who modelled the electric double layer mathematically as a simple capacitor.[49] The theory of the diffuse layer of ions was first studied in 1910 by Gouy[71] and later in 1913 by Chapman[72]. They reported that the electric potential decreases exponentially as a function of distance from the surface and introduced a "diffuse layer" of ions that are not physically adsorbed to the surface and can move freely. Later Stern (1924) combined the two theories of Helmholtz and Gouy-Chapman and added the "Stern layer" (depicted in **Figure 1.12.)** which is located a hydrated ion radius from the particle surface.[73] This double layer model proposed by Stern was later reviewed by Grahame who introduced the outer and inner Helmholtz planes.[74] The inner Helmholtz plane is where dehydrated surface ions are located and the outer Helmholtz plane is the same as the Stern plane.[74] Lyklema[75] and Van der

Hoeven *et al*[76] studied the applicability of electric double layer repulsion for colloidal particles in non-aqueous media. They reported that low polarity solvents increase the Debye length thus reducing the electrostatic repulsive forces and stability. A typical electric double layer pair potential is shown in **Figure 1.13.** in **Section 1.4.1.3.**.

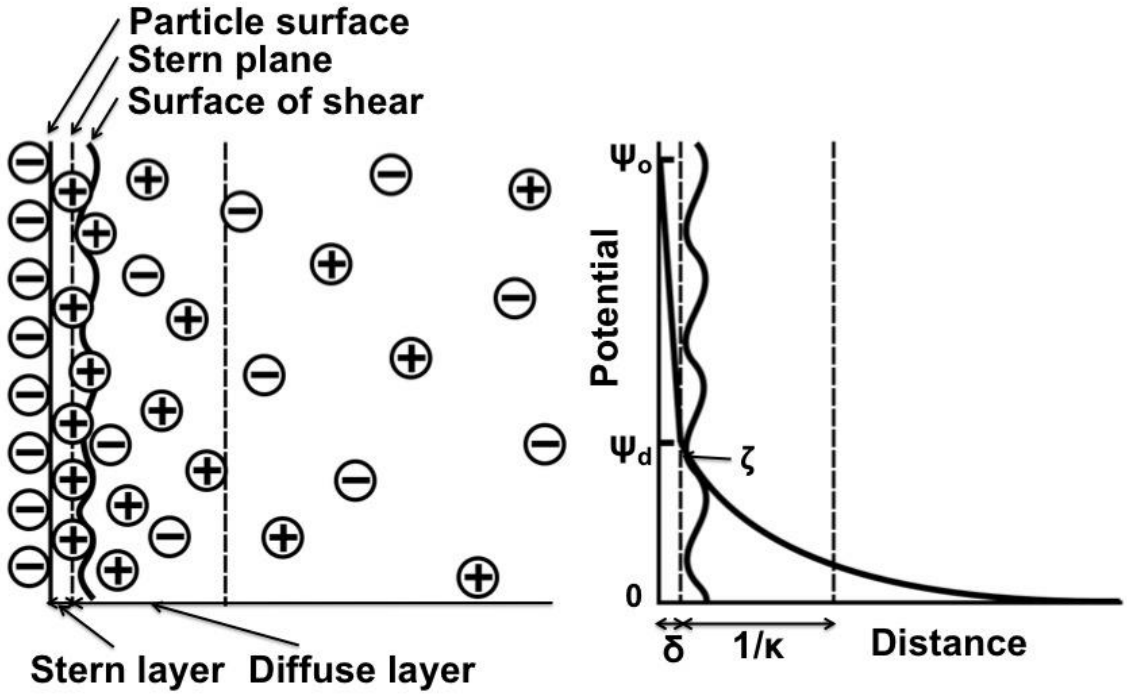

Figure 1.12. Schematic of the double layer for a negatively charged surface according to Stern's theory [Reproduced from reference 16].

1.4.1.3. Attractive and repulsive interactions – DLVO theory

These longer range van der Waals forces introduced by Hamaker and de Boer,[68,77] led to further work by Derjaguin,[69-70] Derjaguin and Landau,[78] and independently by Verwey and Overbeek[79-80] (hence "DLVO").[17,49,53,65-66,80-81] The particles experience electrostatic repulsion at longer distances than they experience attractive forces which gives rise to a repulsive energy barrier (V_{max}, shown in **Figure 1.13.**). The summation of both attractive and repulsive interactions leads to a total interaction energy, V_T, pair potential between two particles as a function of distance, H (a schematic is shown in **Figure 1.13.**). Typically this interaction energy potential

differs for each system where can be repulsive barrier height, primary minimum depth and the presence of a secondary minimum. The repulsive barrier height is affected by surface charge concentration, salt concentration, valency of salt and temperature. The primary minimum depth is assumed irreversible and is when the system coagulates and the existence of a secondary minimum is where flocculation occurs. Not all systems show the presence of a secondary minimum. Overbeek reported the assumption that an energy barrier of kT ≥10 is enough to prevent collisions[82] and lower repulsive energy barriers can cause both slow and fast coagulation depending on the relative height. Finally at very small interparticle distances (<10 nm) a strong repulsive force called Born repulsion is experienced caused from electron cloud overlap between aggregated particles.

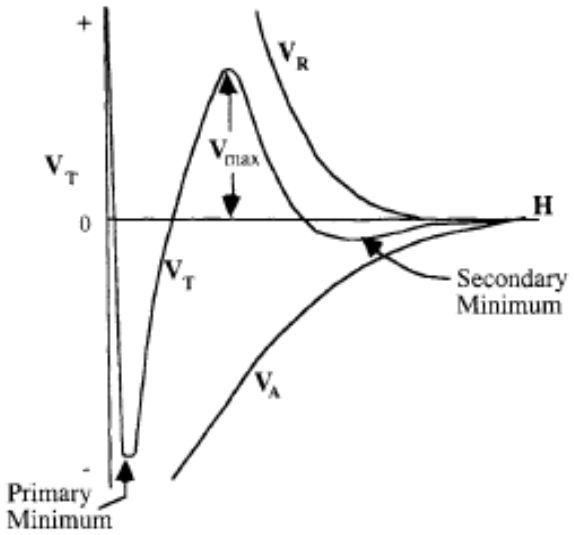

Figure 1.13. Representing the total interaction free energy, V_T, between two charged spheres as a function of separation distance, H. V_T is the addition of both repulsive (V_R) and attractive (V_A) pair potentials [Reproduced from reference 49].

In order to maintain colloidal stability a sufficiently large repulsive energy barrier is required. We discussed earlier that ion valency controls the ccc value for coagulation of the system and the repulsive energy barrier is heavily dependant on the ionic strength, I, of the media due the changes in the Debye length, 1/κ (the thickness of

the double layer). Israelachvili proposed a simplified equation for 1:1, 2:1/1:2 and 2:2 electrolytes at 25 ºC (**Equations 1.1.**) where the energy barrier depends on the inverse square root of I.[34] The Debye length decrease from 30.4 nm to 0.96 nm changing from a $1x10^{-4}$ M to $1x10^{-1}$ M NaCl solution and decreases in Debye length often lead to coagulation of the system. An example of the interaction energy of separation between two charged particles as a function of electrolyte strength[81] is shown in **Figure 1.14.**.

$$\boldsymbol{\kappa^{-1}} = \left(\frac{\boldsymbol{\varepsilon_o \varepsilon k T}}{\boldsymbol{2\rho_\infty e^2}}\right)^{\frac{1}{2}} \text{ and for } e = 1 \text{ (monovalent ion) } \kappa^{-1} = 0.304\times10^{-9}/\sqrt{M}\ m$$

$$\kappa^{-1} = \begin{cases} 0.304/\sqrt{[NaCl]} & nm \quad \text{for 1:1 electrolytes} \\ 0.176/\sqrt{[MgCl_2]} & nm \quad \text{for 2:1 or 1:2 electrolytes} \\ 0.152/\sqrt{[MgSO_4]} & nm \quad \text{for 2:2 electrolytes} \end{cases} \qquad \textbf{Equation 1.1.}$$

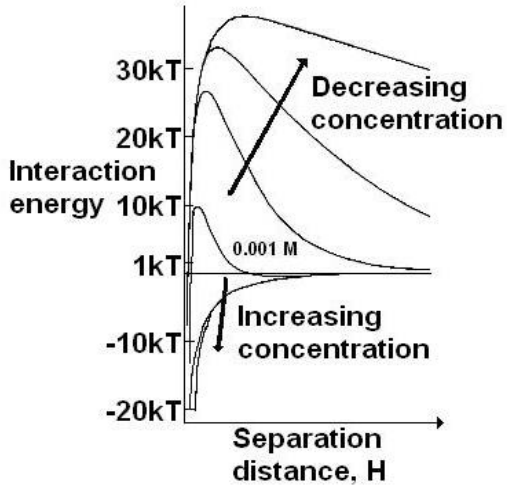

Figure 1.14. Interaction energy pair potential between two charged spheres as a function of separation distance, H. The interaction energy profiles are analysed as a function of the ionic concentration (shown for a 1:1 electrolyte with 10kT being 0.001 M electrolyte) [Reproduced, and adapted, from reference 81].

1.4.2. Non DLVO interactions

Two forces not covered by the DLVO theory are the hydration force and the hydrophobic interaction.[65-66] The hydration force is caused by two polar surfaces separated by a thin film of water and is repulsive and the hydrophobic interaction is an

attractive force caused from entropic rearrangement of water molecules surrounding colloidal particles. The increased entropy caused by water-water interactions (hydrogen bonding) forces the hydrophobic colloids together or even with other phases as discussed earlier with hydrophobic colloids adhering more strongly to collector surfaces and AWI's.

1.4.3.Steric stabilisation

Steric stabilisation is caused from the absorption of polymers onto the particle surface. The polymers need an affinity for the particle surface as well as being sufficiently hydrophilic to extend into the aqueous phase (or continuous phase for different solvents). As particles come closer together the polymer chains compress and inter-penetrate causing a higher concentration of stabiliser chains between particles. Repulsion occurs due to entropic osmotic pressure forcing water molecules between the two particles.

1.5. Outlook and objectives of the thesis

The overall aim of the sponsor was the fabrication of colloidal carrier particles with good soil mobility and root adhesion. The mobility of particles through soil is mainly controlled by particle surface charges, hydrophobicity and environmental factors (less controllable). Adhesion is mainly affected by both surface area (heterogeneities) and the surface charge of the particles and surfaces. Delivery and encapsulation is heavily dependant on the application and whether controlled release (fast or slow) or burst release is required where a rigid wall is required to prevent release being too rapid. A series of aims to try and overcome all of these issue have been formulated.

1. To synthesise polymer particles using soap-free emulsion polymerisation to generate a high surface number of anionic surface groups within the size range 200-1000 nm. For this aim we chose the sulphonate group as the anionic charge and poly(styrene) as the polymer colloid.

2. To utilise soap-free emulsion polymerisation to decorate colloidal seed particles using a range of different hydrophobicities in order to increase the surface area and roughness. We also would like to easily incorporate post surface charge using thiol-Michael addition chemistry to incorporate different functional groups and charges to the decorated surface.

3. To study the encapsulation of a naphthalene based aromatic oil, solvesso 200ND, using interfacial thiol-Michael addition chemistry for capsule formation. To study the capsule sizes and size distributions using both microfluidic methods as well as high shear techniques.

1.5.1. A brief overview of each chapter

Chapter 2 discusses use of sodium vinylbenzenesulphonate in the soap-free emulsion copolymerisations with styrene to synthesise sulphonated colloidal nanoparticles. We report the limitations of the previous methods for the sulphonation of colloids. We designed protected sulphonate particles by the copolymerisation of neopentyl 4-vinylbenzenesulphonate and ethyl 4-vinylbenzenesulphonate with styrene to synthesise colloids under 200 nm with hidden sulphonate groups. Following particle synthesis we discuss the deprotection or hydrolysis of the ethyl protecting groups using high temperature heat (>200^{o}C) where the effects on the particles are studied using thermal gravimetric analysis and differential scanning calorimetry.

In **Chapter 3** we report the synthesis of both hydrophobic styrenic and hydrophilic acrylic monodisperse seed particles *via* soap-free emulsion polymerisation. Seed particles were decorated using nanogel particles (formed using di, tri, and penta-/hexa- functional acrylate crosslinking monomers) to produce raspberry and core-shell latex particles with an increased surface areas and roughness as visualised using scanning electron microscopy. The effects of the seed surface hydrophobicity were investigated where hydrophilic seeds generally led to core-shell type particles and hydrophobic seeds led to raspberry decorated particles. Pendant vinyl groups were quantified and analysed using Raman microscopy where both infra-red and nuclear magnetic resonance were unable. Thiol-Michael addition click reactions between the pendant vinyl groups and various charged thiols (*L*-cysteine, sodium 3-mercapto-1-propanesulphonate, and penta-erythritol tetra-kis(3-mercaptopropionate) was accomplished using nucleophilic *iso*butylamine catalyst. A decrease in the percentage of vinyl groups was observed using Raman microscopy.

In **Chapter 4** we report the main methods for encapsulating an oil for agricultural applications and discuss the common poly(urethane) and poly(urea) polymerisations methods. Using the methodology of thiol-Michael addition from **Chapter 3** we report the synthesis of milli- and microcapsules using an interfacial thiol-Michael addition reaction between a penta-/hexa- functional ene and a tetra- functional thiol using nucleophilic *iso*butylamine catalyst. The use of a microfluidic device led to millimetre sized capsules with controlled capsule sizes and dispersity that could be dried without payload release. The thiol-Michael addition reaction was further tested using high shear techniques (homogenisation) but the capsules were not robust enough to be dried without rupture and the oil release rate occurred after minutes.

The conclusions of the thesis are summarised in **Chapter 5**.

1.6. References

1. Bowes BG, Mauseth JD, Plant structure: a colour guide, 2nd Ed, Manson Publishing, 2008

2. Roberts MBV, Biology: A functional approach, 4th Ed, Nelson Thornes, 1986

3. Mauseth JD, Botany: An introduction to plant biology, 3rd Ed, Jones and Barnett Publishers Inc, 2003

4. Segal E, Kushnir T, Mualem Y, Shani U, Water uptake and hydraulics of the root hair rhizosphere, *Vadose Zone J.*, 2008; **7**:1027-1034

5. Kramer PJ, Boyer JS, Water relations of plants and soils: chapter 5-roots and root systems, Academic Press, 1995

6. Varney GT, Canny MJ, Rates of water uptake into the mature root system of maize plants, *New Phytol.*, 1993; **123**:775-786

7. Ochoa-Villarreal M, Aispuro-Hernández E, Vargas-Arispuro I, Martínez-Téllez MA, "Polymerisation" Chapter 4 - Plant cell wall polymers: function, structure and biological activity of their derivatives, Edited by 2012, ISBN: 978-953-51-0745-3, published by InTech, DOI: 10.5772/46094. (Available to download for free from: http://www.intechopen.com/books/polymerization/plant-cell-wall-polymers-function-structure-and-biological-activity-of-their-derivatives)

8. Schaffner L, Brügger G, Nyffenegger R, Walter R, Rička J, Lkeimann J, Hotz J, Quellet Ch, Surfactant mediated absorption of negatively charged latex particles to a cellulose surface, *Colloid Surface A*, 2006; **286**:39-50

9. Öztürk HB, Vu-Manh H, Bechtold T, Interaction of cellulose with alkali metal ions and complexed heavy metals, *Lenzinger Berichte*, 2009; **87**:142-150

10. Lavelle P, Spain A, *Soil ecology*, Kluwer academic publishers and Springer, Dordrecht, Springer, 2005

11. Ryan JN, Elimelech M, Review- Colloid mobilization and transport in groundwater, *Colloid Surface A*, 1996; **107**:1-56

12. Stevenson FJ, Humus chemistry genesis, composition, reactions, Wiley interscience, New York, 1982

13. Senesi N, Binding mechanisms of pesticides to soil humic substances, *Sci. Total Environ.*, 1992; **124-124**:63-76

14. McCarthy JF, Zachara JM, Subsurface transport of contaminants, *Environ. Sci. Technol.*, 1989; **23**:496-502

15. Pelley AJ, Tufenkji N, Effect of particle size and natural organic matter on the migration of nano- and microscale latex particles in saturated porous media, *J. Colloid Interf. Sci.*, 2008; **321**:74-83

16. Shaw DJ, Introduction to colloid and surface chemistry (4th edition), Butterworth-Heinemann, Elsevier Ltd, ISBN 978075611824, 1992

17. Schramm LL, *Emulsions, foams, and suspensions: fundamentals and applications*, Wiley-VCH, Verlag GmbH & Co, 2005

18. Overbeek JTG, The rule of Schulze and Hardy, *Pure & Appl. Chem.*, 1980; **52**:1151-1161

19. Sen TK, Khilar KC, Review on subsurface colloids and colloid-associated contaminant transport in saturated porous media, *Adv. Colloid Interf.*, 2006; **119**:71-96

20. Grolimund D, Elimelech M, Borkovec M, Barmettler K, Kretzschmar R, Sticher H, Transport of in situ mobilized colloidal particles in packed soil columns, *Environ. Sci. Technol.*, 1998; **32**:3562-3569

21. Bradford SA, Yates SR, Bettahar M, Simunek J, Physical factors affecting the fate and transport of colloid in saturated porous media, *Water Resour. Res.,* **2002**; **38**:63-1—63-12

22. Bradford SA, Simunek J, Bettahar M, Tadassa YF, van Genuchten MT, Yates SR, Straining of colloids at textural Interfaces, *Water. Resour Res.,* 2005; **41**: 1-17

23. Bradford SA, Bettahar M, Simunek J, van Genuchten MT, Straining and attachment of colloids in physically heterogeneous porous media, *Vadose Zone J.*, 2004; **3**:384–394

24. Mishurov M, Yakievich A, Weisbrod N, Colloid transport in a heterogeneous partially saturated sand column, *Environ. Sci. Technol.*, 2008; **42**:1066-1071

25. McDowell-Boyer LM, Chemical mobilization of micron-sized particles in saturated porous media under steady flow conditions, *Environ. Sci. Technol.*, 1992; **26**:586-593

26. Elimelech M, Kinetics of capture of colloidal particles in packed beds under attractive double layer interactions, *J. Colloid Interf. Sci.*, 1991; **146**:337-352

27. Elimelech M, Effect of particle size on the kinetics of particle deposition under attractive double layer interactions, *J. Colloid Interf. Sci.*, 1994; **164**:190-199

28. DeNovio NM, Saiers JE, Ryan JN, Colloid movement in unsaturated porous media: recent advances and future directions, *Vadose Zone J.*, 2004; **3**:338–351

29. Wan J, Wilson JL, Colloid transport in unsaturated porous media, *Water Resour. Res.*, 1994; **30**:857-864

30. Sharma P, Flury M, Zhou J, Detachment of colloids from a solid surface by a moving air-water interface, *J. Colloid Interf. Sci.*, 2008; **326**:143-150

31. Crist JT, Zevi Y, McCarthy JF, Throop JA, Steenhuis TS, Transport and retention mechanisms of colloids in partially saturated porous media, *Vadose Zone J.*, 2005; **4**:184-195

32. Sirivithayapakorn S, Keller A, Transport of colloids in unsaturated porous media: a pore-scale observation of processed during dissolution of air-water interface, *Water Resour. Res.*, 2003; **39**:6-1—6-10

33. Corapcioglu MY, Choi H, Modelling colloid transport in unsaturated porous media and validation with laboratory column data, *Water Resour. Res.*, 1996; **32**:3437-3449

34. Israelachvili JN, Intermolecular and surface forces, 3rd Ed, Academic Press, 1992

35. Dai Z, Fornasiero D, Ralston J, Particle-bubble attachment in mineral flotation, *J. Colloid Interf. Sci.*, 1999; **217**:70-76

36. Wan J, Tokunaga TK, Partitioning of clay colloids at air-water interfaces, *J. Colloid Interf. Sci.*, 2002; **247**:54-61

37. Zhuang J, Qi J, Jin Y, Retention and transport of amphiphilic colloids under unsaturated flow conditions: effect of particle size and surface property, *Environ. Sci. Technol.,* 2005; **39**:7853–7859

38. Harvey RW, Kinner NE, MacDonald D, Metge DW, Bunn A, role of physical heterogeneity in the interpretation of small-scale laboratory and field observations of microorganism, microsphere, and bromide transport through aquifer sediments, *Water Resour. Res.,* 1993; **29**:2713-2721.

39. Ouyang Y, Shinde D, Mansell RS, Harris W, Colloid-enhanced transport of chemicals in subsurface environments: a review, *Crit. Rev. Env. Sci. Tec.*, 1996; **26**:189-204

40. Torkzaban, S, Bradford SA, Colloid transport in unsaturated porous media: the role of water content and ionic strength on particle straining, *J. Contam. Hydrol.*, 2008; **96**:113-127

41. Elimelech M, O'Melia CR, Kinetics of deposition of colloidal particles in porous media, *Environ. Sci. Technol.*, 1990; **24**:1528-1536

42. Elimelech M, O'Melia CR, Effect of particle size on collision efficiency in the deposition of Brownian particles with electrostatic energy barriers, *Langmuir*, 1990; **6**:1153-1163

43. Zvikelsky O, Weisbrod N, Impact of particle size on colloid transport in discrete fractures, *Water Resour. Res.*, 2006; **42**:1-12

44. Roose T, Fowler AC, A model for water uptake by plant roots, *J. Theor. Biol.*, 2004; **228**:155-171

45. Abamectin pesticide data sheet, accessed September 15th 2012 (http://www.drugfuture.com/chemdata/abamectin.html)

46. Farm chemicals handbook, 2000, Meister publishing co. Willoughby OH

47. Gruber VF, Halley BA, Hwang SC, Ku CC, Mobility of Avermectin B1a in soil, *J. Agr. Food Chem.*, 1990; **38:**886-890

48. Solvesso structures obtained from the European chemicals agency (http://echa.europa.eu) using CAS 64742-94-5). Date accessed June 20th 2015

49. Fitch RM, Polymer colloids: a comprehensive introduction, Academic Press, 1997

50. Arshady R, Suspension, emulsion, and dispersion polymerization: a methodological survey, *Colloid Polym. Sci.*, 1992; **270**:717-732

51. Caruso F, Colloids and colloid assemblies, Wiley-VCH Verlag GmbH & Co, 2004

52. Ebewele RO, Polymer science and technology, CRC Press, 2000

53. Chern CS, Principles and applications of emulsion polymerization, John Wiley a& Sons Inc, 2008

54. Chern CS, Emulsion polymerization mechanisms and kinetics, *Prog. Polym. Sci.*, 2006; **31**:443-486

55. Harkins WD, A general theory of the mechanism of emulsion polymerization, *J. Am. Chem. Soc.*, 1947; **69**:1428-1444

56. Harkins WD, General theory of the mechanism of emulsion polymerization. II, *J. Polym. Sci.*, 1950; **5**:217-251

57. Smith WV, Ewart RH, Kinetics of emulsion polymerization, *J. Chem. Phys.*, 1948; **16:**592-600

58. Priest WJ, Particle growth in the aqueous polymerization of vinyl acetate, *J. Phys. Chem.*, 1952; **56**, 1077-1082

59. Roe CP, Surface chemistry aspects of emulsion polymerization, *Ind. Eng. Chem.*, 1968; **60**:20-33

60. Hansen FK, Ugelstad J, Particle nucleation in emulsion polymerization. I. a theory for homogeneous nucleation, *J. Polym. Sci. Polym. Chem.*, 1978; **16**:1953-1979

61. Hansen FK, Ugelstad J, Particle nucleation in emulsion polymerization. II. nucleation in emulsifier-free systems investigated by seed polymerization, *J. Polym. Sci. Polym. Chem.*, 1979; **17**:3033-3045

62. Lichti G, Gilbert RG, Napper DH, The mechanisms of latex particle formation and growth in the emulsion polymerization of styrene using the surfactant sodium dodecyl sulfate, *J. Polym. Sci. Polym. Chem.,* 1983; **21**:269-291

63. Feeney PJ, Napper DH, Gilbert RG, Coagulative nucleation and particle size distributions in emulsion polymerization, *Macromolecules*, 1984; **17**:2520-2529

64. Feeney PJ, Napper DH, Gilbert RG, Periodic nucleation processed in emulsion polymerization systems, *J. Colloid Interf. Sci.*, 1985; **107**:159-173

65. Butt HJ, Kappl M, Surface and interfacial forces, Wiley-VCH Verlag GmbH & Co, 2010

66. Birdi KS, Handbook of surface and colloid chemistry, 2nd Ed, CRC Press, 2003

67. Parsegian AV, Van der Waals forces: a handbook for biologists, chemists, engineers and physicists, Cambridge University Press, 2006

68. Hamaker HC, The London-van der Waals attraction between spherical particles, *Physica*, 1937; **4**:1058-1072

69. Derjaguin B, On the repulsive forces between charged colloidal particles and on the theory of slow coagulation and stability of lyophobe sols, *Trans. Faraday Soc.*, 1940; **35**:203-215

70. Derjaguin B, A theory of heterocoagulation, interaction and adhesion of dissimilar particles in solutions of electrolytes, *Discuss. Faraday Soc.*, 1954; **18**:85-98

71. Gouy G, Constitution of the electric charge at the surface of an electrolyte, *J. Phys.*, 1910; **9**:457-467

72. Chapman DL, A contribution to the theory of electrocapillarity, *Phil. Mag.,* 1913; **25**:475-481

73. Stern O, The theory of the electrolytic double-layer, *Z. Electrochem.*, 1924; **30**:508

74. Grahame DC, The electrical double layer and the theory of electrocapillarity, *Chem. Rev.*, 1947; **41**:441-501

75. Lyklema J, Principles of the stability of lyophobic colloidal dispersions in non-aqueous media, *Adv. Colloid Interfac.*, 1968; **2**:67-114

76. Van Der Hoeven PhC, Lyklema J, Electrostatic stabilization in non-aqueous media, *Adv. Colloid Interfac.*, 1992; **42**:205-277

77. Boer JH, The influence of van der Waals' forces and primary bonds on binding energy, strength and orientation, with special reference to some artificial resins, *Trans. Faraday Soc.*, 1936; **32**:10-37

78. Derjaguin BV, Landau LD, Theory of the stability of strongly charged lyophobic sols and of the adhesion of strongly charged particles in solutions of electrolytes, *Prog. Surf. Sci.*, 1993; **43**:30-69

79. Verwey EJW, Overbeek JThG, Long distance forces acting between colloidal particles, *Trans. Faraday Soc.*, 1946; **42**:B117-B123

80. Verwey EJW, Overbeek JThG, The theory of stability of lyophobic colloids, Elsevier, Elsevier, 1948

81. Verwey EJW, Overbeek JThG, The theory of stability of lyophobic colloids, Elsevier, Dover Publications, 1999

82. Overbeek JThG, Recent developments in the understanding of colloid stability, *J. Colloid Interf. Sci.*, 1977; **58**:408-422

Chapter 2 - Cleavable sulphonated poly(styrene) nanoparticles

2.1. Abstract

Chapter 2 discusses the use of sodium 4-vinylbenzenesulphonate in the soap-free emulsion copolymerisation with styrene to synthesise sulphonated colloidal particles. We report the limitations of the previous methods for the sulphonation of colloids. We designed protected sulphonate monomers by the copolymerisation of neopentyl 4-vinylbenzenesulphonate (NSS) and ethyl *p*-vinylbenzenesulphonate (ESS) with styrene and synthesised colloids under 200 nm with hidden sulphonate groups as studied using Scanning Electron Microscopy (SEM). Following particle synthesis we discuss limitations of both NSS and ESS for use in soap-free emulsion copolymerisation and studied the deprotection or hydrolysis of the ethyl groups from ESS particles using high temperature heat (>200^{o}C) where the effects on the particles are studied using thermal gravimetric analysis and differential scanning Calorimetry.

2.2. Introduction

In this chapter the aim was to synthesise functionalised polymer particles with a high loading of sulphonate groups *via* soap-free emulsion polymerisation. We wanted to find a method that could increase the sulphonate levels using batch emulsion polymerisation with functional comonomer sodium 4-vinylbenzenesulphonate. Sulphonate groups would enable soil mobility due having a high anionic surface charge density thereby minimising the adhesion to negatively charged surfaces. Sulphonate groups also provide colloidal stability at high salt concentrations and have shown an adhesion affinity to air-water interfaces.

2.2.1. Homogeneous sulphonation of particles

The first synthetic route for synthesising sulphonated particles and polymers was using concentrated sulphuric acid. Hazarika *et al* reported the sulphonation of poly(styrene) particles using this method[1] or a less harsh sulphonation using acetyl sulphate as reported by Orler *et al*.[2] Many homogeneous and heterogeneous methods are reported by Kućela *et al*.[3] Unfortunately the harsh reaction conditions required for sulphonation can lead to a number of side reactions (double substitution on phenyl rings and condensation of two sulphonic acids causes crosslinking) which reduces the usefulness of this method as it lowers the sulphonate content.[3]

2.2.2. Soap-free emulsion polymerisation for sulphonation

In **Chapter 1** we discussed soap-free emulsion polymerisation and many authors have shown that the use of different charged thermal initiators such as persulphates, peroxide and azo compounds can generate different surface charges. With persulphate

initiators the sulphate group is unstable and can readily hydrolyse to hydroxyl or oxidise carboxylic acid groups. The use of only initiators to add surface charged groups often limits the size of the final polymer particles to between 400 and 1000 nm[4-5] but the size can be altered by the amount of initiator, pH, electrolyte concentration and temperature.[6]

2.2.2.1. Heterogeneous sulphonation utilising soap-free emulsion polymerisation with ionic comonomers

More commonly the addition of ionic comonomers results in latex particles with an increased content of surface active functional groups. We will only be referencing the methods to add sulphonate surface charge in this chapter. The most commonly used sulphonate comonomer is sodium 4-vinylbenzenesulphonate (or NaSS), which has been shown to provide control over the particle size and improves the colloidal stability of the final latex due to the sulphonate group being hydrolytically stable. The batch soap-free emulsion of styrene with NaSS using potassium persulphate (KPS) has been shown to synthesise 500-800 nm colloids by the addition of 0.02-2 wt% NaSS based on styrene as reported by Peula *et al* and Kim *et al*.[4-5] The particle size can be decreased further by the addition of crosslinkers such as DVB which inhibits swelling of the polymer particles.[7] Unfortunately the use of NaSS in batch soap-free emulsion polymerisation leads to low incorporation of the NaSS monomer and low surface density of sulphonate groups. The latex particle size decreases with higher NaSS amount leading to an increased number of particles so the overall sulphonate charge per particle remains the same. A secondary effect of higher NaSS amounts (above 2 wt%) is the formation of a bimodal size distribution caused by broadening of the nucleation period.[5,8-9] The formation of amphiphilic polymers can also induce bridging and depletion

flocculation/coagulation which reduces the overall colloidal stability.[8] Particles with low sulphonate functional group loading and broad dispersity is a problem when particles with controlled size distributions and high levels of sulfonation is required.

One method that improved on the low sulphonate content in particles was to adapt the batch emulsion polymerisation method with the "shot-addition" method as reported by Peula *et al*, Kim *et al* and others.[4-10] The shot addition method uses a highly concentrated shot of NaSS (in styrene) that is injected into the polymerisation at a high conversion value, typically reported at 90-92% conversion (or 85-95% as reported by Sunkara *et al*[7]). Studies have led to the belief that this method creates a hairy surface layer of electrosterically stabilised sulphonate groups which can have chain lengths hundreds of nm long effectively creating a core-shell type structure (this is shown in **Figure 2.1-B.**).[4] These hairy chains are chemically bound to the surface of the particles and lead to a much greater colloidal stability as shown by electrolyte addition. This means that hairy sulphonated colloids synthesised using the shot-addition method have an increased surface charge density compared to the standard batch made latexes.[5-8] Studies have led to the idea that the particles synthesised using the shot addition method are more colloidally stable due to the hairy layer providing electrostatic stabilisation from the sulphonate polyelectrolyte chains. This effect is combined with the immobilisation of water molecules surrounding the particles that lowers the van der Waals attraction between particles. The advantage of the shot addition method is that size can be tailored easily and therefore monodisperse latexes can be easily prepared with much higher amounts of NaSS compared to batch polymerisation. The surface charge can be tailored by ratio of sulphonated comonomers to monomer used in the shot.

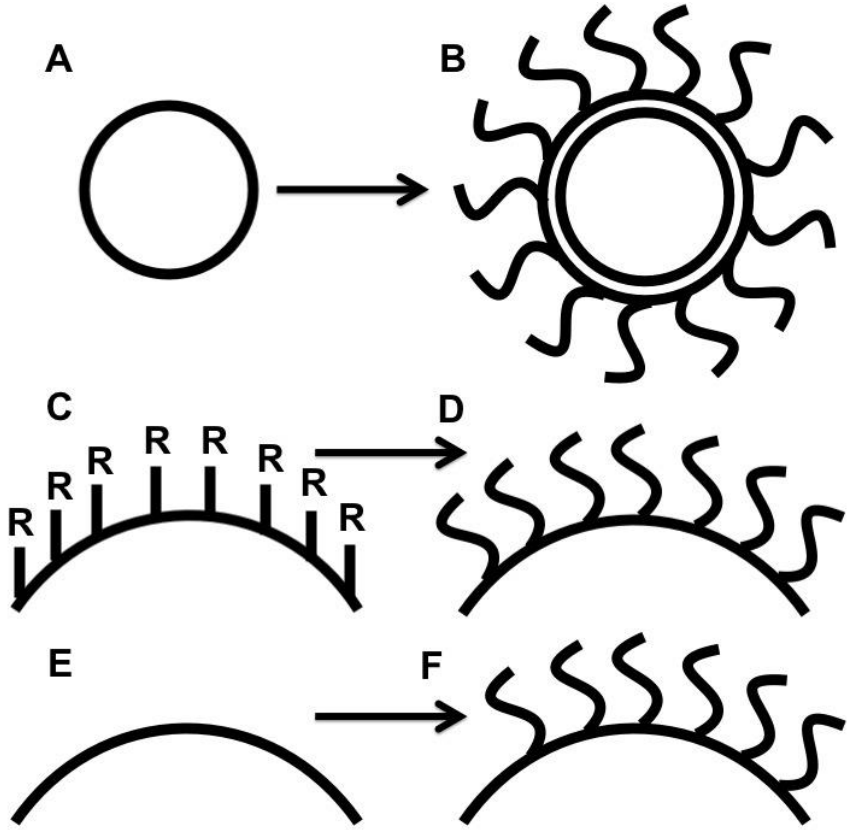

Figure 2.1. Representative figure showing A) a poly(styrene) nanoparticle with smooth morphology *via* soap-free emulsion polymerisation, B) poly(styrene) nanoparticle surface after the shot-addition of NaSS and styrene with hairy electrosteric chains, C) particle surface with functional groups (R), D) polymerisation from reactive surface groups ("grafting from"), E) nanoparticle surface, F) nanoparticle surface after chemisorption or physisorption of polymer chains ("grafting to").

2.2.3. Alternative methods for increasing the sulphonate content at the particle surface

Chemisorption of polyelectrolyte chains to the surface using a shot-addition method with or without crosslinkers can enable attachment of polymer chains to the surface of a particle (or a flat substrate). The chemisorption can be achieved using the "grafting from" and the "grafting to" approach (shown in **Figure 2.1-C** to **Figure 2.1-F.**). The grafting technique is reviewed by Zhao *et al*,[11], Minko[12] and Barbey *et al*.[13] The "grafting to" approach uses physisorption or chemisorption of polymer chains to the surface but suffers the drawback of low grafting rates and low grafting density of polymer chains. The low grafting is caused by either steric hindrance from other already

attached polymer chains that affects the diffusion of polymer grafts[14] or physisorbed chains being reversibly attached. However, the "grafting from" approach allows sufficient brush density to be grown from a surface as brushes grow from every reactive site on the surface. The more surface active initiation sites the higher the density of grafted brushes.[14-15] The "grafting from" approach usually employs living radical polymerisation techniques such as atom transfer radical polymerisation (ATRP) or reversible addition fragment chain transfer (RAFT) polymerisation. Using these two techniques any polymer composition can be grown or attached to a surface of a particle or substrate. Single polymer brushes, block copolymer brushes, altered composition polymers can be synthesisedand the length of the brushes can be tailored by the reaction conditions and monomer addition (see reviews articles).[11-15] Su *et al* have shown the radical polymerisation of NaSS from a silane modified SiO_2 particle results in the formation of polyelectrolyte brushes that extend from the surface[16] and others have shown the use of ATRP[17-18] and RAFT[19] for attaching and growing poly(sulphonate) electrolytes from the particle surface.

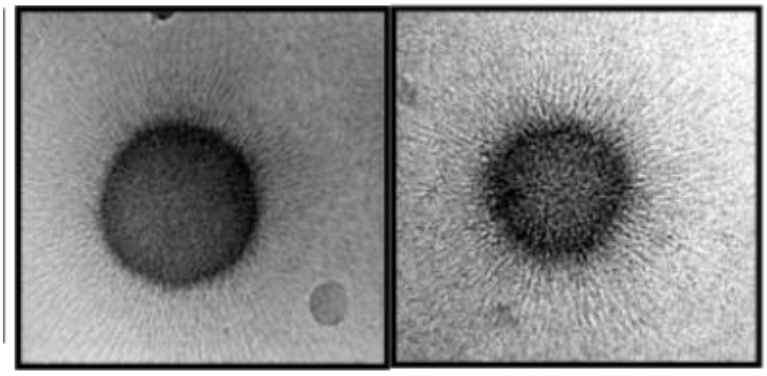

Figure 2.2. SEM micrographs of poly(styrene) particles with poly(NaSS) brushes grafted to the surface [Reproduced from reference 20].

One such method of synthesising poly(NaSS) brushes from a particle surface was reported by Alzhrani during his PhD thesis[20] and also by Chen *et al* (see **Figure**

2.2. for an example of colloids with poly(NaSS) brushes).[17] Firstly a slightly crosslinked poly(styrene) latex was prepared using styrene, NaSS, DVB and a functional tertiary bromine ATRP initiator. The bromine monomer was added using both batch and shot addition methods to vary the surface incorporation of the ATRP initiator. Single electron transfer living radical polymerisation (SET-LRP) was carried out on the particles causing the functional bromine group to grow poly(NaSS) chains from the surface of the particles creating a hairy brush structure wand a high polysulphonate brush density per particle. The reaction proceeded in water using copper zero catalyst at room temperature and the polymer brushes were visualised with the aid of cryogenic transmission electron microscopy (Cryo-TEM). The shot addition method was shown to have a pronounced effect on the concentration of bromine initiator groups at the surface and Cryo-TEM analysis showed polymer brushes extending from the particle surface. These polymer brushes could not be visualised when the batch emulsion polymerisation method was chosen indicating that much less brushes were able to polymerise from the surface. Ballauff *et al* have also reported the synthetic methods for the attachment and grafting of polyelectrolyte brushes from spherical poly(styrene) particles and dumbbells.[21-23]

2.2.4. Protected monomer for use in batch soap-free emulsion polymerisation

In this chapter aimed to overcome the size dependant function of NaSS concentration as well as the dispersity index problems shown by NaSS above 2.5 wt%. By using a protected sulphonate monomer variation of NaSS monomer we aimed to alter the hydrophobicity and locus for nucleation thereby increasing the incorporation of sulphonate monomer to above 2.5 wt% using batch soap-free emulsion polymerisation.

We also hoped to provide control over particle size and the dispersity index. Post polymerisation the protected monomer can be cleaved to release the sulphonate charge at the particle surface.

2.3. Experimental

2.3.1. Materials

Thionyl chloride (purum, >99.0%), 4-*t*-butyl catechol (≥98.0% HPLC grade), dimethylformamide (anhydrous 99.8%), sodium 4-vinylbenzenesulphonate (>90% technical grade, NaSS), neopentyl alcohol (2,2-Dimethyl-1-propanol, 99%), 4-di(methylamine)pyridine (ReagentPlus, ≥99%), triethylamine (≥99.5%), cyclohexane (ACS reagent, ≥99%), styrene (Reagent Plus, >99.0%), divinylbenzene (DVB, 80% mixture of isomers) and potassium persulphate (ACS reagent, ≥99.0%) were all purchased from Sigma-Aldrich and used as received. 2,2'-azobis(2-methylpropionitrile) (AIBN) was supplied by Wacker and used as received. Solvents toluene, methanol, ethanol, diethyl ether, petroleum ether 40-60 ^{o}C, dichloromethane were purchased from fisher scientific and were reagent grade purity. Magnesium sulphate, potassium chloride, potassium carbonate and sodium hydrogen carbonate were of reagent grade purity and were purchased from fisher scientific. Silica gel was also from Sigma Aldrich and was ≥400 mesh.

2.3.2. Equipment

Analysis of ^{1}H NMR measurements was performed on either a Bruker DPX-300 300 MHz or DPX 400 MHz spectrometer and the spectrum was analysed with Mestrec v2.3a. TGA measurements were performed using a Mettler-Tolledo DSC1-Star with autosampler using both air and nitrogen environments in the temperature range 25-1000 ^{o}C. Fisher Scientific supplied all all glassware. Emulsion polymerisations were carried out in double-walled cylindrical glass reactors (250 ml, Asynt) equipped with an external heating bath (Julabo F-25 unit). A four-bladed overhead Teflon stirrer (Cowie

Ltd) approximately 1cm from the bottom of the reaction vessel ensured thorough mixing with typical stirring speeds of 275 rpm. Average hydrodynamic particle sizes and dispersity indexes were measured by dynamic light scattering using a Malvern Zetasizer Nano (data was analysed using the CONTIN algorithm). SEM analyses were performed using a Zeiss Supra 55VP FEG-SEM with an EBSD camera. Sample preparation and analysis using DLS and SEM is reported in **Section 2.3.6.**. A 4 digit analytical balance (Precisa XT 220A) was used for accurate measurements of the monomers, comonomers, initiator and crosslinkers and also for measuring monomer conversion.

2.3.3. Synthesis of protected sulphonate monomer

2.3.3.1. Synthesis of precursor 4-vinylbenzenesulphonyl chloride (SSC)

The SSC precursor was synthesised following the method from literature.[30] Thionyl chloride ($SOCl_2$, 250 mL, 2.64 mol) was added to a mixture of 4-*t*-butylcatechol (1.5 g, 9 mmol) and dimethylformamide (anhydrous DMF, 320 mL) in a 1 L round bottomed flask (RBF) whilst stirring in an ice bath (<0 °C). Sodium *p*-styrene sulphonate (NaSS, 100 g, 0.48 mol) was added in small amounts with constant stirring and then further stirred for 3 hours. The RBF was covered in tin foil and transferred to the fridge for 12 hours where the solution separated into two layers. The solution was poured into ice cold water (carefully due to HCl gas release) and the solution was extracted twice with toluene (2 × 600 mL) using a separating funnel. The organic layer was collected and further washed with water (2 × 600 mL) and KCl brine solution (2× 600 mL). The organic layer was dried for 1 hour using anhydrous $MgSO_4$. Once the solid was filtered off using a Buchner funnel the toluene was removed on a rotary evaporator (<45 °C). Styrene sulphonyl chloride was a yellow oil yield 91.6 g (90%). ^1H

NMR ($CDCl_3$, 300 MHz,) δ_H 1.98 (3H, s, Toluene C*H*$_3$), 5.14-5.18 (1H, d, J_{Trans} 17.5 Hz, CH=C*H*$_2$), 5.56-5.62 (1H, d, J_{Cis} 11.0 Hz, CH=C*H*$_2$), 6.36-6.45 (1H, dd, J_{Trans} 17.5 Hz J_{Cis} 11.0 Hz, C*H*=CH_2), 6.81 (s, $CDCl_3$), 6.76-6.90 (5H, m, Toluene Ar*H*), 7.21-7.24 (2H, d, *J* 8.5 Hz, Ar*H*), 7.60-7.63 (2H, d, *J* 8.5 Hz, Ar*H*).

2.3.3.2. Synthesis of neopentyl 4-vinylbenzenesulphonate (NSS)

The NSS monomer was synthesised following a slightly adapted method from literature reported by Baek.[28] In a 500 ml round bottomed flash 15.03 g *p*-styrene sulphonyl chloride was added dropwise to a solution of 9.79 g neopentyl alcohol, 0.75 g 4-di(methylamino)pyridine, 15 ml triethylamine and 50 ml cyclohexane at 0 ^oC and stirred for 30 minutes. This solution was further stirred for 30 hours at room temperature and then stored at 0 ^oC overnight. The solution was pored into 200 ml deionized water and the aqueous phase was extracted with DCM (2 x 200 ml). The organic layers were combined and washed with water (2 x 200 ml) and dried using magnesium sulphate. DCM was removed using a rotary evaporator and columned using a silica column with 60:40 DCM:Petroleum ether to give a white powder of yield 9.45 g (50%); ^1H NMR ($CDCl_3$, 400 MHz,) δ_H 0.81 (9H, s, C(C*H*$_3$)$_3$), 3.59 (2H, s, OC*H*$_2$C), 5.36-5.39 (1H, d, J_{Cis} 11.0 Hz, CH=C*H*$_2$), 5.80-5.85 (1H, d, J_{Trans} 17.5 Hz, CH=C*H*$_2$), 6.34-6.71 (1H, dd, J_{Trans} 17.5 Hz J_{Cis} 11.0 Hz, C*H*=CH_2), 7.46-7.48 (2H, d, *J* 8.5 Hz, Ar*H*), 7.76-7.78 (2H, d, *J* 8.5 Hz, Ar*H*).

2.3.3.3. Synthesis of ethyl 4-vinylbenzenesulphonate (ESS)

SSC (78.4 g, 0.39 mol) was added dropwise to a stirring solution of potassium carbonate (160 g, K_2CO_3, excess) in ethanol (460 mL, excess) at ambient temperature. After 12 hours the sample was analysed by ^1H NMR. At this point the reaction was concentrated under reduced pressure using the rotary evaporator (<35 °C) for 3 hours and we monitored the volume collected for comparison with the starting amount. Et_2O

(500 mL) and water (500 mL) were added to the RBF and the organic layer was separated and kept. The aqueous layer was then washed with Et_2O (2 × 500 mL) and the organic layers were combined and further washed with both water (2 × 500 mL) and KCl brine solution (2 × 500 mL). The organic layer was dried with $MgSO_4$ and filtered *via* Buchner filtration. A yellow product resulted and removal of the colour was attempted using activated back charcoal yet a pale yellow colour remained which was taken to be the colour of the monomer. After high vacuum a pure pale orange oil product was obtained of yield 42.8564 g (52%). ^{1}H NMR ($CDCl_3$, 400 MHz,) δ_H 1.31-1.34 (3H, t, *J* 7.0 Hz, CH_2CH_3), 4.12-4.17 (2H, q, *J* 7.0 Hz, CH_2CH_3), 5.47-5.50 (1H, d, J_{Cis} 11.0 Hz, CH=CH_2), 5.91-5.95 (1H, d, J_{Trans} 17.5 Hz, CH=CH_2), 6.74-6.82 (1H, dd, J_{Trans} 17.5 Hz J_{Cis} 11.0 Hz, CH=CH_2), 7.57-7.59 (2H, d, *J* 8.5 Hz, Ar*H*), 7.87-7.89 (2H, d, *J* 8.5 Hz, Ar*H*); ^{13}C NMR ($CDCl_3$, 100 MHz) δ_C 14.73, 67.05, 77.79, 77.10, 77.42, 118.05, 126.83, 128.19, 135.18, 142.86; IR (thin film) 3078, 2986, 1597, 1375, 1353, 1190, 1172, 1094, 998, 911, 845, 800, 755, 657 cm^{-1}. HRMS *m/z* (ES$^+$) calculated for $C_{10}H_{12}O_3S$, 212.0399, found 235.0396 $[M + Na]^+$.

2.3.4. Synthesis of poly(styrene-co-NSS-co-DVB) particles via soap-free emulsion polymerisation

In a 250 ml reactor 190 ml water with 0.0723 g NaSS and 0.1017 g sodium hydrogen carbonate was degassed with nitrogen for ~45 minutes. To this solution 8.02 g styrene, 2.017 g NSS and 0.76 g DVB was injected and degassed for a further 10 minutes. The reactor was heated to 70 ^{o}C and equilibrated for 5 minutes and 0.07 g KPS in 1 ml deionized degassed water was injected to begin the polymerisation. Polymerisation proceeded overnight followed by dialysis twice daily against deionized water for 2 weeks.

2.3.5. Synthesis of poly(styrene-co-ESS-co-DVB) particles via soap-free emulsion polymerisation

In a 250 ml round bottomed flask 90 ml water with NaSS and sodium hydrogen carbonate was degassed for ~45 minutes. To this a mixture of styrene, ESS, and DVB was added (refer to **Table 2.1.** in **Section 2.4.6.2.** for exact amounts added). The solution was further degassed for ~10 minutes. The reaction was heated to 70 ^{o}C using a probe controlled oil bath and left for 5 minutes for the temperature to equilibrate. To this 0.1 g KPS in 1 ml DDI water was injected and the reaction was left to polymerise overnight followed by dialysis twice daily against deionized water for 2 weeks per sample.

2.3.6. Analysis preparation

2.3.6.1. DLS sample analysis

Dynamic light scattering (DLS), also known as PCS (photon correlation spectroscopy), is used to measure both the hydrodynamic sizes of the colloids being analysed as well as monitoring the polydispersity of the sample. These measurements were carried out using a Malvern Zetasizer Nano ZS.

Typically for a 10 wt% latex a drop of latex was diluted with 20 ml deionised water. Sample acquisition was carried out in poly(styrene) cuvettes with four clear faces. Approximately 1 cm of the diluted latex was added to the cuvette and the machine was used to analyse it. Typically a two minute equilibration time was used to stabilise the temperature to 25 ^{o}C before the measurement was run using five measurements with 6 second sub runs and 10 total runs.

2.3.6.2. SEM sample analysis

Sample preparation for SEM analysis involved the sticking of silicon wafers (donated by Wacker Chemie AG, Germany) onto an SEM stub (from Agar scientific). Diluted latex sample was dried out onto the top of the wafer where samples were typically diluted by 1 drop of latex to 20 ml of deionized water to ensure that saturation of the grid did not occur. A thin layer of particles is preferable for easy visualisation. Once the samples were prepared onto the silicon wafer they were also sputtered with either metal particles or carbon to provide a conducting surface, which is crucial for imaging. The carbon coater machine was used once it arrived due to the finer and more efficient conductive coating that enables greater surface visualisation. Settings were optimised and best imaging was generally obtained after sputtering 40 seconds at 1.5 kV and 25 mA using the auto mode of a Quorum technologies Polaron SC7640 auto/manual high resolution sputter coater for the gold/palladium or platinum metal. The carbon coater was a EmiTech KX950 was supplied from the Advantage West Midlands: Science City grant and samples was sputtered with carbon using three bursts of 1000 mS. SEM imaging was performed on ZEISS supra 55VP field emission gun scanning electron microscope (FEG-SEM) equipped with an electron backscattered diffraction camera.

2.3.6.3. SEM analysis using ImageJ

(ImageJ was downloaded from the website: http://rsbweb.nih.gov/ij/download.html). SEM images were first opened using ImageJ. The line tool was used to measure the scale bar from the SEM image and the distance in nm was inputted to set the scale. This scale bar allowed other lines to be measured and the distance was tabulated, where high magnification images were used to enable more

accurate size measurements. Typically 100 particle diameters were measured per image using multiple images per sample in order to calculate average the particle diameters and the variation in sizes (coefficient of variation). Contact angles were measured using the angle tool where three points on the picture could be moved around to measure angles between the seed and decorating nanogel particles.

2.4. Results and discussion

2.4.1. Protected ethyl 4-vinylbenzenesulphonate and neopentyl 4-vinylbenzenesulphonate monomers

In 2007 Kazemi *et al* reported the effective tosylation of *p*-toluenesulphonyl chloride (Ts) with alcohols under solvent free conditions.[24] This method allowed methanol, ethanol, benzyl alcohols and valuable ethylene glycols to react with Ts in fast high yield synthesis by simply grinding the two reagents together. Recently, in 2010, Miller reported the protection of dansyl sulphonate using a multitude of functional groups including straight and branched alkyl chains, phenyl groups and fluoro groups.[25] The use of different protecting alcohols allowed different monomer properties such as acidic media stability for *iso*butyl sulphonates or nucleophilic displacement resistance for neopentyl sulphonates. Chen *et al* showed the synthesis of butyl 4-vinylbenzenesulphonate (BuSS) as a means of protecting the sulphonate functional group. The reaction also achieved satisfactory results using *n*-hexyl, *n*-octyl and benzyl groups to synthesise functionalised sulphonate esters.[26] This synthetic method was also adapted by Okamura *et al* for synthesising BuSS and NSS.[27] Baek further adapted the synthesis of NSS and improved the yield from 26% to 51%.[28]

In this chapter we adapted the work done by Kazemi *et al*[24] but replaced the tosyl chloride with SSC so that the vinyl group would make it useful for polymerisations. SSC (2.2) was prepared by the method set out by Jeřábek *et al* which was an adaption of the original work carried out by Kamogawa where NaSS (2.1) and thionyl chloride reacted in DMF to form 2.2 with a 90% yield (synthesis of 2.2 described in **Section 2.3.3.1**).[30-31] The structure of 2.2 is shown in **Scheme 2.1.** and the ^{1}H NMR spectrum is shown in **Figure 2.3.**.

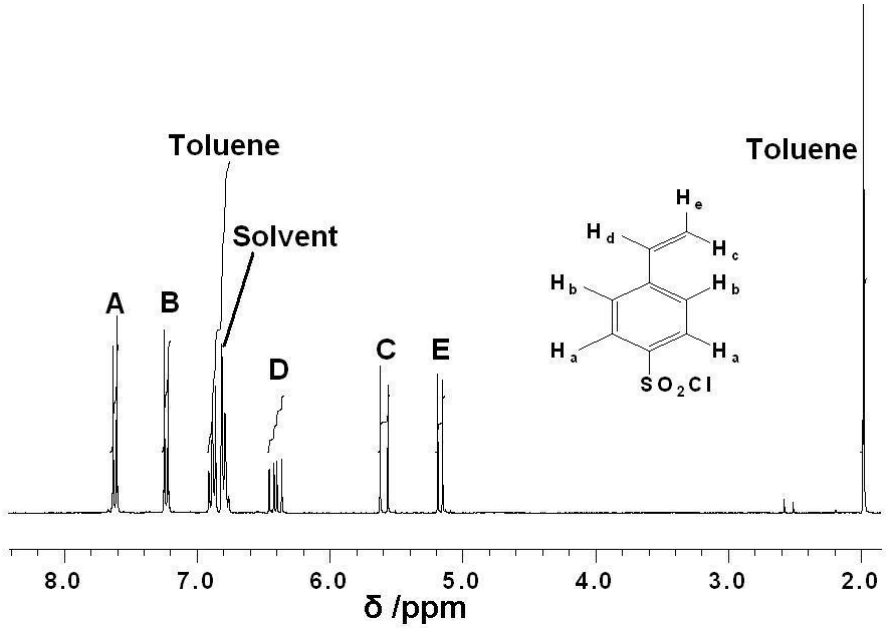

Figure 2.3. ^{1}H NMR spectrum of monomer 2.2.

Utilising monomer 2.2 we prepared the NSS monomer (2.3, structure shown in **Scheme 2.1.**) by reacting 2.2 with neopentyl alcohol. This method was published by Baek and achieved a satisfactory 50% yield (full synthesis described in **Section 2.3.3.2**). Due to the complexity for the synthesis of 2.3 (requiring multiple washing and drying stages and column purification), preparation of 2.3 was initially carried out in small quantities. The protected monomer ESS (2.4, structure shown in **Scheme 2.1.**) was first reported by Woeste in his PhD thesis in 1993 where the reaction of silver 4-vinylbenzenesulphonate with ethyl bromide yielded 79% 2.4 monomer and silver bromide.[29] Kazemi altered this method and used potassium carbonate and ethanol with Ts to form the tosyl ester product. We synthesised 2.4 using the Kazemi method but we reacted potassium carbonate and ethanol with 2.2 to form 2.4 with mass 42.85 g (52% yield, full synthesis described in **Section 2.3.3.3.**).[34]

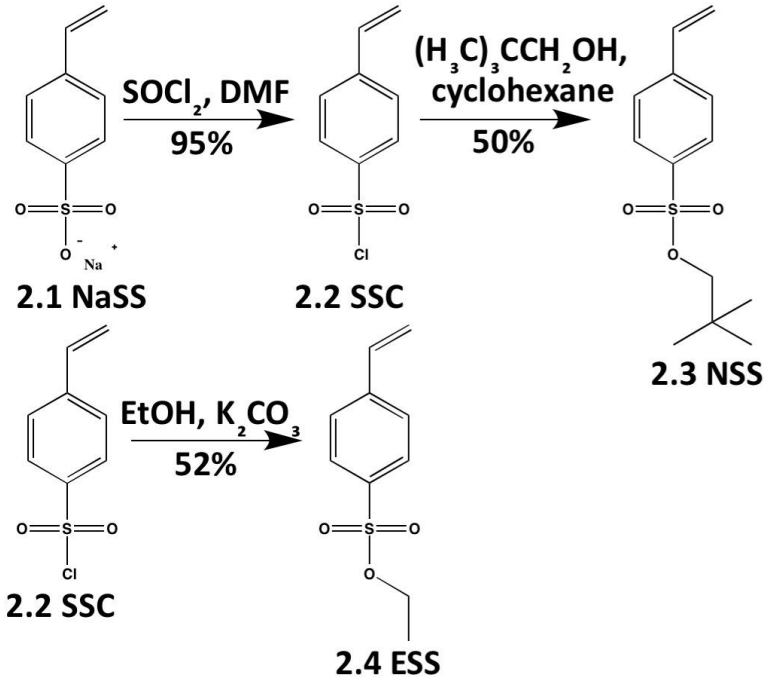

Scheme 2.1. The reaction scheme for the synthesis of ESS and NSS monomers using NaSS and SSC.

The synthesis of 2.3 and 2.4 are shown schematically in **Scheme 2.1.** and the analysis of the monomers 2.3 and 2.4 are shown in **Figure 2.4.**, **Figure 2.5.** and **Figure 2.6.**. Recently Tosoh Organic Chemicals Company developed larger scale production of 2.4 but due to cost and the small scale production the 3 was synthesised in house. The lower yield when compared to the high 90% yield of 2.2 is caused by incomplete esterification of 2.2.

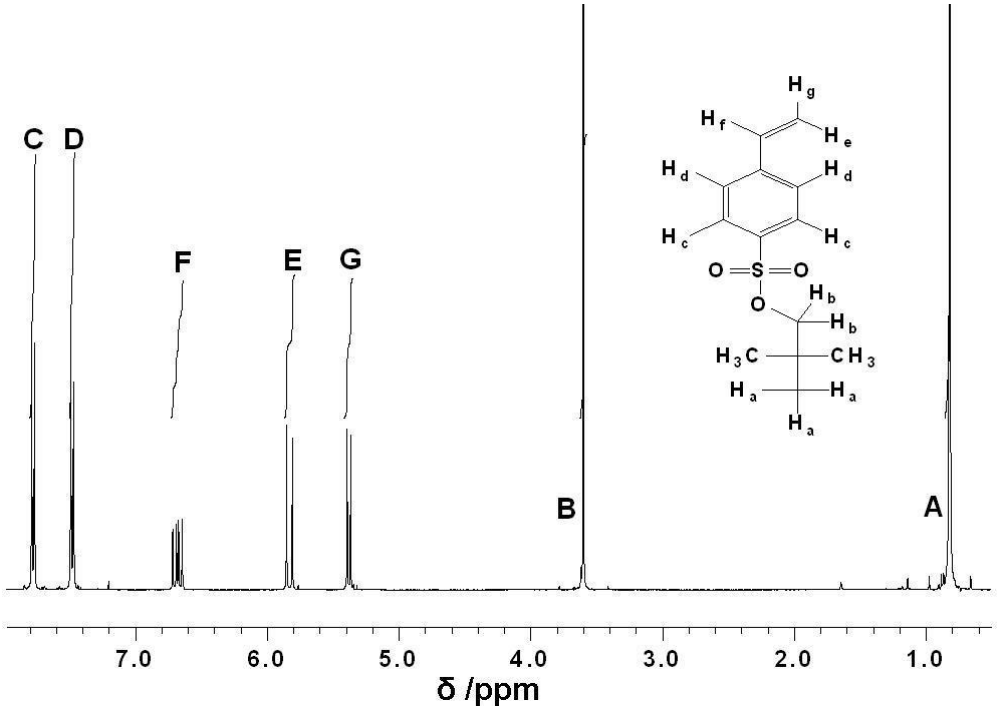

Figure 2.4. [1]H NMR spectrum of monomer 2.3.

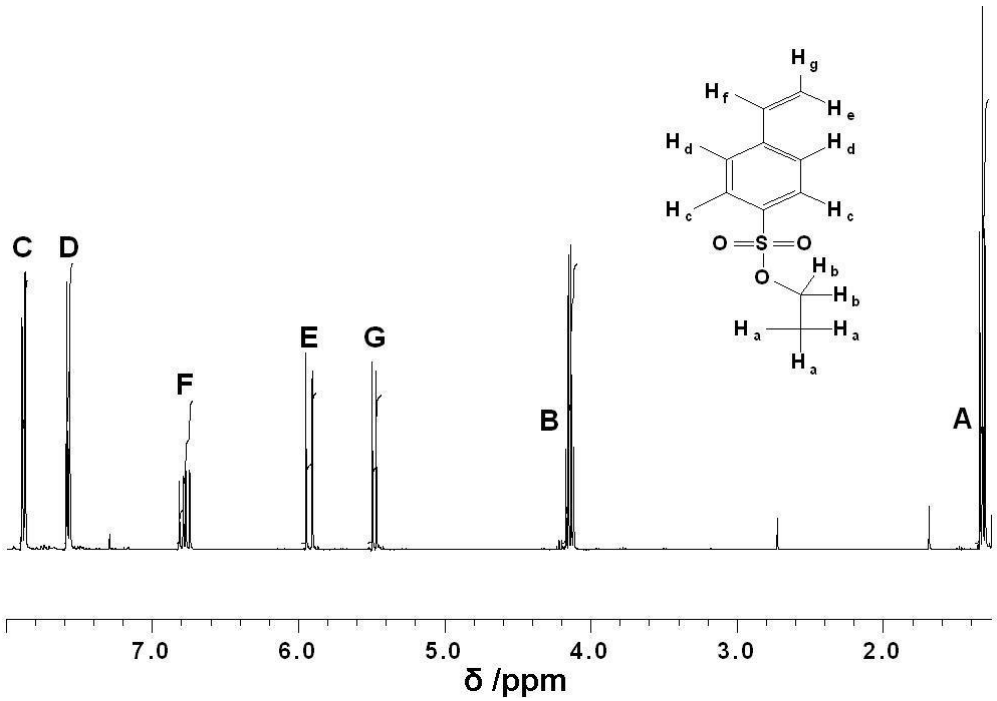

Figure 2.5. [1]H NMR spectrum of monomer 2.4.

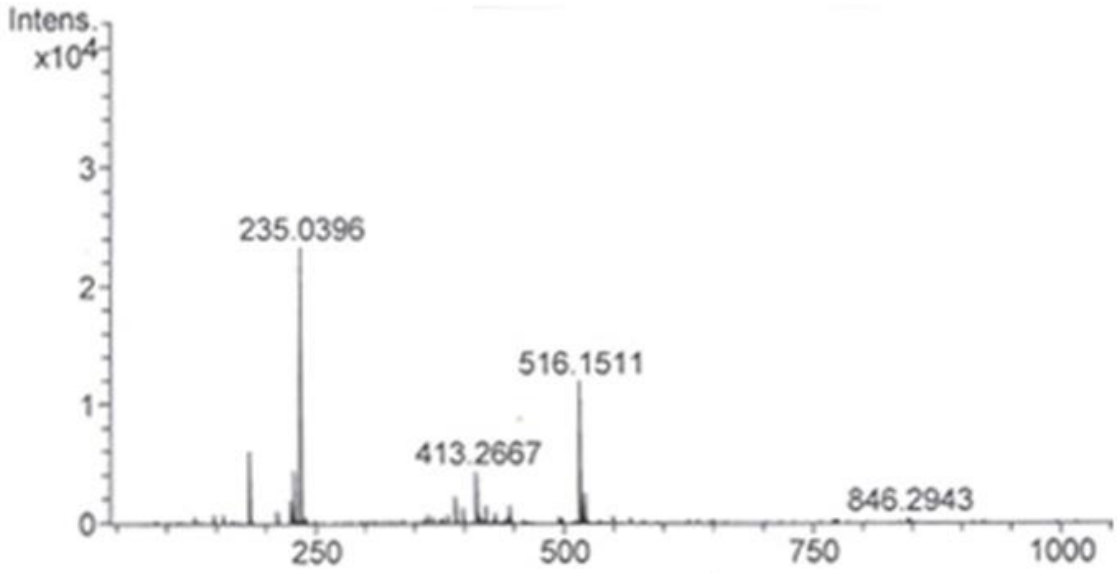

Figure 2.6. MS spectrum of monomer 2.4.

2.4.2. Thermal analysis of poly(NSS)

Initially the polymerisation of 2.3 was carried out in toluene using AIBN initiator (structure shown in **Figure 2.7.**). We dissolved 1 g 2.3 in 9 g toluene, degassed with nitrogen and stirred at 70 ^{o}C where 0.05 g AIBN was injected. Polymerisation was allowed for 8 hours whereby removal of the toluene gave a pale orange powder. Thermal gravimetric analysis (TGA) was used to study the degradation temperatures of poly(2.3). The TGA and Differential Scanning Calorimetry (DSC) spectra for the synthesised homopolymer of poly(2.3), under nitrogen atmosphere are shown in **Figure 2.8.**.

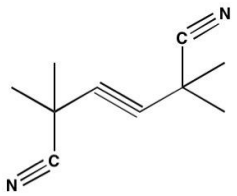

Figure 2.7. Structure of 2,2'-azobis(2-methylpropionitrile) (AIBN).

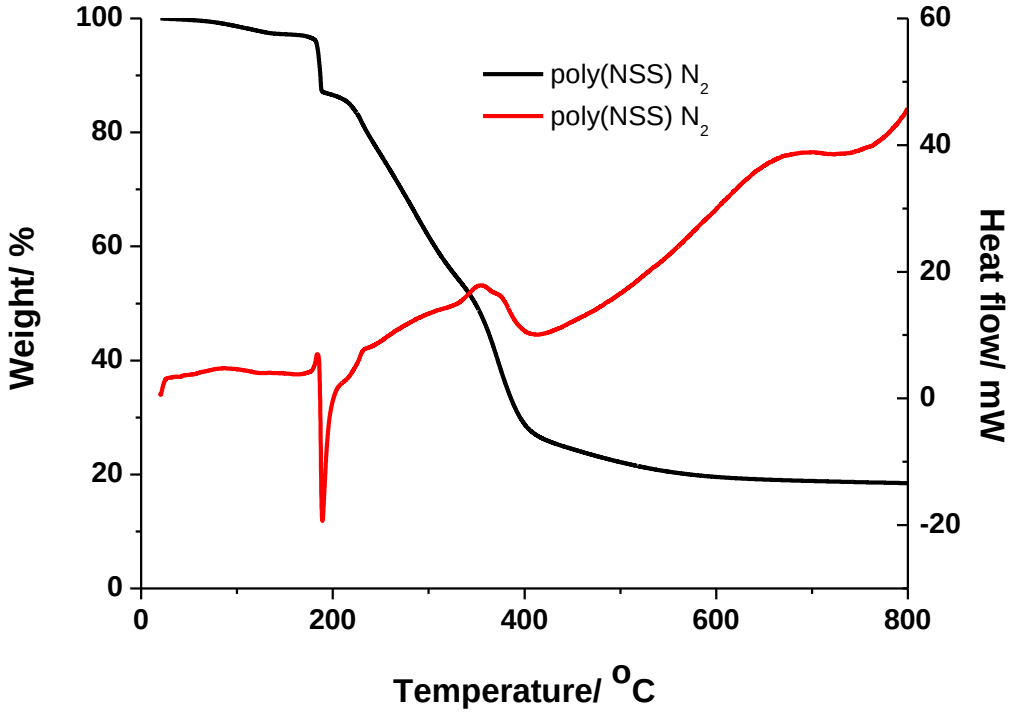

Figure 2.8. TGA and DSC traces for bulk polymer poly(2.3) under N_2 atmosphere from 20-800 °C at a heating rate of 10 °C/min. Black line is the TGA trace, red line is the DSC trace.

The TGA weight loss observed by our poly(2.3) sample follows this same degradation profile as reported by Baek.[28] They assigned the weight loss at 185-188 °C to the thermolysis of the neopentyl radical followed by degradation between 185-380 °C for desulphonation of the polymer chains. The weight loss up to 400 °C was due to degradation of the polymer backbone. The plateau region at >500 °C was caused by the decomposition of polymer fragments in the presence of SO_2 generating sulphur based compounds with higher thermal degradation temperatures.[28] The DSC data also confirms the transition changes for the poly(2.3) weight losses and this is explained in more detail in the next section for poly(2.4) degradation.

2.4.3. Thermal analysis of poly(ESS)

Bulk polymerisation of the 2.4 monomer using AIBN initiator was carried out to produce solid poly(2.4). Initially 0.005 g AIBN was dissolved into 1 g of 2.4 and added

to a sealed glass vial and purged with nitrogen. An oil bath increased the temperature of the monomer to 70 ºC to enable polymerisation and after ~4 hours polymerisation time the reaction vessel was cooled to room temperature and a viscous polymer had formed. Precipitating the polymer into methanol removed any unreacted 2.4 and AIBN was removed and the solid was filtered, washed, and dried. The TGA and DSC spectra for the synthesised homopolymer of poly(2.4), under both air and nitrogen atmospheres, is shown in **Figure 2.9.**.

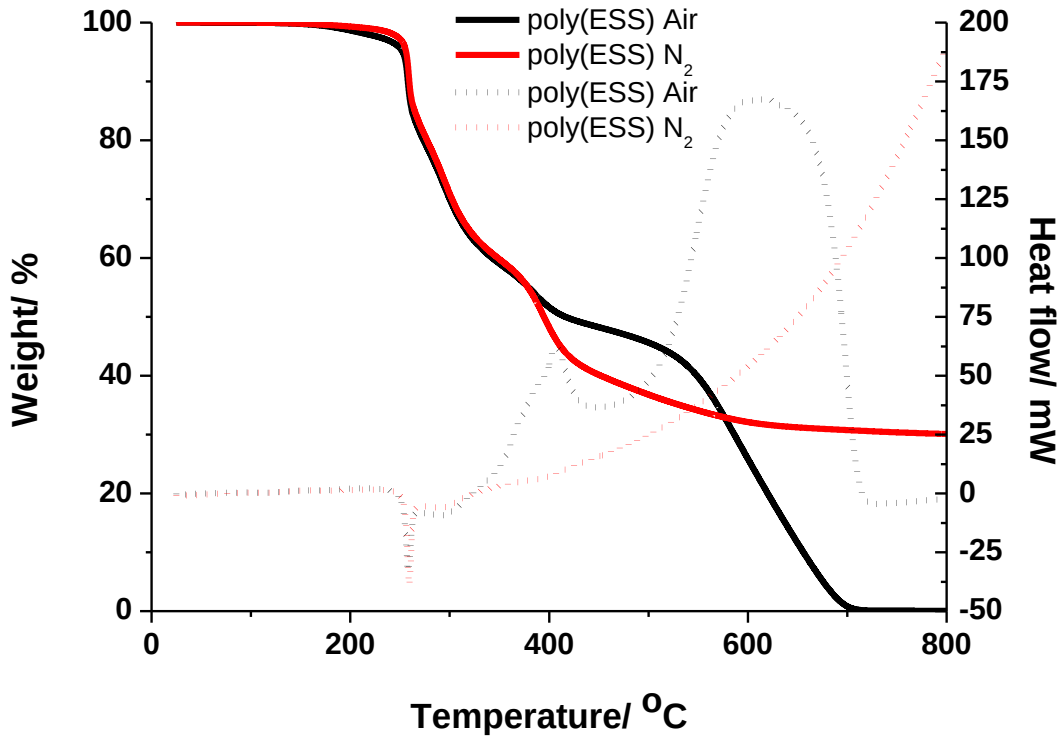

Figure 2.9. TGA and DSC traces for bulk polymer poly(2.4) under air (black line) and nitrogen (red line) atmospheres, from 23-800 ºC at a heating rate of 10 ºC/min. Complete line is TGA traces, dotted line is DSC traces.

2.4.3.1. TGA and DSC of poly(ESS) in air

Jiang *et al* studied the degradation of poly(sodium 4-vinylbenzenesulphonate) using TGA.[32] Both Jiang *et al*[32] and Nasef[33] studied the degradation of poly(sodium 4-vinylbenzenesulphonic acid). The results in their papers indicated that after removal of residual moisture the first loss at 300 ºC is caused from homolytic cleavage of the

sulphonate or sulphonic acid group that releases SO_2 and H_2O. Styrene depolymerisation occurred at 400-490 ^oC. Jiang *et al* showed that partial degradation of sulphonic acid groups occurs as IR of the volatiles indicated remaining sulphonates up to 550 ^oC.

We assign the degradation of poly(2.4) as follows. The weight loss begins with thermolysis of ethyl radicals at 258-260 ^oC and this cleavage is in agreement with the endothermic DSC peak that is shown occurring at the same temperature. Following the ethyl loss, partial homolytic degradation of the sulphonate groups (bond dissociation energy of 259 kJ/mol) occurs from 260-380 ^oC decomposing into SO_2 as well as H_2O. Sulphonic acid and sulphonated polymers have been shown to only partially cleave the sulphonate groups[32] so some sulphur based styrene chains will still exist up to 550 ^oC. This sulphonate cleavage from the polymer chains results in styrene radicals and degradation of the polymer chain will release styrene and various dimers, trimers etc due to hydrogen transfer and back-biting from the polymer backbone from 350-440 ^oC (this is discussed for poly(styrene) in **Section 2.4.7.1.1.**). The weight loss from 440-700 ^oC is due to the decomposition of the carbon and sulphur based compounds that form by the degradation of the polymer chains in the presence of SO_2. Oxidative degradation also occurs in air atmospheres at 400-700 ^oC. The exothermic peak in the DSC spectrum at 410 ^oC and again at 550-700 ^oC could be caused by both crystallisation of polymer chains and oxidative degradation or combustion respectively.

Due to the degradation mechanisms discussed above and the complex mechanism of degradation the exact weight losses for each section are difficult to determine. Many degradation pathways may combine into one steady weight loss as is shown between 260-400 ^oC. When we study the weight loss percentages we notice that the weight losses are in close agreement to the predicted degradation pathways proposed

earlier. The weight loss at 258-260 ^{o}C is approximately ~13% which is similar to the theoretical weight loss of 13.7% for the loss of an ethyl radical. The weight loss from 260-440 ^{o}C shows a further weight loss of ~34% which accounts for the SO_3 group (theoretical loss of 37.2%) which may be lower than predicted due to partial cleavage and possible recombination with other radicals. The remaining 50% weight loss from 440-700 ^{o}C agrees with the weight loss of styrene degradation products. The higher temperatures required are likely due to the formation of other products from such as decomposition of styrene in the presence of SO_2.

Recently Hasegawa *et al* studied the degradation of poly(2.4) grafted PEEK polymers[34] and similar TGA and DSC traces were shown when compared to the results for poly(2.3) and poly(2.4) and the data reported for poly(2.3) by Baek.

Due to the competing degradation pathways a multitude of products may form which could not be analysed with the TGA/DSC machine alone. Linking a TGA machine to pyrolysis-GC could help identify the degradation products and volatiles as reported by Gurman *et al* for poly(styrene).[35]

2.4.3.2. TGA and DSC of poly(ESS) in nitrogen

When we study the nitrogen TGA and DSC curves we notice the same endothermic peak at 410 ^{o}C. However, the two exothermic peaks are not present and the heat flow increased steadily until 800 ^{o}C. We noticed that sample still remained at 800 ^{o}C due incomplete combustion of the material and sulphur and carbon based compounds from SO_2 recombination.

2.4.4. Soap-free emulsion polymerisation of NSS and styrene

Polymer particles are typically synthesised using emulsion, dispersion and suspension polymerisation techniques (refer to **Chapter 1** for references). Emulsion

polymerisation was chosen due to size of the colloids that can be synthesised which is typically 50-1000 nm depending on whether surfactants are used (surfactants allow smaller particle sizes). Initially a 5 wt% latex was made was made using 2.1 and 2.3 (structures shown in **Scheme 2.1.**), styrene (2.5) and DVB (2.6). Addition of 2.1 introduced sulphonate surface charge for colloidal stability and controlled both particle sizes and dispersity. Structures of 2.5 and 2.6 are shown in **Figure 2.10.** along with the initiator potassium persulphate (KPS, referred to as 2.7 throughout). This polymerisation was carried out using a reactor at 70 ^{o}C. The exact procedure for synthesis of this latex is described in **Section 2.3.4** with details of the reactor setup in **Section 2.3.2.**.

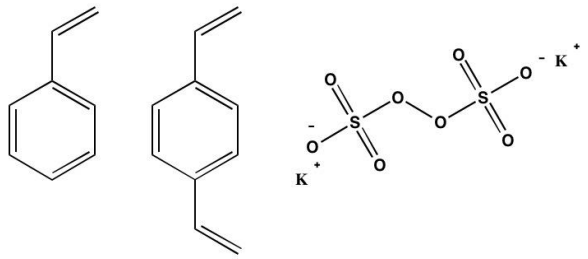

Figure 2.10. Structures of (left to right) styrene, di-vinylbenzene and potassium persulphate.

Scanning electron microscopy (SEM) samples were prepared by diluting the latex sample to ~0.1 wt% solids. The diluted latex was dried onto a silicon wafer SEM stub and the samples were coated using graphite or platinum to provide a uniform conductive coating (see **Section 2.3.6.2.** and **2.3.6.3.** for further details on SEM preparation and analysis using ImageJ). SEM images for the poly(2.5-*co*-2.3-*co*-2.6) copolymer particles are shown in **Figure 2.11.** where it can be seen that the particles are relatively monodisperse with an average particle size of 117 nm (standard deviation – s.d. = 6.1 nm) and a coefficient of variation (CV) of 5.2% (analysed using ImageJ).

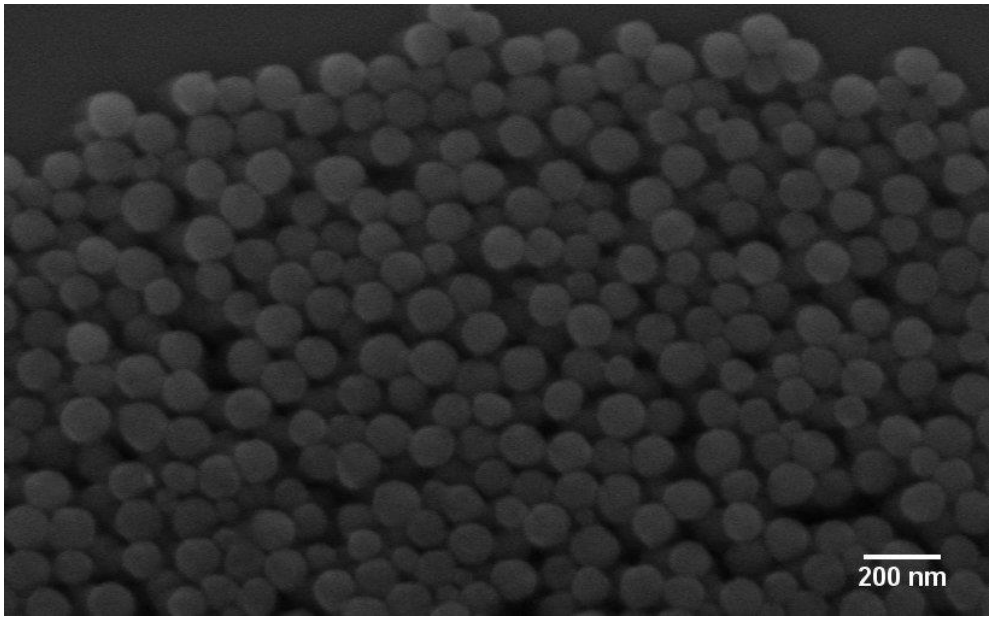

Figure 2.11. SEM micrographs for 10 wt% solids batch soap-free emulsion copolymerisation colloids of styrene with NSS initiated using KPS at 70 ^{o}C. Scale bars is 200 nm.

Due to the synthesis of 2.3 from 2.2 requiring more stages for purification we decided to continue using the monomer 2.4 as it could be made in much larger quantities and requiring simpler purification stages. The second reason for the use of 2.4 over 2.3 was due to the 2.3 hydrolysing at a lower temperature (185 ^{o}C versus 258-260 ^{o}C) and this could affect the stability of the latex (**Section 2.4.8.** discusses hydrolysis and partial hydrolysis can occur at much lower temperatures). The monomer 2.3 was easier to use in emulsion polymerisation due to it being solid and by using monomer 2.4 instead of 2.3 did show a disadvantage in emulsion polymerisation (discussed in **Section 2.4.6.1.**).

2.4.5. Soap-free emulsion polymerisation of ESS and styrene

To allow the incorporation of monomer 2.4 into polymer colloids a number of criteria must be fulfilled. These requirements will be discussed for the copolymerisation of 2.4 with 2.5 as this is the comonomer we are interested in. The monomer 2.5 was chosen as the comonomer alongside 2.4 due to the similarity in structure and the high T_g value of 100 ^{o}C for poly(2.5) enabling easier imaging using SEM.

2.4.5.1. ESS solubility in water

The first requirement for the monomer 2.4 is that it must exhibit sufficient water solubility. Typically three categories of solubility exist, highly soluble monomers such as acrylonitrile (water solubility 70 g/L), monomers of medium solubility such as acrylates (methyl methacrylate 16 g/L) and practically insoluble monomers such as styrene (0.30 g/L).[36] A previous member on the Bonlab group studied the water solubility of 2.4 and reported a value of 0.30 g/L at 25 ºC[37] which is similar to that of styrene.[36] A SciFinder Scholar ACD labs prediction search gave a slightly higher water solubility value of 0.57 g/L at pH 7 and 25 ºC[38] meaning that 2.4 is considered sparingly soluble in water. The ACD labs from SciFinder predicted a water solubility of styrene to be 0.3 g/L,[38] so 2.4 is twice as soluble as styrene but still relatively insoluble in water. Due to the similarities in water solubility we would expect monomer 2.4to be useful in emulsion polymerisation.

2.4.6. Synthesis of protected sulphonate particles via soap-free emulsion polymerisation

2.4.6.1. Density issues of ESS monomer

The first hindrance with performing soap-free emulsion copolymerisation using 2.4 and 2.5 was the density difference between the two monomers. Monomer 2.5 has a density much lower than water (0.909 g/cm^3)[38] but 2.4 has a density of 1.179 g/cm^3 (as predicted using SciFinder Scholar).[38] The monomer 2.4 sank to the bottom of the reactor and remained below the rotor blades that were approximately 1 cm from the bottom. Due to the high density of monomer 2.4 it did not mixed with 2.5 or the aqueous phase and this led to coagulation at the bottom while the 2.5 polymerised into poly(2.5) colloids. Potentially a slight amount of monomer 2.4 would have polymerised

due to slight water solubility but not enough when compared with 2.5. In order to allow incorporation of 2.4 alongside 2.5 a stirrer bar was used in a round bottomed flask (RBF). The stirrer bar forced the 2.4 upwards so that it was mixed into the aqueous phase thus increasing the surface area and helping the 2.4 to solubilise into the aqueous phase.

2.4.6.2. Copolymer particle synthesis

Using 2.1, 2.4, 2.5 and 2.6 in soap-free emulsion copolymerisation in water at 70 ^{o}C synthesised a 10 wt% solids latex. We added 1 wt% 2.1 based on total monomer content again to introduce sulphonate surface charge and controll particle sizes and dispersity. Using 2.1 decreased the polymerisation times for high conversion to be reached as shown with poly(2.1-*co*-2.5) colloids *via* emulsion polymerisation.[41] Using 2.1 in emulsion polymerisation with 2.5 changes the nucleation site to the aqueous phase, adds the gel effect and increases the number of particles thus affecting the rate of polymerisation. Initiation was carried out using 2.7 and detailed experimental conditins are reported in **Section 2.3.5.**. The ratio of the 2.4 to 2.5 was altered where up to 50 wt% 2.4 relative to styrene was used (see **Table. 2.1.**). A latex of pure poly(2.5) was also synthesised as a reference sample.

The soap-free emulsion copolymerisations of 2.4 and 2.5 were left to run overnight to ensure the highest conversion based on the half life of the initiator (2.7 has a half life at 70 ^{o}C of ~5 hours) and the final conversion, X_m, was analysed using gravimetric analysis. However, conversion was unreliable for the samples containing monomer 2.4 due to the relative boiling point of the 2.4 compared to 2.5. Typically gravimetry analysis is useful for low boiling point monomers (the boiling point of 2.5 is 146 ^{o}C but the predicted boiling point for 2.4 is 342+/-21 ^{o}C according to a Scifinder scholar search).[38] Conversion would have also been much lower than expected to due to

the reactor conditions (using an RBF over a reactor) where coagulation on the stirrer bar was strongly visible for the 10:90 wt% poly(2.4-*co*-2.5) sample. Coagulum was also visible on the other latex samples but less than the 10:90 wt% latex sample and for the above reasons conversion isn't reported.

Table 2.1. Relative quantities of ingredients for the synthesis of poly(2.4-*co*-2.5) latexes and poly(2.5) reference.

Sample	2.5 (g)	2.4 (g)	2.6 (g)	2.1 (g)	$NaHCO_3$ (g)	H_2O (ml)	2.7 (g)
Reference poly(2.5)	10.0912	0.00	0.20	0.10	0.10	90	0.10
5.0:95 wt% poly(2.4-*co*-2.5)	9.5948	0.5119	0.20	0.10	0.10	90	0.10
10:90 wt% poly(2.4-*co*-2.5)	9.5456	1.0060	0.20	0.10	0.10	90	0.10
30:70 wt% poly(2.4-*co*-2.5)	7.0125	3.0005	0.20	0.10	0.10	90	0.10
50:50 wt% poly(2.4-*co*-2.5)	5.0235	5.0031	0.20	0.10	0.10	90	0.10

All polymerisations were carried out at 70 ^{o}C. (a) Initiator 2.7 was dissolved into 1 ml of DDI H_2O for injection.

The poly(2.5) and poly(2.4-*co*-2.5) latexes were cleaned and purified using dialysis where the water was changed thrice daily to remove impurities and starting materials before further analysis was done.

2.4.6.3. Particle analysis – dynamic light scattering

Dynamic light scattering (DLS) was used to measure the hydrodynamic diameter (Z_{Ave}) of the colloidal particles. The DLS measurements are shown in **Table 2.2.** where each size measurement was an average of 10 sub-runs of 6 s each giving a total acquisition time of 1 minute per sample. Each sample was analysed three to five times and the average was calculated. Sample preparation is reported in experimental **Section 2.3.6.1.**.

Table 2.2. DLS size analysis of poly(2.4-*co*-2.5) and poly(2.5) latexes.

Sample	Z_{Ave} (nm)	PDI
Reference poly(2.5)	129.1	0.041
5.0:95 wt% poly(2.4-*co*-2.5)	129.7	0.043
10:90 wt% poly(2.4-*co*-2.5)	104.0	0.032
30:70 wt% poly(2.4-*co*-2.5)	195.0	0.009
50:50 wt% poly(2.4-*co*-2.5)	184.2	0.022

DLS measurements carried out at 25 ^{o}C and averaged from 5 measurements.

From the DLS measurements we notice that the hydrodynamic size decreases when only 10 wt% 2.4 is used (compared to the reference poly(2.5) colloids). The samples containing 30 wt% and 50 wt% 2.4 show roughly a 50% increase in hydrodynamic diameter when compared to the reference. A possible reason for the increase in size could be due to partial hydrolysis of the ethyl group. Hydrolysis has been shown to occur at 95 ^{o}C when heated in water for 2-3 days (see section discussing hydrolysis in **Section 2.4.8.**) and Kamogawa et al reported the hydrolysis of aromatic functionalised sulphonate esters occurring at 20 ^{o}C.[52] Therefore, heating of the emulsion to 70 ^{o}C could cause partial hydrolysis to occur over the polymerisation times studied. Cleavage of the ethyl group from 2.4 would cause a sulfonic acid group to form that could affect the affinity of the polymer chains for the aqueous phase. The acidic sulfonic acid group would cause electrostatic (or electrosteric) stabilisation to influence the double layer hydration sphere around the colloids by hydrogen bond.

The poly dispersity index (PDI) of all samples shown in **Table 2.2.** are very low. This is in contrast to using 2.1 where the PDI would have increased dramatically above 2.6 wt% (see Sect**ion 2.2.2.1.** and **Chapter 3** for references). By protecting the monomer 2.1 we achieved greater control over the polymerisation nucleation due to the lower solubility of 2.4 compared to 2.1 in water.

2.4.6.4. Particle analysis – scanning electron microscopy

As we can see from the SEM images shown in **Figure 2.12.** the particles have a mixture of different morphologies as the amount of 2.4 alters. The reference poly(2.5) particles are monodisperse with smooth spherical surfaces. The reference colloids also exhibited Bragg diffraction due to the hexagonal packing that shows upon drying (**Figure 2.12-A.**).

When 5-10 wt% of monomer 2.4 was incorporated into colloidal particles with 2.5 the dispersity broadened and the particles appeared "patchy" in selected surface regions (see **Figure 2.12-B.** and **2.12-C.**). This morphology effect was also observed for the 30 and 50 wt% 2.4 samples (see **Figure 2.12-D.** and **2.12-E.**). However, samples containing 30 wt% and 50 wt% 2.4 showed monodisperse sizes and exhibited Bragg diffraction on drying. A few possible ideas for these changes in shape and morphology are discussed below and represented visually in **Figure 2.13**.

Random copolymerisation between 2.4 and 2.5 could cause copolymer chains to orientate and pack differently inside the particles depending on the relative ratios of poly(2.4) to poly(2.5) in each chain. Due to the increased reactivity of 2.4 the copolymer may have sections of block structure with poly(2.4) sections followed by poly(2.5) sections. The more hydrophilic poly(2.4) sections have a greater affinity for the aqueous phase and may phase separate to the particle surface. Poly(2.5) is more hydrophobic and therefore would position at the core of the particle generating the patchy structures as shown (see **Figure 2.12-B.**).

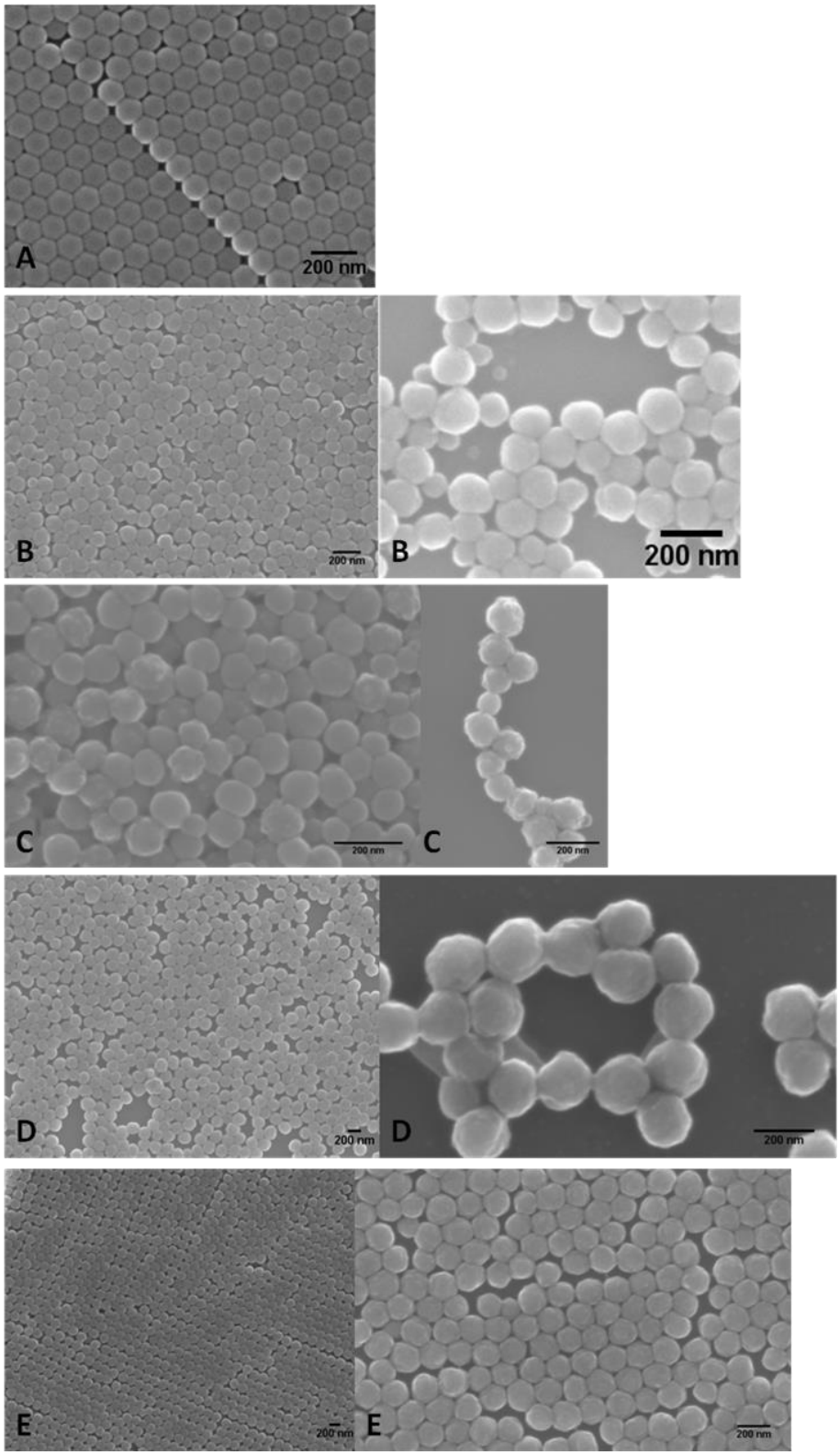

Figure 2.12. SEM micrographs for 10 wt% solids batch soap-free emulsion copolymerisation colloids, A) reference poly(2.5), B) 5.0:95 wt% poly(2.4-*co*-2.5), C) 10:90 wt% poly(2.4-*co*-2.5); D) 30:70 wt% poly(2.4-*co*-2.5) and E) 50:50 wt% poly(2.4-*co*-2.5). All scale bars 200 nm.

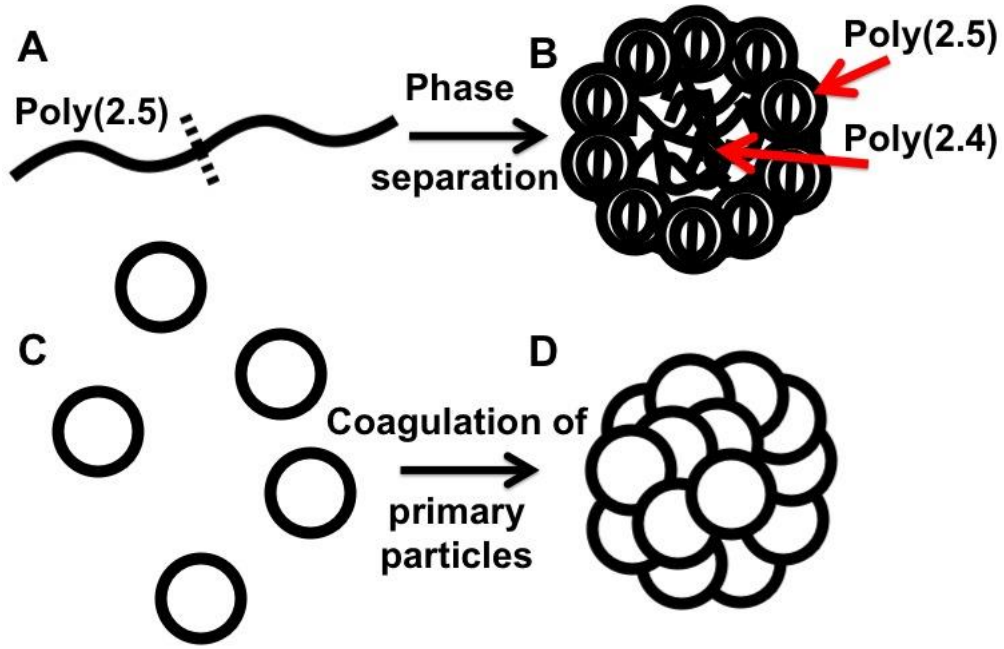

Figure 2.13. Figure showing possible morphology structures from the soap-free emulsion copolymerisation of ESS and styrene. A) formation of block copolymers chains, B) assembly of block copolymer chains and phase separation, C) formation of crosslinked primary particles, D) coagulation of crosslinked primary particles.

Further explanation could be caused from partial hydrolysis of the 2.4 both before, during or after copolymerisation. Hydrolysis would greatly alter the relative hydrophobicity of the polymer that forms and the combination of hydrolysed 2.4 sections and hydrophobic 2.5 sections could cause the patchy structures as shown. Hydrolysis would have been suppressed due to the sodium hydrogen carbonate buffer present in the reaction but hydrolysis can occur even without base being present as shown by Hasegawa[34] and Chen (reference in **Chapter 1**).[53]

Another mechanism could be caused from the coagulative nucleation mechanism. Hansen-Ugelstad and Fitch-Tsai (HUFT theory) and Feeney *et al* (see **Chapter 1** for references) explained homogeneous nucleation and coagulative nucleation mechanisms of primary particles under soap-free conditions. They proposed that unstable primary particles formed early in the reaction aggregate to form stable colloids. This coagulative nucleation mechanism could result in patchy structures

particles due to the incorporation of 2.7 crosslinker that would inhibit the ability for the interfacial tension to reduce the surface area (see **Figure 2.12-D.**).

When low amounts of 2.4 are copolymerised with 2.5 the primary particles may have different amounts of 2.4 and this could affect the coagulative nucleation mechanism. Some particles might have gained sufficient charge to be colloidally stable or hydrolysed during the copolymerisation generating a charged sulpfonic surface charge. Other primary particles might not have sufficient surface charge and will coagulate with many primary particles and lead to larger particle sizes. As the particles grow from further polymerisation the final sizes and dispersity would have been affected by this nucleation period. As the amount of 2.4 increases the cogulation of primary particles would be more equal which would lead to monodisperse final particle sizes.

The factors discussed abovecould explain why the morphology changed from a smooth morphology for that of poly(2.5) to a patchy morphology for the samples containing poly(2.4). These theories could also explain why the dispersity of the samples changed when low (5.0-10) and high (30-50) wt% of 2.4 was added.

The diameters of the poly(2.5) and poly(2.4-*co*-2.5) samples were measured using ImageJ (ImageJ analysis is described in experimental **Section 2.3.**). The results from ImageJ analysis are shown in **Table 2.3.** detailing the average particle sizes, the s.d. and the CV. The particle sizes measured using SEM were in close agreement to those measured earlier using DLS but the advantage of SEM is that exact sizes of the colloids without the hydration sphere can be measured. SEM also allowed the morphology and shaped to be analysed which is not possible using DLS.

Table 2.3. SEM analysis of poly(2.4-*co*-2.5) samples and poly(2.5) reference sample.

Sample	Average diameter (nm)	S.D. (nm)	CV (%)
Reference poly(2.5)	116.1	4.7	4.1
5.0:95 wt% poly(2.4-*co*-2.5)	113.0	24.1	21.3
10:90 wt% poly(2.4-*co*-2.5)	98.7	20.2	20.5
30:70 wt% poly(2.4-*co*-2.5)	189.1	15.0	7.9
50:50 wt% poly(2.4-*co*-2.5)	180.2	13.6	7.6

Average particle diameters, standard deviation and coefficient of variation calculated using ImageJ software. See Experimental Section 2.3.6.

2.4.7. ESS incorporation into poly(styrene) colloids

Determination of the amount of poly(2.4) relative to poly(2.5) into the colloids is important and using thermal analysis (TGA and DSC) we tried to qualitatively determine the amount of 2.4 incorporated in the samples. This method lacks the accuracy as elemental analysis but determination of monomer incorporation is an area of interest. The degradation pathway for poly(2.4) was studied in **Section 2.4.3.** using both TGA and DSC. By combining the degradation traces of poly(2.4) using TGA and DSC with those from poly(2.5) we can analyse of the percentage of 2.4 in the samples.

Arunbabu *et al* used TGA to analyse a series of poly(2.1-*co*-2.5) copolymers and showed that the level of 2.1 in the copolymer affected the degradation profile and correlation existed between the level of 2.1 in the polymer and the weight of char formed above 500 ^{o}C.[41] We did the same analysis method using poly(2.4-*co*-2.5) copolymer particles.

2.4.7.1. Thermal analysis of copolymer particles

2.4.7.1.1.TGA and DSC of poly(styrene) reference

A singular weight loss beginning at 380 ^{o}C and fully decomposing at 450 ^{o}C is shown for poly(2.5) as shown in **Figure 2.14.**. Poly(2.5) decomposes into 2.5, dimer, trimer, and tetramer with the evolution of 2.5 being most pronounced (typically 40-50

wt%).[54-56] The formation of toluene, benzene and methyl styrene from alternate decomposition pathways has also been shown for poly(2.5) by Gurman *et al*.[35] Poly(2.5) degradation has been studied by Yang *et al*[54] and Peterson *et al*[54] where the degradation pathways are discussed with the mechanisms for products formed. Degradation of the polymer chains occurs *via* end chain and random chain scission, intramolecular hydrogen transfer and bimolecular termination.[56] The DSC for poly(2.5) shows an endothermic peak at 407 ^{o}C and 420 ^{o}C for air and nitrogen respectively which is caused by polymer chain degradation. This is in agreement with the TGA trace degradation losses. The degradation trace of poly(2.5) in air shows an exothermic peak at 427 ^{o}C which is caused from oxidative degradation.[55]

2.4.7.1.2. TGA and DSC of poly(styrene-co-ESS) particles in Air

Freeze-drying of the samples prior to analysis allowed more accurate thermal analysis data due to the minimisation of the water loss peak. The 5.0:95 wt% and 10:90 wt% poly(2.4-*co*-2.5) colloids show a similar trace to that of poly(2.5) reference. A slight degradation for a ethyl group is observed (shown in **Figure 2.15.**) followed by a single weight loss at 360-410 ^{o}C due to styrene degradation (~95% loss for the 5.0:95 wt% poly(2.4-*co*-2.5) sample and 89% loss for the 10:90 wt% poly(2.4-*co*-2.5) sample). However, we do notice that residual weight remained above 420 ^{o}C indicating the formation of sulphur based fragments with carbon and this was not observed for poly(2.5). When the DSC traces are studied for the 5.0:95 wt% and 10:90 wt% poly(2.4-*co*-2.5) samples (**Figure 2.16.**) we observed a similar trend as shown from the poly(2.5) reference. No visible hydrolysis peak was observed at 260 ^{o}C in the DSC traces and this is in agreement with the lack of weight loss observed in the TGA degradation traces.

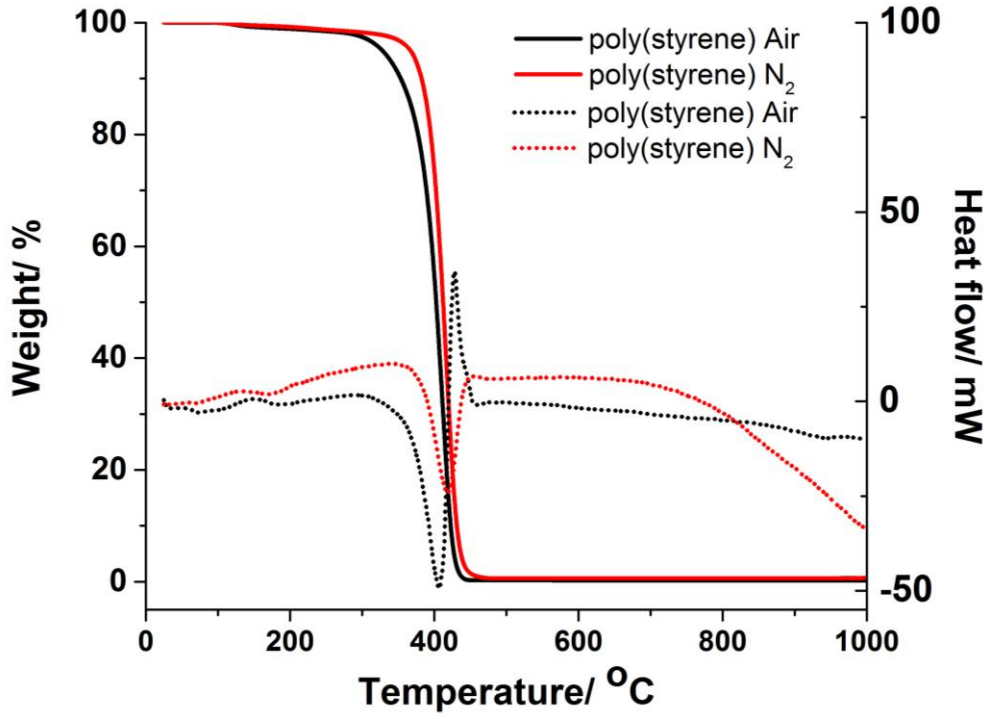

Figure 2.14. TGA and DSC traces for 10 wt% solids poly(2.5) colloids under air and nitrogen atmospheres, 23-1000 °C at a heating rate of 10 °C/min. Complete line is TGA, dotted line is DSC.

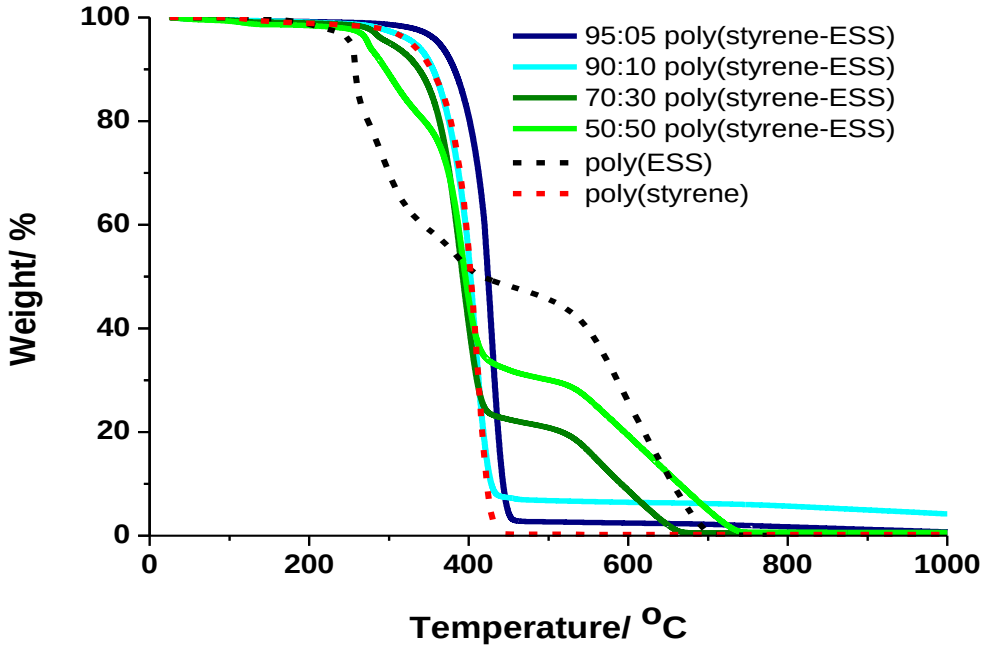

Figure 2.15. TGA traces for 10 wt% solids poly(2.4-*co*-2.5) colloids under air atmosphere, 23-1000 °C at a heating rate of 10 °C/min. Complete line is poly(2.4-*co*-2.5) colloids, dotted line is poly(2.4) and poly(2.5).

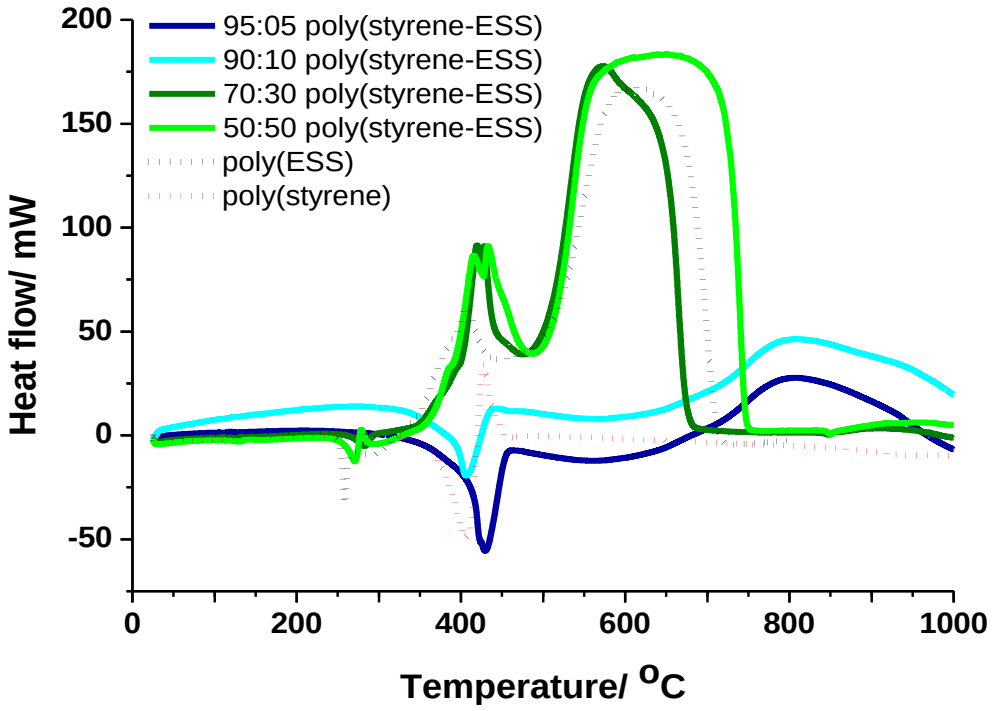

Figure 2.16. DSC traces for 10 wt% solids poly(2.4-*co*-2.5) colloids under air atmosphere, 23-1000 °C at a heating rate of 10 °C/min. Complete line is poly(2.4-*co*-2.5) colloids, dotted line is poly(2.4) and poly(2.5).

The 30:70 wt% poly(2.4-*co*-2.5) sample is similar to the poly(2.5) trace but a slight degradation step is observed at 280 °C (only 3% weight loss). This is significantly lower than we would expect if 30 wt% of 2.4 was incorporated into the colloids (an ethyl group loss of 6.3 wt% would be expected). Based on the hydrolysis stage we clearly incorporated less 2.4 that we had expected but the weight loss does show that incorporation must have occurred. We also note that a higher thermal degradation stability that was observed after 410 °C which also shows incorporation of sulphur from 2.4. When the 50:50 wt% poly(2.4-*co*-2.5) sample was studied we notice a weight loss curve that is between the poly(2.4) and poly(2.5) traces. The theoretical weight loss for the 50:50 wt% poly(2.4-*co*-2.5) sample would be 9.2 % for ethyl cleavage. When we study the TGA trace we notice a 22% weight loss up to 370 °C. This is likely due to thermolysis and partial cleavage of the sulphonate groups as shown with other sulphonated polystyrene polymers.[32] For poly(2.4) we do not detect a sharp drop in

weight from 250-400 ^{o}C but a more gradual weight loss. Assignment of the degradation trace is difficult especially from TGA measurements alone. When we study the DSC traces we notice an endothermic peak at 260 ^{o}C indicating that thermolysis is occurring (this temperature correlated with the TGA trace weight loss).

Between the temperature range 360-410 ^{o}C a weight loss of 69% is shown for the 30:70 wt% poly(2.4-*co*-2.5) sample and 45% for the 50:50 wt% poly(2.4-*co*-2.5) sample. This weight loss shows the degradation of poly(2.5). The differences in the weight loss of monomer 2.5 may bee due to monomer loss during polymerisation, coagulation and potential reactions occurring as monomer gets degraded in the presence of oxygen and SO_2. After the degradation of 2.5 from the samples we notice an exothermic peak in the DSC trace that could be due to further polymerisation of radicals to form the thermally stable sulphur products that degrade after 550 ^{o}C. From 410-550 ^{o}C the 30:70 wt% and 50:50 wt% poly(2.4-*co*-2.5) colloids showed a significant plateau region, this was also noticed earlier for the poly(2.4) sample (discussed in **Section 2.4.3.**). The amount of product that remained up until 550 ^{o}C could be largely related to the amount of sulphonate groups in the sample and that is dependant on the amount of 2.4 incorporated. At 410 ^{o}C the 30:70 wt% poly(2.4-*co*-2.5) sample had 23% weight remaining and the 50:50 wt% poly(2.4-*co*-2.5) sample had approximately 35% remaining. In comparison sample poly(2.4) showed 50% mass remaining at 410 ^{o}C. **Figure 2.17.** shows a graph of the amount of 2.4 in the sample versus the amount of sample remaining at 500 ^{o}C. We can see a straight line graph for both samples heated under an air and nitrogen atmosphere. Due to this linear correlation between the percentage of monomer 2.4 in the sample with the remaining weight at 500 ^{o}C it appears that calculation of the ratio of monomer 2.4 to 2.5 could be possible. So if a sample had

a specific weight remaining at 500 °C then we could quantify the relative weight of monomer 2.4 in the sample.

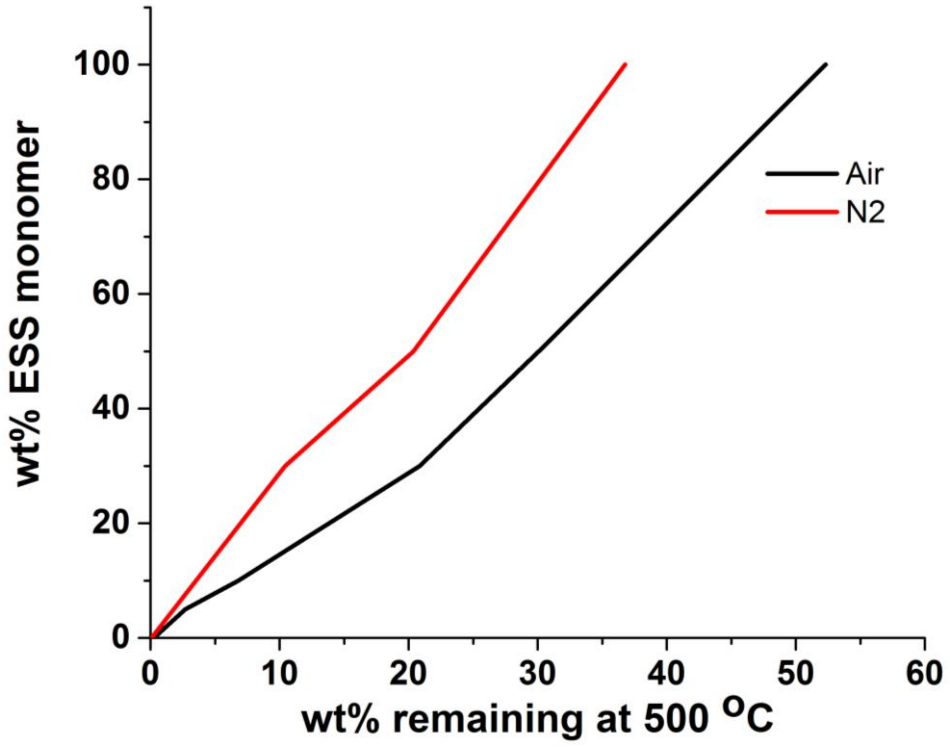

Figure 2.17. Graph showing the relationship between amount of ESS monomer in the sample against the weight percent remaining after heating to 500 °C in the TGA machine.

While analysis of the products was not available with the thermal analysis equipment available so the product structures could not be determined. The 30 wt% and 50 wt% samples show a further exothermic peak from 550-700 °C indicating the combustion and oxidative degradation of the samples.

2.4.8. Hydrolysis of ESS incorporated poly(styrene) colloids

The combined TGA and DSC traces (**Figure 2.14.** and **2.15.**) showed that the first degradation product is the thermolysis of ethyl radicals. In this section we wanted to study the effects of hydrolysis on the sample. Studies have shown that ethyl, butyl and neopentyl protecting groups can be cleaved under specific conditions. Monomer 2.3 was shown to cleave in 30 minutes at 150 °C by Okamura *et al*[27] and Baek.[28] They showed that using trimethylsilyl iodide at room temperature could cause thermolysis.

Woeste *et al*[29] and Biesalski *et al*[57] showed that base catalysed hydrolysis could occur for 2.4 using ammonium carbonate at 50-70 ºC for <60 hours. Hasegawa *et al*[34] and Chen *et al*[53] both reported hydrolysis at 95 ºC for 24 hours. Lienkamp *et al* used NaOH at 80 ºC for 3 hours to hydrolyse the 2.4.[58] Sikkema[63] showed the use of sodium azide in causing hydrolysis and summarised previous work using other bases for base catalysed hydrolysis.[59] The review on protecting groups by Miller showed a variety of hydrolysis methods involving sodium iodide, piperidine, sodium azide, sodium hydroxide, Fe, HBr and BBr_3.[25] All hydrolysis methods showed different hydrolysis capability for different protected sulphonate esters where some showed complete hydrolysis, some hydrolysed partially and many did not hydrolyse at all.

Studying hydrolysis of the poly(2.4-*co*-2.5) functionalised particles was needed to confirm whether selective hydrolysis of the ethyl group could occur. We decided to use a slight modification from previous literature studies and decided to use temperature. In order to study hydrolysis of colloidal particles we decided to heat the sample to a high temperature without the use of base. This was tested using an Autoclave (high temperatures under constant pressure to prevent boiling of water). The sample was heated to 220 ºC in the autoclave for ~8 hours and TGA and DSC traces were measured.

2.4.8.1. TGA and DSC of poly(styrene-co-ESS) colloids after thermolysis

The TGA and DSC data for the 30:70 wt% poly(2.4-*co*-2.5) sample after autoclaving for ~8 hours is shown in **Figure 2.18.**. We can clearly see that the majority of both the TGA and DSC spectra are identical to the sample before autoclaving meaning that the sample has not altered or degraded. The main noticeable difference is at 283 ºC. Before autoclaving we observed a 3% drop in weight due to ethyl cleavage and after autoclaving we notice this drop in mass had disappeared. This change in

weight loss also correlates well with the DSC trace. The original DSC trace showed a small endothermic peak at 280 °C and after autoclaving this endothermic peak has disappeared. This shows that hydrolysis has probably occurred under the conditions of the autoclave. A drop in weight also occurs up to 120 °C which is attributed to the loss of water. Nasef,[33] Hasegawa *et al*[34] and Suleiman *et al*[60] observed this same loss of weight from poly(styrene sulphonic acid) caused by the hydroscopic nature of sulphonic acid groups retaining moisture.

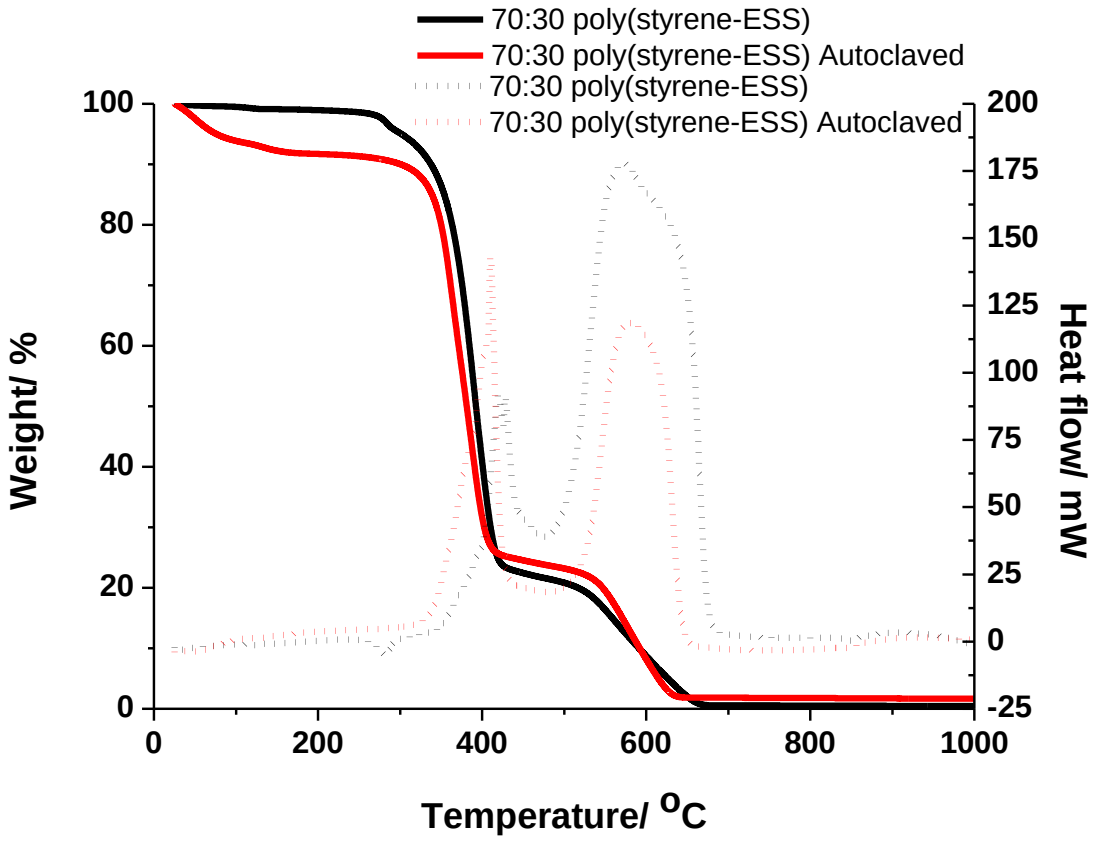

Figure 2.18. TGA and DSC traces for 10 wt% solids 30:70 wt% poly(2.4-*co*-2.5) colloids under air atmosphere before and after ~8 hours in an Autoclave at 240 °C. Heating range 23-1000 °C at a heating rate of 10 °C/min. Complete line is TGA curves and the dotted line is the DSC traces.

2.5. Conclusion

In this chapter we discussed the synthetic methodology for the preparation of intermediate 4-vinylbenzenesulfonyl chloride synthesised from precursor 4-vinylbenzenesulphonate (NaSS). We then report the synthesis of two protected sulphonate monomers neopentyl 4-vinylbenzenesulphonate (NSS) and ethyl 4-vinylbenzenesulphonate (ESS). NSS synthesis required column purification but ESS was synthesised with simpler purification procedures (filtration). Bulk polymers of poly(NSS) and poly(ESS) were synthesised and subjected to TGA and DSC analysis to study the degradation stages and showed a loss of the ethyl group at 185-188 ^{o}C for NSS and 258-260 ^{o}C for ESS. NSS was tested using soap-free emulsion copolymerisation with styrene and DVB but due to the lower hydrolysis temperature we continued the experiments with ESS (ESS was easier to synthesise in bulk quantities as well)

Batch soap-free emulsion copolymerisation of ESS alongside styrene and DVB was carried out using KPS initiator to synthesise a 10 wt% latex composing of 5.0, 10, 30 and 50 wt% of ESS monomer relative to styrene. The particle sizes were all within 100-200 nm as measured using DLS and SEM. Larger particle sizes were observed for the 30 wt% and 50 wt% poly(ESS-*co*-styrene) latexes with very low dispersity. Using SEM we were able to visualise broader particle size distributions for the 5.0 and 10 wt% poly(ESS-*co*-styrene) colloids caused by secondary nucleation.

Following the synthesis of polymer particles incorporating ESS monomer TGA/DSC analysis was used to determine the relative loadings of ESS monomer in the latex particles. The results indicated that the loadings were lower than the predicted values based on the amount of ESS added due to mixing and coagulation problems.

However, the results did indicate that ESS monomer was incorporated into latex particles due to the weight loss curves shifting between the traces for pure poly(styrene) and poly(ESS). The formation of high temperature residue above 500 ^{o}C also indicated the formation of sulphur based products and was used to determine the relative percentage of ESS incorporated into the colloids.

Hydrolysis or thermolysis of the protected particles was carried out by high temperature heating (240 ^{o}C) in an autoclave for ~8 hours. TGA and DSC analysis indicated that no more degradation of the ethyl group occurred and that the polymer particles had been hydrolysed releasing their protecting group.

2.6. References

1. Hazarika M, Malkappa K, Jana T, Particle-size-dependant properties of sulphonated polystyrene nanoparticles, *Polym. Int.*, 2012; **61**:425-1432

2. Orler EB, Dorie JZ and Robert BM, Sulfonation of syndiotactic polystyrene for model semicrystalline ionomer Investigations, *Macromolecules*, 1993; **26**:5157–5160

3. Kućela F, Jańćář J, Homogeneous and heterogeneous sulphonation of polymers: a review, *J. Polym. Eng. Sci.*, 1998; **38**:783-790

4. Peula JM, Fernández-Barbero A, Hidalgo-Álvarez R, de las Nieves FJ, Comparative study on the colloidal stability mechanisms of sulphonated latexes, *Langmuir*, 1997; **13**:3938-3943

5. Kim JH, Chainey M, El-Aasser MS, Vanderhoff JW, Preparation of highly sulphonated polystyrene model colloids, *J. Polym. Sci. Polym. Chem.*, 1989; **27**:3187-3199

6. Juang MS-D, Krieger IM, Emulsifier-free emulsion polymerization with ionic comonomer, *J. Polym. Sci.: Polym. Chem. Ed.*, 1976; **14**:2089-2107

7. Sunkara HB, Jethmalani JM, Ford WT, Synthesis of crosslinked poly(styrene-*co*-sodium styrenesulphonate) Latexes, *J. Polym. Sci. Polym. Chem.*, 1994; **32**:1431-1435

8. Kim JH, Chainey M, El-Aasser MS, Vanderhoff JW, Emulsifier-free emulsion copolymerization of styrene and sodium styrene sulphonate, *J. Polym. Sci. Polym. Chem.*, 1992; **30**:171-183

9. Peula-Garcia JM, , Hidalgo-Álvarez R, de las Nieves FJ, Colloid stability and electrokinetic characterization of polymer colloids prepared by different methods, *Colloid Surf. A.*, 1997; **127**:9-24

10. de las Nieves FJ, Daniels ES, El-Aasser MS, Electrokinetic characterization of highly sulphonated polystyrene model colloids, *Colloid Surf.*, 1991; **60**:07-126

11. Zhao B; Brittain WJ, Polymer brushes: surface immobilized macromolecules. *Prog. Polym. Sci.*, 2000; **25**:677–710.

12. Minko S, Chapter 11: Grafting on solid surfaces: "grafting to" and "grafting from" methods, Polymer Surfaces and Interfaces, Stamm M, Springer, 2008

13. Barbey R, Levanant L, Paripovic D, Schwüver N, Sugnaux C, Tugulu S, Klok HA, Polymer brushes *via* surface-initiated controlled radical polymerization: synthesis, characterization, properties, and applications, *Chem. Rev.*, 2009; **109**:5437–5527

14. Advincula RC, Surface initiated polymerization from nanoparticle surfaces, *J. Disp. Sci. Technol.*, 2003; **24**:343-361

15. Rühe J, Ballauff M, BiesalskiM, Dziezok P, Gröhn F, Johannsmann D, Houbenov N, Hugenberg N, Konradi R, Minko S, Motornov M, Netz RR, Schmidt M, Seidel C, Stamm M, Stephan T, Usov D, Zhang H, Polyelectrolyte brushes, *Adv. Polym. Sci.*, 2004; **165**:79-150

16. Su N, Li HB, Zheng HM, Yi SP, Liu XH, Synthesis and characterization of poly(sodium-*p*-styrenesulphonate)/modified SiO_2 spherical brushes, *Polym. Letters*, 2012; **6**:680-686

17. Chen X, Randall DP, Perruchot C, Watts JF, Patten TE, von Werne T, Armes SP, Synthesis and aqueous solution properties of polyelectrolyte-grafter silica particles by surface-initiated atom transfer radical polymerization, *J. Colloid Interf. Sci.*, 2003; **257**:56-64

18. Lei z, Ren N, Li Y, Li N, Mu B, FeO/SiO-g-PSStNa polymer nanocomposite microspheres (PNCMs) from a surface-initiated atom transfer radical polymerization (SI-ARTP) approach for pectinase immobilization, *J. Agric. Food Chem.*, 2009; **57**:1544-1549

19. Barsbay M, Güven O, Davis TP, Barner-Kowollik C, Barner L, RAFT- mediated polymerization and grafting of sodium 4-styrenesulphonate from cellulose initiated *via* γ-radiation, *Polymer*, 2009; **50**:973–982

20. Alzhrani A, PhD Thesis, Fabrication of anisotropic polymer colloid particles, 2011

21. Ballauff M, Nanoscopic Polymer particles with well-defined surface: synthesis, characterization, and properties, *Macromol. Chem. Phys.*, 2003; **204**:220-234

22. Wittemann A, Drechler M, Talmon Y, Ballauff M, High elongation of polyelectrolyte chains in the osmotic limit of spherical polyelectrolyte brushes: a study by cryogenic transmission electron microscopy, *J. Am. Chem. Soc.*, 2005; **127**:9688-9689

23. Hoffmann M, Lu Y, Schrinner M, Ballauff M, Dumbbell-shaped polyelectrolyte brushes studied by depolarized dynamic light scattering, *J. Phys. Chem. B.*, 2008; **112**:14843-14850

24. Kazemi F, Massah AR, Javaherian M, Chemoselective and scalable preparation of alkyl tosylates under solvent-free conditions, *Tetrahedron*, 2007; **63**:5083-5087

25. Miller SC, Profiling sulphonate ester stability: identification of complementary protecting groups for sulphonates, *J. Org. Chem.*, 2010; **75**:4632-4635

26. Chen CH, Hammett LP, Specific effects in acid catalysts by ion exchange resins. 5. resins prepared from styrenesulphonic esters, *J. Am. Chem. Soc.*, 1958; **80**:1329-1331

27. Okamura H, Takatori Y, Tsunooka M, Shirai M, Synthesis of random and block copolymers of styrene and styrenesulphonic acid with low polydispersity using nitroxide-mediated living radical polymerisation technique, *Polymer*, 2002; **43**:3155-3162

28. Baek KY, Synthesis and characterization of sulphonated block copolymers by atom transfer radical polymerisation, *J. Polym. Sci. Polym. Chem.*, 2008; **46**:5991-5998

29. Woeste G, Meyer WH, Wegner G, Copolymers of ethyl *p*-vinylbenzenesulphonate for the preparation of polyelectrolytes of reproducible ion content., *Die Makromolekulare Chemie*, 1993; **194**:1237-1248

30. Jeřábek K, Hanková L, Functional Polymers prepared from *p*-styrenesulphonyl chloride as the functional monomer, *Ind. Eng. Chem. Res.*, 1995; **34**:2598-2604

31. Kamogawa H, Kanzawa A, Kadoya M, Maito T, Nanasawa M, Conversion of carbonyl compounds *via* their polymeric sulphonylhydrazones into alkenes, alkanes, and nitriles, *B. Chem. Soc. Japan.*, 1983; **56**:762-764

32. Jiang DD, Yao Q, McKinney MA, Wilkie CA, TFA/FTIR studies on the thermal degradation of some polymeric sulphonic and phosphonic acids and their sodium salts, *Polym. Degrad. Stabil.*, 1999; **63**:423-434

33. Nasef MM, Thermal stability of radiation grafted PTFE-g-polystyrene sulphonic acid membranes, *Polym. Degrad. Stabil.*, 2000; **68**:231-238

34. Hasegawa S, Takahashi S, Iwase H, Koizumi S, Morishita N, Sato K, Narita T, Ohnuma M, Maekawa Y, Radiation-induced graft polymerisation of functional

monomer into poly(ether ether ketone) film and structure-property analysis of the grafted membrane, *Polymer*, 2011; **52**:98-106

35. Gurman JL, Baier L, Levin BC, Polystyrenes: a review of the literature on the products of thermal decomposition and toxicity, *Fire Mater.*, 1987; **2**:109-130

36. www.inchem.org (International programme on chemical safety (IPCS) and the Canadian centre for occupational health and safety (CCOHS)

37. Parker Q, MChem thesis, Synthesis and application of styrene sulphonate ester monomers in pickering emulsion polymerisation for the production of flame-retardant intumescent films, 2012

38. SciFinder scholar, *calculated using advanced chemistry development (ACD/labs) softwareV11.02(©1994-2012ACD/labs) (*https://scifinder.cas.org/scifinder/view/scifinder/scifinderExplore.jsf) Date accesed September 4th 2012

39. Siadat B, Lenz RW, Preparation of esters of styrene sulphonic acid and their emulsion copolymerization with isoprene, *J. Polym. Sci.: Polym. Chem. Ed.*, 1980; **18**:3273-3287

40. Odian G, Principles of polymerization, 4th Ed., John Wiley and Sons Inc, 2004

41. Arunbabu D, Sanga Z, Seenimeera KM, Jana T, Emulsion copolymerization of styrene and sodium styrene sulphonate: kinetics, monomer reactivity ratios and copolymer properties, *Polym. Int.*, 2009; **58**:88-96

42. Lewis FM, Walling C, Cummings W, Briggs ER, Mayo FR., Copolymerization. 4. effects of temperature and solvents on monomer reactivity ratios, *J. Am. Chem. Soc.*, 1948; **70**:1519-1523

43. Cameron GG, Esslemont GF, Solvent effects in free radical copolymerisation of styrene and methacrylonitrile, *Polymer*, 1972; **13**:435-438

44. Bontà G, Gallo BM, Russo S, Some kinetic aspects of radical copolymerisation: influence of the reaction medium on the reactivity ratios, *Polymer*, 1975; **16**:429-432

45. Kaim A, Oracz P, Solvent effects on true terminal reactivity ratios for styrene-methyl methacrylate copolymerisation system, *Polymer*, 1999; **40**:6925-6932

46. Matyjaszewski K, Handbook of radical polymerization., John Wiley and Sons Inc, 2002

47. Vanzo E, Marchessault RH, Stannett V, The solubility and swelling of latex particles, *Science*, 1965; **20**:62-71

48. Morton M, Kaizerman S, Altier MW, Swelling of latex particles, *J. Colloid. Sci.*, 1954; **9**:300-312

49. Daswani P, van Herk A, Solubility data of comonomer pairs relevant to aqueous-phase study in the emulsion copolymerization, *Dataset Papers in Materials Science*, 2013:5 pages

50. Maxwell IA, Jurja J, van Doremaele GHJ, German AL, Partial swelling of latex particles with monomers, *Die Makromolekulare Chemie*, 1992; **193**:2049-2063

51. Noël LFJ, Maxwell IA, German AL, Partial swelling of latex particles by two monomers, *Macromolecules*, 1993; **26**:2911-2918

52. Kamogawa H, Haramoto Y, Misaka Y, Asada Y, Ohno Y, Nanasawa M, Chemical release control: sulphonate esters from perfume and herbicide alcohols and *p*-styrenesulphonyl chloride, *J. Polym. Sci.: Polym. Chem. Ed.*, 1985; **23**:1517-1526

53. Chen J, Asano M, Maekawa Y, Yoshida M, Fuel cell performance of polyetheretherketone-based polymer electrolyte membranes prepared by a two-step grafting method, *J. Membrane. Sci.*, 2008; **319**:1-4

54. Yang M, Shibasaki Y, Mechanisms of thermal degradation of polystyrene, polymethacrylonitrile, and their copolymers on flash pyrolysis, *J. Polym. Sci. Polym. Chem.*, 1998; **36**:2315-2330

55. Peterson JD, Vyazovkin S, Wight CA., Kinetics of the thermal and thermo-oxidative degradation of polystyrene, polyethylene and poly(propylene), *Macromol Chem Physic*, 2001; **202**:775-784

56. Beyler CL, Hirschler MM, Chapter 7: thermal decomposition of polymers, The SFPE Handbook of Fire Protection Engineering; 3rd Ed, 2002

57. Biesalski M, Rühe J, Synthesis of a poly (*p*-styrenesulphonate) brush *via* surface-initiated polymerization, *Macromolecules*, 2003; **36**:1222-1227

58. Lienkamp K, Schnell I, Groehn F, Wegner G, Polymerization of styrene sulphonate ethyl ester by ATRP: synthesis and characterization of macromonomers for Suzuki polycondensation, *Macromol. Chem. Physic.*, 2006; **207**:2066-2073

59. Sikkema FD, PhD Thesis, Organic and inorganic biohybrid assemblies of the cowpea chlorotic mottle Virus, 1976

60. Suleiman D, Napadensky E, Sloan JM, Crawford DM, Thermo stability of highly sulphonated poly(styrene-isobutylene-styrene) block copolymers: effects of sulphonation and counter-ion substitution, *Thermochim. Acta.*, 2007; **460**:35-40

Chapter 3 - Nanogel decorated nanoparticles and functionalisation using thiol-Michael addition

3.1. Abstract

In this chapter we report the synthesis of hydrophobic and hydrophilic monodisperse seed particles produced using the soap-free emulsion polymerisation of styrenic and acrylic monomers. The seed particles were decorated using nanogel particles formed from di-, tri-, and penta-/hexa- functional crosslinking monomers. The decoration of the seed nanoparticles led to raspberry-like and core-shell latex particles with increased surface areas and roughness. SEM was used to visualise the morphology and sizes of the seeds and decorated nanoparticles. The effects of the seed hydrophobicity were investigated where hydrophilic seeds led to core-shell particles and hydrophobic seeds led to raspberry-like particles. Unreacted pendant vinyl groups were quantified and analysed using Raman microscopy and both infra-red and nuclear magnetic resonance were unable to prove vinyl group presence. Thiol-Michael addition reactions between the pendant vinyl groups and various charged thiols were accomplished using a nucleophilic amine catalyst. Post thiol-Michael addition a decrease in the percentage of vinyl groups was observed using Raman microscopy.

3.2. Introduction

In this chapter we aimed to synthesise decorated or core-shell type particles with increased surface area and a soft adhesive shell. We also wanted pendant vinyl groups to remain to post functionalise the colloidal particles where the vinyl groups could be reacted under ambient conditions to impart charged group functionality.

3.2.1. Decoration of nanoparticles with raspberry and core-shell type morphologies

Many studies have been done using seed latexes with the aim to create decorated or core-shell type particles. Many advantages exist for decorated particles including an increased surface area useful for catalysis or adhesion to a substrate, surface roughness or altered Tg's between the shell and seed polymers which affects the mechanical and physical properties post film formation. A variety of different morphologies of nanoparticles have been synthesised to date with extensive studies from the Okubo group. Example morphologies include core-shell,[1-10] raspberry,[8-14] popcorn,[10] confetti,[10,15] snowman,[10,15-16,20-22] golf ball like,[17] discs and polyhedral,[18] inverted core-shell particles[2-3,19] and dumbbell particles.[20-22] Examples of some of the above mentioned morphologies are shown in **Figure 3.1.**. Simulation and computational studies by Ferguson *et al* led to the conclusion that both thermodynamic and kinetic factors can play a crucial role in the synthesis of different morphologies.[23] It was reported that decreasing the seed radius, increasing solids content and the use of starved-feed conditions were the most important factors for preventing the formation of

secondary particles.[23] The formation of secondary particles in the polymerisation leads to dispersity and poor control over the morphology.

The main factor that influences the morphology of nanoparticles ais the hydrophobicity of the core and shell polymers where typically a hydrophobic core and hydrophilic shell form core-shell structures.[1] Inverted core-shell structures can be synthesised by crosslinking the seed particles and inhibiting absorption of radicals or polymers.[2-3,10] Typically the synthesis of core-shell structured nanoparticles requires controlled feeding of the shell forming polymer to a seed system under starve-fed conditions or dispersion polymerisation. [1-3,6,10,15,17-18,23] Alternatively the synthesis of a core-shell structure can occur when the system is heated and phase separation of the two polymers can occur. Another method for altering the morphology utilises phase separation of two polymers. Using two different polymers with different Tg values can enable one polymer to phase separate under increased temperature (this can be influenced by crosslinking). This can lead to a lobe or lobes protruding from the surface synthesising dumbbell, snowman[20-22] and popcorn particles or complete engulfment of the seed can produce core-shell structures.[5,9-10,19] Heterocoagulation between two particles using either electrostatic[4-5,8,11-12] or hydrogen bonding interactions[14] leads to the formation of raspberry-like particles.[4,11-13] Further treatment of the raspberry-like particles can lead to core-shell morphologies by heating the shell forming particles above the Tg and allowing surface wetting.[4-5,8] Chaudhuri and Paria recently published a review stating core-shell type morphologies using various organic and inorganic cores and shells and documented both synthetic methodology and applications of such particles.[7] Recently in 2013 Gaulding *et al* discussed the formation of microgel poly(NIPAM) particles and the template driven adhesion onto micron sized polymer

seeds creating raspberry-like particles where the microgel particles are responsive to multiple stimuli.[24] Microgel particles are highly appealing for particle decoration due to the post functionalisation of pendant vinyl groups that remain.

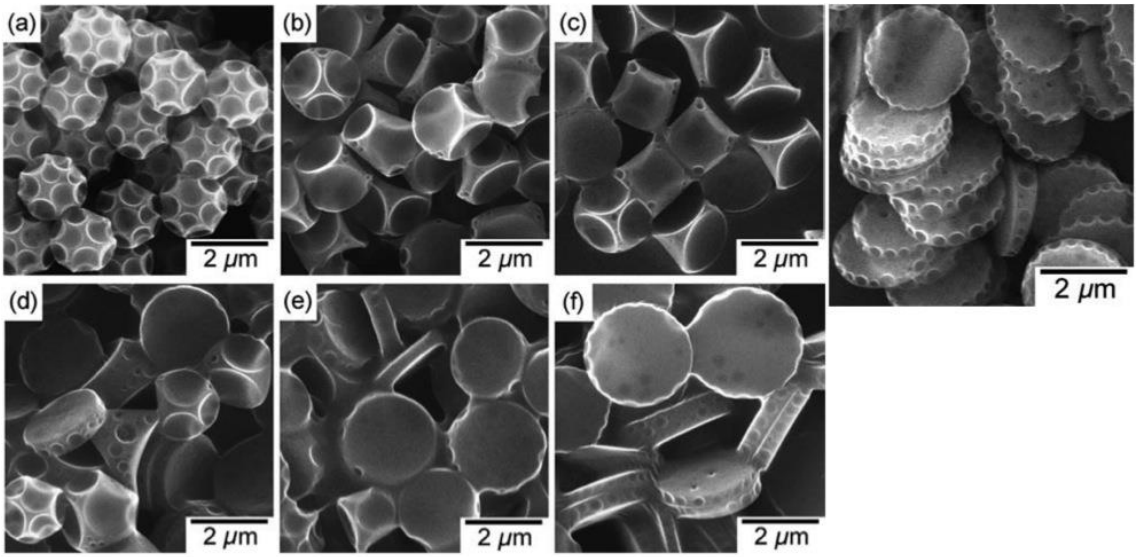

Figure 3.1. SEM micrographs showing a few morphologies of colloidal particles synthesised by the Okubo group [Reproduced from reference 18].

3.2.2. Microgel particles with pendant vinyl groups

Vinyl groups or olefins have been a great interest over the past century due to the breadth of reactions that can be carried out. Synthesis of particles with pendant vinyl groups usually employs the use of crosslinkers such as divinylbenzene[25-28] (DVB) or ethylene glycol dimethacrylate[29-30] (EGDMA) using either dispersion or emulsion polymerisation techniques. Yamamoto *et al*,[25] Okubo *et al*[26] and Bon *et al*[27] have shown that pendant vinyl groups remain from the emulsion and dispersion polymerisation of DVB. They reported that during polymerisation the first vinyl group in DVB provides steric factors and an increased viscosity that reduces the polymerisation rate of the second vinyl group leaving many vinyl groups unreacted. Saunders *et al*[29] and Downey *et al*[31] studied the synthesis of poly(DVB) microspheres *via* dispersion polymerisation

and noted that the microgel structure has a crosslinking gradient from the inside to the outside of the particles where the particle surface contains the most pendant vinyl groups.[29-31] Two review articles by authors Saunders *et al*[29] and Srivastava[32] provided concise reviews on the formation of microgel particles from past five years. Srivastava emphasises the use of methyl methacrylate (MMA) based microgels showing the effects of crosslink density and Tg[32] and Saunders *et al* focuses on all microgel types including DVB, EGDMA and NIPAM. Saunders *et al* and Srivastava discuss the theory behind microgel formation and swelling parameters according to Flory theory as well as the internal structure of microgel particles prepared *via* soap-free emulsion polymerisation.[29]

3.2.3. Olefin based reactions.

The so called "click" reactions were originally developed in the 1940-50's as simple organic reactions until in 2001 Sharpless *et al* reinvented the term "click" chemistry. He proposed that building on simple synthetic chemical reactions we could try and mimic nature and allow the attachment of two species together.[33] This idea was developed to provide simple reactions that could give high yield and high specificity products in a range of benign solvents and conditions with a high scope of reactions and products.[33] Such click reactions include thiol-ene and thiol-Michael,[34-41] thiol-epoxy,[34-35] thiol-isocyanate,[34-35] thiol-halogen[34-33] and the thiol-yne[34-35] addition reactions. These reactions typically proceed *via* two mechanisms of initiation, free-radical (thermal or UV initiated)[34-37] and catalytic (acidic catalysed, base catalysed and nucleophilic catalysed).[34-35,37-41] Over the last decade olefin based chemical reactions have become much more popular in materials chemistry due to the simplicity of the reactions. Click

reactions can synthesise polymers, block copolymers, star and hyperbranched polymers.[34-35,37-39] They can functionalise the surface of particles or flat surfaces with any functional group or polymer chain.[3435,37,40-41] Thiol chemistry allows tailoring of micellar structures[34,37] and formation of responsive polymer networks.[34-37,39] Many recent reviews by authors Hoyle, Bowman, Lowe and Chan have studied the vast range of chemical conditions and reactions between various click reactions. They discuss thiol-ene, thiol-yne and 1,3-Huisgen cycloaddition and report the different initiators and applications as well as the versatility of the reactions.[34-35,37-39] Van Berkel *et al* studied the addition of polyethylene glycol (PEG) chains to the surface of poly(DVB) particles using radical thiol-ene chemistry.[42] Goldman *et al* also reported the synthesis of poly(DVB) microspheres and the post functionalisation using thiol-ene to add poly(NIPAM) chains to the surface.[43] An alternative method for the attachment of poly(alkyl methacrylate) chains was reported by Zheng *et al* who used atom transfer radical polymerisation (ATRP).[44-45]

3.2.4. Decorated colloidal particles with pendant vinyl groups for post functionalisation

In this chapter we aimed to synthesise decorated raspberry or core-shell type nanoparticles where the decoration consists of a polymer nanogel shell to give an increased surface area and pendant vinyl groups. Following the synthesis of decorated particles with vinyl groups we wanted to post-functionalise using a simple versatile technique that can be utilised in water with a range of functional groups. For this reason we chose the increasingly useful thiol-Michael addition reaction.

3.3. Experimental

3.3.1. Materials

Styrene, methyl methacrylate (MMA), ethyl methacrylate (EMA) and poly ethyleneglycol methyl ether acrylate average M_n 480 (PEGMEA) were purchased from Sigma-Aldrich at >99% purity and used as received. Sodium hydrogen carbonate ($NaHCO_3$) and potassium persulphate (KPS) were purchased from Sigma-Aldrich at >99% purity and used as received. Sodium 4-vinylbenzenesulphonate (NaSS) was technical grade (90%) and was used as received. Deionised water was used for all reactions and dilutions. Crosslinkers di-(ethyleneglycol) di-acrylate (DEGDA) and penta-erythritol triacrylate were technical grade (75% assay) from Sigma-Aldrich and were all used as received (the lower purity could be due to mono DEG acrylates, DEGDA dimers and PEG diacrylates). Di-penta-erythritol penta-/hexa acrylate was purchased from Sigma Aldrich at 99% and used as received. Sodium 3-mercapto-1-propanesulphonate (MPS, technical grade, 90%), *iso*butylamine (99.0%), *L*-cysteine (≥97%) and pentaerythritol tetrakis(3-mercaptopropionate) were all used as supplied from Sigma Aldrich.

3.3.2. Equipment

Emulsion polymerisations were carried out in double-walled cylindrical glass reactors (250 ml, Asynt) equipped with an external heating bath (Julabo F-25 unit) and a four-bladed overhead Teflon stirrer (Cowie Ltd) approximately 1cm from the bottom of the reaction vessel. Typical reactor stirrer speeds were 275 rpm for emulsion polymerisation. Harvard syringe pumps were used to feed in the crosslinking monomers with a precision of ±0.00005 ml/min. Average hydrodynamic particle sizes and

dispersities were measured by dynamic light scattering using a Malvern Zetasizer Nano (data was analysed using the CONTIN algorithm). SEM analyses were performed using a Zeiss Supra 55VP FEG-SEM with an EBSD camera and the samples were prepared on silicon wafers (provided by Wacker Chemie AG). SEM samples were sputter coated using Au/Pd for the seed particles and using the carbon coater for the irregular shaped particles with sputter times of 1000 mS and two repeat coatings. A 4 digit analytical balance (Precisa XT 220A) was used for accurate measurements of the monomers, comonomers, initiator and crosslinkers and also for measuring conversion of the latexes. FT-IR measurements were completed using a Perkin Elmer FT-IR Spectrometer 100 with ATR attachment using a scan number of 16 per sample at 4 cm-1 resolution. The ^{13}C SSNMR samples were submitted and run by Jonathan Lamley (Dr Jozef Lewandowski group) using a Bruker ^{13}C CP-MAS NMR Avance III 500 MHz ^{1}H Larmor frequency spectrometer with a 2.5mm HXY probe (in double resonance mode with 20 kHz spinning frequency). The Raman microscope was a Renishaw inVia model with a 514.5 nm Argon laser and a Renishaw CCD detector for visible to near-IR. Samples acquisition was 60 s with 5 runs per sample to reduce the signal to noise ratio enough for smooth spectra.

3.3.3. Soap-free emulsion polymerisation of seed particles

Typically, ~0.10 g NaSS (1 wt% based on monomer) and ~0.10 g $NaHCO_3$ were dissolved into ~90 ml de-ionised water and purged with nitrogen for 45 mins to remove oxygen. The monomer, ~10.0 g (Sty, MMA, EMA or Sty-*co*-PEGMEA), was injected into the reactor and purged for a further 10 minutes (to avoid monomer evaporation). The reaction was heated to ~70 ^{o}C and left for 5 minutes to equilibrate. The polymerisation was initiated by injecting ~0.10 g KPS dissolved in ~2.0 ml degassed

de-ionised water into the reactor and the nitrogen pressure was reduced. See **Table 3.1.** for exact compositions for seed particles.

Polymerisation times were 20 hours for styrenic seeds and 5-8 hours for the acrylic seed latexes. Conversion of the seed latexes was analysed using gravimetry and Particles sizes and morphologies were analysed using a combination of both DLS and SEM. The latexes were dialysed twice daily for two weeks to remove water-soluble starting material and monomer. The dialysis tubing showed Bragg diffraction and this was observed for the dried latex films indicating the monodispersity.

3.3.3.1. Gravimetric analysis of seed latexes

Gravimetry was calculated using **Equation 3.1.**. Sample was removed from the reaction at regular intervals and post polymerisation. Samples weight was recorded as soon as the sample was removed (M_{wet}) and after the water had evapourated (M_{dry}) and the values were used in the equation.

$$X_m = \left(\frac{M_{dry}}{M_{wet}} - \frac{M_{Solid}}{M_{Total}} \right) * \left(\frac{M_{Total}}{M_{Monomer}} \right) \quad \textbf{Equation 3.1.}$$

Where M_{Solid} is the mass of solids in the system, M_{Total} is the total mass of the system and $M_{Monomer}$ is the initial amount of monomer. The ratios account for the volatile and non-volatile compounds other than the monomer and polymer, respectively. So by adding the numbers into the equation allows the instantaneous conversion, X_m, to be calculated for a given time that the sample was removed at. This is useful for measuring how long the polymerisation takes to complete, or at least achieve maximum conversion.

3.3.4. Deposition of crosslinked particles onto the seed surface

The seed latex (~25.0 ml) was diluted to ~100 ml using deionised water in a reaction vessel followed by purging with nitrogen for ~45 minutes to remove oxygen. The reaction was heated to ~70 ^{o}C and left for 5 minutes to equilibrate. KPS (~0.05g) dissolved in ~1.0 ml degassed deionised water was injected into the reaction vessel to begin initiation and the nitrogen pressure was reduced during polymerisation. The crosslinking monomer was injected into the reaction vessel 10 minutes after initiation occurred. Monomer feed rate of 0.11 ml/min was controlled using a Harvard precision syringe pump and syringe tubing (2 mm internal diameter). The crosslinkers used and their relative amounts are shown in **Tables 3.3.** and **3.5.**. The addition of all crosslinking monomer into the reaction was followed by 30 minutes of polymerisation time before cooling the reaction to room temperature. The particles sizes, polydispersity index and particle morphologies were analysed using a combination of DLS and SEM (see **Experimental Section 2.3.6.** in **Chapter 2** for details about sample preparation, acquisition and ImageJ analysis).

3.3.5. Thiol-Michael addition to decorated latexes

Using glass screw cap vials 10 ml latex was added with a small stirrer bar and placed on a simple stirrer plate. To this latex solution 0.1 g of thiol (four thiols were tested -sodium 3-mercapto-1-propanesulphonate, *iso*butylamine, *L*-cysteine, and pentaerythritol tetrakis(3-mercaptopropionate) was added and was allowed to mix for approximately one hour before 100 µL *iso*butylamine catalyst was added. The vial was sealed and then left to stir for two days to ensure completion. Following the reaction the latex was dialysed against deionized water for one weak changing the water thrice daily.

3.4. Results and iscussion

3.4.1. Preparation of hydrophobic sulphonated poly(styrene) seed nanoparticles

Initially a monodisperse 10 wt% latex was prepared by emulsifier free emulsion polymerisation of styrene (referred to as 2.5, see **Figure 2.10.** in **Chapter 2** for structure). The polymerisation was carried out at 70 ^{o}C using 2.5, 1 wt% NaSS (referred to as 2.1, structure found in **Scheme 2.1.** in **Chapter 2**) and potassium persulphate as the initiator (referred to as 2.7, structure shown in **Figure 2.10.** in **Chapter 2**). For the exact latex ingredients refer to **Table 3.1.**.

Table 3.1. Recipe for the preparation of 10 wt% poly(2.5) seed latex.

Sample	Monomer (g)	NaSS (g)	$NaHCO_3$ (g)	H_20 (ml)	KPS[(a)] (g)	$Xn^{(b)}$	Polymerisation time (hours)
Poly(2.5)	10.10	0.10	0.10	90	0.10	0.91	20

Reaction temperature 70 ^{o}C. (a) Initiator 2.7 was dissolved into 1 ml of DDI H_2O. (b) Conversion measured by gravimetry (see experimental).

Monomer 2.5 was chosen due to the high T_g value (100 ^{o}C for poly(2.5) allowing easier SEM analysis (latex particles with low T_g values film form when dried causing difficulty in particle size measurements). The addition of 1 wt% 2.1 controlled the particle sizes at 119 nm (s.d. 5.2 nm) with a CV of 4.4% as characterized by SEM (**Figure 3.2-A.** and **3.2-B.**) and 129 nm from DLS measurements (**Table 3.2.**). Measurements using DLS gives larger particle sizes than observed using SEM due to the addition of the hydration sphere (double layer) surrounding the particle that is required for colloidal stability. A low polydispersity index (PDI) is observed using DLS

with value of 0.041 (**Table 3.2.**) and the SEM images showed a hexagonal packed structure when dried (see **Figure 3.2-A.**).

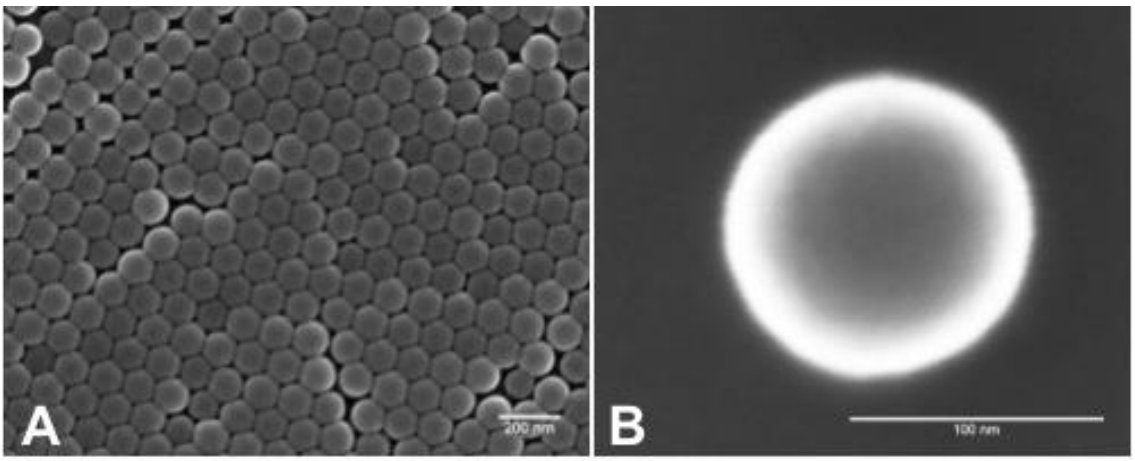

Figure 3.2. SEM micrographs of 10 wt% seed latex using batch soap-free emulsion polymerisation with 1 wt% 2.1 (based on monomer) and 2.7 initiator at 70 ºC. A) poly(2.5) seed, B) close up of a particle for poly(2.5) seed. Scale bars are 200 nm for A and 100 nm for B.

Table 3.2. Size analysis of poly(2.5) seed latex using DLS and SEM.

Sample	Z_{Ave}[(a)] (nm)	PDI[(a)]	Particle diameter[(b)] (nm)	S.D. (nm)	CV (%)
Poly(2.5)	129.0	0.041	119.4	5.2	4.4

(a) DLS measurements carried out at 25 ºC and averaged from 5 measurements. (b) Average particle diameters, standard deviation and coefficient of variation calculated using ImageJ software (see experimental).

The particles sizes of the sulphonate stabilised latex are controlled by the addition of more or less ionic comonomer 2.1 as reported by Juang *et al*[46] and Kim *et al*.[47] They reported a maximum loading of 2.6 wt% 2.1 using batch soap-free emulsion polymerisation with 2.5 and showed that after 2.6 wt% 2.1 the particle size distribution increases. This increase in the size distribution is caused from increased amounts of sulphonated polyelectrolyte chains' forming in the aqueous phase thus affecting the aqueous nucleation mechanism i.e. more nucleation occurs in the aqueous phase. Kim *et al* also showed that the surface charge density of sulphonate groups at the surface

reached a maximum of 35 uC cm^{-2} and the poly(2.1) chains physically adsorb onto the particle surfaces creating hairy polyelectrolyte stabilised colloids.[47]

3.4.1.1. Decorating of poly(styrene) seed nanoparticles with poly(DEGDA) particles

Initial studies were carried out using a 2.5 wt% dialysed poly(2.5) seed latex where initiator 2.7 was injected at 70 ^{o}C. Crosslinking monomer di-ethylene glycol di-acrylate (DEGDA, referred to as 3.1, structure shown in **Figure 3.3.**) was fed into the reactor at a controlled rate under soap-free monomer starved conditions (see experimental for polymerisation setup and **Table 3.3.** for exact amounts). In previous literature studies the starve fed addition of crosslinking monomers leads to the formation of core-shell and inverted core-shell type structures as shown by Hergeth *et al*[1] and Kirsch *et al*.[3] The particle structure is controlled by both hydrophobicity of the seed relative to the shell forming polymer and by the inhibition of secondary particle nucleation which leads to bimodal size distributions.

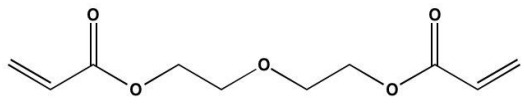

Figure 3.3. Structure of di-(ethyleneglycol) di-acrylate (DEGDA).

The size measurements from both DLS and SEM are shown in **Table 3.4.**, also noted is the contact angle measured between the seed and the decorating nanogel particles which was measured from the SEM images. DLS measurements showed an increase in the hydrodynamic diameter from 129 nm to 166 nm where the PDI remains low between 0.020 and 0.075. The progressive size increase as observed by DLS gave

an indication that the size increased relatively proportionally and following this SEM analysis was used to determine the sizes and morphology of the particles produced.

Table 3.3. Recipe for the preparation of poly(3.1) decorated poly(2.5) latex.

Sample	Seed latex (ml)	H_20 (ml)	KPS[(a)] (g)	Total 3.1 added (ml)
Poly(3.1) decorated poly(2.5)	25	75	0.05	2.5

Feed rate of 3.1 was 0.11 ml/min, temperature 70 ^oC. (a) Initiator 2.7 was dissolved into 1 ml of DDI H_2O. Samples were taken after every 0.5 ml of 3.1 was added. Reaction quenched 30 minutes after feed ended.

The SEM images (shown in **Figure 3.4.**) showed coverage of the seed nanoparticles surfaces by smaller particles followed by growth of the covering nanoparticles. At low 3.1 additions we notice the coverage of the seed by small nanogel particles and the nanogel particles increase in size as more 3.1 is fed in. The nanogel particles consist of crosslinked poly(3.1) latex particles. Typically each poly(2.5) particle has roughly the same number of decorating particles decorating the surface but the orientation of the particles appears random. No ordered surface packing of particles is visualised meaning no strong repulsive forces are present that control the nanogel locations. When we count the decorating particles on a single face and double the number we get a value of 7-12 nanogel particles per seed. However, as 3.1 is fed into the polymerisation with the rate of addition kept constant the number of decorating particles on the surface does not increase. The decorating particles increase in size (see **Figure 3.4-K.**) and the poly(3.1) nanogel particles grow to nearly half the diameter of the poly(2.5) seed particles in some cases. Secondary particle nucleation in the aqueous phase was also observed especially when the amount of 3.1 exceeds 2.0 ml 3.1 and is likely due to seed saturation where the surface area has achieved maximum surface area coverage.

Table 3.4. Size analysis of poly(3.1) decorated poly(2.5) seed latex using DLS and SEM.

Sample	Cross-linker amount (ml)	Z_{Ave} (nm)	PDI	Average particle diameter (nm)	S.D. (nm)	CV (%)	Average nanogel diameter (nm)	S.D. (nm)	CV (%)	Contact angle (°)
Poly(3.1) decorated poly(2.5)	0.1	127.7	0.057	123.8	3.5	2.8	-	-	-	-
	0.5	135.9	0.008	129.8	11.3	8.7	38.8	5.7	14.7	127.5
	1.0	151.3	0.051	148.4	12.7	8.6	49.7	7.8	15.6	116.2
	1.5	153.1	0.018	165.2	14.3	8.7	56.5	9.4	16.7	121.9
	2.0	165.9	0.074	176.1	13.2	7.5	64.1	8.8	13.7	108.4
	2.5	166.3	0.023	185.6	13.0	7.0	68.9	10.0	14.5	112.2

DLS measurements carried out at 25 °C and averaged from 5 measurements. Average particle diameters, standard deviation, coefficient of variation and contact angles calculated using ImageJ software (see experimental).

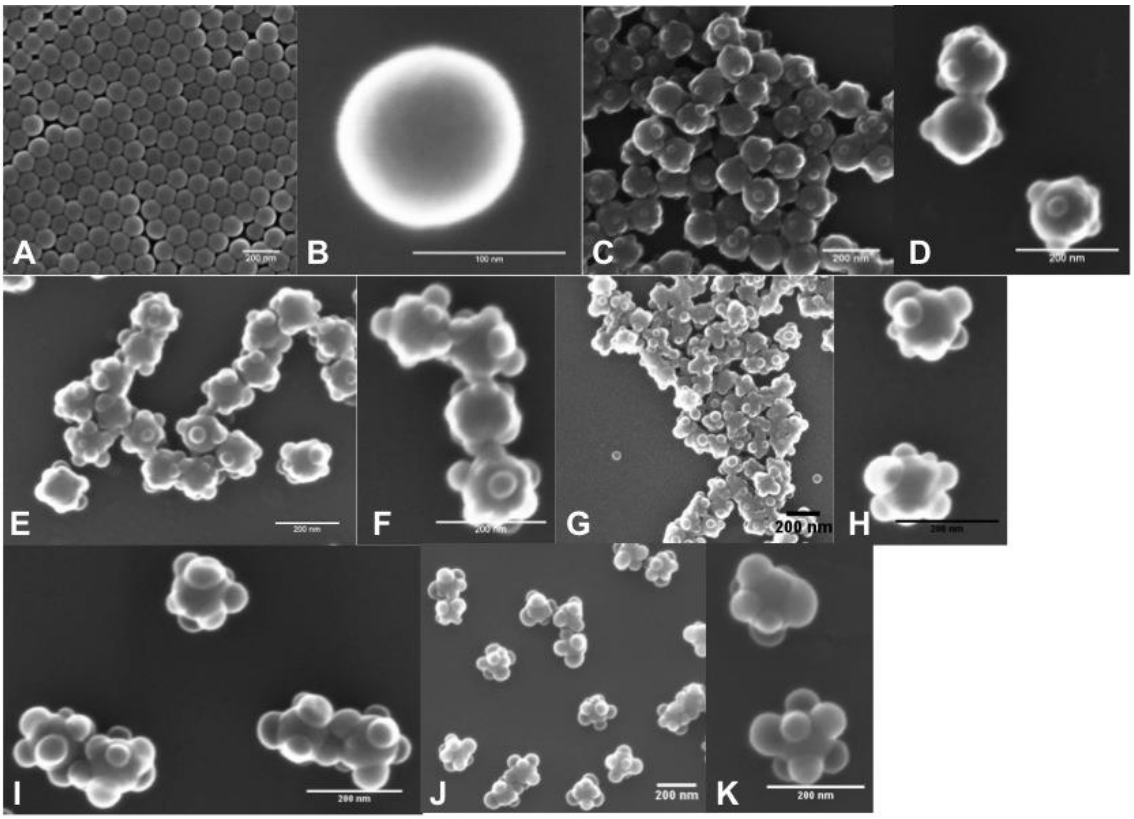

Figure 3.4. SEM micrographs of 2.5 wt% poly(2.5) seed latex with the starve-fed soap-free addition of 3.1, A) reference poly(2.5) seed, B) close up of a poly(2.5) seed particle, C) 0.5 ml 3.1, D) close up of the particles using 0.5 ml 3.1, E) 1.0 ml 3.1, F) close up of particles using 1.0 ml 3.1, G) 1.5 ml 3.1, H) close up of the particles using 1.5 ml 3.1, I) 2.0 ml 3.1, J) 2.5 ml 3.1, K) close up of the particles using 2.5 ml 3.1. All scale bars are 200 nm except for B which is 100 nm.

As 3.1 is fed into the reaction vessel the decorating particles grow in size due to a combination of swelling with monomer as described by Flory (which is heavily dependant on the degree of crosslinking)[29] or from polymerisation occurring at the surface. The step growth of poly(3.1) nanoparticles is shown in **Figures 3.4-G.** to **3.4-K.** where a significant growth of the poly(3.1) particles is observed. The increase in decorating particle sizes appears to be random where some particles grow significantly more than others. The growth of some nanogels over others is likely due to in-homogeneity in the crosslinked networks for each polymer nanogel and diffusion limited growth. Some nanogel particles could be more cross-linked and some particles might adsorb more monomer and grow to larger sizes. The SEM images were analysed

using ImageJ to determine the average particle sizes for different amounts of 3.1 injected into the polymerisation as reported in **Table 3.4..** Typically the poly(3.1) particles begin with an average size of 39 nm and grow to be up to 69 nm in size (69 nm is half of the seed latex particle size). The decorating particles did not spread efficiently over the seed surface as shown by large contact angles of 110-130^{o}. Contact angles were difficult to measure for the poly(3.1) decorated poly(2.5) seed due to vast differences in sizes of the nanogel particles. The lack of spreading is caused by the differences in hydrophobicity between the poly(2.5) seed and the poly(3.1) particles. Poly(3.1) will have a greater affinity for the aqueous phase due to the semi-porous crosslinked nanogel structure and the polarity of the ethylene glycol groups. The decorating nanogel particlesand therefore position them to have the most surface in the aqueous phase and less interaction with the hydrophobic seed particles.

We propose the following mechanism for the formation, adhesion and growth of the crosslinked nanogel particles as shown in **Figure 3.5.**. The monomer 3.1 is a relatively hydrophilic monomer and will polymerise in the aqueous phase until a certain molecular weight has been achieved. After polymer formation occurs the polymers will diffuse to the seed particle surface where they will penetrate the outer shell. Due to the high Tg value of 100 ^{o}C for pol(2.5) compared to the reaction temperature (70 ^{o}C) the polymers will likely only diffuse to the shell and not the core of the seed particles as discussed by Sundberg *et al* (see next paragraph). Polymerisation and growth will cause the polymers to crosslink and swell until polymer particles are formed that will try to position them into the aqueous phase. Due to the crosslinking of the nanogel particles that locate at the seed surface a degree of spreading can occur where for the hydrophobic seed and hydrophilic nanogel particles the degree of spreading is minimal

due to unfavourable conditions. The relative eleasticity of amount of spreading that the nanogel particles can achieve will be dependant on the mechanism for crosslinking (intermolecular or intramolecular crosslinking is discussed on Page 98). Secondary nucleation is visible at greater crosslinking monomer amounts due to a combination of seed surface saturation and crosslinking or branching of polymer chains before they are able to diffuse and penetrate the seed particles. They will then form primary particles in the aqueous phase where sufficient stability will be caused by the ethylene glycol chains in the nanogel particles.

Sundberg *et al* studied the effects of polymer diffusion into seed particles for non crosslinked seed particles and second stage polymers and later discussed the use of a crosslinker in the second stage.[48] He proposed that the monomer will propagate in the aqueous phase and diffuse into the seed particles where the diffusion into the seed is heavily affected by the Tg of the seed particles (discussed more in **Section 3.4.6.2.** for poly(3.1) decorated poly(3.4)). Sundberg *et al* discussed that once a radical chain becomes part of a crosslinked polymer network that it will no longer be able to diffuse into particles. He also discussed that crosslinking or branching of a polymer chain will most likely only occur after diffusion into the particle could occur (most particle penetration occurs within the first 10-20 propagation steps) and so a crosslinker will not affect the diffusion into the seed particles.

The same deformation of microgel particles has been shown by Gaulding *et al*[24] where poly(NIPAM) microgel particles adhered to micron sized poly(styrene) seed particles. Gualding *et al* reported that the microgel particles can be thought of as somewhere between hard rigid spheres and soft deformable jelly so as the particles

attach to a surface they can deform and spread depending on the relative degree of crosslinking. The microgel particles have elastic properties and can deform over the seed surface thus providing surface coverage. This affects the packing potential of particles at the surface (similarly hard microgel particles will have less deformation and so more surface packing is visualised).

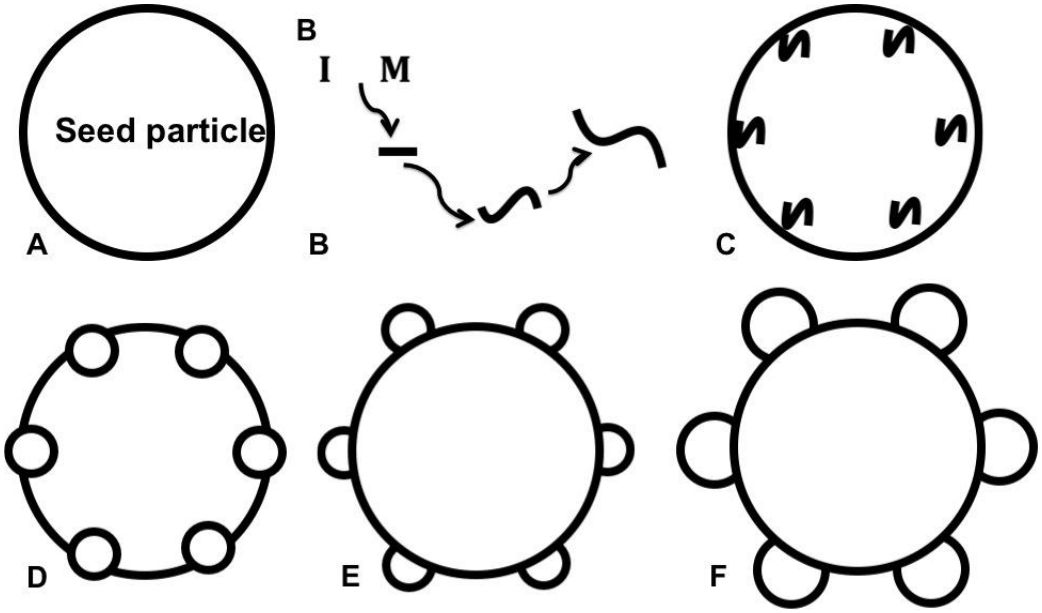

Figure 3.5. Image showing the growth of polymer chains and penetration and growth inside seed particles. A) seed particle, B) Initiator polymerising with polymer creating polymer chains, C) diffusion of polymer chains into the seed particles, D) phase separation of polymer nanogel particles at the surface, E) and F) further swelling and growth of phase separated nanogel particles.

In 2005 Bouvier-Fontes *et al* reviewed the crosslinking of di-acrylates and showed that shorter di-acrylate monomers have a greater chance for primary cyclisation (intramolecular crosslinking) of the same polymer chain.[49] Primary cyclisation of short di-acrylates lead to more elastically inactive polymers.[50] However, longer di-acrylate monomers have a reduced chance for primary cyclisation due to the distance between the vinyl groups and therefore the polymer is more favourable for both secondary cyclisation and crosslinking reactions (intramolecular crosslinking and intermolecular crosslinking). As the chain length of the di-vinyl monomer increases polymers with

higher crosslinking density and elasticity form. Using different multifunctional crosslinking monomers (tri-, tetra-, penta- and hexa-) will alter this crosslinking density further as the distance between vinyl groups' changes thus inhibiting cyclisation polymerisation.

Analysis was studied on the formation of microgel particles using bulk and emulsion polymerisation by Tobita *et al.*[28] They reported that during emulsion polymerisation the amount of crosslinking is relatively high from the very beginning of the polymerisation due to the differences in the amount of polymer. In bulk polymerisation the crosslink density increases as polymerisation progresses due to an increase in polymer concentration over time whereas for emulsion polymerisation the polymer concentration inside the locus of polymerisation is high from the start.

To overcome the lack of surface spreading and decorating particle packing for the hydrophobic poly(2.5) seed we tried two different approaches.

1) Modifying the poly(2.5) seed to become more hydrophilic or changing to a hydrophilic monomer e.g. acrylic seed particles

2) Varying the decorating crosslinker by using multi-functional acrylates instead of di-acrylates

3.4.2. Preparation of hydrophilic sulphonated poly(styrene) seed nanoparticles

We next copolymerised 2.5 with 5 wt% poly(ethylene glycol) methyl ether acrylate (PEGMEA, referred to as 3.2, see **Figure 3.6.** for structure) using batch soap-free emulsion polymerisation to synthesise a more hydrophilic styrenic seed latex (see **Table 3.5.** for the recipe). The seed will be slightly more hydrophilic due to the

increased water solubility of the PEG chains incorporated into the nanoparticles (water solubility of 3.2 is 1.090 g/L at 25 ^{o}C). The monomer 2.5 has a water solubility of 0.03 g/L so is very hydrophobic.

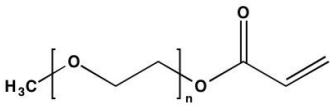

Figure 3.6. Structure of poly ethyleneglycol methyl ether acrylate average M_n 480 (PEGMEA).

Table 3.5. Recipe for the preparation of 10 wt% poly(2.5-*co*-3.2) seed latex.

Sample	2.5 (g)	3.2 (g)	NaSS (g)	$NaHCO_3$ (g)	H_20 (ml)	KPS[(a)] (g)	*X*n[(b)]	Polymerisation time (hours)
Poly(2.5-*co*-3.2) seed	9.52	0.51	0.10	0.10	90	0.10	0.81	8

Reaction temperature 70 ^{o}C. (a) Initiator 2.7 was dissolved into 1 ml of DDI H_2O. (b) Conversion measured by gravimetry (see experimental).

Table 3.6. Size analysis of poly(2.5-*co*-3.2) seed latex using DLS and SEM.

Sample	Z_{Ave}[(a)] (nm)	PDI[(a)]	Particle diameter[(b)] (nm)	S.D. (nm)	CV (%)
Poly(2.5-*co*-3.2) seed	321.7	0.010	274.2	7.1	2.6

(a) DLS measurements carried out at 25 ^{o}C and averaged from 5 measurements. (b) Average particle diameters, standard deviation and coefficient of variation calculated using ImageJ software (see experimental).

The particle sizes were 274 nm (s.d. 7.1 nm) with a CV of 2.6% from SEM analysis and 322 nm with a PDI of 0.010 from DLS analysis (**Table 3.6.**). Again we notice the monodispersity of the seed latex where a hexagonal packed structure is visible when film formed (see **Figure 3.7.**). The calculated sizes were larger than the hydrophobic poly(2.5) latex particles and a possible reason for this could be caused from a shift in the nucleation site (more aqueous phase nucleation). Monomer 3.2 is more water soluble than 2.5 and will be more likely to homopolymerise or copolymerize with 2.1 in the aqueous phase leading to the formation of polyelectrolyte chains. The

formation of more polymer chains in the aqueous phase typically increases the number of primary particles that form.[47] The lack of surfactant means that homogeneous and coagulative nucleation mechanisms dominate (discussed both in **Chapter 1)** as reported by Feeney *et al*.[51] Coagulation combined with adsorption of sterically stabilised polymer chains with poly(PEG) units extending into the aqueous phase provides electrosteric repulsion. These poly(PEG) chains will stabilise the particles like poly(2.1) chains do as Kim *et al* reported.[47]

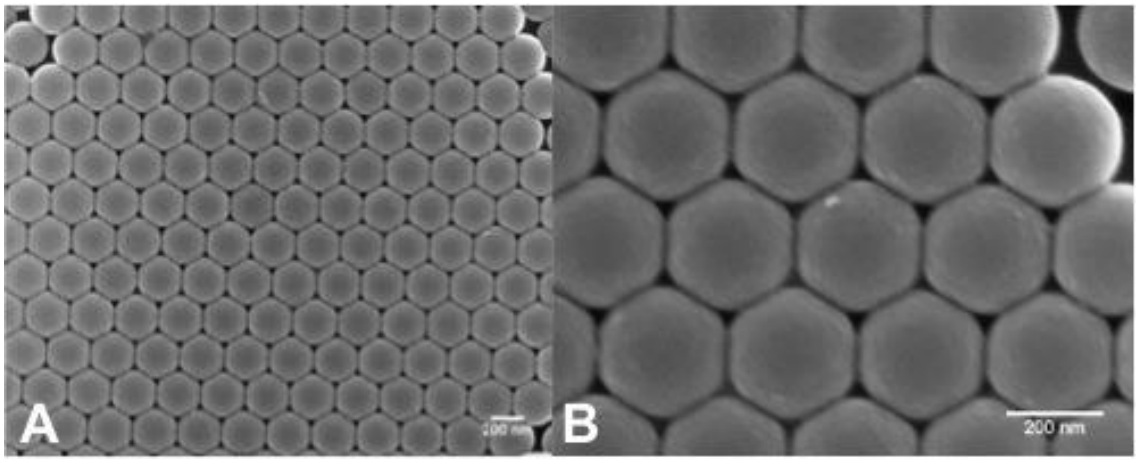

Figure 3.7. SEM micrographs of 10 wt% seed latex using batch soap-free emulsion polymerisation with 1 wt% 2.1 (based on monomer) and 2.7 initiator at 70 ºC. A) 95:05 wt% poly(2.5-*co*-3.2) seed, B) close up of the particles from 95:05 wt% poly(2.5-*co*-3.2) seed. Scale bars are 200 nm.

3.4.2.1. Decorating of poly(styrene-co-PEGMEA) seed nanoparticles with poly(DEGDA) particles

We again studied the same deposition of poly(3.1) nanogel particles onto the surface of the seed using starve-fed emulsion polymerisation (see **Table 3.7.**). The SEM analysis and DLS analysis are shown in **Figure 3.8.** and **Table 3.8.**. From the DLS analysis the PDI increased substantially with a very large hydrodynamic radius (indicating a very polydisperse sample or aggregated clusters) so to determine the actual sizes and morphology we decided to use SEM analysis. The SEM data showed the same mechanism as shown previously for the poly(2.5) seed with poly(3.1) addition where

nanogel particles spread over the seed surface followed by growth of the decorating nanogel particles. The size of the seed is much greater than the hydrophobic poly(2.5) seed (274 nm compared to 119 nm) and so the decorating particles had a much greater surface area available for adhesion and coverage.

Table 3.7. Recipe for the preparation of poly(3.1) decorated poly(2.5-*co*-3.2) latex.

Sample	Seed latex (ml)	H_20 (ml)	KPS[(a)] (g)	Total 3.1 added (ml)
Poly(3.1) decorated poly(2.5-*co*-3.2)	25	75	0.05	2.0

Feed rate of 3.1 was 0.11 ml/min, temperature 70 ^oC. (a) Initiator 2.7 was dissolved into 1 ml of DDI H_2O. Samples were taken after every 0.5 ml of 3.1 was added. Reaction quenched 30 minutes after feed ended.

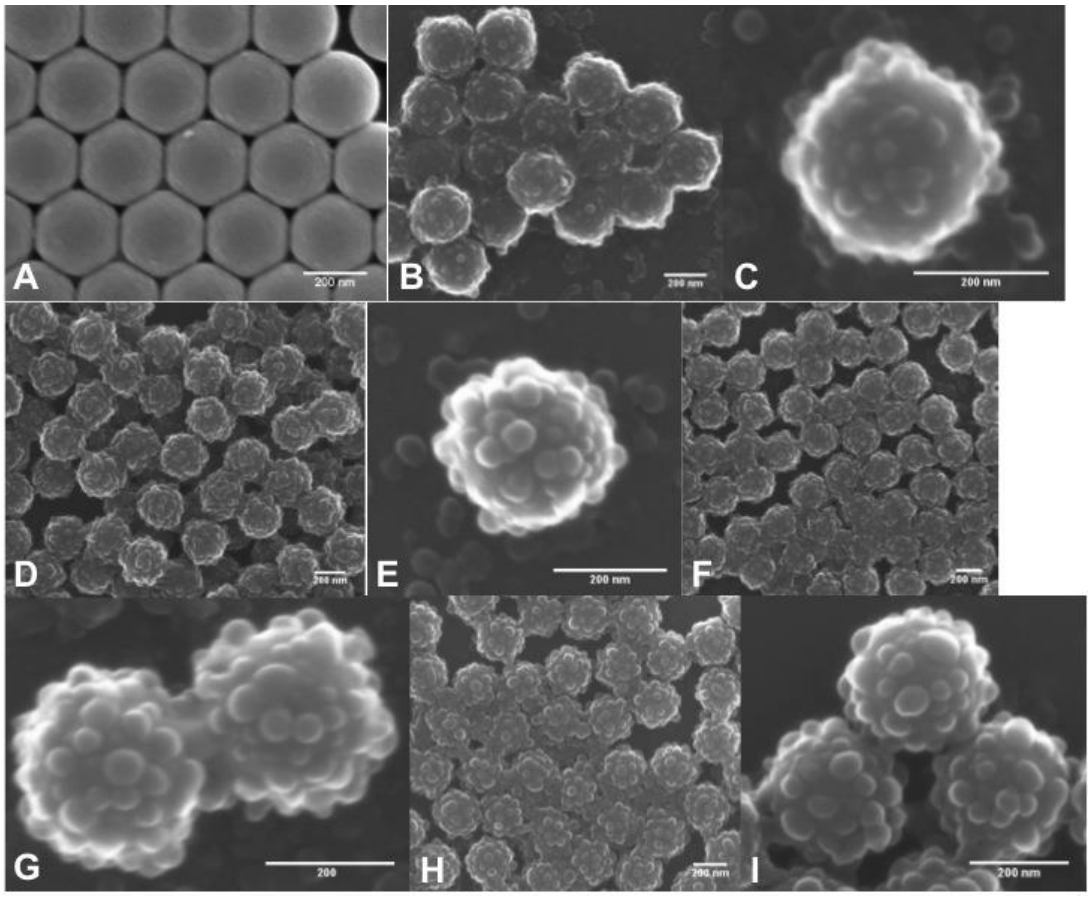

Figure 3.8. SEM micrographs of 2.5 wt% poly(2.5-*co*-3.2) seed latex (ratio 95:05) with the starve-fed soap-free addition of 3.1 crosslinker, A) reference poly(2.5-*co*-3.2) seed, B) 0.5 ml 3.1, C) close up of a particle using 0.5 ml 3.1, D) 1.0 ml 3.1, E) close up of a particle using 1.0 ml 3.1, F) 1.5 ml 3.1, G) close up of the particles using 1.5 ml 3.1, H) 2.0 ml 3.1, I) close up of the particles using 2.0 ml 3.1. All scale bars are 200 nm.

Table 3.8. Size analysis of poly(3.1) decorated poly(2.5-*co*-3.2) seed latex using DLS and SEM.

Sample	Cross-linker amount (ml)	Z_{Ave} (nm)	PDI	Average particle diameter (nm)	S.D. (nm)	CV (%)	Average nanogel diameter (nm)	S.D. (nm)	CV (%)	Contact angle (°)
Poly(3.1) decorated poly(2.5)	0.5	1246	0.713	312.8	21.9	7.0	34.8	5.3	15.2	107.2
	1.0	1319	0.863	313.8	17.3	5.5	44.6	8.5	19.0	107.4
	1.5	2182	0.425	305.2	15.7	5.1	47.8	8.5	17.7	104.4
	2.0	1635	0.902	317.3	19.2	6.0	-	-	-	-

DLS measurements carried out at 25 °C and averaged from 5 measurements. Average particle diameters, standard deviation, coefficient of variation and contact angles calculated using ImageJ software (see experimental).

Visually we see an increase in the number of particles that had adhered to the seed surface when compared to the poly(2.5) seed. We also noticed that the poly(3.1) nanogel particles have identical average particle sizes of 35 nm as was shown previously for the poly(2.5) seed latex but only grew to approximately 48 nm which was not as large as the nanogel particles grew for the poly(2.5) seed. As the number of decorating nanogel particles is greater then each particle can absorb less monomer overall and so the particles do not grow as much. The growth of the decorating particles as 3.1 was fed in was more uniform and the amount of surface coverage is much higher (even at 0.5 ml 3.1 feedings). Typically the number of nanogel particles that adhered to a single poly(2.5-*co*-3.2) seed particle was in the range of 50-100 particles, which is significantly more than shown previously to more hydrophobic poly(2.5) seed particles. We notice the random shapes and sizes of the decorating particles where no apparent order or periodicity is shown (see **Figure 3.8.**) so repulsive forces are not present on the nanogel particles.

As the feeding of 3.1 increases we observe monodisperse raspberry-like decorated particles with relatively uniform decorating particle sizes meaning the colloids are more spherical than the decorated poly(2.5) seed. Again we notice secondary nucleation occurring indicating that too many new particles were formed before diffusion onto the seed particles can occur and subsequently when the saturation of the seed surface was reached. Many poly(3.1) nanogel particles remained in the aqueous phase. As well as a higher degree of decorating particle coverage the contact angle between the decoration and the seed is nearly the same as for the poly(2.5) seed with values of 104-108^{o} as reported in **Table 3.8.**. Due to the similarities in the nanogel

particle sizes measurements of contact angles was more accurate than for the poly(3.1) decorated poly(2.5) seeds.

3.4.3. Decoration of poly(styrenic) seed nanoparticles with poly(DEGDA-co-PEGMEA) particles

We also tried altering the styrenic seed nanoparticles poly(2.5) and poly(2.5-*co*-3.2) with the use of a slightly more hydrophilic decorating nanogel. We altered the composition of the feeding crosslinking monomer 3.1 by addition of 10 wt% 3.2 (see **Table 3.9.** for quantities). The morphology of the nanoparticles produced using the poly(2.5) seed nanoparticles are identical when either poly(3.1) and poly(3.1-*co*-3.2) decoration is added i.e. final latex size and nanogel particles sizes are equivalent (compare **Table 3.4.** with **Table 3.10.**). One discernable difference was a lower contact angle of 122^{o} and 119^{o} as shown in **Table 3.10.** and **Figure 3.9-E.** and **Figure 3.9-F.** when we compare the two different decorating particles. This lower contact angle is likely caused from poly(3.2) chains extending from the nanogel particle surface and forcing the nanogel to cover more surface. By wetting the surface more efficiently then more poly(3.2) chains can be in the more favourable aqueous phase in order to stabilise the nanoparticles.

Table 3.9. Recipe for the preparation of poly(3.1-*co*-3.2) decorated latexes.

Sample	Seed latex (ml)	H_20 (ml)	KPS[(a)] (g)	Total 3.1 added (ml)
Poly(3.1-*co*-3.2) decorated poly(2.5)	25	75	0.05	1.0
Poly(3.1-*co*-3.2) decorated poly(2.5-*co*-3.2)	25	75	0.05	1.0

Feed rate of 3.1-*co*-3.2 was 0.11 ml/min, temperature 70 ^{o}C. (a) Initiator 2.7 was dissolved into 1 ml of DDI H_2O. Samples were taken after every 0.5 ml of 3.1-*co*-3.2 was added. Reaction quenched 30 minutes after feed ended.

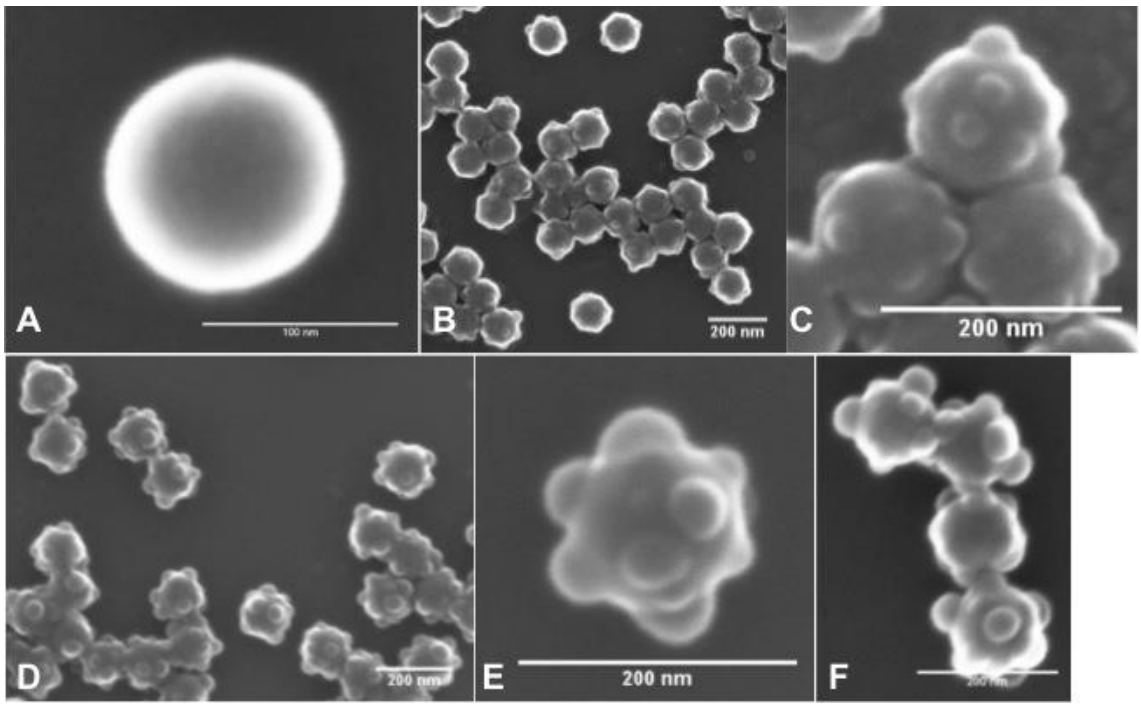

Figure 3.9. SEM micrographs of 2.5 wt% poly(2.5) seed latex with the starve-fed soap-free addition of 3.1-*co*-3.2 (ratio 50:50 wt%), A) reference poly(2.5) seed particle, B) 0.5 ml 3.1-*co*-3.2, C) close up of the particles using 0.5 ml 3.1-*co*-3.2, D) 1.0 ml 3.1-*co*-3.2, E) close up of a particle using 1.0 ml 3.1-*co*-3.2, F) 1.0 ml 3.1. Scale bars all 200 nm except for A which is 100 nm.

Table 3.10. Size analysis of poly(3.1-*co*-3.2) decorated poly(2.5) and poly(2.5-*co*-3.2) seed latex using DLS and SEM.

Sample	Cross-linker amount (ml)	Z_{Ave} (nm)	PDI	Average particle diameter (nm)	S.D. (nm)	CV (%)	Average nanogel diameter (nm)	S.D. (nm)	CV (%)	Contact angle (°)
Poly(3.1-*co*-3.2) decorated poly(2.5)	0.5	231.5	0.335	137.9	7.8	5.7	32.2	4.6	14.2	122.1
	1.0	259.4	0.271	153.4	10.9	7.1	44.0	6.8	15.5	119.7
Poly(3.1-*co*-3.2) decorated poly(2.5-*co*-3.2)	0.5	517.0	0.699	289.2	11.7	4.0	35.2	3.3	9.3	120.1
	1.0	508.3	0.897	307.4	17.9	5.8	48.1	5.7	11.9	117.9

DLS measurements carried out at 25 °C and averaged from 5 measurements. Average particle diameters, standard deviation, coefficient of variation and contact angles calculated using ImageJ software (see experimental).

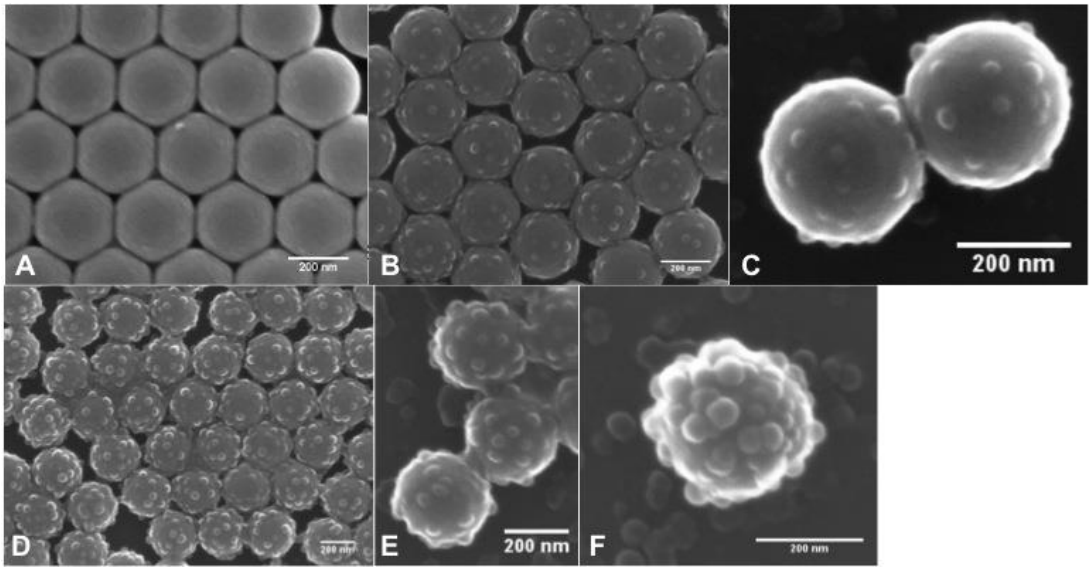

Figure 3.10. SEM micrographs of 2.5 wt% poly(2.5-*co*-3.2) seed latex with the starve-fed soap-free addition of 3.1-*co*-3.2 (ratio 50:50 wt%), A) reference poly(2.5-*co*-3.2) seed particles, B) 0.5 ml 3.1-*co*-3.2, C) close up of the particles using 0.5 ml 3.1-*co*-3.2, D) 1.0 ml 3.1-*co*-3.2, E) close up of the particles using 1.0 ml 3.1-*co*-3.2, F) 1.0ml 3.1. All scale bars are all 200 nm.

The poly(2.5-*co*-3.2) seed nanoparticles decorated using poly(3.1-*co*-3.2) nanogel particles did show a decrease in the number of decorating particles (see **Figure 3.10.**) and an increase in the number of secondary particles that did not adhere to the seed surface. The lack of decoration is likely due to the hydroxyl groups from the 3.2 chains causing more repulsive forces, which means the nanogel particles have greater colloidal stability and therefore do not require coagulation. Again a lower contact angle is observed between decorating microgel particles and the seed surface with a value of 120^{o} and 118^{o}. Comparison of the poly(3.1) and poly(3.1-*co*-3.2) nanogel decorated poly(2.5-*co*-3.2) nanoparticles is shown in **Figure 3.10-E.** and **Figure 3.10-F.** and a comparison of sizes and contact angles are reported in **Table 3.8.** and **Table 3.10.**. The lower contact angle is likely caused from van der Waals interactions between poly(3.2) chains from the seed and nanogel particles which allows greater coverage. The lower number of decorating nanogel particles is likely due to the nanogel particles being more colloidally stable where poly(3.2) groups can create steric stability and steric polymer

chains from the nanogel particles already covering the surface could inhibit the coverage and spreading of other particles.

3.4.4. Surface analysis of poly(DEGDA) decorated seed nanoparticles for vinyl group quantification

In order to try and prove the presence or relative quantity of vinyl groups remaining from the poly(3.1) nanogel particles we utilised a variety of solid state techniques. Fourier transform infra-red spectroscopy (FT-IR) and solid-state nuclear magnetic resonance (^{13}C SSNMR) were chosen due analysis of solid samples being possible (vinyl group analysis of nanoparticles can not be analysed using ^{1}H NMR and ^{13}C NMR unless the polymer particle is dissolved). The FT-IR and ^{13}C SSNMR spectra are shown in **Figure 3.11.** and **Figure 3.12.** respectively. The FT-IR spectra showed no vinyl peaks at 1639 cm^{-1} but did show the presence of a new peak at 1739 cm^{-1} from the carbonyl group in 3.1. The problem we encountered using ^{13}C NMR analysis was overlap between the vinyl group region and the aromatic carbons from the poly(2.5). This overlap was located at 125-130 ppm for the ^{13}C SSNMR (large aromatic carbon peaks) and the vinyl group peak was expected to be at 120-125 ppm. These techniques proved inconclusive for styrenic seed particles and poly(2.5) was subsequently removed from further experiments.

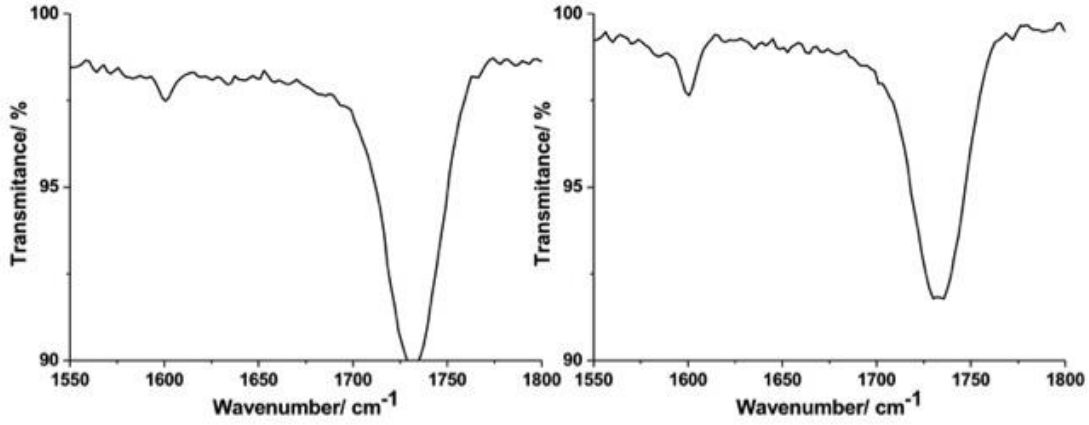

Figure 3.11. FT-IR spectra of an extended region between 1550 and 1800 cm-1, left) 2.5 ml poly(3.1) decorated poly(2.5), right) 1.0 ml poly(3.1-*co*-3.2) decorated poly(2.5-*co*-3.2).

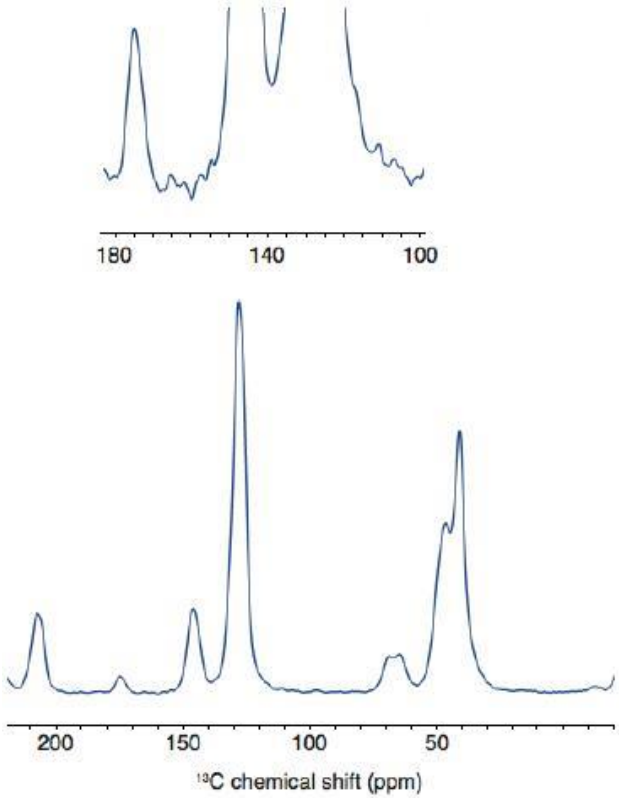

Figure 3.12. ^{13}C 500 MHz SSNMR spectrum of 0.5 ml poly(DEGDA) decorated poly(styrene) particles, acquisition range 0-200 ppm,with zoom region between 100 and 180 ppm.

3.4.5. Preparation of hydrophilic sulphonated poly(acrylic) seed nanoparticles

In order to remove the overlap problem experienced with styrenic seed nanoparticles we next tried the same polymerisations using acrylic seed nanoparticles. We repeated the batch soap-free emulsion polymerisation to synthesise a 10 wt% latex

incorporating 1 wt% 2.1 but using monomers methyl methacrylate (MMA, referred to as 3.3) and ethyl methacrylate (EMA, referred to as 3.4). Exact compositions are shown in **Table 3.11.** and structures for 3.3 and 3.4 are shown in **Figure 3.13.**.

Table 3.11. Recipe for the preparation of 10 wt% poly(acrylic) seed latex.

Sample	3.3 (g)	3.4 (g)	NaSS (g)	$NaHCO_3$ (g)	H_20 (ml)	KPS[(a)] (g)	$Xn^{(b)}$	Polymerisation time (hours)
Poly(3.3) seed	10.13	-	0.10	0.10	90	0.10	0.81	8
Poly(3.4) seed	-	10.12	0.10	0.10	90	0.10	0.80	5

Reaction temperature 70 ^{o}C. (a) Initiator 2.7 was dissolved into 1 ml of DDI H_2O. (b) Conversion measured by gravimetry (see experimental).

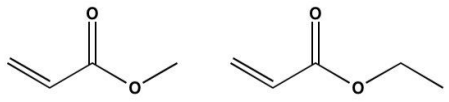

Figure 3.13. Structures of methyl methacrylate (MMA, left) and ethyl methacrylate (EMA, right).

The monomers 3.3 and 3.4 have T_g values of 105 ^{o}C (atactic) and 66 ^{o}C respectively and the seed particles synthesised are shown in **Figure 3.14.** Particle sizes for poly(3.3) were calculated to be 249 nm with a PDI of 0.034 from DLS measurements and 180 nm (s.d. 7.8 nm) with a CV of 4.3% from SEM analysis (**Table 3.12.**). Particle sizes for poly(3.4) were 207.2 nm with a PDI of 0.025 from DLS measurements and 167.4 nm (s.d. 10.0 nm) with a CV of 6.0% from SEM analysis (**Table 3.12.**). The hydration sphere from DLS measurements is much larger than the hydration sphere from the poly(2.5) seed latex due to the relative interaction between the acrylic seeds and water. Hydrogen bonding and dipolar interactions attract more water into the diffuse layer surrounding the particles so acrylic latexes have a larger double layer than styrenic latexes. The water solubility values for 3.3 and 3.4 are much greater than those from using monomer 2.5 and the seed particles will be more

hydrophilic (water solubility of 3.3 is 16 g/L and of 3.4 is 5 g/L both at 25 ºC according to the MSDS data from Sigma Aldrich).

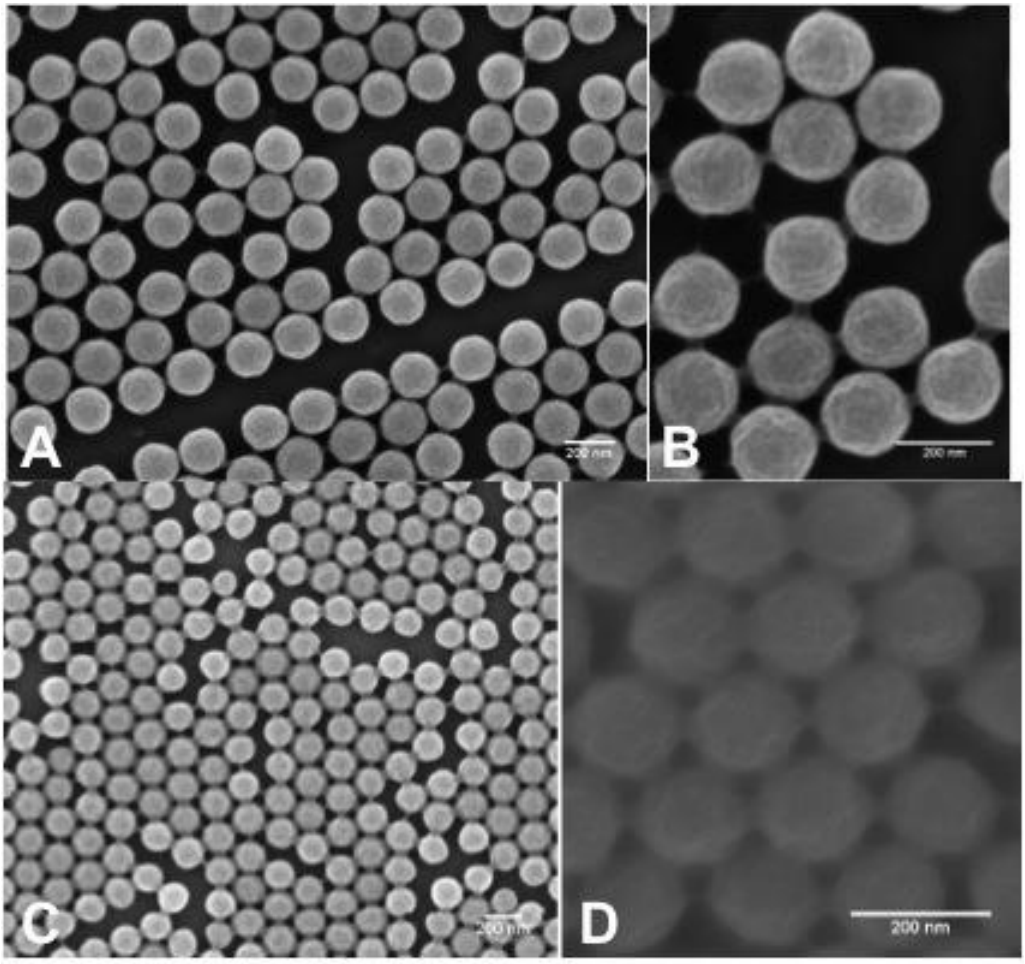

Figure 3.14. SEM micrographs of 10 wt% seed latex from batch soap-free emulsion polymerisation with 1 wt% 2.1 (based on monomer) and 2.7 initiator at 70 ºC. A) poly(3.3) seed, B) close up of poly(3.3) seed, C) poly(3.4) seed, D) close up of the poly(3.4) seed. All scale bars are 200 nm.

Table 3.12. Size analysis of poly(acrylic) seed latex using DLS and SEM.

Sample	Z_{Ave}[(a)] (nm)	PDI[(a)]	Particle diameter[(b)] (nm)	S.D. (nm)	CV (%)
Poly(3.3)	249.1	0.034	180.1	7.8	4.3
Poly(3.4)	207.2	0.025	167.4	10.0	6.0

(a) DLS measurements carried out at 25 ºC and averaged from 5 measurements. (b) Average particle diameters, standard deviation and coefficient of variation calculated using ImageJ software (see experimental).

3.4.6. Decoration of poly(MMA) and poly(EMA) seed nanoparticles with poly(DEGDA) particles

3.4.6.1. Poly(MMA) seed particles decorated with poly(DEGDA) particles

When the seed particle was changed to poly(3.3) we noticed a greater surface coverage when compared with the poly(2.5) and poly(2.5-*co*-3.2) latexes. This is shown in **Figure 3.15.** and the latex information and data is shown in **Table 3.13.** and **Table 3.14.**. We did notice a slight difference to the poly(2.5-*co*-3.2) seed where the amount of surface coverage of the poly(3.1) microgels as well as the shape of the decorating particles is different. The shape of the nanogels decorating the poly(3.3) seed are mainly non-spherical and many elongated above 2 ml of 3.1 (see **Figures 3.15-H.** to **Figure 3.15-J.**). The difference is caused by favourable interactions between both hydrophilic decorating particles and hydrophilic seed particles and this leads to increased spreading of the nanogel particles over the surface of the seed particles.. The poly(3.1) nanogel particles wet the surface of a hydrophilic seed more effectively due to an increase in van der Walls interactions between polar surfaces (refer to DLVO theory in **Chapter 1**). Contact angles are not reported for the latexes described from this point forth due to difficulty in measurements and contrast for the decorated poly(3.4) seed particles.

Table 3.13. Recipe for the preparation of poly(3.1) decorated poly(acrylic) latex.

Sample	Seed latex (ml)	H_20 (ml)	KPS[(a)] (g)	Total 3.1 added (ml)
Poly(3.1) decorated poly(3.3)	25	75	0.05	2.5
Poly(3.1) decorated poly(3.4)	25	75	0.05	0.5

Feed rate of 3.1 was 0.11 ml/min, temperature 70 ^{o}C. (a) Initiator 2.7 was dissolved into 1 ml of DDI H_2O. Samples were taken after every 0.5 ml of 3.1 was added. Reaction quenched 30 minutes after feed ended.

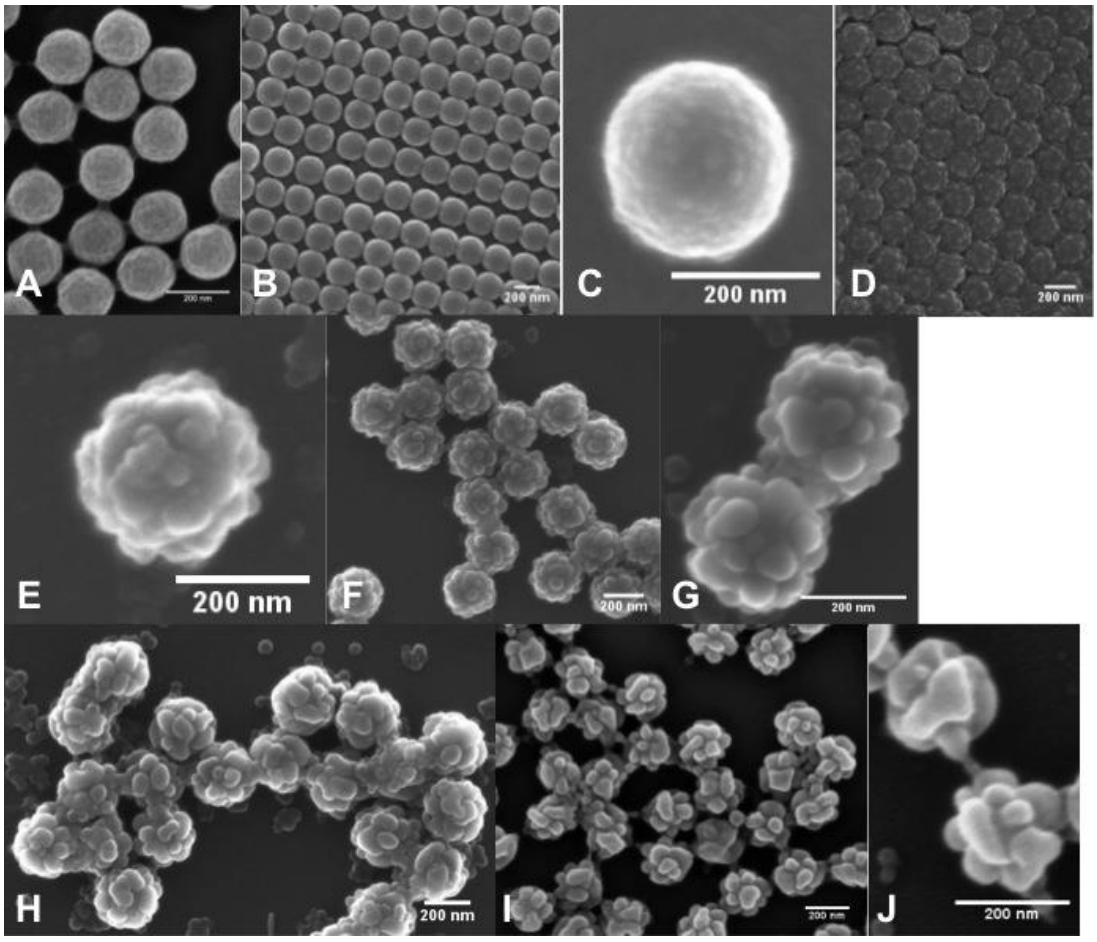

Figure 3.15. SEM micrographs of 2.5 wt% poly(3.3) seed latex with the starve-fed soap-free addition of 3.1, A) reference poly(3.3) seed particles, B) 0.1 ml 3.1, C) close up of a particle using 0.1 ml 3.1, D) 0.5 ml 3.1, E) close up of a particle using 0.5 ml 3.1, F) 1.0 ml 3.1, G) close up of the particles using 1.0 ml 3.1, H) 2.0 ml 3.1, I) 2.5 ml 3.1, J) close up of the particles using 2.5 ml 3.1. All scale bars are 200 nm.

3.4.6.2. Poly(EMA) seed particles decorated with poly(DEGDA) particles

The decoration of the poly(3.4) seed latex using poly(3.1) is shown in **Figure 3.16.** and **Table 3.14.**. Only 0.5 ml 3.1 was added to try and prevent increased nanogel particle sizes and secondary nucleation (secondary nucleation was visible when 1.0 ml to 2.5 ml 3.1 was added, see **Figure 3.15-H.**). The poly(3.4) seed showed a drastic difference when compared to all the previous decorated latexes. The morphology is much smoother and an almost core-shell morphology is observed. When we look at the sizes of the particles before and after decoration we notice a growth of ~40 nm (206.6 nm after decoration and 167.4 nm before).

Table 3.14. Size analysis of poly(3.1) decorated poly(3.3) and poly(3.4) seed latex using DLS and SEM.

Sample	Cross-linker amount (ml)	Z_{Ave} (nm)	PDI	Average particle diameter (nm)	S.D. (nm)	CV (%)	Average nanogel diameter (nm)	S.D. (nm)	CV (%)
Poly(3.1) decorated poly(3.3)	0.1	273.9	0.128	202.9	10.8	5.3	-	-	-
	0.5	274.4	0.071	267.6	13.3	5.0	35.6	8.6	24.0
	1.0	294.1	0.168	271.0	13.5	5.0	51.7	14.3	27.6
	1.5	282.1	0.150	288.6	13.9	4.8	54.2	13.8	25.5
	2.0	271.2	0.184	287.7	16.4	5.7	34.0	23.7	69.7
	2.5	296.7	0.326	2295	12.5	5.4	70.2	24.6	35.0
Poly(3.1) decorated poly(3.4)	0.5	230.4	0.038	206.6	9.0	4.3	47.8	6.4	13.5

DLS measurements carried out at 25 ^{o}C and averaged from 5 measurements. Average particle diameters, standard deviation and coefficient of variation calculated using ImageJ software (see experimental).

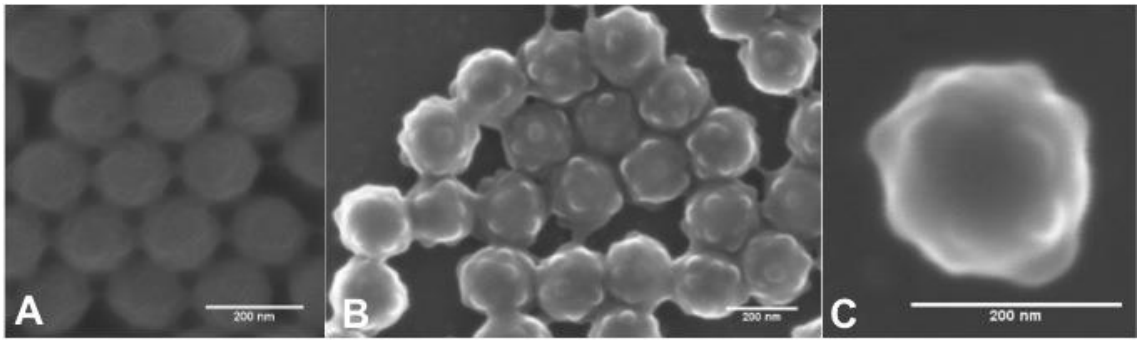

Figure 3.16. SEM micrographs of 2.5 wt% poly(3.4) seed latex with the starve-fed soap-free addition of 3.1, A) reference poly(3.3) seed particles, B) 0.5 ml 3.1, C) close up of a particle using 0.5 ml 3.1. All scale bars are 200 nm.

The nanogel domains show much less phase separation when compared to the harder Tg polymers (2.5 and 3.3) and the lower Tg of the seed plays an important role on the polymer diffusion into the seed particles as reported by Sundberg *et al.*[52] They discussed that Tg values 18 ^{o}C below the reaction temperature can allow significant polymer diffusion more towards the core of the seed particles. The poly(3.4) seed particles are ~4 ^{o}C below the reaction temperature and this likely leads to more polymer diffusion into the particles than poly(2.5) or poly(3.3) which have Tg values of 100 ^{o}C and 105 ^{o}C respectively. If more polymer diffuses towards the particle core then polymerisation will occur inside the particles and the nanogel particles will growth inside the seed particles rather than growing at the surface.

3.4.7. Influence of the seed nanoparticles on the decorating nanogel particles

Overall the results from the poly(3.1) decorated latexes indicate that the degree of decoration is influenced heavily by the seed hydrophobicity. Hydrophobic poly(2.5) showed less surface coverage and spreading of nanogel particles when compared to more hydrophilic poly(2.5-*co*-3.2), poly(3.3) and poly(3.4) seed particles. The Tg of the seed also has an influence on the morphology where high Tg polymers poly(2.5) and

poly(3.3) showed very phase separated raspberry domains and the low Tg poly(3.4) showed a smooth almost core-shell morphology.

3.4.8. Vinyl analysis of poly(DEGDA) decorated poly(acrylic) latexes

Unfortunately analysis of the poly(3.1) decorated acrylic latexes gave no indication of vinyl groups being present even with removal of the styrenic group overlaps. **Figure 3.17.**, **Figure 3.18.** and **Figure 3.19.** show the FT-IR and ^{13}C SSNMR spectra for the poly(3.1) decorated poly(3.3) and poly(3.4) seed latexes. Due to these results we decided to next try varying the decorating nanogel particles by the use of multifunctional acrylate crosslinkers.

3.4.9. Decoration of poly(EMA) seed nanoparticles using multi-functional acrylate nanogel particles

For the next multifunctional acrylate decorated latexes only the poly(3.4) seed was used. The feed monomer was altered by using two other crosslinking monomers penta-erythritol tri-acrylate (referred to as 3.5) and di-penta-erythritol penta-/hexa-acrylate (referred to as 3.6) whose structures are shown in **Figure 3.20.**. The monomer 3.5 was fed into the polymerisation vessel neat as it was a non-viscous liquid but the monomer 3.6 needed dissolution into either monomers 3.1 or 3.5 to allow feeding.

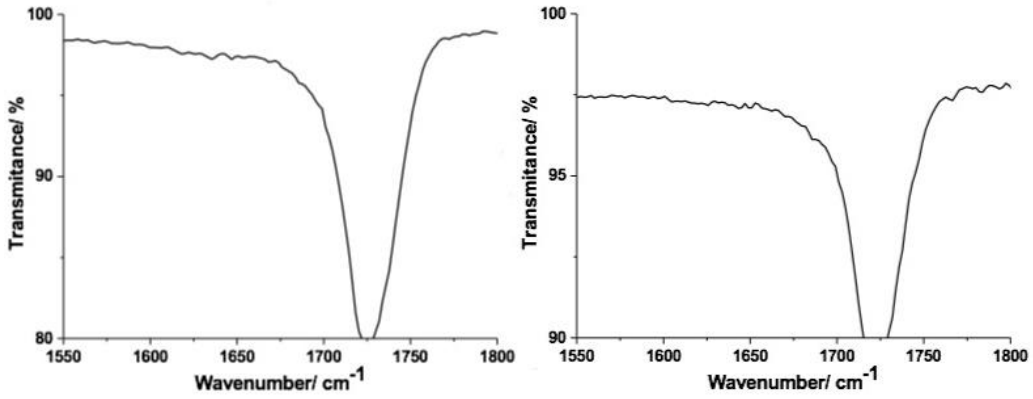

Figure 3.17. FT-IR spectra of an extended region between 1550 and 1800 cm-1, left) 2.5 ml poly(3.1) decorated poly(3.3), right) 1.0 ml poly(3.1) decorated poly(3.4).

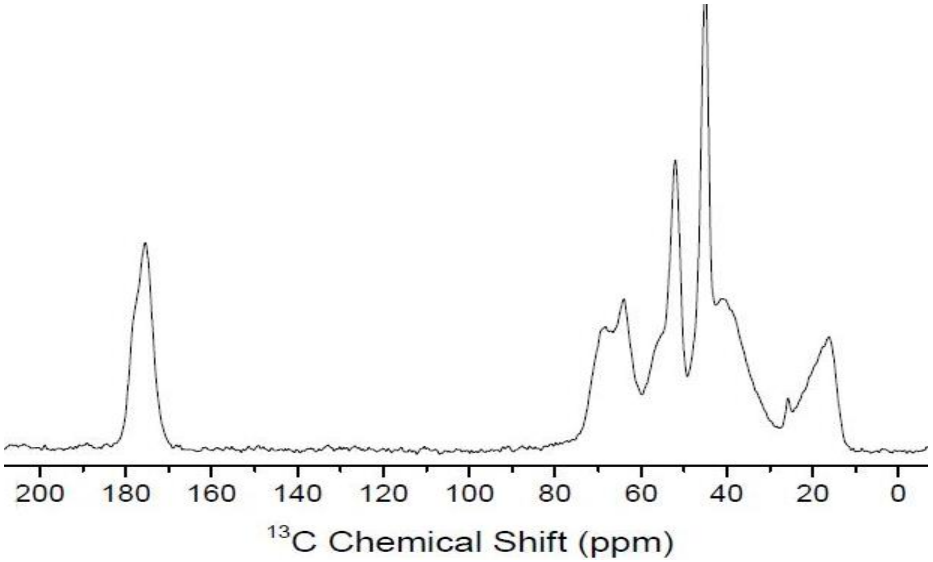

Figure 3.18. ^{13}C 500 MHz SSNMR spectrum of 2.5 ml poly(3.1) decorated poly(3.3) particles. 14000 scans. Acquisition range 0-200 ppm.

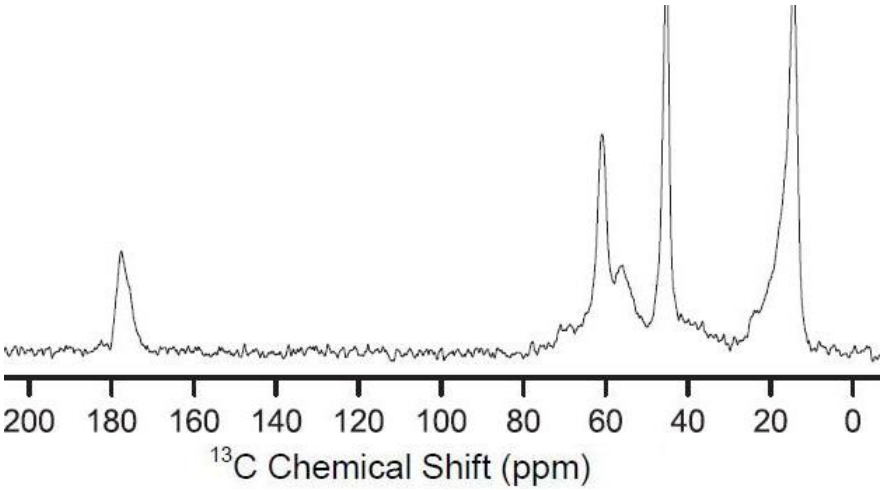

Figure 3.19. ^{13}C 500 MHz SSNMR spectrum of 0.5 ml poly(3.1) decorated poly(3.4) particles 1024 scans. Acquisition range 0-200 ppm.

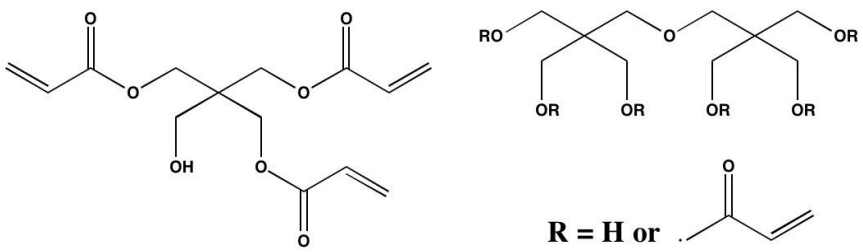

Figure 3.20. Structures of penta-erythritol tri-acrylate (left) and di-penta-erythritol penta-/hexa- acrylate (right).

3.4.9.1. Decoration of poly(EMA) seed nanoparticles with poly(DEGDA-co-tri-acrylate) particles

We combined two crosslinking monomers (50 wt% 3.1 and 50 wt% 3.5) and fed them into the reaction vessel at the same rates used for the addition of 3.1 (see **Table 3.15.** for latex ingredients). When we compare the poly(3.4) seed covered with poly(3.1-*co*-3.5) nanogel particles with the same seed covered with the poly(3.1) particles we observe a similar morphology *via* SEM analysis (see **Figure 3.16.** and **Figure 3.21.**). Full surface coverage was achieved by the nanogel particles (see **Figure 3.21.**). The decorating nanogel particle sizes (**Table 3.16.**) do not increase to the same extent as observed when poly(3.1) was used.

Table 3.15. Recipe for the preparation of poly(3.1-*co*-3.5) decorated poly(3.4) latex.

Sample	Seed latex (ml)	H_20 (ml)	KPS[(a)] (g)	Total 3.1-*co*-3.5 added (ml)
Poly(3.1-*co*-3.5) decorated poly(3.4)	25	75	0.05	1.0

Feed rate of 3.1-*co*-3.5 was 0.11 ml/min, temperature 70 ^{o}C. (a) Initiator 2.7 was dissolved into 1 ml of DDI H_2O. Samples were taken after every 0.5 ml of 3.1-*co*-3.5 was added. Reaction quenched 30 minutes after feed ended.

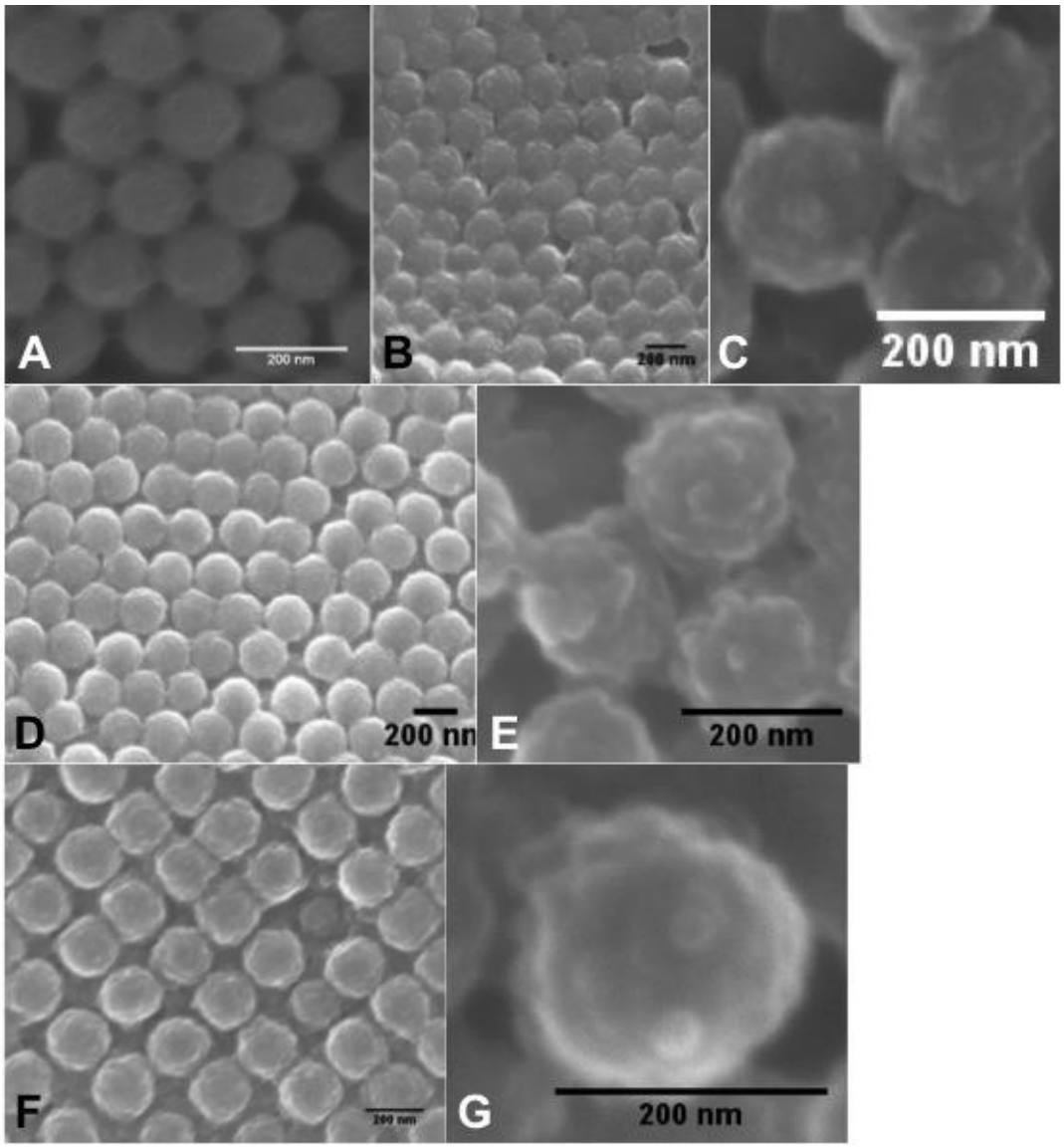

Figure 3.21. SEM micrographs of 2.5 wt% poly(3.4) seed latex with the starve-fed soap-free addition of 3.1-*co*-3.5 (ratio 50:50); A) reference poly(3.4) seed particles, B) 0.5 ml 3.1-*co*-3.5, C) close up of the particles using 0.5 ml 3.1-*co*-3.5, D) 1.0 ml 3.1-*co*-3.5, E) close up of the particles using 1.0 ml 3.1-*co*-3.5, F) 1.0 ml 3.1-*co*-3.5 after 30 minutes G) close up of the particles using 1.0 ml 3.1-*co*-3.5 after 30 mins. All scale bars are 200 nm.

However, we notice that the decorating nanogel particles at the surface are more spherical in shape than was visualised using poly(3.1). The boundaries between each nanogel particles are more pronounced when using poly(3.1-*co*-3.5) and a rougher surface is visualised. The cause is most likely due to the elasticity difference of the polymer network that forms as well as an altered crosslinking density of the nanogel. The use of a tri-functional acrylate crosslinker alters the polymer network that forms

where more reactive sites are present due to the increase in vinyl groups and therefore levels of branching sites. The length of the crosslinker will affect the T_g value of the polymer microgels due to an increase in the molecular weight.[21,32,50]

Table 3.16. Size analysis of poly(3.1-*co*-3.5) decorated poly(3.4) seed latex using SEM.

Sample	Cross-linker amount (ml)	Average particle diameter (nm)	S.D. (nm)	CV (%)	Average nanogel diameter (nm)	S.D. (nm)	CV (%)
Poly(3.1-*co*-3.5) decorated poly(3.4)	0.1	205.8	10.9	5.3	-	-	-
	0.5	211.8	6.8	3.2	31.6	6.6	20.8
	1.0	216.8	7.5	3.4	34.4	5.6	16.3

Average particle diameters, standard deviation and coefficient of variation calculated using ImageJ software (see experimental).

The 0.5 ml poly(3.1-*co*-3.5) nanogel decorated poly(3.4) seed shows a smoother morphology when compared to the poly(3.1) decorated poly(3.3) seed and a rougher morphology compared to the poly(3.1) decorated poly(3.4) seed. The crosslinker functionality clearly affects how the nanogel particles form and how they grow when after spreading onto the seed surface. Contact angle measurements were difficult to measure for this latex due to the lack of spherical shaped nanogel particles as well as more of core-shell type morphology (raspberry particles are easier to measure nanogel particle sizes and contact angles due to well phase separated domains)..

3.4.9.2. Decoration of poly(EMA) seed nanoparticles with poly(tri- acrylate) particles

We continued the above synthesis but this time the seed nanoparticles were decorated using poly(3.5) nanogel particles instead of poly(3.1-*co*-3.5) and similar morphology particles were produced (see **Table 3.17.** for latex ingredients).

Table 3.17. Recipe for the preparation of poly(3.5) decorated poly(3.4) latex.

Sample	Seed latex (ml)	H_20 (ml)	KPS[(a)] (g)	Total 3.5 added (ml)
Poly(3.5) decorated poly(3.4)	25	75	0.05	1.0

Feed rate of 3.5 was 0.11 ml/min, temperature 70 ºC. (a) Initiator 2.7 was dissolved into 1 ml of DDI H_2O. Samples were taken after every 0.5 ml of 3.5 was added. Reaction quenched 30 minutes after feed ended.

No definitive differences could be found as the shapes and sizes of the nanogel particles are almost identical (see **Figure 3.22.** for SEM micrograph and **Table 3.18.** for DLS and SEM results). However, the surface of the decorated nanoparticles appeared slightly smoother when poly(3.5) was used over poly(3.1-*co*.3.5). Only the 1.0 ml poly(3.5) sample is shown *via* SEM analysis due to the difficulty with gaining a clear image.

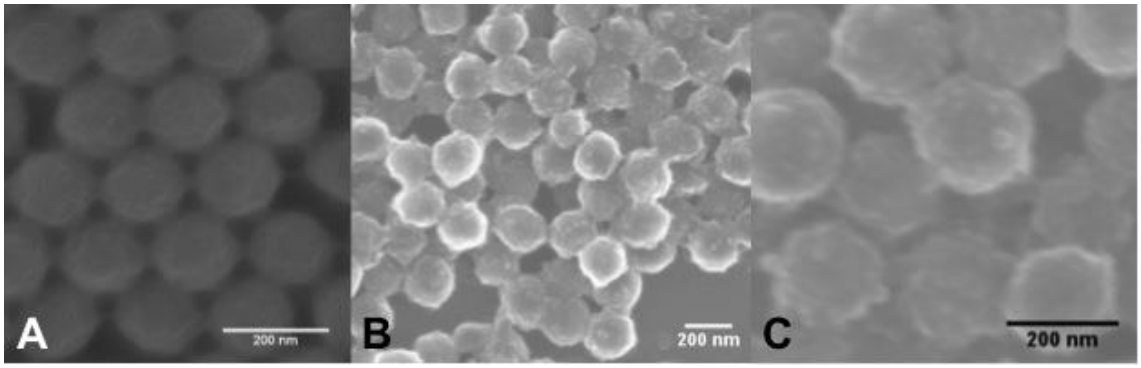

Figure 3.22. SEM micrographs of 2.5 wt% poly(3.4) seed latex with the starve-fed soap-free addition of 3.5 (ratio 50:50), A) reference poly(3.4) seed particles, B) 1ml 3.5, C) close up of the particles using both 1.0 ml 3.5. All scale bars are 200 nm.

Table 3.18. Size analysis of poly(3.5) decorated poly(3.4) seed latex using DLS and SEM.

Sample	Cross-linker amount (ml)	Z_{Ave} (nm)	PDI	Average particle diameter (nm)	S.D. (nm)	CV (%)	Average nanogel diameter (nm)	S.D. (nm)	CV (%)
Poly(3.5) decorated poly(3.4)	0.1	-	-	203.9	9.0	4.4	-	-	-
	0.5	-	-	212.1	8.0	3.8	31.7	7.1	22.5
	1.0	271.1	0.029	213.5	9.8	4.6	-	-	-

DLS measurements carried out at 25 ^{o}C and averaged from 5 measurements. Average particle diameters, standard deviation and coefficient of variation calculated using ImageJ software (see experimental).

3.4.9.3. Decoration of poly(EMA) seed nanoparticles with poly(DEGDA-co-penta-/hexa- acrylate) particles

We synthesised a poly(3.1-*co*-3.6) nanogel decorated poly(3.4) seed latex using the recipe shown in **Table 3.19.** and the SEM and DLS results are reported in **Table 3.20.**. The SEM images are shown in **Figure 3.23.** and we notice a similarity with the poly(3.1) decorated poly(3.3) seed showed earlier (**Figure 3.15.**). Long irregular nanogel particle shapes were observed leading to an overall smoother surface shell and more of a core-shell morphology. Clearer boundaries exist between each nanogel particles and growth of the nanogel particles is very irregular in shape. This irregular growth and spreading mechanism provides very effective surface coverage as shown in **Figure 3.23-C.** and **3.23-D.**.

Table 3.19. Recipe for the preparation of poly(3.1-*co*-3.6) decorated poly(3.4) latex.

Sample	Seed latex (ml)	H_20 (ml)	KPS[(a)] (g)	Total 3.1-co-3.6 added (ml)
Poly(3.1-*co*-3.6) decorated poly(3.4)	25	75	0.05	1.0

Feed rate of 3.1-*co*-3.6 was 0.11 ml/min, temperature 70 ^{o}C. (a) Initiator 2.7 was dissolved into 1 ml of DDI H_2O. Samples were taken after every 0.5 ml of 3.1-*co*-3.6 was added. Reaction quenched 30 minutes after feed ended.

Again we note the low dispersity of the sample where DLS analysis gave a PDI of 0.020 (**Table 3.20.**) and the hexagonal packed structure is shown in **Figure 3.23-B.** and **Figure 3.22-D.**. Particle size measurements using SEM image analysis with ImageJ showed that the poly(3.1-*co*-3.6) decorated poly(3.4) nanoparticles have the smallest particle sizes of the multi acrylate decorated latexes. The particle sizes for the poly(3.1-*co*-3.6) decorated poly(3.4) latex were 178.2 nm (0.5 ml) and 182.5 nm (1.0 ml) whereas the particle sizes for the poly(3.1-*co*-3.5), poly(3.5) and poly(3.5-*co*-3.6)

decorated latexes were 203-216 nm (**Table 3.12.**). DLS analysis also shows a larger value for the hydrodynamic diameter at ~235 nm again due to a hydration sphere caused by hydrogen bonded water molecules or swelling of the nanogel particles.

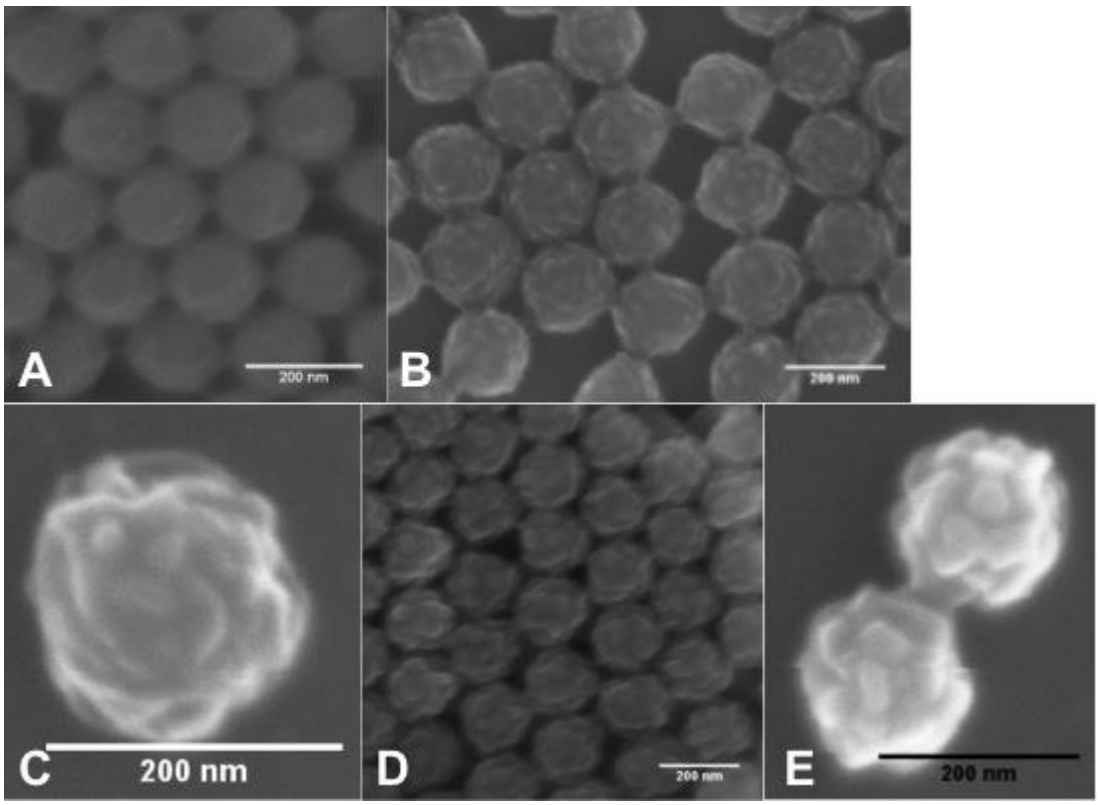

Figure 3.23. SEM micrographs of 2.5 wt% poly(3.4) seed latex with the starve-fed soap-free addition of 3.1-*co*-3.6 (ratio 50:50); A) reference poly(3.4) seed particles, B) 0.5 ml 3.1-*co*-3.6, B)close up of a particles using 0.5 ml 3.1-*co*-3.6, C) 1.0 ml 3.1-*co*-3.6, D) close up of the particles using 1.0 ml 3.1-*co*-3.6. All scale bars are 200 nm.

3.4.9.4. Decoration of poly(EMA) seed nanoparticles with poly(tri- acrylate-co-penta-/hexa- acrylate) particles

The final multi-functional decorated seed latex used monomers 3.5 and 3.6 as reported in **Table 3.21.** and the results are reported in **Table 3.22.**. The SEM analysis for the poly(3.5-*co*-3.6) decorated nanoparticles are shown in **Figure 3.24.**. A similarity with the poly(3.1-*co*-3.5) and poly(3.5) decorated poly(3.4) latexes is apparent. Uniform

surface coverage of the nanogel particles is observed and the decorating nanogel particles increase in size as shown as more crosslinker is added.

Table 3.20. Size analysis of poly(3.1-*co*-3.6) decorated poly(3.4) seed latex using DLS and SEM.

Sample	Cross-linker amount (ml)	Z_{Ave} (nm)	PDI	Average particle diameter (nm)	S.D. (nm)	CV (%)	Average nanogel diameter (nm)	S.D. (nm)	CV (%)
Poly(3.1-*co*-3.6) decorated poly(3.4)	0.5	-	-	178.2	8.4	4.7	25.7	6.0	23.5
	1.0	235.9	0.020	182.5	8.8	4.8	32.2	6.9	18.0

DLS measurements carried out at 25 °C and averaged from 5 measurements. Average particle diameters, standard deviation and coefficient of variation calculated using ImageJ software (see experimental).

The surface morphology appears to be the smoothest compared to all the other nanogel decorated latexes even when 1.0 ml crosslinking monomer is used Unlike the poly(3.1-*co*-3.6) decorated poly(3.4) latex we can visualise distinct hemi-spherical nanogel particles. The morphology of the decorated particles is more similar to the poly(3.1) decorated poly(2.5-*co*-3.2) latex particles in that clear boundaries are observed between nanogel particles (see **Figure 3.24-F.**).

Table 3.21. Recipe for the preparation of poly(3.5-co-3.6) decorated poly(3.4) latex.

Sample	Seed latex (ml)	H_20 (ml)	KPS[(a)] (g)	Total 3.1-co-3.6 added (ml)
Poly(3.5-*co*-3.6) decorated poly(3.4)	25	75	0.05	1.0

Feed rate of 3.5-*co*-3.6 was 0.11 ml/min, temperature 70 ^{o}C. (a) Initiator 2.7 was dissolved into 1 ml of DDI H_2O. Samples were taken after every 0.5 ml of 3.5-*co*-3.6 was added. Reaction quenched 30 minutes after feed ended.

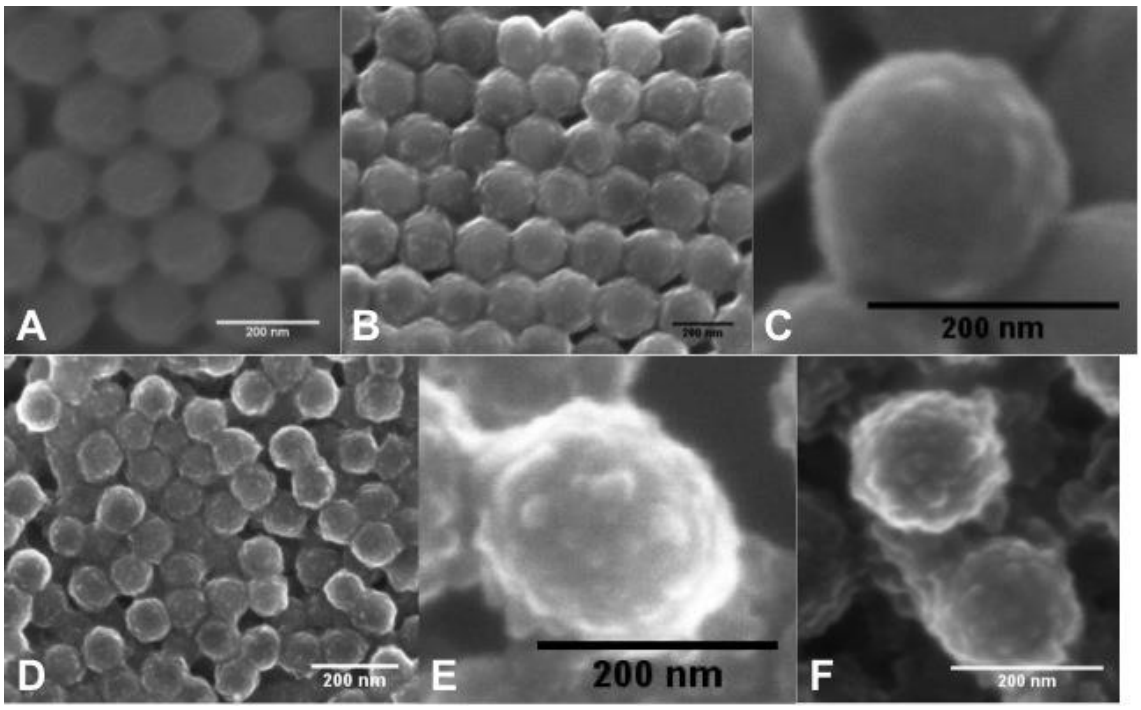

Figure 3.24. SEM micrographs of 2.5 wt% poly(3.4) seed latex with the starve-fed soap-free addition of 3.5-*co*-3.6 (ratio 50:50), A) reference poly(3.4) seed particles, B) 0.25 ml 3.5-*co*-3.6, C) close up of the particles using 0..25 ml 3.5-*co*-3.6, D) 0.5 ml 3.5-*co*-3.6, E) close up of the particles using 0.5 ml 3.5-*co*-3.6, F) 1.0 ml 3.5-*co*-3.6 after 30 mins. All scale bars are 200 nm.

Table 3.22. Size analysis of poly(3.5-*co*-3.6) decorated poly(3.4) seed latex using SEM.

Sample	Cross-linker amount (ml)	Average particle diameter (nm)	S.D. (nm)	CV (%)	Average nanogel diameter (nm)	S.D. (nm)	CV (%)
Poly(3.5-*co*-3.6) decorated poly(3.4)	0.5	204.3	8.2	4.0	27.9	5.4	19.5
	1.0	214.4	11.6	5.4	20.4	4.7	19.6

DLS measurements carried out at 25 ^{o}C and averaged from 5 measurements. Average particle diameters, standard deviation and coefficient of variation calculated using ImageJ software (see experimental).

3.4.10. Vinyl analysis of poly(multi-functional acrylate) decorated poly(EMA) latexes

Having synthesized a variety of multi acrylate nanogel decorated poly(3.4) particles we decided to try detect or quantify vinyl groups at the surface. We tried ^{13}C SSNMR on the poly(3.1-*co*-3.6) decorated poly(3.4) latex which we believed would possess a high number of pendant vinyl groups (^{13}C SSNMR spectrum is shown in **Figure 3.25.**). Unfortunately ^{13}C NMR still showed no visible vinyl peak around 120-125 ppm even when a 500 MHz spectrometer and higher scan number of 18000 was used. If vinyl groups did exist on our particles either the quantity was too low to analyse (less than 1%) or the detection resolution of the NMR was too low.

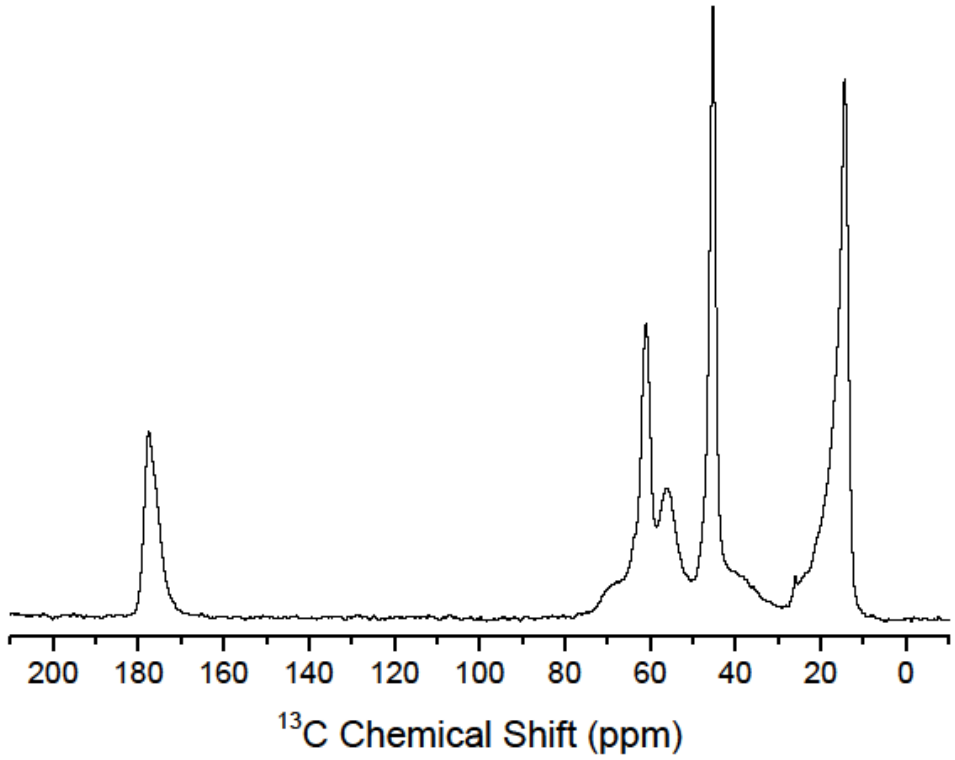

Figure 3.25. ^{13}C SSNMR spectrum for poly(3.1-*co*-3.6) decorated poly(3.4) latex using 18000 scans on a 500 MHz spectrometer.

From ^{13}C SSNMR we tried Raman spectroscopy to try and find the presence of vinyl groups. Raman microscopy has a much faster acquisition time compared to ^{13}C SSNMR (^{13}C SSNMR required specialist training and was run by the Lewandowski group) where acquisition times are similar to that of FT-IR spectroscopy. Using longer scan times for Raman spectroscopy allows reduction in the signal to noise ratio providing a smoother spectra for analysis. Due to time consumption, training and cost of use more samples were analysed using Raman spectroscopy than was possible for ^{13}C SSNMR. The spectra obtained using Raman spectroscopy are shown in **Figure 3.26.** for the poly(3.1-*co*-3.5), poly(3.5), poly(3.1-*co*-3.6) and poly(3.5-*co*-3.6) decorated poly(3.4) latexes.

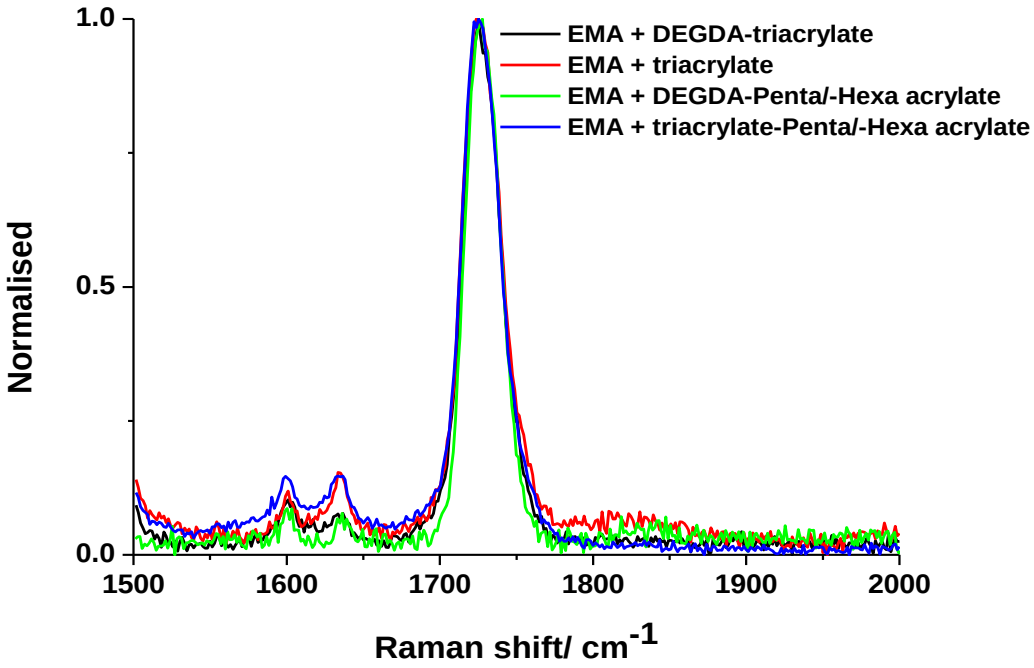

Figure 3.26. Normalised Raman spectra of four decorated poly(3.4) latexes where spectra had baseline subtraction followed by normalising with respect to the peak at 1739 cm^{-1}. The region 1500-2000 cm^{-1} is shown.

Raman microscopy has the advantage or being able to run any sample type making it ideal for latex powder or films and most solvents do not interfere with the

Raman spectra. The major factors affecting the Raman spectra are the sample acquisition time and surface that the sample is analysed on. Glass and aluminium are often the best choice of substrates and give the least interference or fluorescence. The peak at 1739 cm^{-1} is from the carbonyl C=O group. The peaks located at 1600 cm^{-1} is due due to C-H bond vibrations. The peaks at 1643 cm^{-1} is clearly visible for all four latexes using multi-acrylate nanogel decoration and this peak is attributed to the vinyl group stretching frequency. The vinyl group is typically located around 1635-1650 cm^{-1} (depending on the vinyl group and further substituent groups).[53-57] The vinyl peak is a much stronger peak for Raman spectroscopy compared with FT-IR spectroscopy due to the polarisability of the C=C bond. The use of IR and Raman spectroscopy has been studied by Gauthier *et al*,[54] Rueggeberg *et al*[55] and other authors for analysing the degree of conversion of dental resins or studying other vinyl polymerisations. The polarisability of the vinyl group helps quantify the conversion.[54-59]

By studying the peaks located between 1500 and 2000 cm^{-1} we normalised the peaks with respect to the carbonyl peak at 1739 cm^{-1}. By integrating the vinyl peak relative to the carbonyl peak, using both area and height, we are able to estimate the ratio of vinyl groups relative to the carbonyl peaks. Gauthier *et al*[54] and Reuggenberg *et al*[55] showed that quantification of acrylate polymers using Raman uses the carbonyl C=O peak as a reference. Rueggeberg *et al* analysed the differences between integrating the vinyl and carbonyl peaks using both area and height and no discernable differences were found.[55] The ratios of the three peaks at 1600 cm^{-1}, 1643 cm^{-1} and 1739 cm^{-1} are shown in **Table 3.23.** for the four decorated poly(multiacrylate) latexes where the carbonyl peak is set at a value of 1.

Table 3.23. Raman peak integration and the analysis of ratios between the carbonyl and vinyl groups in determining relative amounts of pendant vinyl groups for poly(multi-acrylate) decorated poly(3.4) latexes.

Sample	Wavenumbers (cm^{-1})	Peak area[(a)]	Peak height[(a)]	RI C=O/ RO C=C Area	RI C=O/ RO C=C Height	Percentage of vinyl groups (Area %)	Percentage of vinyl groups (Height %)
Poly(3.1-*co*-3.5)	1600	0.041	0.089	34.76	16.39	1.5	3.1
	1636	0.029	0.061				
	1725	1.000	1.000				
Poly(3.5)	1600	0.040	0.097	15.24	7.86	3.3	6.4
	1633	0.066	0.127				
	1723	1.000	1.000				
Poly(3.1-*co*-3.6)	1600	0.045	0.096	33.55	12.89	1.5	3.9
	1636	0.030	0.078				
	1726	1.000	1.000				
Poly(3.5-*co*-3.6)	1599	0.049	0.098	17.20	9.90	2.9	5.0
	1636	0.058	0.100				
	1725	1.000	1.000				

(a) Baseline subtraction was done using Microcal origin, followed by integration of the peaks for both area and height.

From the Raman spectra peak intensities calculated using the area and height of the peaks it appears that the smallest vinyl peaks were shown for both poly(3.1) decorated poly(3.4) latex meaning that 3.1 crosslinks the most. The lowest group ratios are shown for both poly(3.5) and poly(3.5-*co*-3.6) decorated poly(3.4) latexes indicating that the multi-functional crosslinkers polymerise to a lesser degree than the single chained crosslinkers. This leaves more pendant vinyl groups available that may be inside or at the surface or the nanogel particles. Using an octa-functionalised acrylate monomer would hypothetically provide a greater degree of vinyl groups but would likely be a solid and therefore would require other liquid crosslinkers for solubility to be of use. From the ratio values calculated from both area and height intensities the order of increasing pendant vinyl groups is as follows: 3.1-*co*-3.5>3.1-*co*-3.6>3.5-*co*-3.6>3.5. Also noticed is that using integration of the peak area for C=O/C=C ratios gives roughly double the values of the corresponding peak height ratios.

We also decided to compare the values shown in **Table 3.23.** to those of the monomer before polymerisation where the decrease in the vinyl group can be viewed as a percentage of the starting material. In the book by Nyquist[57] specified ratios of the C=C to C=O groups have been measured for various acrylate monomers.[57] When we study the structures for the monomers 3.5 and 3.6 we note that each arm comprises of an ethyl acrylate group which either has 3 arms or five/six arms respectively (see **Figure 3.20.**). From the data available in the book[57] and the sigma Aldrich FT-Raman spectra (available only for monomer 3.5) we noted relative intensities for methyl and propyl acrylates to average out to a value of 0.50 (C=O/C=C). This means that the C=C is approximately twice the intensity of the C=O peak in its monomeric state. Comparison of the monomeric peak intensity ratio to those analysed from the decorated poly(3.4)

nanoparticles we tried to quantify the percentage conversion of the monomers (**Table 3.23.**). The values we obtained for conversion are calculated from the ratio of C=O/C=C values for monomer conversions of 0% and 100%. Analysis of the Raman spectra data and integration of the peaks indicated relative vinyl group concentrations to be below 6.4% with a lowest value of 1.5%. All the integration by height values gave roughly double the percentage of unreacted vinyl groups compared to integrating using area.

Okubo reported a slightly different approach to quantification of the amount if vinyl groups from poly(DVB) microspheres prepared using dispersion polymerisation. Pre-reacting the vinyl groups with bromine allowed elemental analysis to be carried out generating accurate quantification of the surface vinyl groups. Vinyl groups under the particle surface would not react with the bromine so the true number of vinyl groups throughout the particle may be much greater than those reported.[25]

3.4.11. Thiol-Michael addition chemistry

Due to the presence of vinyl groups on the nanogel decorated colloids shown by Raman spectroscopy we decided to try a post-functionalisation reaction to further functionalise the surface of the particles. Recently the thiol-Michael addition reaction has shown widespread use for the functionalisation of vinyl polymers in a variety of solvents especially water.[33] Recent reviews have highlighted the conditions for both radical and catalytic approaches where we are more interested in the catalytic approach which can follow either base catalysed or nucleophilic initiation mechanisms (see **Scheme 3.1.** for the thiol-Michael nucleophilic addition reaction mechanism).[34-35]

Li *et al* did a recent review of the conditions required for the thiol-Michael addition reaction using various vinyl monomers (or olefins) with different thiols. The

mechanism of initiation and the products were studied using MALDI-TOF, FT-IR and NMR spectroscopy.[41] They reported that catalytic amounts of straight chained primary amines such as hexylamine provided a nucleophilic rather than basic initiation of the thiol-Michael addition reaction. The thiol-Michael addition reaction could be completed in under 500s for most vinyl monomers (the exceptions are methacrylates and styrenics which can take considerably longer). They also showed the use of phosphine compounds dimethylphenylphosphine and tris(2-carboxyethyl) phosphine hydrochloride (DMPP and TCEP respectively) as a method to increase the rate of reaction between thiol and olefin even when the concentration of catalyst was an order of two lower than for the amines. The advantages of the reaction between a thiol and olefin using amine and phosphine catalysts is that solubilities can be achieved in all the major solvents and side product formation is prevented under certain conditions (alternatively side reactions are highly likely *via* radical initiation). Unfortunately the amine and phosphine catalysts did suffer from side reactions occurring when the ratio of catalyst to monomer was much greater than one.

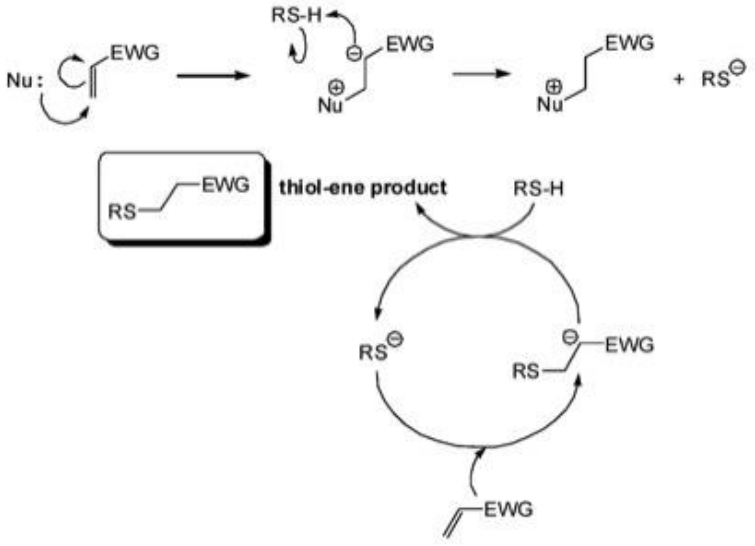

Scheme 3.1. Reaction scheme for the nucleaophilic thiol-Michael addition reaction [Reproduced from reference 34].

For the chosen multi-functional acrylate system we tested three different thiols to monitor the loss of vinyl peaks: sodium 3-mercapto-1-propanesulfonate (referred to as 3.7), *L*-cysteine (referred to as 3.8) and penta-erythritol tetra-kis(3-mercaptopropionate) (referred to as 3.9). The addition of thiol to the latex is discussed in the experimental **Section 3.3.5.** (thiol structures are shown in **Figure 3.27.**) where an excess of thiol was added to the poly(3.1-*co*-3.6) decorated poly(3.4) latex under stirring. Followed 1 hour of stirring a slight excess of *iso*butylamine was injected to initiate the thiol-Michael addition reaction (structure of isobutylamine shown in the next **Chapter 4 Figure 4.3.**). A slight excess of thiol was added so that the chances of the thiolate reacting with a pendant surface vinyl group is increased especially as the concentration of surface vinyl groups may be low indicated from the Raman spectra analysis (see **Table 3.23.**). Following the addition of thiol we allowed two days of stirring to try and ensure high conversion under the dilute latex conditions and afterwards the latex was dialysed to remove any amine catalyst and unreacted thiol. Raman spectroscopy was carried out on the dialysed latex film for the three thiols tested and this these spectra are shown in **Figure 3.28.**.

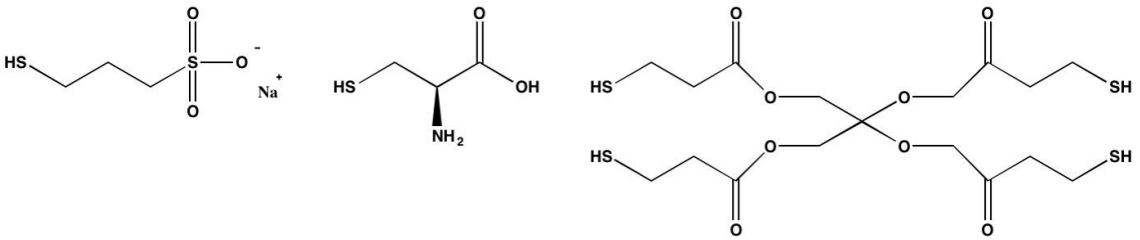

Figure 3.27. Structures of thiols used for thiol-Michael addition reaction, sodium 3-mercapto-1-propanesulphonate (left), *L*-cysteine (middle), penta-erythritol tetra-kis(3-mercaptopropionate) (right).

In **Figure 3.28.** all three samples still show peaks at 1600 cm^{-1} and 1736-1739 cm^{-1}. In the majority of samples the vinyl peak at 1646 cm^{-1} has practically disappeared. The only exception to this decrease in vinyl band occurs for the latex functionalised

using 3.7. One possible reason for this peak occurring could be due to an absorption property of sulphonated compounds that are typically hygroscopic in nature. Raman spectroscopy has been reported for 3.7 by Houlton *et al*[60] where a water peak was located at 1645 cm^{-1} and Reed *et al* showed that sulphonates with carbon chain lengths below octyl have a very hygroscopic nature and will absorb moisture.[61]

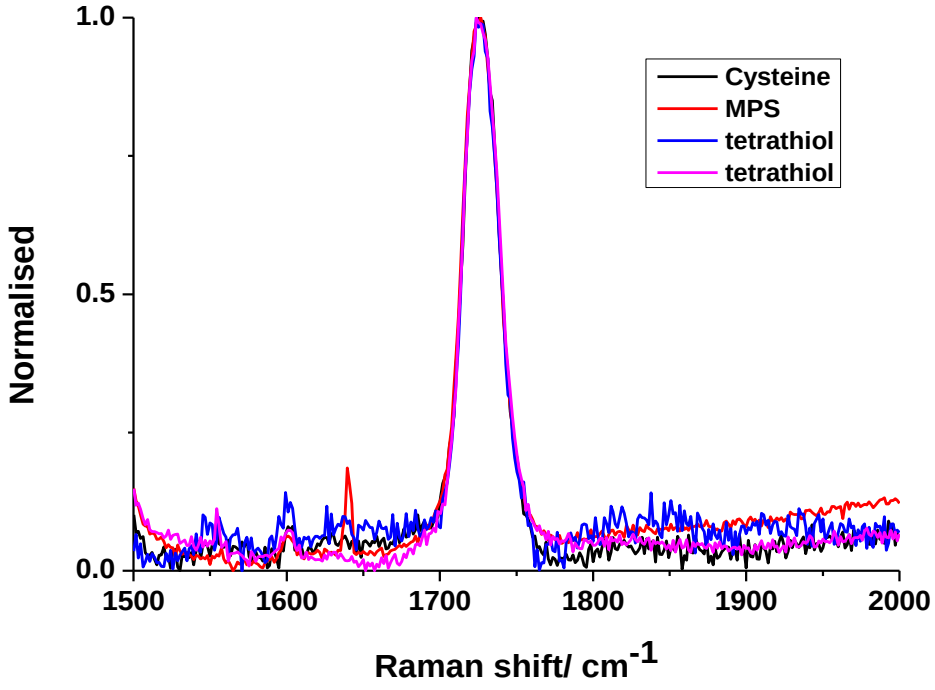

Figure 3.28. Normalised Raman spectra of poly(3.1-*co*-3.6) decorated poly(3.4) latexes reacted with 3.7, 3.8 and 3.9. All spectra had baseline subtraction followed by normalising with respect to the peak at 1739 cm^{-1}. The region 1500-2000 cm^{-1} is shown.

If we again study the integration ratio between the normalised vinyl peak and carbonyl peak intensities (**Table 3.24.**) we can clearly see a decrease in the carbonyl to vinyl ratios possibly indicating that vinyl bonds have been reacted that were previously pendant (the concentration was identical). Nearly all the vinyl peak ratios show a decrease where up to 50% of the vinyl groups are shown to have reacted for the 3.9 reacted poly(3.1-*co*-3.6) decorated poly(3.4) latex.

Table 3.24. Raman peak integration and the analysis of ratios between the carbonyl and vinyl groups in determining relative amounts of pendant vinyl groups for poly(3.1-*co*-3.6) decorated poly(3.4) latexes after thiol-Michael addition reactions.

Sample	Wavenumbers (cm^{-1})	Peak area[(a)]	Peak height[(a)]	RI C=O/ RO C=C Area	RI C=O/ RO C=C Height	Percentage of vinyl groups (Area %)	Percentage of vinyl groups (Height %)
3.7	1600	0.017	0.050	31.8	5.8	1.6	8.6
	1629	0.031	0.172				
	1725	1.000	1.000				
3.8	1600	0.027	0.076	39.6	19.7	1.3	2.5
	1630	0.025	0.051				
	1723	1.000	1.000				
3.9	1600	0.031	0.065	72.2	32.4	0.7	1.5
	1630	0.014	0.031				
	1723	1.000	1.000				

(a) Baseline subtraction was done using Microcal origin, followed by integration of the peaks for both area and height.

Again we see slight variation between the measurements using both area under the peak and the peak height but both shows a similar decrease in vinyl group percentage. Unfortunately this decrease in vinyl group percentage is not conclusive that the thiol-Michael addition reaction occurred. It could be caused from side reactions occurring and reacting with the vinyl groups or possibly resolution limitations of the techniques used to study the vinyl group intensities.

3.5. Conclusion

In this chapter we reported the use of starve fed soap-free emulsion polymerisation for the synthesis of nanogel decorated raspberry and core-shell morphology nanoparticles. We synthesised nanogel decorated polymer latexes by feeding of di-, tri- and multi- functional acrylate crosslinkers to a range of hydrophobic and hydrophilic styrenic and acrylic seed latexes. We report differences is surface wetting and coverage for each seed with different sizes and relative hydrophobicities. The results indicated that decoration of hydrophilic seeds such as poly(EMA) and poly(MMA) gave the lowest contact angles and greatest surface coverage of nanogel particles. Hydrophobic polymer particles such as poly(styrene) showed low surface coverage and higher contact angles. Hydrophilic poly(styrene) particles were prepared by copolymerisation of styrene with poly ethyleneglycol methyl ether acrylate which further increased the amount of surface covering nanogel particles. The size of the polymer seed particles played a factor in the number of decorating particles where larger particles allowed more surface adhesion. Changing the crosslinker of the decorating nanogel particles from di-functional to tri-functional and finally to multi-functional drastically altered the surface morphology. Synthesis of raspberry and core-shell type structures were observed and particle shapes and morphologies were analysed using SEM and DLS.

Spectroscopic studies NMR, FT-IR and Raman could not detect pendant vinyl groups for the di-acrylate crosslinked nanogel particles but changing to tri-acrylate and penta-/hexa-acrylate monomers allowed pendant vinyl groups to be visualised by Raman spectroscopy. Raman microscopy allowed utilisation of the stronger vinyl group

absorption that FT-IR and NMR lacked. Following the quantification on vinyl groups on the particles from the Raman spectra a thiol-Michael addition reaction was carried out. The thiol-Michael addition reaction used nucleophilic catalyst *iso*butylamine (under aqueous conditions at room temperature) to react the vinyl groups with sodium 3-mercapto-1-propanesulphonate, cysteine and penta-erythritol tetra-kis 2-mercapto propionate. Raman microscopy was again used to show a decrease in the vinyl peak intensity.

3.6. References

1. Hergeth WD, Bittrich HJ, Eichhorn F, Schlenker S, Schmutler K, Steinau UJ, Polymerizations in the presence of seeds: core-shell structure using two-stage emulsion polymers, *Polymer*, 1989; **30**:1913-1917
2. Lee CF, The morphology of composite particle: produced by multistage soapless seeded polymerization, *Colloid Poly. Sci.*, 2002; **280**:116-123
3. Kirsch S, Doerk A, Bartsch E, Sillescu H, Landfester K, Speiss HW, Maechtle W, Synthesis and characterization of highly cross-linked, monodisperse core-shell and inverted core-shell colloidal particles. polystyrene/poly(*tert*-butyl acrylate) core-shell and inverse core-shell particles, *Macromolecules*, 1999; **32**:4508-4518
4. Pham HH, Kumacheva E, Core-shell particles: building blocks for advanced polymer materials, *Macromol. Symp.*, 2003; **192**:191-205
5. Ottewill RH, Schofield AB, Waters JA, Preparation of composite latex particle by engulfment, *Colloid Polym. Sci.*, 1996; **274**:763-771
6. Okubo M, Izumi J, Takekoh R, Production of micron-sized monodispersed core/shell composite polymer particles by seeded dispersion polymerization, *Colloid Polym. Sci.*, 1999; **277**:875-880
7. Chaudhuri RG, Paria S, Core/shell nanoparticles: classes, properties, synthesis mechanisms, characterization, and applications, *Chem. Rev.*, 2012; **112**:2373-2433
8. Li H, Han J, Panioukhine A, Kumacheva E, From heterocoagulated colloids to core-shell particles, *J. Colloid Interf. Sci.*, 2002; **255**:119-128
9. Park JM, Core-shell polymerization with hydrophilic polymer cores, *Korea Polymer J.*, 2001; **9**:51-65

10. Shi S, Kuroda SI, Kubota H, Anomalous particles formed in two-stage soap-free emulsion polymerization of styrene on poly(2-acetoxyethyl methacrylate), *Colloid Polym. Sci.*, 2003; **281**:331-336

11. Li G, Yang X, Wang J, Raspberry-like polymer composite particles *via* electrostatic heterocoagulation, *Colloid Surface A*, 2008; **332**:192-198

12. Li G, Yang X, Bai F, Huang W, Raspberry-like composite polymer particles by self-assemble heterocoagulation based on charge compensation process, *J. Colloid Interf. Sci.,* 2006; **297**:705-710

13. Okubo M, Lu Y, Production of core-shell composite polymer particles utilizing the stepwise heterocoagulation method, *Colloid Surface A*, 1996; **109**:49-53

14. Li R, Yang X, Li G, Li S, Huang W, Core-corona polymer composite particles by self-assembled heterocoagulation based on a hydrogen-bonding interaction, *Langmuir*, 2006; **22**:8127-8133

15. Okubo M, Fujibayashi T, Yamada M, Minami H, Micron-sized, monodisperse, snowman/ confetti-shaped polymer particles by seeded dispersion polymerization, *Colloid Polym. Sci.*, 2005; **283**:1041-1045

16. Okubo M, Yamashita T, Minami H, Konishi Y, Preparation of micron-sized monodispersed highly monomer- ‘‘adsorbed’’ polymer particles having snow-man shape by utilizing the dynamic swelling method with tightly crosslinked seed particles, *Colloid Polym. Sci.*, 1998; **276**:887-892

17. Okubo M, Murakami Y, Fujiwara T, Formation mechanism of anomalous "golf ball-like" composite polymer particles by seeded emulsion polymerization, *Colloid Polym. Sci.*, 1996; **274**:520-524

18. Okubo M, Fujibayashi T, Terada A, Synthesis of micron-sized, monodisperse polymer particles of disc-like and polyhedral shapes by seeded dispersion polymerization, *Colloid Polym. Sci.*, 2005; **383**:793-798

19. Lee DI, Ishikawa T, The formation of “inverted” core-shell latexes, *J. Polym. Sci.: Polym. Chem. Ed.*, 1983; **21**:147-154

20. Sheu HR, El-Aasser MS, Vanderhoff JW, Uniform nonspherical latex particles as model interpenetrating polymer networks, *J. Polym. Sci. Polym. Chem.*, 1990; **28**:653-667

21. Sheu HR, El-Aasser MS, Vanderhoff JW, Phase separation in polystyrene latex interpenetrating polymer networks, *J. Polym. Sci. Polym. Chem.*, 1990; **28**:629-651

22. Kim JW, Larsen RJ, Weitz DA, Uniform nonspherical colloidal particles with tunable shapes, *Adv. Mater.*, 2007; **19**:2005-2009

23. Ferguson CJ, Russell GT, Gilbert RG, Modelling secondary particle formation in emulsion polymerisation: application to making core–shell morphologies, *Polymer*, 2002; **43**:4557-4571

24. Gaulding JC, Saxena S, Montanari DE, Lyon LA, Packed colloidal phases mediate the synthesis of raspberry- structured microgel heteroaggregates, *ACS Macro. Lett.*, 2013; **2**:337-340

25. Yamamoto Y, Okubo M, Iwasaki Y, Estimation of distribution of vinyl groups in micron-sized monodisperse polymer microspheres by bromine titration method, *Colloid Polym. Sci.*, 1991; **269**:1126-1132

26. Okubo M, Katayama Y, Yamamoto Y, Preparation of micron-size monodisperse polymer microspheres having crosslinked structures and vinyl groups, *Colloid Polym. Sci.*, 1991; **269**:217-221

27. Bon SAF, van Beek H, Piet P, German AL, Emulsifier-free synthesis of monodisperse core-shell polymer colloids containing chloromethyl groups, *J. Appl. Polym. Sci.*, 1995; **58**:19-29

28. Tobita H, Kumagai M, Aoyagi N, Microgel formation in emulsion polymerization, *Polymer*, 2000; **41**:481-487

29. Saunders BR, Vincent B, Microgel particles as model colloids: theory, properties and applications, *Adv. Colloid Interf.*, 1999; **80**:1-25

30. Guo H, Hamielec AE, Zhu S, Experimental study of emulsion polymerization with crosslinking, *J. Appl. Polym. Sci.*, 1997; **66**:935-957

31. Downey JS, Frank RS, Li WH, Stöver HDH, Growth mechanism of poly(divinylbenzene) microspheres in precipitation polymerization, *Macromolecules*, 1999; **32**:2838-2844

32. Srivastava S, Co-polymerization of acrylates, *Des. Monomers Polym.*, 2009; **12**:1-18

33. Kolb HC, Finn MG, Sharpless KB, Click chemistry: diverse chemical function from a few good reactions, *Angew. Chem. Int. Ed.*, 2001; **40**:2004-2021

34. Hoyle CE, Lowe AB, Bowman CN, Thiol-click chemistry: a multifaceted toolbox for small molecule and polymer synthesis, *Chem. Soc. Rev.*, 2010; **39**:1355-1387

35. Lowe AB, Harvison MA, Thiol-based 'click' chemistries in polymer synthesis and modification, *Aust. J. Chem.*, 2010; **63**:1251-1266

36. Clark T, Kwisnek L, Hoyle CE, Nazarenko S, Photopolymerization of thiol-ene systems based on oligomeric thiols, *J. Polym. Sci. Polym. Chem.*, 2009; **47**:14-24

37. Hoyle CE, Bowman CN, Thiol-ene click chemistry, *Angew. Chem. Int. Ed.*, 2010; **49**:1540-1573

38. Chan JW, Hoyle CE, Lowe AB, Bowman M, Nucleophile-initiated thiol-Michael reactions: effect of organocatalyst, thiol, and ene, *Macromolecules*, 2010; **43**:6381-6388

39. Hoyle CE, Lee TY, Roper T, Thiol-enes: chemistry of the past with promise for the future, *J. Polym. Sci. Polym. Chem.*, 2004; **42**:5301-5338

40. Khire VS, Lee TY, Bowman CN, Surface modification using thiol-acrylate conjugate addition reactions, *Macromolecules*, 2007; **40**:5669-5677

41. Li GZ, Randev RK, Soeriyadi AH, Rees G, Boyer C, Tong Z, Davis TP, Becer CR, Haddleton DM, Investigation into thiol-(meth)acrylate Michael addition reactions using amine and phosphine catalysts, *Polym. Chem.,* 2010; **1**:1196-1204

42. Van Berkel KY, Pierarski AM, Kierstead PH, Pressly ED, Ray PC, Hawker CJ, A simple route to multimodal composite nanoparticles, *Macromolecules*, 2009; **42**:1425-1427

43. Goldmann AS, Walther A, Nebhani L, Joso R, Ernst D, Loos K, Barner-Kowollik C, Barner L, Müller AHE, Surface modification of poly(divinylbenzene) microspheres *via* thiol-ene chemistry and alkyne-azide click reactions, *Macromolecules*, 2009; **42**:3707-3714

44. Zheng G, Stöver HDH, Grafting of polystyrene from narrow disperse polymer particles by surface-initiated atom transfer radical polymerization, *Macromolecules*, 2002; **35**:6828-6834

45. Zheng G, Stöver HDH, Grafting of poly(alkyl (meth)acrylates) from swellable poly(DVB80-*co*-HEMA) microspheres by atom transfer radical polymerization, *Macromolecules*, 2002; **35**:7612-7619

46. Juang MSD, Krieger IM, Emulsifier-free emulsion polymerization with ionic comonomer, *J. Polym. Sci. Polym. Chem. Ed.*, 1976; **14**:2089-2107

47. Kim JH, Chainey M, El-Aasser MS, Vanderhoff JW, Emulsifier-free emulsion polymerization of styrene and sodium styrene sulphonate, *J. Polym. Sci. Polym. Chem.*, 1992; **30**:171-183

48. Karlsson LE, Karlsson OJ, Sundberg DC, Nonequilibrium particle morphology development in seeded emulsion polymerisation. II. Influence of seed polymer T_g, *J. Appl. Polym. Sci.*, 2003; **90**:905-915

49. Feeney PJ, Napper DH, Gilbert RG, Surfactant-free emulsion polymerizations: predictions of the coagulative nucleation theory, *Macromolecules*, 1987; **20**:2922-2930

50. Bouvier-Fontes L, Pirri R, Magnet S, Asua JM, Leiza JR, Effect of the diacrylate ester size on the semicontinuous crosslinking emulsion copolymerization of BA, *Macromolecules*, 2005; **38**:2722-2728

51. Bouvier-Fontes L, Pirri R, Asua JM, Leiza JR, Seeded semicontinuous emulsion copolymerization of butyl acrylate with crosslinkers, *Macromolecules*, 2005; **38**:1164-1171

52. Stubbs JM, Sundberg DC, Nonequilibrium morphology development in seeded emulsion polymerisation. V. The effect of crosslinking agent, *J. Appl. Polym. Sci.*, 2006; **102**:2043-2054

53. Anseth KS, Wang CM, Bowman CN, Reaction behaviour and kinetic constants for photopolymerizations of multi(meth)acrylate monomers, *Polymer*, 1994; **35**:3243-3250

54. Gauthier MA, Stangel I, Ellis TH, Zhu XX, A new method for quantifying the intensity of the C=C band of dimethacrylate dental monomers in their FTIR and Raman spectra, *Biomaterials*, 2005; **26**:6440-6448

55. Rueggenberg FA, Hashinger DT, Fairhurst CW, Calibration of FTIR conversion analysis of contemporary dental resin composites, *Dent. Mat.*, 1990; **6**:241-249

56. Socrates G, Infrared and Raman characteristic group frequencies. tables and charts, 3rd Ed, John Wiley & Sons 2001

57. Nyquist RA, Interpreting infrared, Raman, and nuclear magnetic resonance spectra. vol 1, Academic Press 2001

58. O'Donnell JH, O'Sullivan PW, A kinetic study of crosslinking vinyl polymerization by laser Raman spectroscopy free radical polymerization of diethylene glycol bis(allyl carbonate), *Polym. Bull.*, 1981; **5**:103-110

59. Reis MM, Uliana M, Sayer C, Araújo PHH, Guidici R, Monitoring emulsion homopolymerization reactions using FT-Raman spectroscopy, *Braz. J. Chem. Eng.*, 2005; **22**:61-74

60. Houlton HG, Tartar HV, Raman spectra of sodium alkyl sulphonates and sulphinates, *J. Am. Chem. Soc.*, 1938; **60**:544-548

61. Reed RM, Tartar HV, The preparation of sodium alkyl sulfonates, *J. Am. Chem. Soc.*, 1935; **57**:570-571

Chapter 4 - Interfacial thiol-Michael addition capsules

4.1. Abstract

Chapter 4 reports the main methods for encapsulating an oil for agricultural applications with the main attention is trying to improve on existing poly(urethane) and poly(urea) polymerisation reactions. Using a microfluidic device allowed synthesis of milli- and micron sized capsules using nucleophilic thiol-Michael addition interfacial polymerisation. The interfacial polymerisation between a penta-/hexa- olefin with a tetra- functional thiol using nucleophilic *iso*butylamine catalyst synthesised capsules containing solvesso 200ND. The thiol-Michael addition reaction was applied to try and synthesise capsules using high shear homogenisation techniques and the capsules showed stability while aqueous. However, the homogenised capsules showed release of the solvesso 200ND after 1-2 minutes for the homogenised capsules whereas the microfluidic capsules did not appear to show rupture.

4.2. Introduction

4.2.1. Encapsulation of a liquid for agricultural application

Encapsulation of an active ingredient is a very important aspect for a range of colloid areas including cosmetics, agriculture, medicine and pharmaceuticals. In these fields encapsulation and selective release of ingredients is highly appealing. Sufficient encapsulation is preferable as many active ingredients (AIs), specifically drug AIs, are valuable or expensive. For agricultural purposes the encapsulation of oil can allow pesticides and herbicides to be transported through soil towards the root system. This protects the AI from leaching into the groundwater, which is undesirable due to the relative toxicity of many AIs and the oils used for their encapsulation. Typically a solid insecticide is dissolved into solvesso 200ND oil (and potentially alongside Xylene) in order to be encapsulated (structure of solvesso 200ND is reported in **Chapter 1**, **Section 1.2.6.** and **Figure 1.9.**). The encapsulation of AIs and solvesso 200ND has been studied using interfacial polycondensation reactions (discussed below) and their methodology is reported in a number of patents.[1-8]

4.2.2. Capsule wall formation around droplets

There are many synthetic methods for microcapsule formation and each method has specific advantages and disadvantages over others depending on whether a solid, a liquid/oil or a gas is being encapsulated. The main methods for the encapsulation of a liquid or oil are shown in **Figure 4.1.**. Colloidosomes form when solid particles assemble at an interface followed by fusing of particles, the core can be an altered to suit the specific application e.g. an oil for agriculture.[10-11] Polymer precipitation by phase separation includes both polymerisation induced phase separation and solvent

extraction and evaporation.[10,12-19] Phase separation of polymer (*via* polymerisation or solvent removal) forces the polymer to move to the interface. Interfacial polymerisation includes polycondensation and coacervation between cationic and anionic molecules that react at the interface forming a shell polymer.[10,12-13,15-28] Layer-by-layer assembly of anionic and cationic polyelectrolytes uses the addition of a single layer to a surface and then alternating the polymer layer until a shell is formed.[1012-13,15,29-34] Polymer growth by surface polymerisation uses vinyl or other reactive groups to crosslink a surface layer to create a shell.[10,13,15] Emulsification polymerisation is where droplets of oil are formed by emulsification and subsequent polymerisation at the interface leads to a shell.[12-13,15-16] Vesicles/polymersomes uses the self assembly of block copolymers to generate micellar type structures.[10,15] Flow focusing/doublet emulsions forces droplets of oil into a narrow channel of a solvent followed by stability of the droplets or capsule wall formation.[12-13] The above methods for capsule formation allow capsules of sizes between 0.02 μm and 1200 μm to be achieved depending on the specific system and application required.[13] Choice of the technique can greatly influence the capsule produced e.g. capsule wall thickness, wall porosity, surface functionality. Reviews by authors Yow and Routh,[9] Esser-Kahn *et al*,[11] Ghosh[12] and Jabbari[19] go into great detail about how these techniques have been used in the past and discuss specific reagents, methodologies and the effects this has on the final capsules produced. They also discuss the advantages and disadvantages of the different approaches to encapsulation.

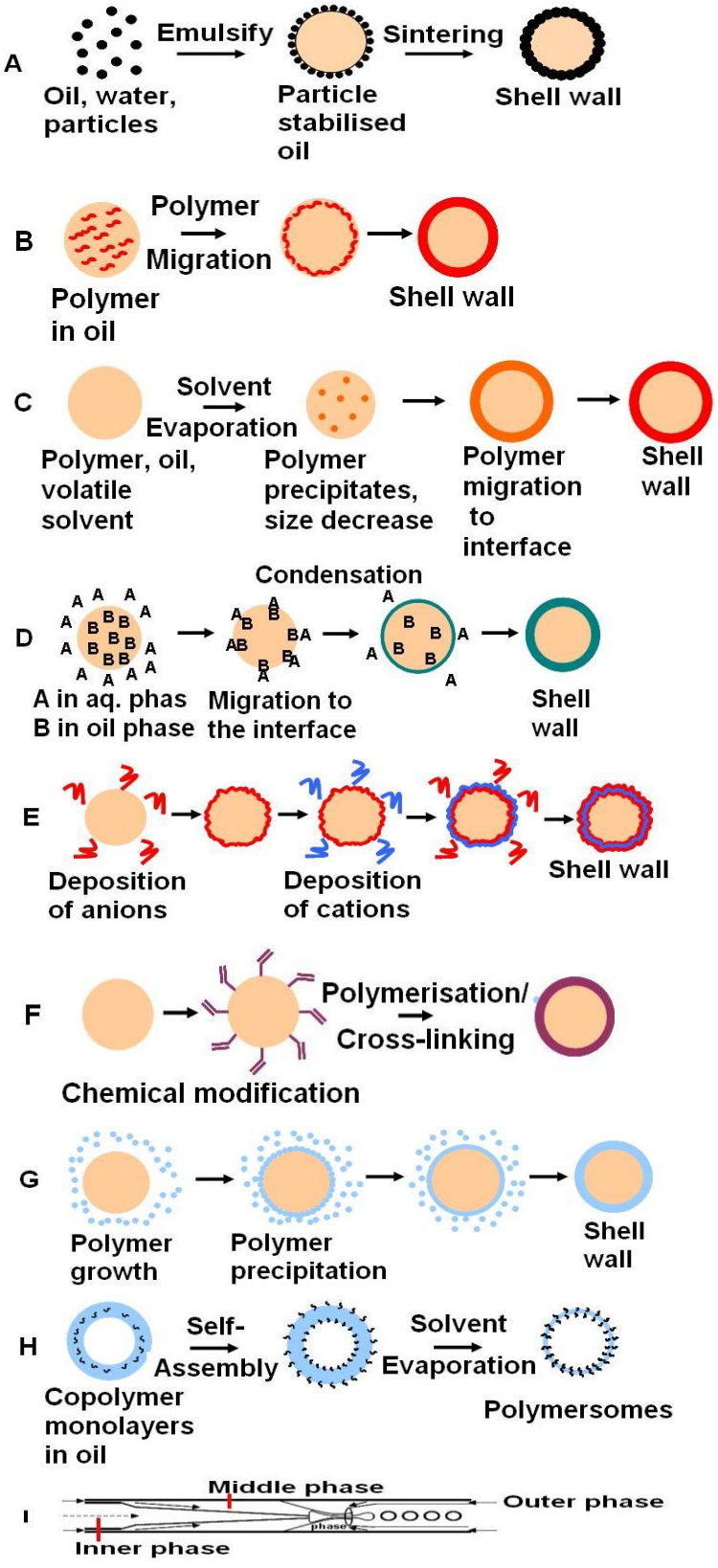

Figure 4.1. Visual representation of the different methods for encapsulation of liquid or oil. A) Colloidosomes, B) polymerisation induced phase separation, C) solvent extraction and evaporation, D) interfacial polymerisation, E) layer-by-layer assembly, F) surface polymerisation, G) emulsification polymerisation, H) vesicles/polymersomes, I) flow focusing/doublet emulsions formation.

4.2.3. Poly(urethane) and poly(urea) microcapsules

Typically the encapsulation of oil for agricultural purpose is carried out using interfacial polymerisations or polycondensation reactions. Such chemical reactions produce poly(urethanes),[17,21-25,35-38] poly(ureas),[1-3,17-18,20,22,24,26-28,32,39] urea-formaldehydes,[4-5] poly(amides)[17,24,40-41] or poly(esters).[17,24] The mechanism for poly(urethane) and poly(urea) formation is shown in **Scheme 4.1.**, technically these reactions are not condensation reactions because no small molecules are lost.[24] Poly(urea) and poly(urethane) techniques are the most commonly used by Syngenta UK for the encapsulation of pesticides and herbicides.

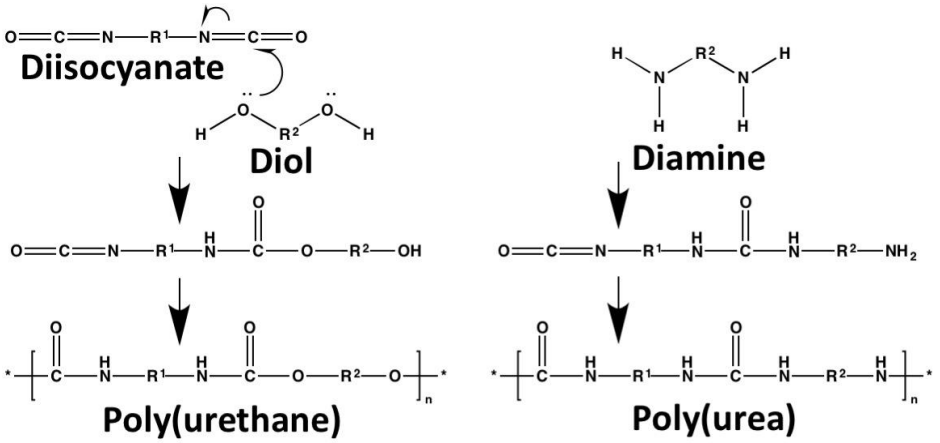

Scheme 4.1. Scheme showing the chemical reaction between a di-isocyanate and a diol (left) or diamine (right) forming poly(urethane) or poly(urea) polymers respectively. R^1 and R^2 can be tailored using a range of commercial diols and diamines.

Both poly(urea) and poly(urethane) methods lead to broader size distributions of capsules typically between 0.2-20 μm (the average capsule sizes are altered using homogenisation and sonication techniques). Poly(urea) and poly(urethane) capsules allow easy control over wall thickness, wall functionality, wall porosity, surface functionality and release mechanisms of the oil containing the dissolved AI. The capsules wall porosity can be tailored by alteration of the diisocyanate as well as the

diol and diamine crosslinkers. Surface functional groups can be incorporated by the addition of hydroxyl or amine molecules that can help with stabilisation of the capsules.

4.2.4. Controlling droplet size and stability

Many methods exist for the control of droplet sizes including stirring, hand shaking, microfluidics/flow focussing[12-13,49] and homogenisation or sonication. These methods are used to generate mm to micron sized droplets where greater shear generates smaller droplet sizes. Sonication and membrane emulsification are typically reported for synthesising droplets with diameters in the nanosize range.[42-43] However, nearly all of these methods give broad size distributions. Membrane emulsification and microfluidic devices can give very monodisperse droplet sizes of 200-400 nm and 5.0 μm to millimetres respectively. Recently Malloggi *et al* reported achieving droplet sizes of 1.0-3.0 μm using a microfluidic device.[43] Droplet sizes can be altered using varying power of homogenisation (low or high shear homogenisation and low and high amplitude sonication), changing pore sizes for membrane emulsification, altered flow rates and viscosities for microfluidics and the employment of surfactants.

4.2.5. Triggered release of an active ingredient

The release of an encapsulated AI is of great interest for agriculture. Controlling where and how the AI is released is very important as ideally the AI should reach the plant roots (discussed in **Chapter 1**). Reviews by Esser-Khan[4] and others[23,26,29] provided insight into triggered release mechanisms that involve the use of biological (enzyme and receptor), chemical (pH, ionic, solvent and electrochemical) and physical (photo, thermal, electrical and magnetic) approaches. The two main release profiles of an AI from capsules are burst release (released in one go) and controlled release (release

over time by absorption/diffusion through the capsule wall).[1f] The release can be tailored to be between the above situations. Release of the active ingredient is altered by wall thickness, wall polymer composition and degradability, wall porosity and structural wall weak links.

4.2.6. Interfacial nucleophilic thiol-Michael addition chemistry for encapsulation of solvesso 200ND

In this chapter we aimed to use interfacial polymerisation to encapsulate solvesso 200ND under milder conditions than required for polyurethane and polyurea reactions. We wanted to synthesise capsules with monodisperse sizes if possible and control over capsule sizes where ideally 200-500 nm capsules would be ideal. We decided to try out the thiol-Michael nucleophilic addition reaction from **Chapter 3** where a polymer network could form at the oil-water interface using an amine catalyst under ambient conditions. Large microcapsules on the submillimetre lengthscale were prepared using a microfluidic device for emulsion droplet generation. Smaller microcapsules were prepared using a more standardised homogenisation approach.

4.3. Experimental

4.3.1. Materials

All chemicals were used as supplied. Penta-erythritol penta-/hexa- acrylate, penta-erythritol tetrakis(3-mercaptopropionate), *iso*butylamine (99%), hexylamine (99.5%), and tri-ethyl amine and were also purchased from Sigma Aldrich. Solvesso 200ND was supplied courtesy of Syngenta (originally from ExxonMobil). The surfactants poly(vinyl alcohol) (M_w 85000-124000, 87-89% hydrolysed) was purchased from Sigma Aldrich, gohsenol GL05 was from Nippon-Gohsei (86.5-89.0% hydrolysed), lomar D (also known as agnique NSC 11NP) was from GEO speciality chemicals and tergitol XD (M_w 2990) was from the DOW chemical company and were all used as received.

4.3.2. Equipment

All standard glassware was supplied by Fisher Scientific (beakers, vials etc). The microfluidic device was developed and operated by Dr Gabit Nurumbetov where the fluid flow rates were controlled using PHD2000 Harvard apparatus precision pumps. Glass capillaries (from Harvard Apparatus) used had inner diameter 1.62 mm and outer diameter 3.0 mm or inner diameter 0.58 mm and outer diameter 1.0 mm. Glass capillaries were altered using a diamond scribe, a mini drill kit (Farnell UK) and a P-2000 Laser Capillary Puller (Sutter Instruments). Tubing used for microfluidic connectors was Transparent FLEX^R tubing with internal diameter 1/32" and external diameter 3/32" (from Cole-Parmer). Homogenisation was done using a Heidolph Silent crusher M. Optical micrographs were taken using a Leica DM2500 microscope and

attached Nikon® D5100 DSLR camera. All measurements on micrographs were performed using ImageJ software (see **Chapter 2. Section 2.3.6.3.**).

4.3.3. Microfluidic device fabrication

The borosilicate glass capillary used for the main channel of the microfluidic device was narrowed by heating and pulling using a P-2000 laser capillary puller. A bent 32 gauge needle (inner diameter 0.108 mm) was inserted into a cut short capillary tube and epoxy glue was used to fix them together (**Figure 4.2-B.**). The other end of the bent needle was inserted into the narrowed main channel section (this focused the dispersed phase and decreased the droplet sizes). This component was then attached to a glass slide (**Figure 4.2-C.**). The dispersed phase component was then glued to another glass capillary tube in order to produce a co-flow device as shown in **Figure 4.2-D.**. The microfluidic device was connected to the syringe pumps using flexible PVC tubing and the final device is shown in **Figure 4.4.**.

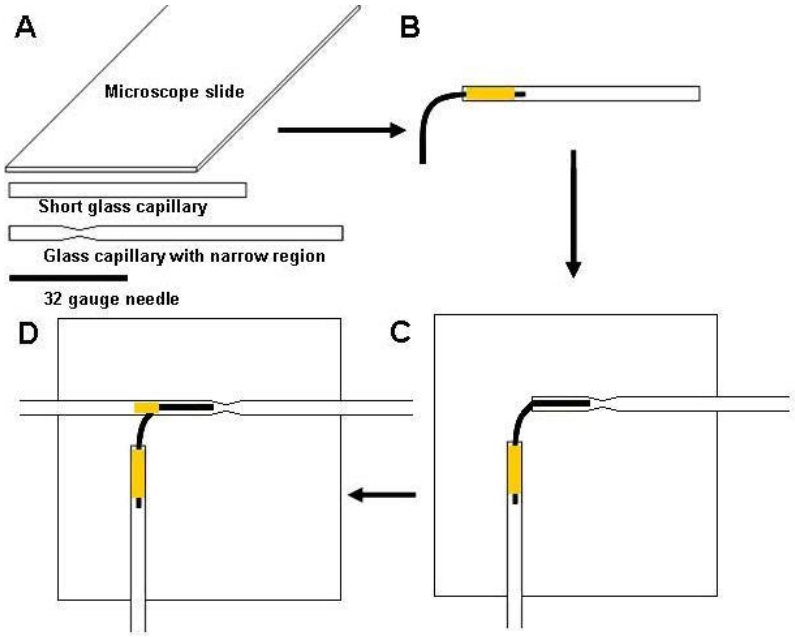

Figure 4.2. Schematic representation of the fabrication of simple microfluidic devices. A) materials required for fabrication of a microfluidic device, B) the short capillary is cut and the bend needle is glued into one end using epoxy glue, C) the other needle end is then inserted into the main narrowed capillary main channel, D) the other piece of short capillary is then added to the end of the main channel and connected with epoxy glue.

4.3.4. Microfluidic capsule approach

The above mentioned fabricated co-flow device was used (device shown in **Figure 4.4.**) where flow rates were 0.2 ml/min for the inner oil phase and 0.115 ml/min for the outer aqueous phase (according to the pump feed rates). These flow rates were found by a trial and error method until stable droplets were produced. The thiol-Michael reagents, 1.01 g penta-erythritol penta-/hexa- acrylate and 1.29 g penta-erythritol tetra-kis(3-mercaptopropionate), were dissolved into 10.0 ml solvesso 200ND oil (sonic bath aided the dissolution of the penta-/hexa- acrylate monomer). The oil phase was fed into the outer aqueous phase (with or without poly(vinyl alcohol) surfactant) at the rates specified above. The droplets that formed were dropped into a aqueous solution with *iso*butylamine catalyst (used in slight excess so that fast thiol-Michael network formation could occur). Instantaneous capsules formed upon addition to the amine catalyst whereby the large capsules sank to the bottom of the vial (shown later in **Figure 4.6.**). The capsules were easily washed by removal of the water followed by addition of water and then repeated. The exact amounts used for the synthesis of microfluidic capsules are reported in **Table 4.1.**.

Table 4.1. Reagents required for the synthesis of microcapsules using a microfluidic approach.

Sample	Acrylate (g)	Thiol (g)	Solvesso 200ND (g)	PVA
PVA capsules	1.01	1.29	10	1.0 wt% in H_2O
No surfactant capsules	1.01	1.29	10	-

Molar ratio of acrylate to thiol was calculated using average ratios of 1.25 and 1.5 (assuming 50% penta- and 50% hexa- acrylate monomer). Flow rates were 0.2 ml/min inner solvesso 200ND phase and 0.115ml/min outer aqueous phase (according to the syringe pumps)

4.3.5. Homogenisation capsule approach

4.3.5.1. Gohsenol, lomar D and tergitol XD stabilised capsules

Penta-erythritol penta-/hexa- acrylate (1.23 g) and penta-erythritol tetra-kis(3-mercaptopropionate) (1.02 g) were both dissolved into the solvesso 200ND oil phase (12.75 g) using a sonic bath was used to aide the dissolution of the penta-/hexa acrylate monomer. A 100 ml beaker containing an aqueous solution of either gohsenol GL05 or lomar D and tergitol XD surfactant (exact amounts used are reported in **Table 4.2.** with a total amount of 50 g) was emulsified and the organic phase was added drop wise. The two phases were pre-mixed using a stirrer bar and then further homogenised at 3500 rpm for one minute (low shear) followed by 8100 rpm for two minutes (high shear) to decrease the droplet size (droplet sizes were checked under a microscope). The homogenised sample was transferred to a glass jar (containing a stirrer bar) and under stirring two drops of *n*-butylamine was added to allow the thiol-Michael addition reaction to occur. The capsules were monitored under a light microscope by adding a droplet of the capsules to a microscope slide.

Table 4.2. Reagents required for the synthesis of microcapsules using a homogenisation approach.

Sample	Acrylate (g)	Thiol (g)	Solvesso 200ND (g)	Gohsenol (g)	Lomar D (+tergitol XD) (g)	H_2O (g)
Gohsenol capsules	1.25	1.04	12.6	8.33 (15 w/w)	-	26.7
Lomar D capsules	1.24	1.04	12.7	-	12.5 (+1.25 g 20 w/w)	21.3

Molar ratio of acrylate to thiol was calculated using average ratios of 1.25 and 1.5 (assuming 50% penta- and 50% hexa- acrylate monomer). Lomar D was combined with tergitol XD (a non-ionic alkyl EO/PO copolymer). Total emulsion mass was 50 g.

4.4. Results and discussion

4.4.1. Thiol-Michael addition reaction overview and applicability for capsules

In **Chapter 3** (**Section 3.4.11.**) we reported the kinetics, versatility and applications of the thiol-Michael click reaction by various authors. This reaction has applicability using a range of functional thiols and olefins with mono-, di-, tri-, tetra- and multi- functionalities. We also discussed the use of amines as nucleophilic catalysts. The results showed that the thiol-Michael addition reaction using primary amine catalysts is very rapid and can occur in seconds to minutes depending on the choice of thiol, olefin and the amine being used. The reports show that using nucleophilic catalysts then side reactions can be minimised (refer to **Chapter 3** for references). This reaction between a thiol and an olefin is the basis for our proposed methodology (see **Scheme 3.1.** in **Chapter 3** for the nucleophilic thiol-Michael addition reaction mechanism). Using this method we can achieve almost instantaneous reaction between the thiol and olefin to produce a polymer. By using multi- functional thiol and olefin we aimed to try and create a highly networked polymer that could build up a shell at an interface of two immiscible liquids (water and solvesso). The advantages for nucleophilic thiol-Michael addition being that water can be the solvent under ambient conditions and using low concentrations of catalyst.

4.4.2. Poly(urethane), poly(urea) and the encapsulation of solvesso 200ND

We discussed in the introduction that typically interfacial polymerisation or polycondensation reactions are usually employed to produce capsules for agricultural purposes with the most common being poly(urethane) and poly(urea) (**Scheme 4.1.** on

Page 140). These methods typically require raised temperatures (40-80^{o}C),[20,22-23,27-28,32,36,38-39] homogenisation to control droplet sizes and distributions and multiple solvents to afford a capsule wall (the solvent evaporation technique requires vast quantities of acetone when scaled up). One requirement for agricultural capsules is that they must have a chemically robust wall to maintain the encapsulation of the AI. The AI under interest (Abamectin) needs dissolution into organic oils such as solvesso (produced by ExxonMobil Chemical) or xylenes.[7,26,32] Solvesso typically consists of 99 wt% of C_{10-14} aromatic compounds and < 1 wt% of various alkylnapthalene compounds. Chemical compounds include tetra-methyl benzene, undecyl benzene, dodecyl benzene, tetra- hydronapthalene, di-dodecyl benzene, octyl- benzene, naphthalene, methylnaphthalene, ethylnapthalene, *iso*propyl napthalenes, di-iso-propyl napthalenes and dimethylnapthalene (see **Chapter 1**, **Section 1.2.6.** and **Figure 1.9.** for solvesso 200ND chemical structures).[7-8] Solvesso 200ND is regarded as toxic to the environment and aquatic organisms which is why targeted delivery and controlled release is essential to prevent leeching into the groundwater.

4.4.3. Thiol-Michael addition polymer network test reaction

Most reported polymer networks synthesised using the thiol-Michael addition reaction reported photopolymerisation methods to initiate the "click" reaction. Zhou *et al* published the results of the photopolymerisation of a range of multifunctional thiols and acrylates and reported that conversion was higher as the functionality of both thiol and ene increased.[44] Using tetra- or hexa- functional acrylates and thiols led to a greater thiol-Michael addition bond formation (greater degree of crosslinking) and increased the T_g values of the polymer network. Connal *et al* reported the synthesis of thiol-Michael addition capsules utilising the layer-by-layer technique whereby alternating layers of

poly(vinylpyrollidone) and poly(methylmethacrylate) functionalised with thiol or ene end groups were hydrogen bonded around silica particles.[32] Initiation of the thiol-ene reaction using UV light and subsequent removal of the core followed by dissolution of the poly(vinylpyrollidone) layers caused capsules to form with a poly(methylmethacrylate) network shell.

In order to test out the thiol-Michael addition reaction for the formation of a polymer network or film using nucleophilic initiation we first carried out a test reaction. We dissolved both the penta-erythritol penta-/hexa- acrylate (referred to as 3.6) and penta-erythritol tetra-kis (2-mercaptopropionate) (referred to as 3.9) in solvesso 200ND (structures of 3.6 and 3.9 are shown in **Chapter 3 Figure 3.20.** and **Figure 3.27** respectively). We choose monomers 3.6 and 3.9 as they were both the most multifunctional thiol and acrylate and should provide a dense crosslinked polymer network as reported by Zhou *et al*.[44] The addition of water to the system caused the solvesso 200ND phase to float due to the lower density (0.984g/cm^{-3}). After equilibration of the two phases a droplet of hexylamine catalyst was added to initiate the reaction between 3.6 and 3.9 where a polymer skin formed between the two phases that was soft and elastic. This initial test gave good reason to believe that we could synthesise capsules using this reaction. The predicted reaction scheme between our monomers 3.6 and 3.9 is shown in **Scheme 4.2.** portraying the reaction of the amine catalyst with the acrylate to yield a thiolate anion. This thiolate anion them reacts with the acrylate monomer to create the thiol-Michael addition reaction and produces a further thiolate anion to continue the reaction. Our designed reaction between the multi-functional acrylate and multi-functional thiol is represented in **Figure 4.3.** for the formation of a thiol-Michael network at an interface.

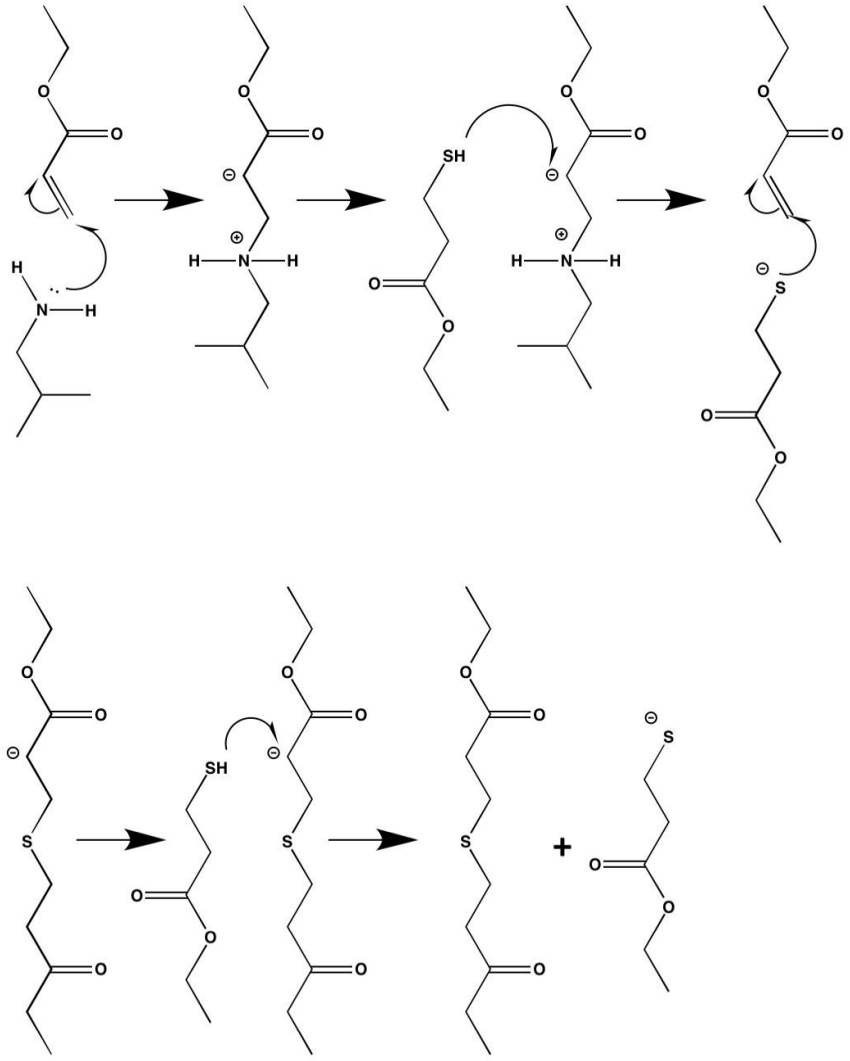

Scheme 4.2. Thiol-Michael reaction scheme for tetra thiol and penta-/hexa- acrylate. Top scheme, amine reaction with acrylate monomer followed by hydrogen abstraction from the thiol to yield a thiolate anion. Bottom scheme, reaction of thiolate with acrylate monomer followed by hydrogen abstraction to yield the thiol-Michael addition product and a new thiolate anion.

4.4.3.1. Choice of nucleophilic amine initiator

Due to the promising reaction in the previous test experiment we tried a similar test but this time trying to create capsules instead of a polymer skin. We hand shook a vial containing solvesso 200ND (containing dissolved 3.6 and 3.9) and water and stirred the sample using a stirrer bar and stirrer plate. This method of hand shaking and stirring produced oil-in-water (O/W) droplets of 2-3 mm in size. To initiate the thiol-Michael addition reaction wetried three different catalysts (*iso*butylamine, hexyl-amine and tri-ethylamine) whose structures are shown in **Figure 4.4.**. The tri-ethylamine catalyst

caused crosslinking of the system and was removed from subsequent reactions. The hexyl-amine and *iso*butylamine catalysts led to large stable capsules that were visible with the naked eye due to their size. Both primary amines worked effectively but we choose *iso*butylamine because shorter chained amines catalyse the thiol-Michael addition reaction faster and also have greater water solubility (see **Chapter 3 Section 3.4.5.** for references on nucleophilic thiol-Michael addition reactions using amines). For agricultural applications capsules of 2-3 mm are not very sufficient especially when the pore sizes of soil are much smaller (mm to micron sized depending on soil types). We aimed to reduce the sizes of the capsules and first tried synthesis of polymer network stabilised capsules using a microfluidic approach.

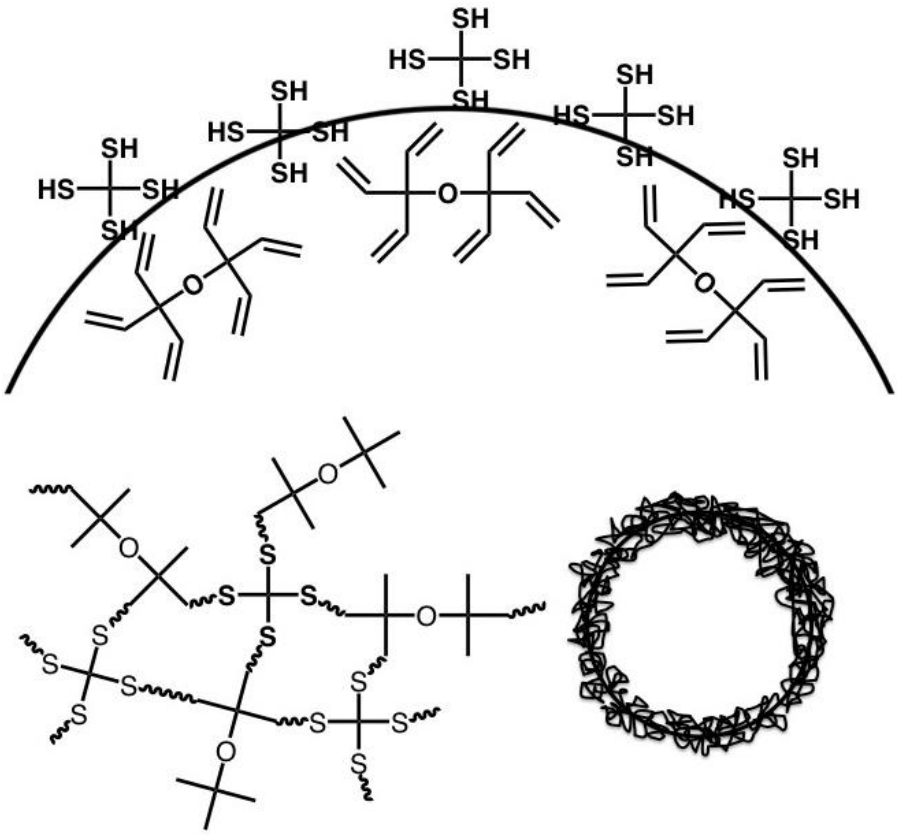

Figure 4.3. Representation of the formation of a thiol-Michael addition polymer network at an interface. Reaction between penta-/hexa- acrylate and tetra-thiol at an interface (top), formation of a polymer network (bottom left) and the polymer network forming at an interface to create a capsule wall (bottom right).

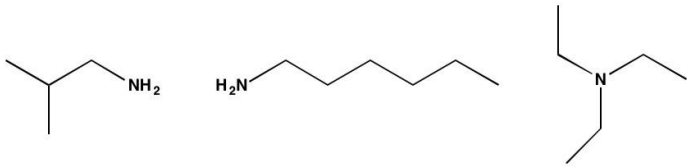

Figure 4.4. Chemical structures for the various amine catalysts, *iso*butylamine (left), hexyl-amine (middle) and tri-ethyl amine (right).

4.4.4. Microfluidic thiol-Michael addition capsule approach

In the **Experimental Section 4.3.3.**, we described the fabrication of a single emulsion microfluidic device (see **Figure 4.5.** for the device and set up and **Section 4.3.4.** for pump flow rates). This device was supplied courtesy of Dr Gabit Nurumbetov who both fabricated the device and helped with finding the required flow rates to achieve stable droplet formation. **Figure 4.5.** shows the use of 2 pumps to control the dispersed and continuous phases into the microfluidic device. The co-flow device shown on the right of **Figure 4.5.** shows the formation of droplets as the dispersed phase is pushed into the continuous phase and the surfactant stabilised droplets exit the channel at the bottom of the picture. Droplets formation occurs due to the interfacial tension seeking to reduce the interfacial area of the droplets.

Recently Prasath *et al* have reported a similar methodology of thiol-Michael addition reaction in microfluidics where firstly an O/W droplet was formed using a microfluidic device.[45] A tetra- functional thiol and a di- or tri- functional acrylate were mixed with photoinitiator 2,2-di-methoxy-2-phenylacetophenone (DMPA) for the reagent phase and light mineral oil or water for the continuous phase. Initiation using UV irradiation allowed a thiol-Michael addition polymer network to form. This created thiol-Michael addition polymer beads of 200-500 μm in size (UV can penetrate the entire droplet which is why beads were synthesised). The use of mineral oil as the continuous phase led to non-porous polymer beads and using porogen in the aqueous

phase led to porous beads. We aimed to create capsules instead of beads and for this reason we chose nucleophilic catalytic initiation for the thiol-Michael addition reaction to ensure that the reaction would occur at the droplet surface upon contact with the water soluble amine.

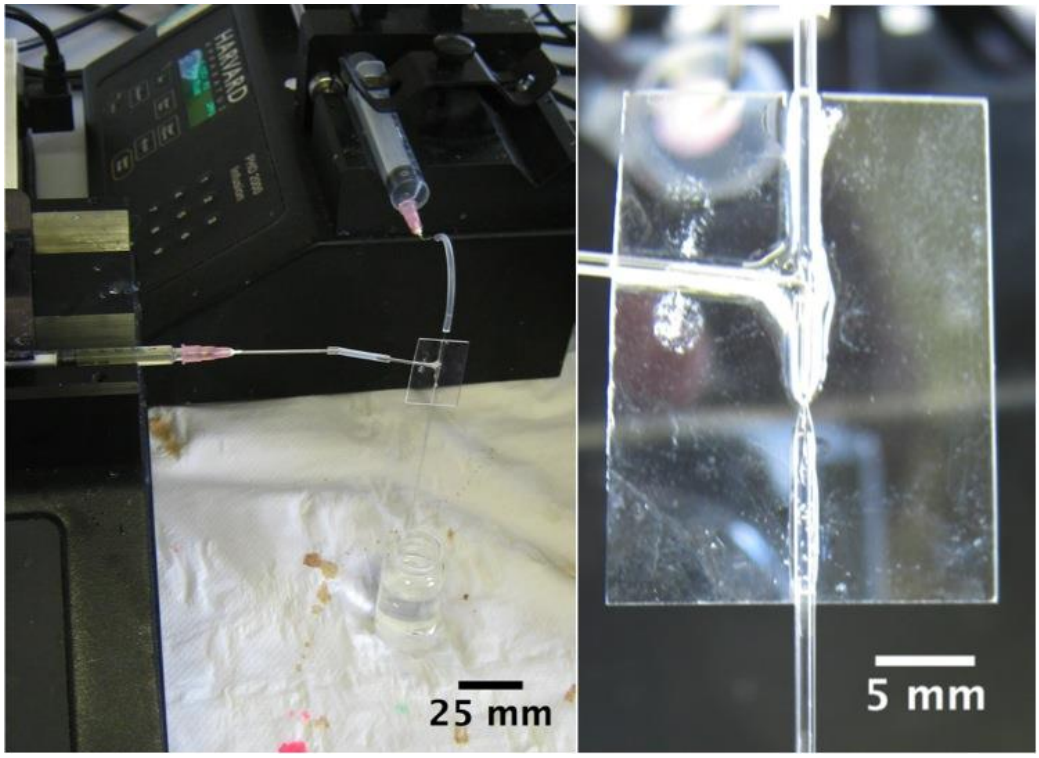

Figure 4.5. Camera image showing set up of the single emulsion microfluidic device using two Harvard syringe pumps to control the outer and inner phase flow rates (left) and an enlargement of the droplet formation zone (right). Scale bars are 25 mm for the left and 5 mm for the right.

4.4.4.1. Surfactant stabilised capsules via nucleophilic thiol-Michael addition reaction

The first synthesised capsules tried using the microfluidic device used surfactant to control the droplet stability. Typically colloid stabilisers are required to produce stable capsules where surfactants exist with anionic, cationic, zwitterionic and non-ionic nature.[47] Surfactants provide steric or electrostatic repulsion to prevent coagulation of droplets and they reduce the surface tension between two phases. Surfactants enable droplets to form that do not coalesce over time caused by collisions. "Bancrofts' rule"

states that the phase that the surfactant is more soluble in will become the continuous phase.[46] This rule ties in with the rule proposed by Griffin[47-48] and later Davies[50] who used a scale to measure the balance between the two phases based on the proportion of hydrophilic to hydrophobic potions. This scale is called the hydrophilic-lipophilic balance (HLB) and typically ranges from 1-20 where values 3-6 produce stable W/O emulsions and values 8-18 produce O/W emulsions.[19,48-49]

The first surfactant we tried for capsule formulation was poly(vinyl alcohol) (referred to as 4.1, structure shown in **Figure 4.6.**) of molecular weight 85000-124000 with 87-89% hydrolysed. The unhydrolysed 4.1 will exist as poly(vinyl acetate) as shown in **Figure 4.6.**. Surfactant 4.1 is a commonly used stabiliser in both microfluidics and emulsion formulations for generating robust droplets. Again the monomers 3.6 and 3.9 were both dissolved into the solvesso 200ND to be used as the inner phase (molar ratio of 3.6 to 3.9 was 1:1.5). The exact masses of 3.6 and 3.9 are reported in **Table 4.1.** in **Section 4.3.4.** and synthesis is reported in experimental **Section 4.3.4.**. When the required flow rates had been found for producing stable spherical droplets (0.2 ml/min for inner phase and 0.115 ml/min for outer phase) the O/W droplets that formed dropped into an aqueous *iso*butylamine solution to cause the thiol-Michael addition reaction to occur and form a capsule wall. The actual flow rates for the dispersed and continuous phases might differ from the values on the pumps.

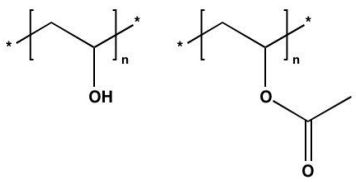

Figure 4.6. Structure of poly(vinyl alcohol), hydrolysed poly(vinyl alcohol) is shown on the left and unhydrolysed poly(vinyl acetate) on the right.

As soon as the produced droplets hit the water they instantly formed a capsule wall around the solvesso droplets. The capsules sedimented to the bottom of the glass

vial as shown in **Figure 4.7.**. Polymer formation has a higher density than water and for this reason the capsules sunk even when the oil being encapsulated is less dense than the aqueous phase.

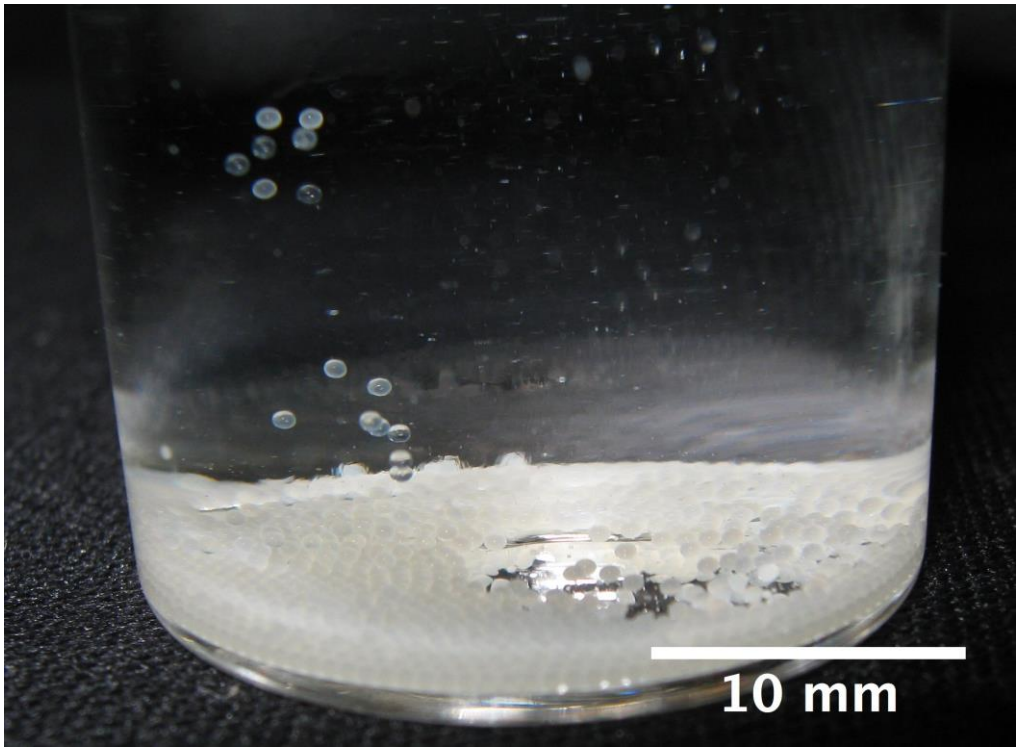

Figure 4.7. Formation of O/W capsules as they hit a basic *iso*butylamine aqueous solution. O/W capsules used solvesso 200ND containing penta-erythritol penta-/hexa- acrylate and penta-erythritol tetra-kis (2-mercaptopropionate) as the inner phase and water containing poly(vinyl alcohol) surfactant solution as the outer phase. Scale bars is 10 mm.

In 2012 Patil reviewed the thiol-ene and thiol-Michael addition reaction between various multi-functional thiols and acrylates and showed that under solvent free conditions many can polymerise in fast times. It has been reported that thiol propionates are the most reactive of thiol compounds and offer less sensitivity towards oxygen than other thiols.[51-52] Patil reported that the monomer reaction between 3.6 and 3.9 occurred in 20 minutes at room temperature with no catalysts or solvent and the polymer formed was transparent and elastic. They also reported that the hardness of the polymer network was dependant on the functionality of the thiol and acrylate being used where more functionality increases the crosslinking density.

The capusles were allowed to dry out on a microslope slide while being monitored using a light microscope with a 20x magnification lens. The capsules were monitored at regular intervals to observe changes during water removal. The capsules did not break down when the water was removed which meant that the wall thickness was thick enough to maintain the structure of the capsule and prevent rupture or bursting. The light microscope images for the capsules synthesised are shown in **Figure 4.8.**. The capsules shown in **Figure 4.8-A.** stuck together when they were dried as the capsule walls fused with the walls of the neighbouring capsules. We believe that the polymerisation between the tetra-thiol and tetra-acrylate leaves many unreacted thiol and vinyl groups. When the capsules come into contact with each other due to the removal of water the free thiol and vinyl groups are still able to react which causes crosslinking between capsules. **Figure 4.8-B.** shows the capsules using the reflectance mode where the light source is from above the sample rather than below it allowing the surface to be more clearly visible. The capsules appear to have an irregular surface where dips and ridges are visible and this is likely caused by more polymer formation in some areas and less polymer formation in other areas. Once the thiol-Michael addition capsule wall forms the crosslinked polymer network might inhibit diffusion of further monomer to the interface. As the catalyst is water soluble then the polymer that forms once the droplets hit the water might not grow over time compared to bulk studies of the thiol-Michael network formation. When we study **Figure 4.8-A.** and **Figure 4.8-B.** we notice that the capsules appear to have different diameters when we study the scale bars. The reason for this is likely due to the reflectance image of the microcapsules only showing the top part of the capsule that is sticking out of the water. This would explain why the capsules appear buckled under reflectance mode and why they looked dry (shown later in **Figure 4.10-B.** and **Figure 4.10-C.**).

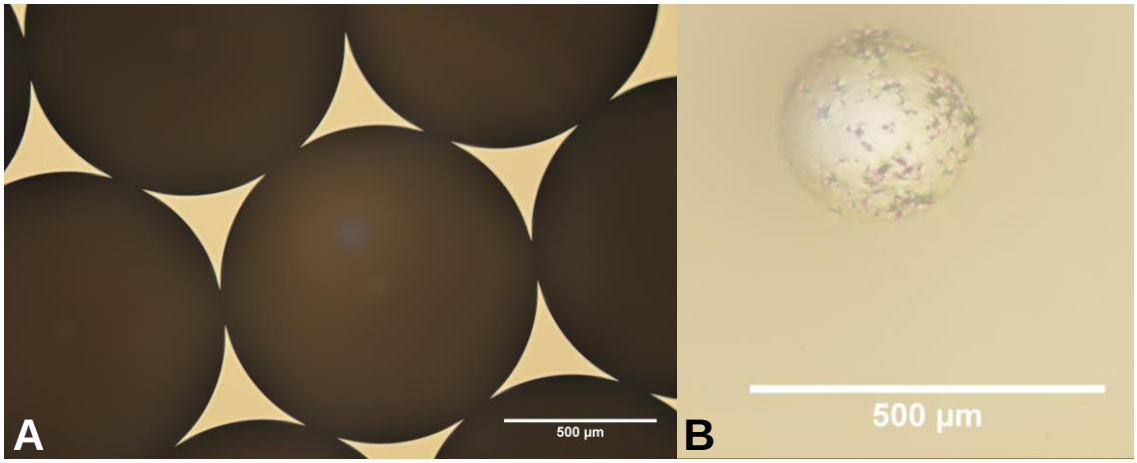

Figure 4.8. Light microscope image using a Leica DM2500 microscope A) poly(vinyl alcohol) stabilised capsules stabilised with 20x magnification lens under normal illumination mode, B) capsule viewed under reflectance mode. All scale bars are 500 µm.

Unfortunately we could not do SEM analysis as the solvesso 200ND is not allowed under the SEM microscope due to the volatility. The capsules synthesised using this method had average sizes of 1040 µm in size (s.d. 8.9 µm) with a CV of 0.86%. (as measured using ImageJ, discussed in **Chapter 2 Experimental Section 2.3.6.3.**). The capsule dispersity is very monodisperse and this is due to the rates selected for the flow of the dispersed and continuous phases. Our flow rates caused a dripping mechanism for droplet formation, which typically favours monodisperse droplet sizes whereas a jetting scheme of droplet formation can lead to broad droplet sizes.[53] Unfortunteately this capsule size is not sufficient for agricultural delivery applications and being able to synthesise smaller capsules would be preferable.

4.4.4.2. Surfactant-free capsules via nucleophilic thiol-Michael addition reaction

The same method was used as reported in **Section 4.4.3.1.** for the synthesis of thiol-Michael addition capsules only this time the aqueous phase contained no surfactants. Surfactants that are physically bound to the surface of particles or capsules are typically hard to remove and synthesis without surfactants allows a cleaner surface

of the capsules (surfactants often give a surface charge which can affect the applications for plant delivery). Robust capsules were synthesised that were visible under no magnification as shown in **Figure 4.9.**. The capsules produced using surfactant free conditions exhibited a slight orange hue (from solvesso 200ND) as shown in **Figure 4.9.** When we look at the capsules synthesised with or without the presence of surfactant 4.1 we notice that without surfactant leads to capsules with a slight orange hue whereas the surfactant stabilised capsules show a transparent white colour. The reason for this colour difference is caused by the surfactant 4.1. The 4.1 can cause microphase separation of the wall which can lead to enhanced scattering and thus gives a white haze.

When the capsules were dried no apparent degradation was observed and no oil release was visualised (capsule release is easy to visualise under the microscope due to the orange colour of the solvesso 200ND). The Light microscope images of the capsules synthesised without the use of surfactants are shown in **Figure 4.10.**. ImageJ analysis of the light microscope images gave capsule sizes of 548 μm (s.d. 8.8 μm) with a CV of 1.61%. The capsules stuck together once dried exactly the same as the surfactant stabilised capsules from the previous section. The reflectance mode of the light microscope again showed a rough surface with much deformation (**Figure 4.10-B.** and **4.10-C.**). This reason was discussed earlier where the sizes are smaller with a buckled surface due to the image only showing a small section of the capsule surface. From the image we can see the buckled surface and a pale white spherical region and this part is the actual capsule size.

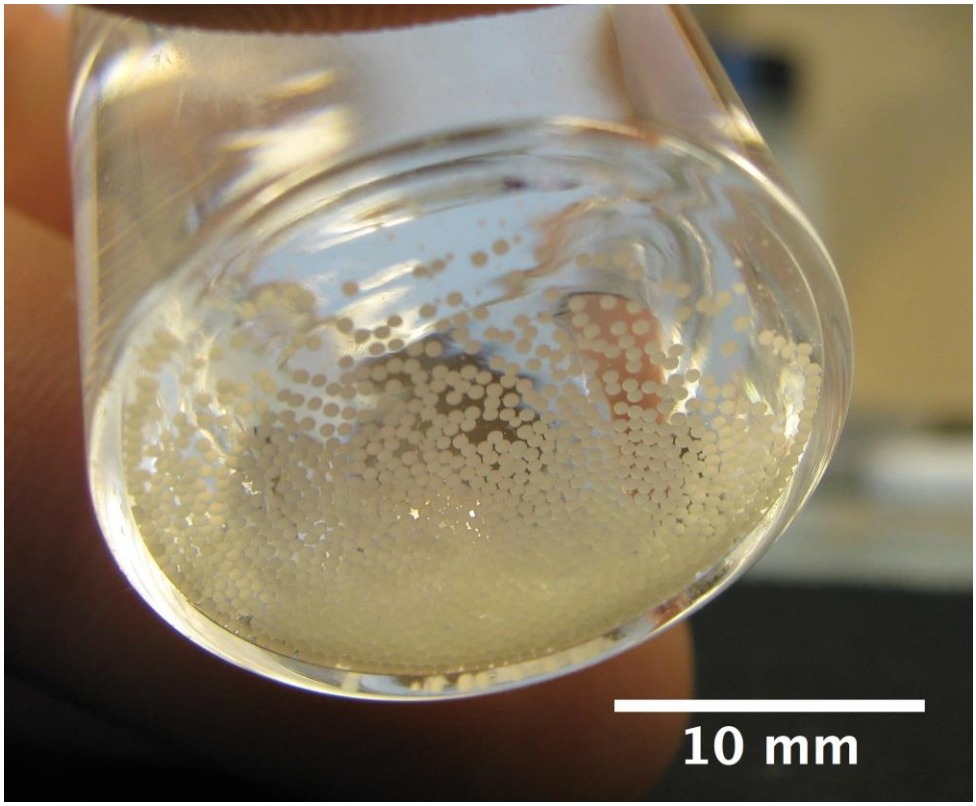

Figure 4.9. Slight orange hue of the synthesised capsules using the microfluidic approach. O/W capsules used solvesso 200ND containing penta-erythritol penta-/hexa- acrylate and penta-erythritol tetra-kis (2-mercaptopropionate) as the inner phase and water as the outer phase. Scale bar is 10 mm.

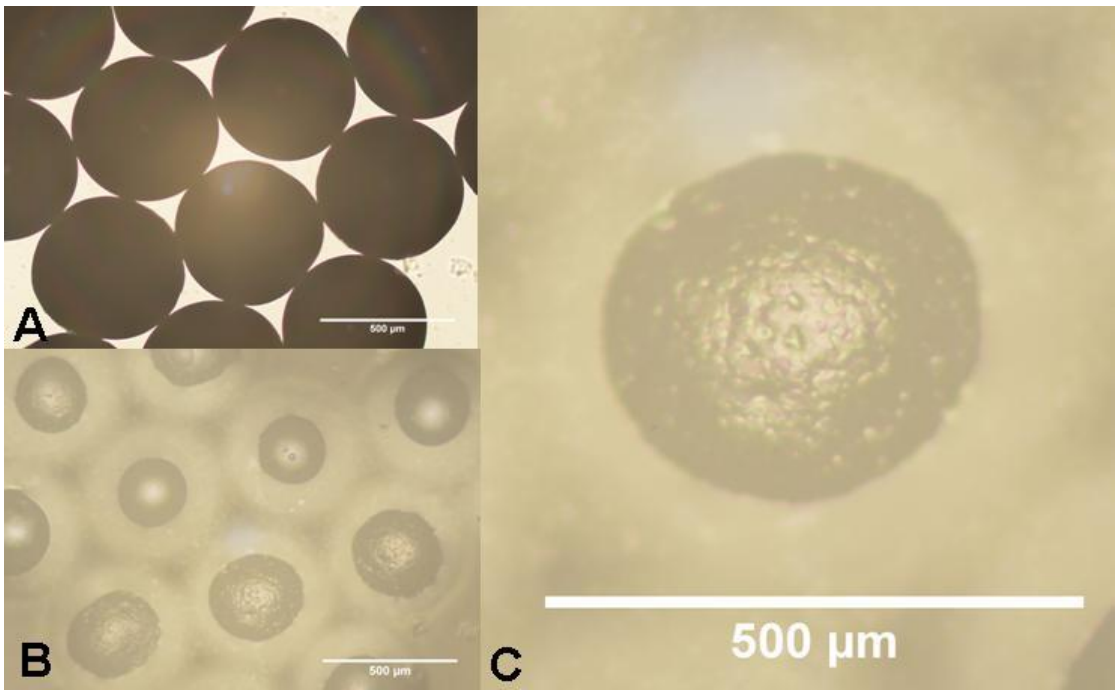

Figure 4.10. Light microscope images using a Leica DM 2500 microscope, A) surfactant-free capsules with 20x magnification lens under normal illumination mode, B) capsules viewed using reflectance mode, C) a close up of a capsule shell using reflectance mode. All scale bars are 500 µm.

4.4.4.3. Comparison between poly(vinyl alcohol) stabilised capsules and soap-free thiol-Michael capsules using microfluidics

4.4.4.3.1. Effect of surfactant on droplet formation

When we compared the two sets of capsules, surfactant free and 4.1 stabilised we notice that the capsules stabilised using surfactant produced capsules of nearly double the size of the capsules with no surfactant (1040 μm compared with 548 μm). When we view the flow rates we notice that the inner phase flow rate is much higher than the outer phase flow rate. In practise these flow rates on the pumps will be different due to the differences between the needle diameter for the inner phase (0.11 mm according to the Sigma Aldrich guide) and the capillary diameter of the outer phase (1.62 mm). The inner needle is so small that the actual flow rate will be much faster leading to larger Weber numbers and so larger droplets will form as the viscous forces from the outer phase are lower.[53] Theoretical explanation would predict that the surfactant stabilised droplets should be smaller. However, the increased viscosity of the continuous phase in the dripping regime for droplet generation makes the droplets bigger. The latter is the dominant effect and so bigger droplets form when surfactant 4.1 is used.

When the outer phase contains surfactant the droplets are stabilised sterically and electrostatically (from the hydroxyl group and large molecular weight chains). This stabilisation of the droplets helps maintain these large 1040 μm droplets before capsule wall formation occurs. If we study the sample without the use of surfactants we can explain the smaller droplet sizes in terms of the surface tension forces. The surface tension between the inner and outer phases will be greater when no surfactant is employed. The higher surface tension leads to a decreased Weber number, We (the

equation for calculating Weber number is shown in **Equation 4.1.**) which would cause droplet break-off to occur earlier. As the droplets break-off sooner then they are smaller as less dispersed phase is forced into the droplet.[53]

$$We = \frac{\rho V^2 D}{\sigma} \qquad \textbf{Equation 4.1.}$$

Where V is the fluid velocity, d is the hydynamic diameter of the channel and σ is the surface tension coefficient.[49,53]

Another possible reason for the differences in the capsule sizes could be the wall formation rather than the droplet formation process. Upon addition of the surfactant-free droplets to the *iso*butylamine solution the capsule could shrink due to solvesso 200ND being released before the wall has time to form. When a surfactant is used it could prevent release of the solvesso 200ND which would explain the larger capsule sizes. Due to the instantaneous reaction for the thiol propionate with an acrylate the wall formation should occur in very fast reaction times so diffusion of the amine should not be important for this interfacial addition reaction.

4.4.4.3.2. Wall structure of microcapsules

When we studied the microfluidic capsules under the microscope we could clearly see the perfect packing of the capsules due to their monodisperse size (**Figure 4.8-A.** and **4.10-A.)**. This is an advantage of generating capsules using a microfluidic device. The capsules were spherical in shape but the surface did have surface irregularities. When we study the reflectance mode microscope images we can visualise the capsule wall and the morphology of the capsule surface (**Figures 4.8-B.**, **4.10-B.** and **4.10-C.**). When we study the surface of the capsules we notice that the morphology is not completely smooth most likely due to the porous thiol-Michael network structure

that forms at the interface. The crosslinking process between 3.6 and 3.9 will likely have a random ordering and heterogeneities in the network due to steric hinderance leaving many unreacted thiol and acrylate groups. This leads to structural irregularities at the interface caused from some sections of the wall having a greater formation of polymer while other sections are constrained by the crosslinking mechanism and form less polymer network. When the dried out capsules were squashed using a needle (under the microscope) rupture did occur and orange solvesso 200ND was released.

We can also estimate the wall thickness for the two synthesised capsules using the theoretical equations (**Equations 4.2.** and **4.3.**) by making two assumptions. We will assume that all solvesso 200ND was encapsulated inside the droplets. We will also assume that the density of the polymer is 1.2 g/ml and that the thiol-Michael addition reaction achieved full conversion. By using **Equation 4.2.** and incorporating this into **Equation 4.3.** we can determine the value of R. We found the values of R for both capsules and the values were 32 μm for the 4.1 stabilised capsules and 16 μm for the surfactant-free capsules. These thicknesses are enough to maintain the stability of the capsule after drying.

$$\boldsymbol{V_d . N = V_t} \qquad \textbf{Equation 4.2.}$$

$$\boldsymbol{m = \rho . V_c . N} \qquad \textbf{Equation 4.3.}$$

4.4.5. Homogenisation thiol-Michael addition capsule approach

Clearly we have thus far been able to utilise the thiol-Michael addition reaction to synthesise capsules in the size range 500-1000 μm using a nucleophilic amine catalyst. The next overall aim was to try and decrease the capsule sizes to produce smaller microcapsules that are more applicable for our aims where nanocapsules would

be ideal. In literature, small capsule sizes are achieved using homogenisation emulsification techniques. Homogenisation is an important means for emulsification as the shear can be controlled (low or high shear). Increasing the shear forces can enable droplets of 500 nm to 20 µm to be produced (depending on the homogenisation speed and the employment of surfactants).

We decided to test the thiol-Michael addition reaction using homogenisation emulsification as a means to synthesise capsules. The monomers 3.6 and 3.9 were dissolved into the solvesso 200ND oil and this phase was added to the aqueous phase under stirring. For the homogenised capsules we tried two different surfactant solutions which are both employed by Syngenta in synthesis of poly(urea) and poly(urethane) capsules. Gohsenol was the first (referred to as 4.2, a slightly different poly(vinyl alcohol) surfactant) and is shown in **Figure 4.11.**. The second system used a combination of lomar D (referred to as 4.3, a poly(naphthalene sulphonate) sodium salt condensate)[45] with tergitol XD (referred to as 4.4, a non-ionic alkyl ethyleneoxide/propyleneoxide copolymer).[55] These three surfactant structures are shown in **Figure 4.11.**. The solution of oil and aqueous phase was initially pre-emulsified followed by further homogenisation at 7100-8100 rpm for two minutes to decrease the droplet sizes to <20 µm as studied using light microscopy. The emulsion was kept stirring and the *iso*butylamine catalyst was added to initiate the reaction between the monomers 3.6 and 3.9. The exact procedure for the two different surfactant stabilised thiol-Michael addition capsules is discussed in **Experimental Section 4.3.5.1.** and quantities of reagents are reported in **Table 4.2.** (**Section 4.3.5.1.)**.

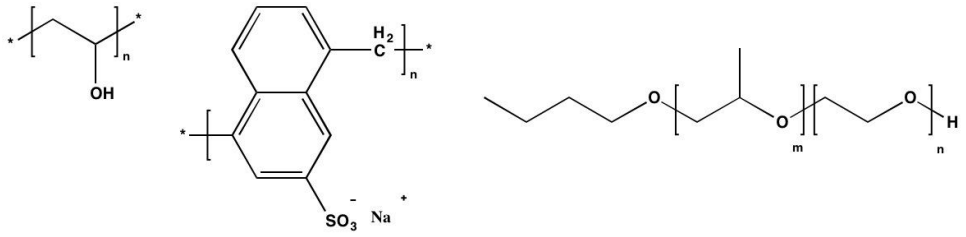

Figure 4.11. Structures of surfactants, gohsenol GL-05 (left), lomar D (middle) and tergitol XD (right).

The homogenised capsules were monitored using light microscopy using a 40x magnification lens to enable visualisation of the capsules (capsule sizes <1 μm are not visible using light microscopy). The capsules produced using surfactant 4.2 are shown in **Figure 4.12.** and the capsules using surfactants 4.3 and 4.4 are shown in **Figures 4.13.**. The capsules synthesised using either surfactant solutions do not show any major differences. The sizes of the capsule and their stability towards drying were roughly equivalent as discussed next (average droplet sizes of the pre-emulsions were 7.35 μm (s.d. 3.5 μm) with a CV of 45.7% and 8.12 μm (s.d. 2.9 μm) with a CV of 47.7%). These CV values are much greater in contrast to the microfluidic device technique.

4.4.5.1. Using gohsenol poly(vinyl alcohol) surfactant

If we study the samples synthesised using gohsenol as the surfactant we notice that the emulsion is stable when water is present and the capsules did not coalesce over time (**Figure 4.12-A.)**. The average capsule sizes after approximately 1 hour 20 minutes of reaction time was 7.8 μm (s.d. 3.6 μm) with a CV of 45.8%. The sample was left to dry on a microscope slide where we noticed that the capsules clustered together and decreased in size as they moved towards the solvent drying front (shown in **Figure 4.12-B.**). Once the capsules reached the drying front they had already began to breakdown. The capsules are less rigid or robust compared to the previously synthesised microfluidic capsules and wall buckling occured after the water is removed from the sample. The buckling is caused from evapouration of the solvesso 200ND from inside

the capsules and capillary underpressure due to the evapouration of water. The combination of these effects leads to rupture of the capsule wall. The capillary underpressure due to water evapouration is bigger for clusters of smaller capsules explaining while this effect did not occur for the microfluidic synthesised capsules. This wall degradation could be burst release of the solvesso 200ND or diffusion of the solvesso 200ND through the thiol-Michael addition polymer network causing the reduction of capsule sizes as observed.

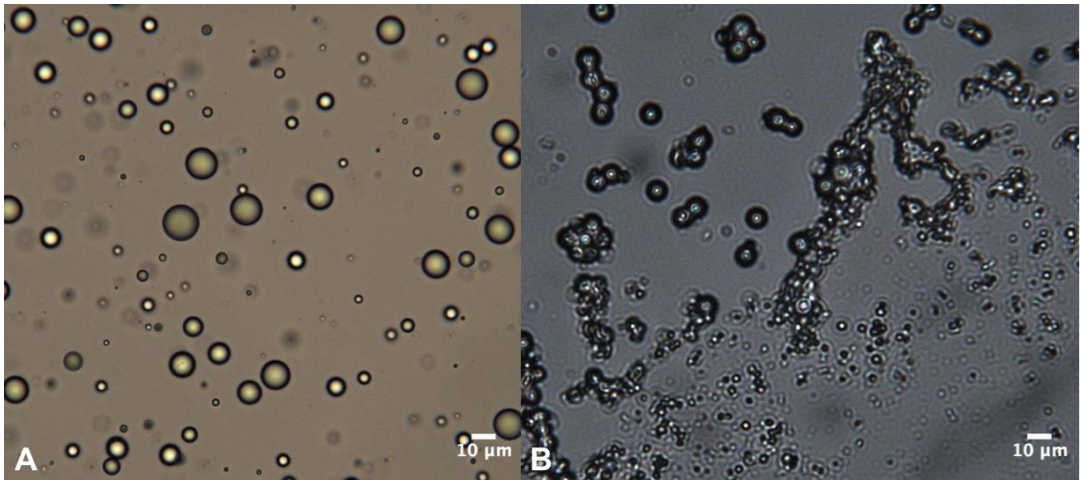

Figure 4.12. Light microscope images of the gohsenol stabilised capsules using a Leica DM 2500 microscope with 40x magnification lens under normal illumination mode, A) wet emulsion, B) drying edge of the capsules. All scale bars 10 µm.

4.4.4.2. Using lomar D poly(naphthalene sulphonate) surfactant with tergitol XD

Again the wet emulsion appears the same as the capsules stabilised using gohsenol surfactant (**Section 4.4.4.1.**). The capsule average sizes was 7.4 µm (s.d. 3.2 µm) with a CV of 46.7%. Lomar D is a colloid stabiliser and tergitol XD is used to lower the surface tension to enable easier droplet break-up. The capsules clustered together and decreased in size as the solvent was removed (**Figure 4.13-B.**). The capsules deformed once dry into hexagonal and polyhedral shapes (see **Figure 4.13-C.**) and eventually they coalesced and fully degraded. Once complete drying has occurred

all that remains are small polymer mass with sizes less than 2 µm (see **Figure 4.13-D.**). The time scale to disintegration of the capsules and solvesso 200ND release was not very long and was typically in the order of two minutes or less.

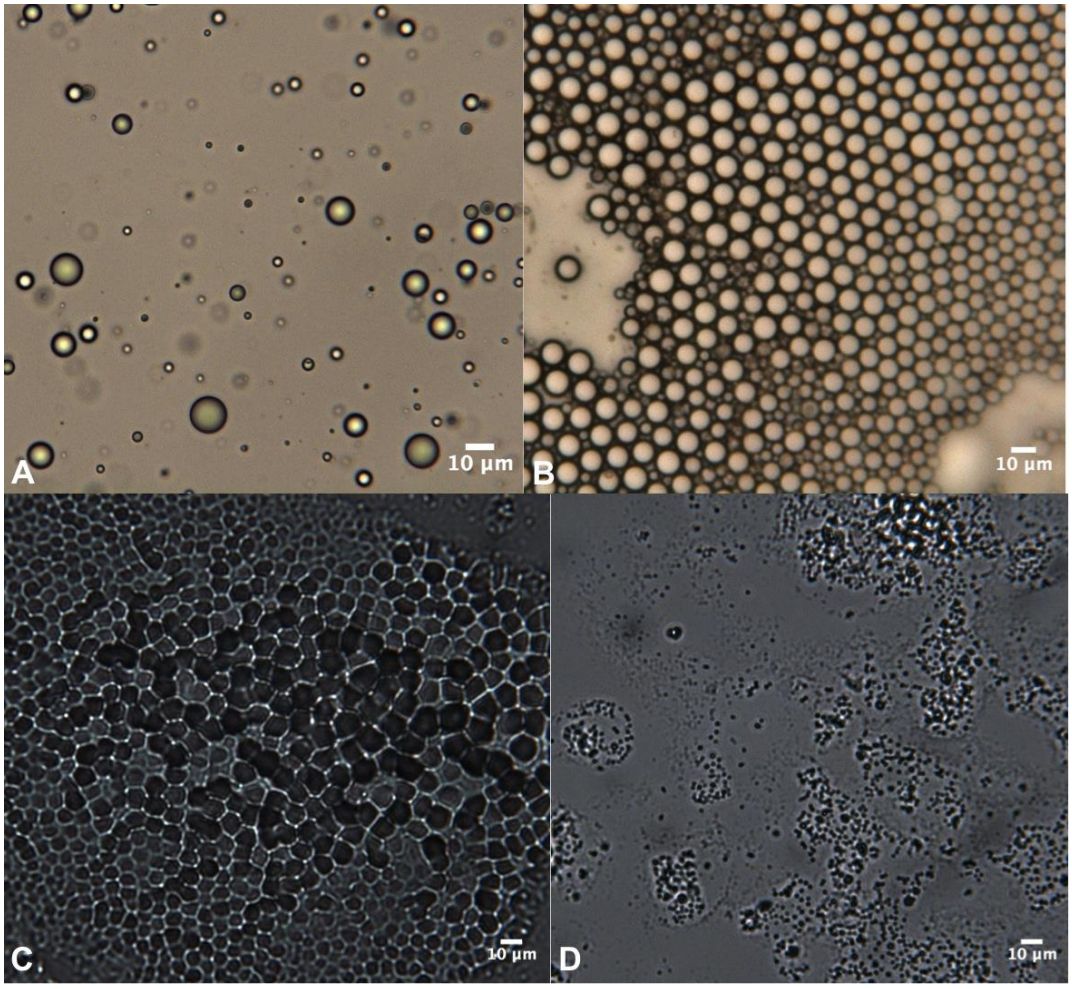

Figure 4.13. Light microscope images of the lomar D and tergitol XD stabilised capsules using a Leica DM 2500 microscope with 40x magnification lens under normal illumination mode, A) wet emulsion, B) drying and clustering capsules near to the water front, C) merging of clustered capsules, D) complete capsule breakdown and remaining residue. All scale bars 10 µm.

4.4.5.3. Failure of homogenised capsules using thiol-Michael addition reaction

The capsules synthesised using homogenisation emulsification did not have enough stability towards drying like the millimetre sized capsules using microfluidics showed. Due to the failure to synthesise stable robust capsules in the size range 2-20 µm

then synthesising capsules smaller in diameter would not be achievable using this current methodology. The main reasons for the failure to create a robust capsule wall is likely due to the increased surface area of the system and capsule wall thicknesses. In the microfluidic approach the surface area per droplet was very large and the amount of monomer able to react per droplet would be generally high. With the homogenised approach the total amount of thiol and acrylate monomers per droplet would be much less due to the drastic increase in the surface area of the system. This could mean that incomplete coverage of the solvesso 200ND droplets occurred which would explain the ease of release of the dispersed phase. In order to try and synthesise more physically robust capsules we would need to increase the quantity of monomeric reagents in the reaction. Another possible solution would be to try the layer-by-layer approach of adding alternating reactants to try and build up the capsule wall layers. We tried to estimate the wall thickness for the homogenised capsules and for the capsule average size of 7.35 μm then the estimated wall thickness would be only 225 nm. This wall is much thinner when compared to the microfluidic capsules and rupture is likely caused by this wall thickness not being enough or the wall being to porous.

Unfortunately capsules smaller than the above would have less stability towards drying due to the increase in internal pressure as the size decreases. This is shown in the Young-Laplace equation, **Equation 4.2.**.[49]

$$\boldsymbol{\Delta P = \frac{2\gamma}{R}} \qquad \textbf{Equation 4.2.}^{49}$$

Where ΔP is the Laplace pressure, γ is the surface tension, and R is the radii of curvature.[49]

This equation states that the internal pressure difference between the inside and outside of the droplet increases as the size decreases. So decreasing the droplet diameter

from one micron to 100 nm would increase the pressure by a factor of ten. This is why surfactants are required for stabilising nano and micro emulsions as they reduce the pressure difference (lowering surface tension values and electrostatic or steric effects).[50]The formation of smaller droplets diameters woud also lead to an increased surface area which would mean more thiol-Michael addition polymer network would need to form and on such small sizes the polymer network would likely be too porous to be robust. Unfortunately this meant that our current experimental method using the thiol-Michael addition reaction could not synthesise smaller capsules and a different method would have to be used to strengthen the capsule wall. The next stage to improving on this method would be to increase the thickness of the capsule walls and try to alter the porosity to reduce the loss of solvesso 200ND by diffusion and wall rupture. There is a chance that the formation of polymer for the capsules could be diffusion controlled. However, to follow whether the polymerisation reaction is diffusion controlled or not would require following capsule wall thickness as a function of time. This would not be very straightforward for this method and would be rather complex.

4.5. Conclusions

In conclusion we describe the use of an interfacial *iso*butylamine catalysed thiol-Michael addition reaction between pentaerythritol penta-/hexa- acrylate and pentaerythritol tetrakis (2-mercaptopropionate) to create capsules. The thiol-Michael addition reaction occurred in water where an elastic polymer network formed at the interface with solvesso 200ND oil as shown in the test reactions. The use of a microfluidic device allowed oil droplets to be generated of sizes 500 to 2000 μm leading. Poly(vinyl alcohol) stabilised and surfactant-free capsules were synthesised by the reaction of pentaerythritol penta-/hexa- acrylate with pentaerythritol tetrakis (2-mercaptopropionate) when dropped into an *iso*butylamine aqueous solution. The capsules produced *via* the microfluidic approach were studied using light microscopy and did not show any signs of breakdown or release of solvesso 200ND before or after drying. However, the microfluidic capsules did adhere to each other when they became dry could not be redispersed into water.

The interfacial thiol-Michael addition reaction capsules were scaled using homogenisation emulsification enabling droplet sizes of 2-9 μm. These microcapsules showed excellent stability when hydrated but lacked stability once dried and full degradation of the capsules was observed after only 1-2 minutes. We have shown that there is potential for the thiol-Michael addition reaction to allow efficient capsule synthesis but more research is needed until tailored nanocapsules can be synthesised.

4.6. References

1 Follows RR *et al* (Syngenta Ltd), Acid-triggered release microcapsules, European patent Application, EP1100327 B1, Mar 12, 2003

2 Chen JL *et al* (Syngenta Ltd), Microencapsulated compositions, European patent Application, EP0902724 B1, Dec 5, 2001

3 Chen JL *et al* (Syngenta Ltd), Microcapsules, United States patent Application, US8173159 B2, May 8, 2012

4 Follows RR *et al* (Syngenta Ltd), Base-triggered release microcapsules, European patent Application, EP1100326 B1, Apr 23, 2003

5 Rodson M, Scher HB (Zeneca Inc), Microcapsules, United States patent Application, US5332584 A, Jul 26, 1994

6 Shirley IM *et al* (Syngenta. Ltd), Variable release microcapsules, United States patent Application, US6485736 B1 Nov 26, 2002

7 Kozuki Y, Agrochemical composition comprising as solvent a mixture of an aromatic hydrocarbon, propylene glycol diacetate, and 1,3-dimethyl-2-imidazolidinone, European patent Application, EP2073633 B1, Feb 13, 2013

8 Damo Z, Fears MA (AgrEvo UK Ltd), Fungicidal formulations, European patent Application, EP0505053 A1, Sep 23, 1992

9 Yow HN, Routh AF, Formation of liquid core-polymer shell microcapsules, *Soft Matter*, 2006; **2**:940-949

10 Dinsmore AD, Hsu MF, Nikolaides MG, Marquez M, Bausch AR, Weitz DA, Colloidosomes: selectively permeable capsules composed of colloidal particles, *Science*, 2002; **298**: 1006-1009

11 Esser-Kahn AP, Odom SA, Sottos NR, White SR, Moore JS, Triggered release from polymer capsules, *Macromolecules*, 2011; **44**:5539-5553

12 Ghosh SW, Functional coatings by polymer microencapsulation, WILEY-VCH, 2006

13 Dowding PJ, Atkin R, Vincent B, Bouillot P, Oil core-polymer shell microcapsules prepared by interfacial phase separation from emulsion droplets. 1. characterization and release rates for microcapsules with polystyrene shells, *Langmuir*, 2004; **20**:11374-11379

14 Wu D, PhD Thesis, Liquid-core capsules *via* interfacial polymerization and alternating copolymerisation, 2007

15 Perlatti B, de Souza Bergo PL, da Silva MTGF, Fernandes JB, Forim MR, Polymeric nanoparticle-based insecticides: a controlled release purpose for agrochemicals

from the book "insecticides - development of safer and more effective technologies, chapter 20", InTech, 2013

16 Wilkins R, Controlled release formulation, agricultural from the book "encyclopedia of polymer science and technology, John Wiley and Sons Inc, 2002

17 Scher HB, Rodson M, Lee KS, Microencapsulation of pesticides by interfacial polymerisation utilising isocyanate or aminoplast chemistry, *Pestic. Sci*. 1998; **54**:394-400

18 Mathiowitz E, Encyclopedia of controlled drug delivery, Volumes 1 and 2, John Wiley and Sons Inc, 1999

19 Jabbari E, Characterization of microcapsules prepared by interfacial polycondensation of methylene bis(phenyl isocyanate) with hexamethylene diamine, *Iran Polym. J.*, 2001; **10**:33-43

20 Su JF, Wang LX, Huang Z, Meng XW, Preparation and characterization of polyurethane microcapsules containing *n*-octadecene with styrene-maleic anhydride as a surfactant by interfacial polycondensation, *J. Appl. Polym. Sci.*, 2006; **102**: 4996-5006

21 Crespy D, Stark M, Hoffmann-Richter C, Ziener U, Landfester K, Polymeric nanoreactors for hydrophilic reagents synthesized by interfacial polycondensation on miniemulsion droplets, *Macromolecules*, 2007; **40**:3122-3135

22 Gaudin F, Sintes-Zydowicz, Poly(urethane-urea) nanocapsules prepared by interfacial step polymerization in miniemulsion. the droplet size: a key factor for the molecular and thermal characteristics of the polymeric membrane of the nanocapsules?, *Colloid Surface A*, 2011; **384**:698-712

23 Wittbecker EL, Katz M, Interfacial polycondensation. 7. polyurethanes, *J. Polym. Sci.*, 1959; **40 (137)**:367-375

24 Wittbecker EL, Morgan PW, Interfacial polycondensation. I, *J. Polym. Sci.*, 1959; **40**: 289-297

25 Ley SV, Ramarao C, Lee AL, Ostergaard N, Smith SC, Shirley IM, Microencapsulation of osmium tetroxide in polyurea, *Org. Lett.*, 2003; **5 (2)**:185-187

26 Li J, Hitchcock AP, Stöver HDH, Shirley IM, A new approach to studying microcapsule wall growth mechanisms, *Macromolecules*, 2009; **42**:2428-2432

27 Ramarao C, Ley SV, Smith SC, Shirley IM, DeAlmeida N, Encapsulation of palladium in polyurea microcapsules, *Chem. Comm.*, 2002; **10**:1132-1133

28 Antipov AA, Sukhorukov GB, Polyelectrolyte multilayer capsules as vehicles with tunable permeability, *Adv. Colloid. Interface.*, 2004; **111**:49-61

29 Sukhorukov GB, Fery A, Möhwald H, Intelligent micro- and nanocapsules, *Prog. Polym. Sci.*, 2005; **30**:885-897

30 De Geest BG, Sanders NN, Sukhorukov GB, Demeester J, De Smedt SC, Release mechanisms for polyelectrolyte capsules, *Chem. Soc. Rev.*, 2007; **36**: 636-649

31 Li J, Mazumder J, Stöver HDH, Hitchcock AP, Shirley IM, Polyurea microcapsules: surface modification and capsule size control, *J. Polym. Sci. Polym. Chem.*, 2011; **49**:3038-3047

32 Connal LA, Kinnane CR, Zelikin AN, Caruso F, Stabilization and functionalization of polymer multilayers and capsules *via* thiol-ene click chemistry, *Chem. Mater.*, 2009; **21**:576-578

33 Delcea M, Möhwald H, Skirtach AG, Stimuli-responsive LbL capsules and nanoshells for drug delivery, *Adv. Drug. Deliver. Rev.*, 2011; **63**:730-747

34 Hong K, Park S, Preparation of polyurethane microcapsules with different soft segments and their characteristics, *React. Funct. Polym.*, 1999; **42**: 193-200

35 Ramanathan LS, Shukla PG, Sivaram S, Synthesis and characterization of polyurethane microspheres, *Pure & Appl. Chem.*, 1998; **70**:1295-1299

36 Rosenbauer EM, Wagner M, Musyanovych A, Landfester K, Controlled release from polyurethane nanocapsules *via* pH -, UV-light – or temperature-induced stimuli, *Macromolecules*, 2010; **43**:5083-5093

37 Tsuda N, Ohtsubo T, Fuji M, Preparation of self-bursting microcapsules by interfacial polymerisation, *Adv. Powder Technol.*, 2012; **23**:724-730

38 Hashemi SA, Zandi M, Encapsulation process in synthesizing polyurea microcapsules containing pesticide, *Iran Polym. J.*, 2001; **10**: 265-270

39 Soto-Portas ML, Argillier JF, Méchin F, Zydowicz N, Preparation of oily core polyamide microcapsules *via* interfacial polycondensation, *Polym. Int.*, 2003; **52**:522-527

40 Beaman RG, Morgan PW, Koller CR, Wittbecker EL, Interfacial polycondensation. 3. polyamides, *J. Polym. Sci.*, 1959; **40**: 329-336

41 Joscelyne SM, Trägårdh, Membrane emulsification – a literature review, *J. Membrane Sci.*, 2000; **169**:107-117

42 Charcosset C, Limayem I, Fessi H, The membrane emulsification process – a review, *J. Chem. Technol. Biotechnol.*, 2004; **79**: 209-218

43 Malloggi F, Pannacci N, Attia R, Monti F, Mary P, Williame H, Tabeling P, Monodisperse colloids synthesised with nanofluidic technology, *Langmuir*, 2010; **26**:2369-2373

44 Zhou J, Zhang QY, Chen SJ, Zhang HP, Ma AJ, Ma ML, Liu Q, Tan, JJ, Influenece of thiol and ene functionalities on thiol-ene networks: photopolymerisation, physical, mechanical, and optical properties, *Polym. Test.*, 2013; **32**:608-616

45 Prasath RA, Gokmen MT, Espeel P, Du Prez FE, Thiol-ene and thiol-yne chemistry in microfluidics: a straightforward method towards macroporous and nonporous functional polymer beads, *Polym. Chem.*, 2010; **1**:685-692

46 Rosen MJ, Surfactants and interfacial phenomena, 3rd Ed, John Wiley & Sons Inc, 2004

47 Griffin WC, Classification of surface active agents by "HLB", *J. Soc. Cosmet. Chem.*, 1949; **1**:311-326

48 Griffin WC, Calculation of HLB values of non-ionic surfactants, *J. Soc. Cosmet. Chem.*, 1954; **5**:249-235

49 Baroud CN, Gallaire F, Dangla R, Dynamics of microfluidic droplets, *Lab Chip*, 2010; **10**:2032-2045

50 Davies JT, A quantitative kinetic theory of emulsion type, I. Physical chemistry of the emulsifying agent, *Gas/liquid and liquid/liquid interface*, 426-438

51 Patil S, Schmidt DF, Safer adhesives *via* thiol-ene chemistry, Toxic use reduction reports (TURI) technical reports number 72, 2012

52 O'Brien AK, Cramer NB, Bowman CN, Oxygen inhibition in thiol-acrylate photopolymerisations, *J. Polym. Sci. Polym. Chem.*, 2006; **44**:2007-2014

53 Nurumbetov G, Synthesis of anisotropic microparticles and capsules *via* droplet microfluidics, PhD thesis, 2013

54 Lange FT, Merklinger M, Wenz M, Brauch HJ, Lehmann M, Pinter I, Occurrence and solid-liquid partition of sulphonated naphthalene-formaldehyde condensated in the aquatic environment, *Environ. Sci. Technol.*, 2005;**39**:1523-1531

55 Polyalkylene glycol monobutyl ether (PGME) Handling/processing MSDS technical evaluation report, compiled by USDA AMS agricultural analytics division, 2013

Chapter 5 - Conclusions

Studies on what move through soil, what bind to plants and how active ingredients are delivered to roots has been of widespread interest for Agricultural applications. Due to large inconsistencies between soils types, soil porosity and plant systems and size designing particles and capsules that can be used for targeted delivery is a challenge for chemists. The purpose of this work was to synthesise and tailor colloidal particles and capsules for the purposes of 1) mobility through soil, 2) adhesion to roots, 3) targeted delivery of microcapsules. For these aims we designed three specific methods of synthesis that could achieve this aim: to synthesise colloidal particles with a great degree of anionic surface groups to provide mobility through soil and stability towards electrolytes where for this thesis the sulphonate group was chosen. To synthesise colloidal particles with adhesive properties that could be functionalised to target root systems. To encapsulate solvesso oil for delivery of an active ingredient

In **Chapter 2** we reported the synthesis and limitations of sulfonated colloidal poly(styrene) particles in the size range 100-200 nm using soap-free emulsion polymerisation with sodium 4-vinylbenzenesulphonate. We studied the protection of sodium 4-vinylbenzenesulphonate monomer using both neopentyl and ethyl functional groups and discuss the deprotection temperatures required for cleavage as well as the limitations both monomers exhibit. Using ethyl 4-vinylbenzenesulphonate over sodium 4-vinylbenzenesulphonate allowed an increase of the monomer loading capacity inside polymer particles. Monodisperse particles synthesised were visualised and characterised by electron microscopy and light scattering and the loading of protected monomer was reported up to 50 wt% as shown using thermal gravimetric analysis. Deprotection of the protected monomer particles was carried out using thermolysis and further thermal analysis led to the report that further cleavage of the ethyl group no longer occurred meaning that the thermolysis caused full deprotection.

Chapter 3 described the synthesis of both hydrophobic, and hydrophilic, poly(styrene) and hydrophilic poly(methylmethacrylate) and poly(ethylmethacrylate) seed particles using soap-free emulsion polymerisation. Seed particles sizes were tailored by the addition of ionic comonomers. By feeding di-, tri-, and penta-/hexa-functional acrylate crosslinking monomers onto seed latex, nanogel decorated raspberry-like and core-shell type particles with a greater surface area were produced. The results showed that hydrophilic acrylic seeds led to a much greater coating percentage of nanogel particles than the hydrophobic seeds. We showed that the hydrophobicity of poly(styrene) seeds can be tailored to make them more hydrophilic increasing the surface coverage of nanogel particles. Seed diameter also played a role in the number of deposited particles onto the seed surface where larger seeds accommodated more decorating particles. Di- functional acrylate crosslinkers led to raspberry-like decorated structures but the morphology changed to core-shell type when the functionality was increased to tri- and penta-/hexa- acrylates. Surface functionality was analysed using spectroscopic methods where Raman microscopy was used to show the presence of pendant vinyl functionality for the tri- and penta-/hexa- nanogel decorated poly(ethylmethacrylate) latex particles. Raman microscopy after a nucleophilic thiol-ene click reaction led to a decrease in the vinyl group percentages.

In **Chapter 4** we described the fabrication of a simple microfluidic device for producing solvesso in water droplets using PVA surfactant and surfactant-free conditions. By utilising an interfacial nucleophilic thiol-ene click reaction we synthesised capsules of 1.1 μm and 0.55 μm capsules using PVA stabilised and surfactant-free respectively. Capsules were studied using light microscopy where the dry down properties of the capsules were studied and release of the oil was prevented on this size scale. No oil release was observed after drying when measured for days.

Capsule sizes were decreased using high shear homogenisation which synthesised capsules in the size range 1-10 microns. The capsules only showed dry down stability for minutes when dried down and the oil was released which was not preferable for our aims.

5.1. Future work

Further characterisation of the sulphonated particles using elemental analysis would be carried out. To test the possibility of a 100% loading of ethyl *4*-vinylbenzenesulphonate inside particles followed by further studies on the deprotection and characterisation. Electron microscopy would be used to monitor the surface effects after deprotection and FT-IR TGA could monitor the release of chemicals during the deprotection to prove whether the protecting group is released. The particles would also be used to study colloid mobility in soil columns using both real soil and using silica particles of varying sizes. An increase in colloid mobility would be expected once the particles were deprotected due to the presence of sulphonate groups.

To further study the effects of particle size on the absorption and spreading of crosslinked nanogel particles onto the surface. Synthesising a range of seed particles of the same polymer with different sizes would enable to study the seed size effects. Also by testing out different rates of crosslinking monomer addition and different temperatures we would aim to find the requirement for synthesising coree-shell particles with a high degree of pendant vinyl groups for reacting. To further study the effects of thiol-Michael addition reaction and prove whether the reaction was a success or not. To tailor the functionality with a range of thiols and study the spatial charge density of vinyl groups that have reacted. Study of the adhesive properties of the particles on model surfaces such as silica, quartz or glass (representing idealised soil) and cellulose

(representating plant roots). To functionalise nanogel decorated particles with various surface charge groups to study the effects of multiple surface charges on mobility of colloids as well as functionalised systems involving zwitterionic charges.

To further study the formation of capsule walls using the interfacial thiol-Michael addition reaction. Using both electron microscopy and NMR we could study the surface and wall thickness quantify the degree of polymerisation of the shell. To study the addition and effects of multi functionality acrylate and thiols acting as linkers and altering the surface porosity. This could enable the homogenised capsules to be more stable towards drying if the wall was made more rigid or the porosity decreased. This could enable smaller capsule sizes to be achieved with a primary aim of nanosized capsules. To study post thiol-Michael addition functionalisation of microcapsules whereby either layer-by-layer technology could be used to build up thicker walls or post functionalisation using charged thiols or enes could synthesise charged polymeric capsules.